Electrochemical Society

AN IMPORTANT MESSAGE FOR ELECTROLYTIC CELL OPERATORS

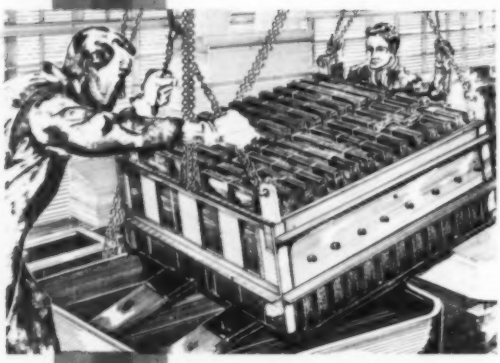

Extra dividends in the form of increased cell operating economies are now available to users of GLC Anodes.

These dividends have been developing during the past several years as a result of exchanges between GLC engineers and those of GLC customers.

Among the results, depending upon the requirements of the individual electrolytic cell operator, are longer anode life, longer diaphragm life, reduced power consumption, and reduced labor costs.

As you know, it takes months to translate technical objectives into anode characteristics—and many months more to check on the results of these changes in cell operations.

The time has now come when the hoped-for results are actually being achieved by GLC Anode customers.

If you, as an electrolytic cell operator, are not as yet fully informed about the GLC program of technical exchanges with GLC Anode customers, and the results of this program which are now becoming evident, we will be happy to furnish such information to you.

We feel sure you will find these facts a profitable step forward in improving the operating efficiency of your electrolytic cells also.

PRODUCTS YOU CAN TRUST

GREAT LAKES CARBON CORPORATION

18 EAST 48TH STREET, NEW YORK 17, N. Y. OFFICES IN PRINCIPAL CITIES

EDITORIAL STAFF

H. H. Uhlig, Chairman, Publication Committee

Cecil V. King, Editor

Norman Hackerman, Technical Editor

Ruth G. Sterns, Managing Editor

U. B. Thomas, News Editor

H. W. Salzberg, Book Review Editor

Natalie Michalski, Assistant Editor

DIVISIONAL EDITORS

W. C. Vosburgh, Battery

Milton Stern, Corrosion, I

R. T. Foley, Corrosion, II

T. D. Callinan, Electric Insulation

Seymour Senderoff, Electrodeposition

H. C. Froelich, Electronics

Ernest Paskell, Electronics—Semiconductors

Sherlock Swann, Jr., Electro-Organic, I

Stanley Wawzonek, Electro-Organic, II

John M. Blocher, Jr., Electrothermics and Metallurgy, I

A. U. Seybolt, Electrothermics and Metallurgy, II

N. J. Johnson, Industrial Electrolytic

C. W. Tobias, Theoretical Electrochemistry, I

A. J. deBethune, Theoretical Electrochemistry, II

ADVERTISING OFFICE

ECS
1860 Broadway, New York 23, N. Y.

ECS OFFICERS

W. C. Gardiner, President
Olin Mathieson Chemical Corp., Niagara Falls, N. Y.

R. A. Schaefer, Vice-President
The Bunting Brass and Bronze Co., Toledo, Ohio

Henry B. Linford, Vice-President
Columbia University, New York, N. Y.

F. L. LaQue, Vice-President
International Nickel Co., Inc., New York, N. Y.

Lyle I. Gilbertson, Treasurer
Air Reduction Co., Murray Hill, N. J.

I. E. Campbell, Secretary
National Steel Corp., Weirton, W. Va.

Robert K. Shannon, Executive Secretary
National Headquarters, The ECS, 1860 Broadway, New York 23, N. Y.

Manuscripts submitted to the Journal should be sent, in triplicate, to the Editorial Office at 1860 Broadway, New York 23, N. Y. They should conform to the Instructions to Authors, last published in the August 1959 issue, pp. 232C-233C. Manuscripts so submitted become the property of The Electrochemical Society and may not be published elsewhere, in whole or in part, unless permission is requested and granted by the Editor.

Inquiries re positive microfilm copies of volumes should be addressed to University Microfilms, Inc., 313 N. First St., Ann Arbor, Mich.

Journal of the
Electrochemical Society

FEBRUARY 1960 **VOL. 107 • NO. 2**

CONTENTS

Editorial

Chemical Industry Runs the Show 28C

Technical Papers

The Reaction of Germanium with Aqueous Solutions, II. Dissolution Kinetics in Electrolytes and the Role of Specific Adsorption. *W. W. Harvey and H. C. Gatos* 65

Corrosion Mechanisms in the Reaction of Steel with Water and Oxygenated Solutions at Room Temperature and 316°C. *M. B. Strauss and M. C. Bloom.* 73

Corrosion of Nickel Coated Mild Steel. *B. C. Banerjee* 80

The Kinetics of the Corrosion of Low-Hafnium Zirconium in Aqueous Sulfuric Acid Solutions. *T. Smith* 82

The Relationship between Brightness and Structure in Electroplated Nickel. *R. Weil and R. Paquin* 87

The Adhesion of Electrodeposited Nickel to Chromium at Elevated Temperatures. *W. E. Reid, Jr. and F. Ogburn* 91

Temperature and Space-Charge Effects in Liquid Hydrocarbons. *R. Coelho and M. Bono* 94

Silicon Nitride Thin Film Dielectric. *C. R. Barnes and C. R. Geesner* 98

Tin-Activated Calcium Orthosilicate Phosphors. *R. W. Mooney* 100

Luminescent Properties of Silver-Activated Magnesium Borate Phosphors. *Y. Uehara, Y. Kobuke, and I. Masuda* 104

Chemical Etching of Silicon, II. The System HF, HNO_3, H_2O, and $HC_2H_3O_2$. *H. Robbins and B. Schwartz* 108

High-Purity Silicon from an Iodide Process Pilot Plant. *C. S. Herrick and J. G. Krieble* 111

The Preparation and Properties of Aluminum Antimonide. *W. P. Allred, W. L. Mefferd, and R. K. Willardson* 117

A Phase Equilibrium Study of the System Na_2WO_4-Na_2CO_3-H_2O. *R. L. Pilloton and G. E. Crawley, Jr.* 122

Production of Thorium Powder by Calcium Reduction of Thorium Oxide. *N. Fuhrman, R. B. Holden, and C. I. Whitman* 127

Batteries with Solid Ion-Exchange Membrane Electrolytes, II. Low-Temperature Hydrogen-Oxygen Fuel Cells. *W. T. Grubb and L. W. Niedrach* 131

The Influence of Cations on the Differential Capacity of the Dropping Mercury Electrode in Solutions of Electrolytes in Methanol and Ethanol. *S. Minc and J. Jastrzebska* 135

Chloride Content of the Diffusion Layer at a Silver Anode. *P. A. Krasley* 139

Technical Notes

Oxidation Rates of K and Rb between −79°C and −20°C. *J. V. Cathcart and G. P. Smith* 141

The A-C Resistance of a Polarized Stainless Steel Wire Cathode. *G. M. Schmid and N. Hackerman* 142

Brief Communication

Measurement of the Segregation Coefficients of Impurity Elements in Aluminum Antimonide. *D. Hazelby and J. L. Parmee* 144

Current Affairs 31C-42C

Published monthly by The Electrochemical Society, Inc., from Manchester, N. H., **Executive Offices, Editorial Office and Circulation Dept.,** and **Advertising Office** at 1860 Broadway, New York 23, N. Y., combining the JOURNAL and TRANSACTIONS OF THE ELECTROCHEMICAL SOCIETY. Statements and opinions given in articles and papers in the JOURNAL OF THE ELECTROCHEMICAL SOCIETY are those of the contributors, and The Electrochemical Society assumes no responsibility for them. Nondeductible subscription to members $5.00; subscription to nonmembers $18.00. Single copies $1.25 to members, $1.75 to nonmembers.

Copyright 1960 by The Electrochemical Society, Inc.

Entered as second-class matter at the Post Office at Manchester, N. H., under the act of August 24, 1912.

The New SARGENT Model XV
RECORDING POLAROGRAPH®

offers you—

- **FULL 10 INCH CHART**
- **1/10% ACCURACY OF MEASUREMENT**
- **TEN STANDARDIZED POLARIZING RANGES**

This new Sargent Polarograph gives you a large 250 mm (10 inches) chart and the highest accuracy and current sensitivity at the lowest price of any pen writing polarographic instrument on the market.

It offers you optimum specifications based on over twenty years of leadership in design, manufacture and service in this specialized field of analysis.

The polarographic method is capable of reproducibility to 1/10% and analytical accuracy to ½%. To make use of this facility, the instrument must be accurate to 1/10% and chart space must be provided for recording large steps to achieve measuring precision. We strongly advise against the purchase of any polarographic instrument using miniature (5 inch) charts and low gain balancing systems in the 1% order of precision.

This Model XV is adaptable to 10^{-8} M determinations with the S-29315 Micro Range Extender.

®Registered Trade Mark, Patents Pending

Current Ranges:	19, from .003 to 1.0 μA/mm.
Current Sensitivity:	standard specifications, 10^{-4}μA/mm.
Polarizing Ranges, volts:	0 to −1; −1 to −2; −2 to −3; −3 to −4; +.5 to −5; 0 to −2; −2 to −4; +1 to −1; 0 to −3; +1.5 to −1.5.
Balancing Speed:	standard, 10 seconds; 1 second or 4 seconds optional.
Bridge Drive:	synchronous, continuous repeating, reversible; rotation time, 10 minutes.
Chart Scale:	current axis, 250 mm; voltage axis, 10 inches equals one bridge revolution.
Current Accuracy:	1/10%
Voltage Accuracy:	¼%
Chart Drive:	synchronous, 1 inch per minute standard; other speeds optional.
Writing Plate:	10½ x 12½ inches; angle of slope, 30°.
Standardization:	manual against internal cadmium sulfate standard cell for both current and voltage.
Damping:	RC, four stage.
Pen:	ball point; Leroy type optional.
Suppression:	zero displacement control, mercury cell powered, 6 times chart width, upscale or downscale.
Potentiometric Range:	2.5 millivolts, usable as general potentiometric recorder.
Finish:	case, enameled steel; panels, anodized aluminum; writing plate, polished stainless steel; knobs and dials, chromium plated and buffed.
Dimensions:	23 x 17 x 10.
Net Weight:	65 pounds.

Catalog number **S-29310** with accessories and supplies. . . . **$1585.00**

For complete information write for Sargent Bulletin P

SARGENT *SCIENTIFIC LABORATORY INSTRUMENTS • APPARATUS • SUPPLIES • CHEMICALS*

E. H. SARGENT & CO., 4647 W. FOSTER, CHICAGO 30, ILLINOIS
DETROIT 4, MICH. • DALLAS 35, TEXAS • BIRMINGHAM 4, ALA. • SPRINGFIELD, N.J.

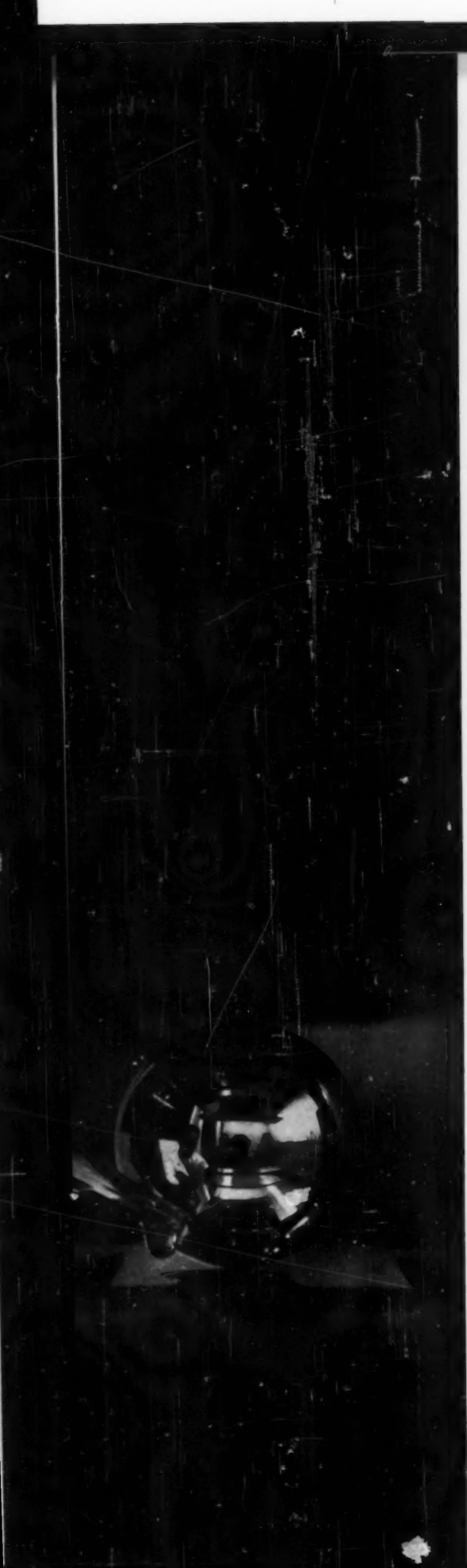

One of a series

On the riddle of rolling friction

It doesn't take much to roll a hard ball across a hard, smooth, level surface – actually only about 0.00001 times the normal force acting vertically on the ball. But by careful measurement of this tiny rolling force, scientists at the General Motors Research Laboratories are helping to unravel the riddle of rolling friction.

An important relationship recently uncovered in this fundamental study: the rolling force is proportional to the volume of material that is stressed above a certain level. As a result, a GM Research group have not only confirmed the hypothesis of *how* a rolling ball loses energy (Answer: elastic hysteresis) but also have learned *where* this lost energy is dissipated (Answer: in the interior of the material, not on the surface). Mathematical analyses have indicated the exact shape of the elastically stressed volume in which all the significant frictional loss takes place.

The purpose of friction research at the GM Research Laboratories is to learn more about the elastic and inelastic behavior of materials. This knowledge – of academic interest now – will eventually give GM engineers greater control of energy lost through friction. This is but one more example of how General Motors lives up to its promise of "More and better things for more people."

General Motors Research Laboratories
Warren, Michigan

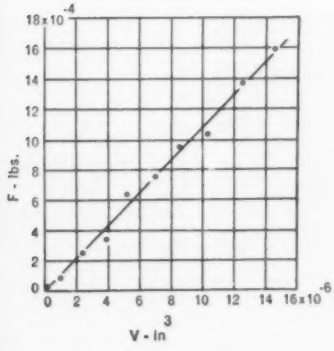

Relationship of rolling force to elastically stressed volume.

Editorial

Chemical Industry Runs the Show

THE 27th exhibition of Chemical Industries, held last November 30-December 4 in the New York Coliseum, was in its way as glamorous as any Midway Fair. This was the biggest of the Chem Shows, with more than 500 firms exhibiting materials listed in 259 categories ranging from *Abrasives* to *X-Ray Equipment*. Many thousands of visitors roamed the four floors of exhibits each day, some of them hurrying through the aisles to get a bird's-eye view, others pausing to examine, pick up literature and samples, and ask for demonstrations.

From year to year, the Exposition does not change in a large way but, over a period of several years, the progress of industry is impressive. A considerable amount of the equipment shown this year did not exist say in 1940, and much of the rest has been improved almost beyond recognition. For example, laboratory balances have been undergoing a revolution, and almost certainly most weighing of this type will some day be completely automatic. Wired television for remote inspection and control is relatively new and will have many applications in other than nuclear installations. Gas heaters for industrial use, and even laboratory burners, have seen vast improvement. Large-scale semiconductor rectifiers, tantalum-lined equipment for hot acids, automatic cathodic protection for ships, were not seen at the early Chem Shows.

A cursory trip through the exhibits was enough to convince one that the chemical industry spends a tremendous amount of effort in mixing some materials together, and an equal amount of effort in separating others from each other. Consequently, many machines were exhibited for pumping, conveying, grinding, crushing, pulverizing, disintegrating, screening, mixing, stirring, blending, homogenizing, colloidizing, emulsifying, milling, kneading, masticating, dissolving; and for distillation (including continuous operation molecular stills), fractionation, extraction, flotation, magnetic separation, centrifuging, filtering, absorbing, decolorizing, and clarifying. Vibratory conveyors, screeners, and classifiers are always popular exhibits. One firm regularly provides a vibrator on which the weary visitor may stand to rejuvenate his feet; or he can sit on the platform if he wishes.

Electrochemical industry was represented, but rather indirectly, no firms being listed under *Electrochemical* or under *Batteries*, for example. However, 13 companies were listed under *Anodes* (none under *Cathodes*) and 23 under *Electronic Equipment*.

An anomaly: 15 firms under *Tubes*, 47 under *Tubing*, 61 under *Pipe and Fittings*, only 1 under *Tube Expanders*. On the other hand, 18 companies handle *Flexible Joints*, so old-fashioned plumbing methods do have competition. Outstanding developments are being made in the field of plastic tubes and pipes; among other necessary equipment for modern living, we can look foward to complete plastic plumbing in buildings and under city streets. The plastics industry has gone a long way since it first exhibited an automatic molding machine which turned out souvenir golf tees—a most appropriate use for the plastics of those days.

—CVK

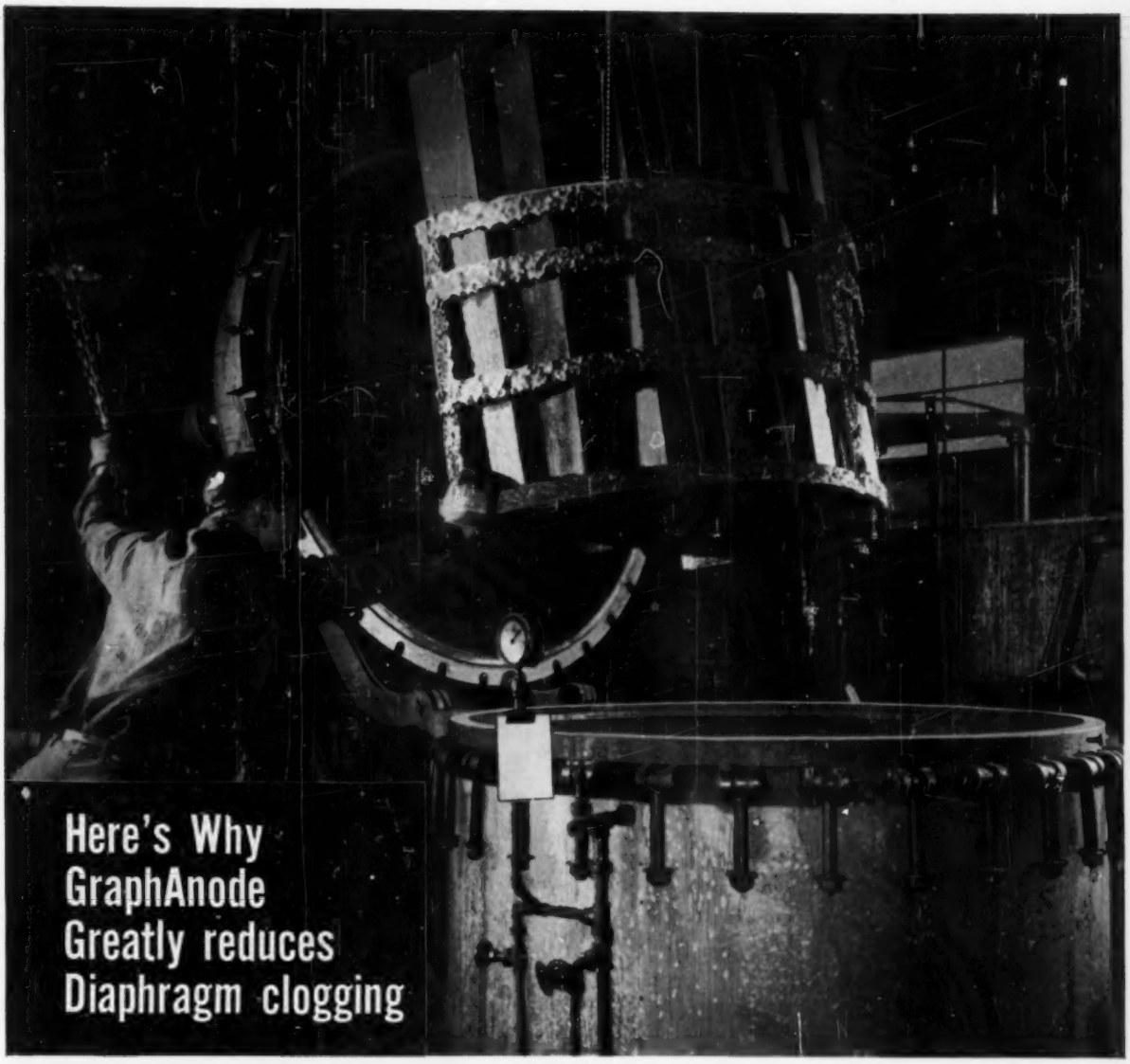

Here's Why GraphAnode Greatly reduces Diaphragm clogging

. . . and whack down cell maintenance costs accordingly

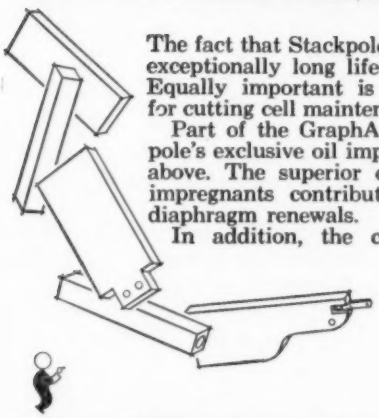

The fact that Stackpole GraphAnode anodes have exceptionally long life is only part of the story. Equally important is their enviable reputation for cutting cell maintenance costs.

Part of the GraphAnode "secret" is in Stackpole's exclusive oil impregnation process pictured above. The superior chemical resistance of the impregnants contributes substantially to fewer diaphragm renewals.

In addition, the carefully-machined GraphAnode anodes present outstandingly uniform, low-porosity surfaces to the electrolyte. The graphite is consumed slowly and evenly. It does not slough off to contaminate the cell.

Inevitably, the result is many more useful cell operating hours — and with the added advantage of low cell voltages. For a convincing demonstration on your own equipment, we suggest you get in touch with Stackpole now.

STACKPOLE CARBON CO., St. Marys, Pa.

CATHODIC PROTECTION ANODES • TUBE ANODES • BEARINGS • SEAL RINGS FLUXING & DE-GASSING TUBES • SALT BATH RECTIFICATION RODS • ELECTRODES & HEATING ELEMENTS • POROUS CARBON • WELDING CARBONS • ROCKET NOZZLES • VOLTAGE REGULATOR DISCS • MOLDS & DIES • "CERAMAGNET"® CERAMIC MAGNETS • ELECTRICAL CONTACTS • BRUSHES for all rotating electrical equipment • and many other carbon, graphite and electronic components

STACKPOLE
GraphAnode®
ELECTROCHEMICAL ANODES

FUTURE MEETINGS OF
The Electrochemical Society

Chicago, Ill., May 1, 2, 3, 4, and 5, 1960

Headquarters at the Lasalle Hotel
Sessions will be scheduled on
Electric Insulation (including a symposium on "Electrolytic Capacitors"), Electronics (including Luminescence, Semiconductors, and Thermionics), Electrothermics and Metallurgy (including symposia on Refractory Metals, "High-Purity Vanadium—Its Preparation, Properties, and Alloys," and on Rhenium, and a round table on "Methods of Reducing Iron Ores"), Industrial Electrolytics, and Theoretical Electrochemistry (general sessions, and a Symposium on "Electrochemical Engineering" co-sponsored by the Theoretical and Industrial Electrolytic Divisions)

★ ★ ★

Houston, Texas, October 9, 10, 11, 12, and 13, 1960

Headquarters at the Shamrock Hotel
Sessions probably will be scheduled on
Batteries, Corrosion, Electrodeposition, Electronics (Semiconductors), Electro and Electrothermics and Metallurgy

★ ★ ★

Indianapolis, Ind., April 30, May 1, 2, 3, and 4, 1961

Headquarters at the Claypool Hotel

★ ★ ★

Detroit, Mich., October 1, 2, 3, 4, and 5, 1961

Headquarters at the Statler Hotel

Papers are now being solicited for the meeting to be held in Houston, Texas, October 9-13, 1960. Triplicate copies of each abstract *(not exceeding 75 words in length)* are due at Society Headquarters, 1860 Broadway, New York 23, N. Y., *not later than June 1, 1960* in order to be included in the program. *Please indicate on abstract for which Division's symposium the paper is to be scheduled and underline the name of the author who will present the paper.* Complete manuscripts should be sent in triplicate to the Managing Editor of the JOURNAL at 1860 Broadway, New York 23, N. Y.

Papers submitted for presentation at the meeting become the property of The Electrochemical Society and may not be published elsewhere, in whole or in part, unless permission is requested and granted by the Society. Papers already published elsewhere, or submitted for publication elsewhere, are not acceptable for oral presentation except on invitation by a Divisional program Chairman.

The Reaction of Germanium with Aqueous Solutions

II. Dissolution Kinetics in Electrolytes and the Role of Specific Adsorption

Walter W. Harvey and Harry C. Gatos

Lincoln Laboratory, Massachusetts Institute of Technology, Lexington, Massachusetts

ABSTRACT

The dissolution of single-crystal germanium has been studied in electrolyte solutions containing dissolved oxygen. The following electrolytes were considered: KF, KCl, KBr, KI, $NaNO_3$, Na_2SO_4, CsCl, $BaCl_2$, and $LaCl_3$. In the range 10^{-4} to 1.0N, the dissolution rate typically goes through a maximum as the electrolyte concentration is increased. The concentration corresponding to maximum dissolution rate is different for the various electrolytes but, in general, is less than $10^{-2}N$. In the case of KF, two distinct maxima were observed; in $BaCl_2$ solutions the maximum is followed by a minimum. The activation energy for the reaction in O_2-saturated KCl solutions was found to be about 19 kcal/mole. At very low oxygen partial pressures, the activation energy was less than 5 kcal/mole, indicative of diffusion-controlled kinetics.

For single-crystal as well as for powdered germanium samples, the reaction rates were not altered measurably by changes in mobile-carrier concentration brought about by doping or illumination. The experimental results are related to germanium electrode behavior and can be interpreted on the basis of specific adsorption rather than solution conductance and oxygen solubility. The interaction of germanium surface atoms with aqueous solutions is discussed in terms of probable electronic configurations.

In a previous communication (1) it was reported that, in the absence of dissolved oxygen, germanium is inert to water and nonoxidizing electrolytes up to 100°C and over a broad range of pH. In oxygen-saturated water, the germanium dissolution rate at room temperature is approximately 1 $\mu g/cm^2/hr$, and the reaction is controlled by the activated reduction of oxygen. The dissolution mechanism was found to be the same for the various surface orientations, although the absolute dissolution rates decreased in the order $\{100\} > \{110\} > \{111\}$ [see also Ellis (2)].

An unusual feature of the surface chemistry of germanium is that its common oxide, hexagonal GeO_2, is moderately soluble in water and aqueous electrolytes [forming metagermanic acid (3)], whereas germanium itself is not attacked by nonoxidizing acids (including HF) and bases. As a result, it is possible to follow the reaction of properly prepared germanium surfaces with mild oxidizing agents in aqueous solutions without the complicating effects of surface oxides. Germanium surfaces prepared by conventional etching techniques, however, generally are covered with an oxide layer consisting at least in part of an insoluble modification (possibly tetragonal GeO_2). With the chemical polishing agent CP-4[1] difficultly soluble surface oxide is likely formed by continued reaction of the etchant on removal of the germanium from the etching bath [cf. Ellis (4)]. The formation of the difficultly soluble oxide is avoided by displacing the etchant[2] with a large volume of water or dilute HF. It is believed that in this way, oxide-free germanium surfaces are obtained, whose subsequent behavior is independent of their prior etching treatment.

The obvious advantages of studying the surface properties of a semiconductor without the complicating effects of a surface oxide, as well as the continued importance of surface reactions in the science and technology of semiconductor materials, motivated this study of the influence of electrolytes in the reaction of germanium with aqueous solution. Elucidation of the role of the adsorptive properties of various ions was considered of particular importance. Our earlier finding (1), that changes in the mobile carrier concentration in germanium are without effect on the kinetics of the reaction with water containing dissolved oxygen, in contrast to the results reported by Schwab (6), was confirmed using both single-crystal and powdered germanium samples. Furthermore, no mobile-carrier effect was found in the presence of added electrolyte.

Experimental

The experimental techniques employed were, in many respects, similar to those described earlier (1). The reagent grade salts employed were not further purified, since consistent results were obtained with such salts from different sources. The KHF_2 was purified by recrystallization. Certain improvements in the procedure for single-crystal samples, as well as the technique employed with powdered samples, will be described briefly.

Powdered samples.—These experiments were performed using a conventional Warburg apparatus.

[1] CP-4 consists of conc. HNO_3 (5 parts by volume), glacial CH_3COOH (3 parts), 48% HF (3 parts), and Br_2 (0.06 part).

[2] A similar technique has been employed for cleaning silicon surfaces (5).

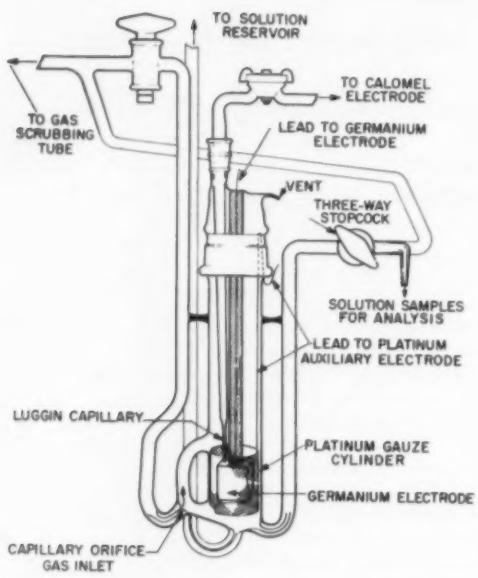

Fig. 1. Cell for dissolution and electrochemical measurements.

The method is similar to that employed by Schwab, *et al.* (6). Consumption of oxygen gas during the reaction was measured by means of a differential micromanometer to within 1 microliter. Our illuminating source consisted of two fluorescent lamps, providing an incident intensity of about 6500 meter-candles, or a photoflood lamp providing approximately 20,000 meter-candles. Radiation from the latter source was filtered through 1 in. of water.

The powdered samples were prepared by crushing germanium crystals of known type under water in an agate mortar. The particle size varied up to several hundred microns; extremely fine particles were removed by washing. For certain runs, powders of nearly uniform particle size were obtained by sieving. In a number of cases, on completion of the run, the solution was analyzed for total dissolved germanium for the purpose of comparison with the total amount of oxygen consumed.

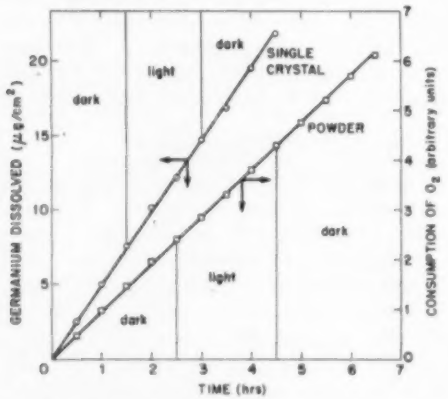

Fig. 2. Typical results of photo experiments with single-crystal and powdered germanium samples in oxygen-saturated solutions at 30°C and pH 6. ○ = 10^{-4}N Na_2SO_4; □ = 10^{-4}N KCl.

Single-crystal samples.—The single crystals employed were rectangular parallelepipeds measuring initially 1.5 x 1.5 x 2.5 cm, all faces having {100} orientation. This geometry was chosen for convenience. An electrical lead was soldered to the crystal, which was mounted as shown in Fig. 1. A thin layer of Apiezon W wax held the sample against the flat end of a heavy-walled capillary tube, through which the electrical lead passed. The saturating gas was introduced through a side tube so as to provide vigorous circulation of the solution past the specimen without permitting direct contact between gas bubbles and germanium. The partial pressure and, hence, the concentration of dissolved oxygen was varied by means of metered admixtures of nitrogen. A platinum auxiliary electrode made possible electrolytic pretreatment of the germanium whenever this procedure was required for the establishment of a stable rest potential. During pretreatment and subsequent equilibration, the solution in the cell was replaced continuously with presaturated solution from the reservoir.

Dissolution rates were obtained by withdrawing portions of solution periodically and analyzing for germanium. At least four samples were taken for each rate reported. For investigating photoeffects, sequences of three stages of alternating darkness and strong light were used in order to distinguish illumination effects from occasional small variations of rate due to other causes. Under the conditions of the experiment, illumination resulted in a considerable enhancement of the minority carrier densities.

Results

Role of mobile carriers.—In agreement with our earlier findings with single-crystal samples, no change in dissolution rate resulted from illumination of either n- or p-type germanium powder. This was the case not only in water, but also in 0.1*N* and 10^{-4}*N* KCl. Similarly, light was without effect on the reaction of n- and p-type germanium single crystals in electrolytes generally. In the latter experiments, total bulk carrier densities ranged from 5×10^{13} (intrinsic) to about 10^{18} carrier/cm³. Typical results are shown in Fig. 2.

It is also significant that the average activation energy for the dissolution of powdered samples was found to be 20 kcal/g-atom, in agreement with the value previously reported for single-crystal samples (1). Furthermore, absolute dissolution rates for the sieved powders were the same as for single crystals, within the uncertainty of estimating actual surface areas. The ratio of moles of O_2 consumed to gram-atoms of germanium dissolved had an average value of 0.85 in 13 runs. However, in view of the experimental uncertainties in the quantitative determination of oxygen consumption, no significance is attached to the deviation of the average value from unity.

Influence of solution variables.—In a given electrolyte solution, as in pure water, the germanium dissolution rate remained constant with time for periods exceeding those employed in this study. With increasing electrolyte concentration, the dissolution rate goes through a maximum, as shown

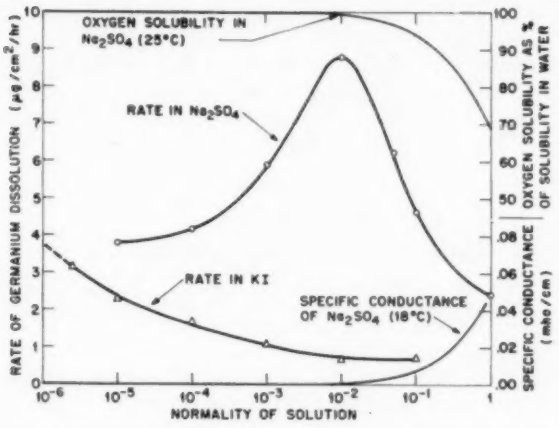
OXYGEN SOLUBILITY IN Na_2SO_4 (25°C)
RATE IN Na_2SO_4
RATE IN KI
SPECIFIC CONDUCTANCE OF Na_2SO_4 (18°C)
RATE OF GERMANIUM DISSOLUTION (μg/cm²/hr)
OXYGEN SOLUBILITY AS % OF SOLUBILITY IN WATER
SPECIFIC CONDUCTANCE (mho/cm)
NORMALITY OF SOLUTION

Fig. 3. Germanium dissolution rate, oxygen solubility, and specific conductance in Na_2SO_4 solutions. Oxygen solubility data from ref. (11). Conductance data from ICT 6:231, 236, 240. The maximum rates in KI and Na_2SO_4 solutions occur at the lowest and highest concentrations, respectively, of the electrolytes studied.

in Fig. 3 for Na_2SO_4 solutions. In addition to the dependence on electrolyte concentration, the effects of pH, oxygen partial pressure, and temperature were studied systematically with the following results.

It was found that the dissolution rate of germanium is not affected by pH changes below approximately pH 6. Above this value, the dissolution rate increases with increasing pH, as shown in Fig. 4(b) for O_2-saturated 0.1*N* KCl. The average of 12 determinations in the pH range 3 to 6.5 was 1.09 ± 0.11 μg/cm²/hr. (This value also indicates the degree of reproducibility of the data generally.) There is evidence that in certain more concentrated solutions, e.g., 1*N* CsCl, the rate in alkaline solutions is even more strongly dependent on pH, but this behavior was not studied in detail. Since working at low pH values would preclude consideration of very dilute salt solutions, all studies were carried out at pH 6.0 ± 0.1, unless otherwise specified.

The dependence of the dissolution rate on the concentration of dissolved oxygen is shown in Fig. 5 for 0.1*N* and 10^{-4}*N* KCl. Although rates are higher

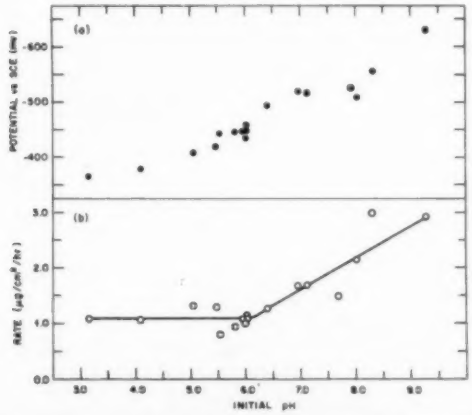

Fig. 4. Variation of (a) mixed potential and (b) dissolution rate with pH in 10^{-1}N KCl at 30°C.

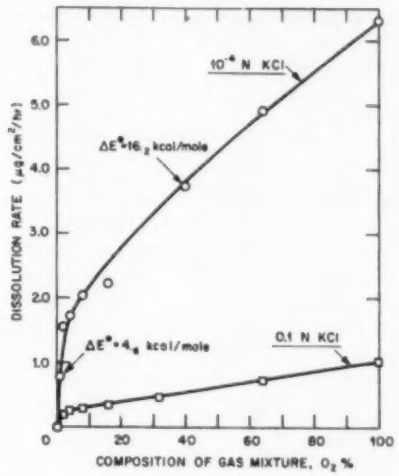

Fig. 5. Effect of oxygen partial pressure on the dissolution rate in 10^{-1}N and 10^{-4}N KCl at 30°C and pH 6.

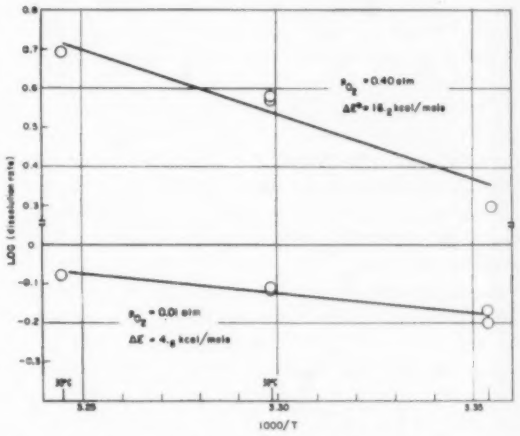

Fig. 6. Temperature dependence of the dissolution rate in 10^{-4}N KCl at two concentrations of dissolved oxygen.

in the latter, the general features of the oxygen dependence are the same in the two solutions, namely, an approximately linear decrease of rate with decreasing oxygen partial pressure, down to about 0.04 atm, and a more rapid decrease (to zero) below this value.

The temperature dependence of the reaction rate in 10^{-4}*N* KCl is shown in Fig. 6 for two values of P_{O_2}. The activation energy at 0.4 atm was 16 kcal/mole, in contrast to the value of less than 5 kcal/mole at 0.01 atm. These results indicate that diffusion is rate limiting only at low concentrations of dissolved oxygen.

Nature of the electrolyte.—The nature of the anion has a marked influence on the dissolution kinetics, as illustrated in Fig. 7 for the potassium halides. In view of the fact that in pure water the dissolution rate is 0.7 μg/cm²/hr at the same temperature, the maximum for KI evidently occurs at concentrations below 10^{-6}*N*.[8] Considering for the present only the second of the two maxima in KF

[8]Actually, the maximum occurs below 10^{-7}M I⁻, as found by extending the concentration range to this value using H_2SO_4, rather than HI, for adjusting the pH to 6. The dissolution rate at 10^{-7}M I⁻ was 5.4 μg/cm²/hr.

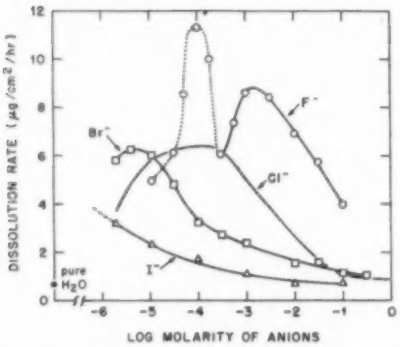

Fig. 7. Specific effects of halogen ions on the dissolution rate-oxygen-saturated solutions of potassium salts at 30°C and pH 6. The anion molarities have been corrected for additions of the corresponding acids in pH adjustments. The experimental points for KCl, omitted for clarity, are included in Fig. 8.

(full line in Fig. 7), a systematic shift of the maximum rate toward higher concentrations occurs in going from KI to KF.

The influence of the nature of the cations present was studied in a series of chlorides (Fig. 8). With the exception of $BaCl_2$, the maximum rates occur at nearly the same Cl^- ion concentration. There is, however, a significant variation in the absolute value of the maximum rate. It is also of interest to note that for $BaCl_2$, the dissolution rate does not decrease indefinitely with concentration after the initial maximum.

Electrode potential measurements.—The electrode behavior of germanium in aqueous solutions presents

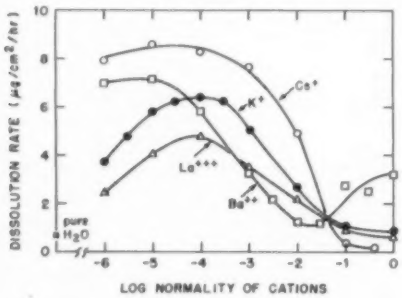

Fig. 8. Specific effects of cations on the dissolution rate-oxygen-saturated chloride solutions at 30°C and pH 6.

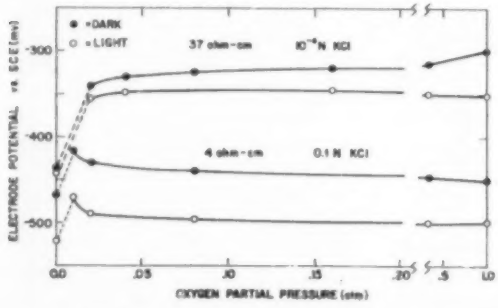

Fig. 9. Variation of the steady-state electrode potential with concentration of dissolved oxygen for n-type germanium electrodes and the effect of illumination.

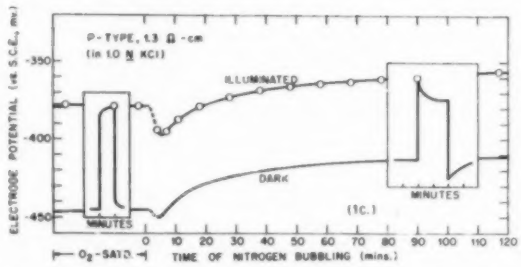

Fig. 10. Transient behavior of the photopotential of a p-type germanium electrode in moderately concentrated electrolyte.

certain aspects peculiar to semiconductors. Effects of oxygen and electrolytes on certain electrical properties of the surface have been described elsewhere (7). Some observations pertinent to the electrochemistry of the dissolution reaction are presented here. In dilute electrolytes, the steady-state mixed potential becomes more cathodic with increasing partial pressure of oxygen, as shown in Fig. 9 for an n-type electrode in $10^{-4}N$ KCl. The photopotentials obtained in the same solutions under steady illumination also are shown in Fig. 9. In more concentrated electrolytes, however, the steady-state potential becomes somewhat more anodic with increasing oxygen partial pressure, following a cathodic shift at very low oxygen partial pressures (illustrated in Fig. 9 for an n-type electrode in $0.1N$ KCl).

From Fig. 10 it will be noted that the combination of p-type electrode and moderately concentrated electrolyte results in a mixed potential which becomes more cathodic with light (i.e., the surface region is more n-type than the bulk). In the example shown, the potential under steady light in nearly oxygen-free solution undergoes a relaxation with a time constant of the order of tens of seconds. Comparably slow changes of the photopotential under no external polarization were not observed in dilute electrolytes for germanium of either type.

The mixed potentials recorded during steady-state dissolution in $10^{-4}N$ KCl at various pH's are plotted in Fig. 4(a) above the corresponding dissolution rates. The dependence of mixed potential on pH was studied more quantitatively in O_2-satu-

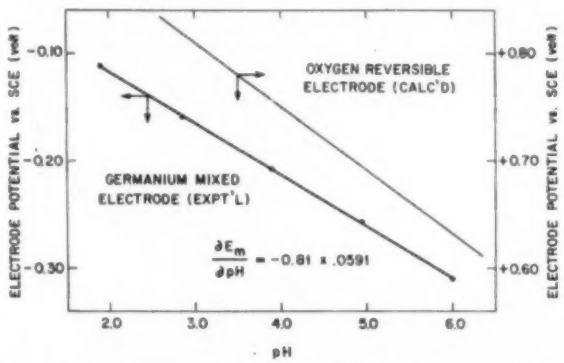

Fig. 11. Dependence of the germanium mixed potential on pH in oxygen-saturated 1.0N Na_2SO_4 + 0.001M GeO_2 + H_2SO_4.

rated 1.0*N* Na_2SO_4 solutions (sulfate-bisulfate buffers). Here the potential varied linearly with pH (Fig. 11) with a slope equal to −0.0478 v/pH unit at room temperature. It will be noted that the mixed potential is far removed from the oxygen reversible potential in these solutions.

Discussion

Comparison with Metal Behavior

The dependence of the germanium dissolution rate on the concentration of inert electrolyte resembles the behavior of metals in similar environments. In the case of metals, however, the maximum in dissolution rate occurs in the vicinity of 0.5*N* (8) and is attributed by Akimov (9) to the combined effects of solution conductivity and oxygen solubility. Thus, the increase in rate with increasing electrolyte concentration is ascribed to the increase in solution conductivity, leading in turn to an increase in the corrosion current. The subsequent decrease in rate in concentrated solutions is attributed to a decrease in oxygen solubility with electrolyte concentration. Evans (10) treats the subject in a more quantitative way but on a similar basis.

In the case of the germanium dissolution reaction, the maxima in rate occur at electrolyte concentrations below $10^{-2}N$. In this range, the solubility of oxygen is the same to within less than 1% as that in pure water (11), so that the decrease in rate with increasing concentration of electrolyte cannot be ascribed solely to diminishing oxygen solubility, although this is a contributory factor at concentrations greater than approximately 0.1*N* It is also unlikely that solution conductance alone is responsible for the initial increase of rate with concentration, since, at very low concentrations of electrolyte, marked differences in dissolution rate are observed in solutions of comparable conductivity.[4] Furthermore, for a given electrolyte, a maximum in rate is reached while the solution conductance continues to increase and the oxygen solubility remains essentially unchanged. This is shown in Fig. 3 for Na_2SO_4 and KI solutions, which represent the extremes of behavior observed in our experiments.

Clearly, the interpretation proposed for the dependence of the corrosion rates of metals on the concentration of electrolyte (9, 10) cannot account for the present findings. In fact, it appears that, even in the case of metals, it is inconsistent with some experimental results. For example, Schaschl and Marsh (12) have found recently that in inert electrolyte solutions at concentrations as low as $10^{-2}N$, the dissolution of iron is controlled by the amount of dissolved oxygen and is independent of conductivity and pH.

Specific Adsorption of Anions

In view of the dependence of the dissolution rate on the nature of the anion (Fig. 7) and the fact that the electrolytes considered are chemically inert toward germanium and oxygen, we believe that anions influence the kinetics of the dissolution process through specific adsorption. Specifically adsorbed anions are considered to be bonded covalently to the metal surface (13). The present results suggest that specific adsorption of anions onto germanium may be represented as follows

$$Ge\cdot + X^- \rightarrow Ge\text{-}X + e^- \qquad [1]$$

where Ge· is a surface atom having an unpaired electron (dangling bond) resulting from termination of the covalent lattice. The transfer of the anionic charge according to Eq. [1] presumably facilitates the reduction of oxygen at an adjacent site. Adsorbed anions regain their charge on detachment of underlying germanium atoms and in essence function as catalysts for the reduction of oxygen. With increasing concentration of adsorbable anions, however, competition for active surface sites between anions and oxygen molecules results eventually in a decrease in the number of sites available for the adsorption and reduction of oxygen and, hence, in a decrease in the dissolution rate. The more strongly adsorbed the anion, the more dilute the solution in which the maximum dissolution occurs. Based on this argument, the data of Fig. 3 and 7 indicate that the anions studied adsorb onto germanium in the order

$$I^- > Br^- > Cl^- > F^- > SO_4^=$$

(in the case of F^- ions the maximum occurring at $10^{-3}N$ is considered as the pertinent one in this regard, as will be discussed below). The same order of specific adsorbability of the halides has been found for mercury (14) and platinum (15). The tendency of sulfate ions to adsorb less than the halogen ions is consistent with data on other solid surfaces (16). In nitrate solutions, the position of the maximum dissolution rate was poorly defined. The unsatisfactory reproducibility of the measured rates may have been due to the presence of adsorbable impurities, especially NO_2^- ion. Nevertheless, the data indicate that the adsorbability of NO_3^- ion on germanium is close to that of Cl^- ion.

Fluoride Solutions

While it is generally considered that F^- ions are not specifically adsorbed on mercury (17), it is possible that they adsorb on germanium, especially since not only the tetrafluoride but also stable fluogermanates (18) are known. The possibility exists that one of the two maxima in KF solutions is associated with a change in the anodic mechanism, e.g., oxidation of germanium to H_2GeF_6 rather than H_2GeO_3. However, this is unlikely in view of the fact that measured solubilities of high-purity GeO_2 in 0.1*N* solutions of KI, KBr, KCl, KF, as well as in $10^{-4}N$ KF, all at pH 6, were the same as that measured in pure water. The absence of complexing action by the principal anions considered is thus indicated.

It is likely that the "anomalous" maximum occurring at $10^{-4}N$ in KF solutions is associated with specific adsorption of HF molecules rather than HF_2^- for the following reasons: (*a*) the residual bonding power of the HF molecule is indicated by the formation of H_2F_2 in the vapor and pure liquid and by the formation of HF_2^- in F^- solutions, and

[4] The conductivity of germanium is orders of magnitude greater than that of very dilute electrolyte solutions. At room temperature the conductivity of intrinsic germanium is 0.02 mho/cm.

(*b*) in the solution considered, the concentration of HF is about $10^{-7}N$ while that of HF_2^- is about $10^{-10}N$ (Table I). The subsequent increase of dissolution rate at higher KF concentrations probably results from displacement of adsorbed HF. At still higher concentrations, adsorption of F^- ions results in the eventual decline of the dissolution rate (Fig. 7).

The displacement of adsorbed HF is considered to result from association with F^- to form HF_2^-

$$HF_{(adsorbed)} + F^- \rightarrow HF_2^- \qquad [2]$$

The postulated interface reaction corresponds to the association of HF and F^- in the solution phase. Adsorption and displacement of HF may be considered as the net result of competition between F^- ions in the double layer and surface atoms having an unshared electron pair (—Ge:$^-$ or $\rangle$Ge: —see below.)

The foregoing interpretation was tested with solutions of KHF_2. In the range 10^{-5} -10^{-3}M F^-, the concentrations of HF and HF_2^- are greater in the KHF_2 solutions than in the corresponding KF solutions and, moreover, increase much more rapidly with increasing $[F^-]$ (Table I). Accordingly, it was found that the anomalous maximum shifted from $[F^-] = 10^{-4}$M in KF to $F^- < 10^{-5}$M in KHF_2. The "normal" maximum also was observed in KHF_2 solutions, but could not be mapped accurately owing to chemical attack of the glassware.

Specific Effects of Cations

Figure 8 shows that the nature of the cation modifies the influence of the anion on the kinetics of the germanium dissolution reaction. No differences were observed between Na^+ and K^+ ions. The case for specific adsorption of inorganic cations is not nearly as well established as that for anions. Owing to the greater polarizability of anions, however, it is likely that their electrical centers are displaced closer to the electrode surface than those of cations. Thus, the larger the charge and the closer the approach of the cation, the greater is its effect in opposing the transfer of anionic charge and, hence, the smaller is the rate of oxygen reduction for equal concentrations of the same anion. For the cations considered, the charge-to-radius ratios are in the order $La^{+++} > Ba^{++} > K^+ > Cs^+$. The data for Cs^+, K^+, and La^{+++} are consistent with this interpretation over a very wide range of concentration (Fig. 8).

Of the cations considered, Cs^+ ions are most likely to undergo specific adsorption (19) and in the present case this seems to occur at concentrations greater than about 0.05*N*. The sharply reduced dissolution rates may be accounted for by specific adsorption of Cs^+ ions leading to increased polarization of the cathodic step, i.e., increase in the potential barrier for electron transfer to oxygen (or hole transfer to germanium).

The minimum in the dissolution rate at about $10^{-2}N$ $BaCl_2$ suggests a change in sign of the electrical double layer such as encountered in the coagulation of collodial particles by electrolytes. Since there is nothing unusual in the chemistry of Ba^{++} ion, its unique behavior suggests specific interaction with the germanium surface. A further study of this phenomenon could prove of special interest.

In view of the predominant role of adsorption in the kinetics of the germanium dissolution process, it is clear that solution conductance can have no more than a minor effect. Rather, it is suggested that in the case of metals, the dissolution rates in inert electrolytes containing dissolved oxygen are not entirely controlled by solution conductance and oxygen solubility, but are also influenced by specific adsorption. Recently, in fact, a correlation has been made between adsorption of anions and the pitting corrosion behavior of stainless steels(20).

Chemical Model of Interactions at Germanium Surfaces

Surface atoms[5] triply bonded to the lattice (—Ge· or, simply, Ge·) are considered to have each of their four valence electrons in sp^3 hybrid orbitals, three of which are involved in bond formation and the fourth constituting a "dangling bond." Doubly bonded surface atoms ($\rangle$Ge: or, simply, Ge:) are usually described as possessing two dangling bonds; however, it is probably more accurate to consider their electrons as being in sp^2 hybrid orbitals, with two electrons forming a lone electron pair [cf. Handler (21)].

[5] Taking into account irregularities of atomic dimensions, any real germanium surface must consist of atoms doubly and triply bonded to the lattice; atoms attached to the crystal by a single bond are probably capable of only transitory existence at a surface in contact with an aqueous solution.

Table I. Composition of fluoride and bifluoride solutions*

KF (pH adj. to 6.0)				KHF_2			
M_{KF}	[HF]	$[HF_2^-]$	$[F^-]$	M_{KHF_2}	[HF]	$[HF_2^-]$	pH
1.0×10^{-6}	3.0×10^{-9}	2.3×10^{-14}	2×10^{-6}	1.0×10^{-6}	3.0×10^{-9}	2.3×10^{-14}	6.0
9.0×10^{-6}	1.5×10^{-8}	5.8×10^{-13}	1×10^{-5}	6.0×10^{-6}	7.4×10^{-9}	2.9×10^{-12}	5.3
9.9×10^{-6}	1.5×10^{-7}	5.8×10^{-11}	1×10^{-4}	5.3×10^{-5}	6.9×10^{-8}	2.7×10^{-9}	4.3
1.0×10^{-3}	1.5×10^{-6}	5.8×10^{-9}	1×10^{-3}	7.1×10^{-4}	4.3×10^{-4}	1.6×10^{-6}	3.5
1.0×10^{-2}	1.5×10^{-5}	5.8×10^{-7}	1×10^{-2}	9.7×10^{-3}	8.8×10^{-6}	3.4×10^{-4}	3.2
0.10	1.5×10^{-4}	5.8×10^{-5}	0.1	0.137	9.9×10^{-5}	3.8×10^{-3}	3.2
1.0	1.5×10^{-3}	5.8×10^{-3}	1	4.85	1.00	3.86	3.2

Note: All concentrations are expressed as gram-formula weights per liter of solution.
* Calculations are based on the equilibrium data of Broene and DeVries, *J. Am. Chem. Soc.*, **69**, 1644 (1947).

Processes such as trapping, generation, and recombination of carriers can be visualized more readily in terms of triply bonded surface atoms and will be described accordingly. Conduction electrons and/or holes may be captured by surface atoms having unpaired electrons; an atom capturing both an electron and a hole functions as a recombination center:

$$\begin{array}{ccccc} \diagdown & & \diagdown & & \diagdown \\ -\mathrm{Ge}^{\cdot} & e^{-} & -\mathrm{Ge}^{\cdot} & e^{-} & -\mathrm{Ge}^{:-} \\ \diagup & \rightleftharpoons & \diagup & \rightleftharpoons & \diagup \\ & e^{-} & & e^{+} & \end{array} \qquad [3]$$

electron trap — recombination center — hole trap

Charged surface atoms may trap electrons or holes, as in Eq. [3], and so constitute localized surface states. Surface states on clean germanium generally are considered to be "fast," whereas "slow" states are believed to lie either in the oxide layer or at the oxide-gas interface (22). Long-time changes in the photopotential (Fig. 10) in moderately concentrated electrolytes[6] indicate that slow states may also result from adsorptive interaction of ions with an oxide-free surface.

In water or very dilute electrolyte solutions, oxygen makes the germanium electrode potential more cathodic and the surface more p-type (Fig. 9); this behavior is consistent with the nature of the oxygen molecule as an electron acceptor. The tendency of dissolved oxygen to drive the surface p-type is opposed by anions of the electrolyte (ref. 7 and Fig. 9 and 10), suggesting that nonoxidizing anions behave as electron donors during the dissolution reaction. This result further supports the view that adsorbed anions are covalently bonded to the lattice; adsorption of anions without transfer of charge would lead to changes in electrode potential and surface conductivity opposite to those observed.

Mechanism of the Dissolution Reaction

The insensitivity of the rates to changes in carrier concentration as brought about by illumination and doping indicates that holes and electrons are in adequate supply for the reaction of germanium with dissolved oxygen in aqueous solutions. Actually, the highest rates observed correspond to a corrosion current density of only about 15 μamp/cm^2, which is well below the region of measured limiting carrier currents (23). Moreover, the existence of an electron-limiting current recently has been disputed (24, 25).

Evidently, the rate-limiting step of the over-all dissolution reaction lies in the activated transfer, rather than supply, of electrons to oxygen. Although formal mechanisms can be written for the reduction of O_2 at Ge$^{\cdot}$ and Ge: sites, the decrease in surface recombination velocity on adsorption of O_2 from aqueous solution (7) indicates that the former sites are involved in the first stage of the reduction.

The following mechanism[7] is compatible with the results of the previous discussion, including the pH dependence of the dissolution rate and mixed potential:

$$\text{acid solution} \begin{cases} O_2 + H^{\cdot} + e^{-} \rightarrow -O_2H & \text{(cathodic)} \quad [4] \\ \mathrm{Ge}^{\cdot} + H_2O \rightarrow \mathrm{Ge\text{-}OH} + H^{\cdot} + e^{-} & \text{(anodic)} \quad [5] \end{cases}$$

$$\text{alkaline solution} \begin{cases} O_2 + H_2O + e^{-} \rightarrow -O_2H + OH^{-} & \text{(cathodic)} \quad [6] \\ \mathrm{Ge}^{\cdot} + OH^{-} \rightarrow \mathrm{Ge\text{-}OH} + e^{-} & \text{(anodic)} \quad [7] \end{cases}$$

where $-O_2H$ represents the surface intermediate $\begin{array}{c} H\text{—}O \\ | \\ -\mathrm{Ge}\text{—}O \end{array}$. Subsequent steps in the mechanism can lead to the formation of metagermanic acid, $OGe(OH)_2$ [or $HGeO_3^-$ in alkaline solution (3)]. In this mechanism, the intermediate formation of GeO or GeO_2 is not essential [cf. Rösner (26)].

Provided the equilibrium between holes and electrons in the germanium is not disturbed, as by carrier injection or illumination, the measured potentials are the same for n-type and p-type electrodes. Hence, the quantity $\partial E_m/\partial pH$ (Fig. 11) measures the same variation of potential as for a metal electrode, irrespective of possible changes of the space charge potential drop inside the germanium. Generalizing the treatment given by Ammar and Riad (20) for the dependence upon pH of the mixed potential of a metal corroding by reaction with dissolved oxygen, we obtain for the case of activation controlled kinetics:

$$\partial E_m/\partial pH = -\frac{(\nu_c - \nu_a)}{n_c\beta_c + n_a\beta_a} \times \frac{RT \ln 10}{F} \qquad [8]$$

where ν's are the chemical coefficients of H$^{\cdot}$ (negative for OH$^-$) in the rate-determining anodic and cathodic steps; n's, the numbers of electrons transferred; β's, the corresponding symmetry factors; and $RT \ln 10/F = 0.0591$ at room temperature. Assuming symmetrical energy barriers ($\beta_c = \beta_a = 0.5$), the mechanism represented by Eq. [4] and [5] or by [6] and [7] gives $\partial\epsilon_m/\partial pH = -0.0591$ v/pH unit. The experimental slope (Fig. 11) is -0.81×0.0591. The experimental value of $\partial E_m/\partial pH$ can be reconciled with the mechanism proposed and Eq. [8] if the reasonable assumption is made that the energy barrier for germanium dissolution is lower than that for the reverse process.

From a study of the anodic dissolution of germanium, Turner (27) concluded that the rate-determining step involves the capture of two holes. This has been considered improbable by Beck and Gerischer (28), who propose that one hole and one OH$^-$ are required in the limiting step during anodic dissolution. These mechanisms are not discussed further here, since the anodic partial process of the reaction with O_2 and H_2O is not necessarily identical with the mechanism of electrolytic anodic dissolution. Moreover, we have made no attempt to distinguish on the basis of purely chemical evidence between the roles of conduction and valence electrons in the dissolution mechanism.

[6] Depending on the type and resistivity of the electrode and the composition of the solution, transient behavior can be more complicated than for the system shown in Fig. 10.

[7] The symbol e^- in the equations is used for valence as well as conduction electrons. It is recognized that holes can be consumed by the anodic reaction and that holes may be injected by the cathodic reaction, but these features are not essential to the present discussion.

The increase of dissolution rate with increasing pH (Fig. 4) is ascribed to depolarization of the cathodic reaction in alkaline solutions as a result of specific adsorption of OH^- ions on sites adjacent to those of adsorbed oxygen:

$$\begin{matrix} Ge\cdot + O_2 & & Ge-O_2H \\ & + H_2O \rightarrow & \\ Ge\cdot + OH^- & & Ge-OH \end{matrix} \quad + OH^- \qquad [9]$$

This is similar to the scheme proposed earlier in this discussion for the accelerating effect of anions. However, since both $-O_2H$ and $-OH$ are consumed in the formation of H_2GeO_3, it is readily understandable that the germanium dissolution rate increases continuously with increasing OH^- concentration in contrast to the behavior with other anions. Actually, experiments showed that differences in rate for the various electrolytes virtually are eliminated in strongly alkaline solutions.

The only previously published work on the reaction of germanium with oxygen in aqueous solutions is that reported by Schwab (6), who proposed that the reaction takes place according to

$$Ge \rightarrow Ge^+ + e^- \text{ and } O_2 + e^- \rightarrow O_2^- \qquad [10]$$

This mechanism does not account for the dependence of mixed potential on pH, and in other respects is incompatible with the results of our experiments.

The barrier-layer theory of chemisorption (29), applied with considerable success to reactions at the semiconductor-gas interface, leads in charge-transfer adsorption to a coverage whose magnitude is determined by the carrier density in the semiconductor bulk. For the reacting system germanium-aqueous solution, on the other hand, our results indicate that the steady-state surface configuration in a given environment is the same for n- and p-type germanium [cf. Bohnenkamp and Engell (30)], at least under mildly oxidizing conditions. In fact, for the reactions studied, the arrangement and predominantly covalent character of the bonds in the germanium crystal are of considerably greater significance than its semiconductor properties.

Acknowledgment

The authors are indebted to A. A. Menna, W. J. LaFleur, and M. J. Button for technical assistance, to A. P. P. Malinauskas for conducting the experiments with the powdered samples, and to S. Sheff for confirming some of the authors' results and performing the experiments in KHF_2 solutions.

Manuscript received June 22, 1959. The work reported in this paper was performed by Lincoln Laboratory, a center for research operated by Massachusetts Institute of Technology with the joint support of the U.S. Army, Navy, and Air Force. This paper was prepared for delivery before the Ottawa Meeting, Sept. 28-Oct. 2, 1958.

Any discussion of this paper will appear in a Discussion Section to be published in the December 1960 JOURNAL.

REFERENCES

1. W. W. Harvey and H. C. Gatos, *This Journal*, **105**, 654 (1958).
2. R. C. Ellis, Jr., *J. Appl. Phys.*, **25**, 1497 (1954).
3. Mme. Lourijsen-Teyssèdre, *Bull. soc. chim. France*, **1955**, 1118.
4. S. G. Ellis, *J. Appl. Phys.*, **28**, 1262 (1957).
5. H. E. Farnsworth, R. E. Schlier, T. H. George, and R. M. Burger, *ibid.*, **29**, 1150 (1958).
6. G.-M. Schwab, "Semiconductor Surface Physics," p. 294, R. H. Kingston, Ed., University of Pennsylvania Press, Philadelphia (1957); "Advances in Catalysis," Vol. IX, p. 234, A. Farkas, Ed., Academic Press, New York (1957).
7. W. W. Harvey and H. C. Gatos, *J. Appl. Phys.*, **29**, 1267 (1958).
8. C. W. Borgmann, *Ind. Eng. Chem.*, **29**, 814 (1937).
9. G. V. Akimov, "Théorie et Méthodes d'Essai de la Corrosion des Métaux," p. 218, Dunod, Paris (1957).
10. U. R. Evans, "Metallic Corrosion, Passivity and Protection," 2nd ed., p. 347, Edward Arnold and Co., London (1946).
11. C. G. MacArthur, *J. Phys. Chem.*, **20**, 495 (1916).
12. E. Schaschl and G. A. Marsh, *Corrosion*, **13**, 243t (1957).
13. B. Breyer, *Rev. Pure and Appl. Chem.*, **6**, 249 (1956).
14. D. C. Grahame, *Chem. Rev.*, **41**, 441 (1947); D. C. Grahame, M. A. Poth, and J. I. Cummings, *J. Am. Chem. Soc.*, **74**, 4422 (1952).
15. P. V. Popat and N. Hackerman, *J. Phys. Chem.*, **62**, 1198 (1958).
16. N. A. Balaschova, *Z. physik. Chem. (Leipzig)*, **207**, 340 (1957).
17. D. C. Grahame and B. A. Soderberg, *J. Chem. Phys.*, **22**, 449 (1954).
18. O. H. Johnson, *Chem. Rev.*, **51**, 431 (1952).
19. B. B. Damaskin, N. V. Nikolaeva-Fedorovich, and A. N. Frumkin, *Doklady Akad. Nauk*, **121**, 129 (1958).
20. M. A. Streicher, *This Journal*, **103**, 375 (1956).
21. P. Handler, "Semiconductor Surface Physics," p. 23, R. H. Kingston, Editor, Univeristy of Pennsylvania Press, Philadelphia (1957).
22. R. H. Kingston, *J. Appl. Phys.*, **27**, 101 (1956).
23. W. H. Brattain and C. G. B. Garrett, *Bell System Tech. J.*, **34**, 129 (1955).
24. H. Gerischer and F. Beck, *Z. physik. Chem.*, **13**, 389 (1957).
25. E. A. Efimov and I. G. Erusalimchik, *Zhur. Fiz. Khim.*, **32**, 1967 (1958).
26. O. Rösner, *Z. Metallk.*, **46**, 225 (1955); *ibid*, **48**, 137 (1957).
27 D. R. Turner, *This Journal*, **103**, 252 (1956).
28. F. Beck and H. Gerischer, *Z. Elektrochem.*, **63**, 500 (1959).
29. A number of references to the original literature are tabulated by F. S. Stone, "Chemisorption," p. 188, W. W. Garner, Editor, Academic Press, New York (1957).
30. K. Bohnenkamp and H. J. Engell, *Z. Elektrochem.*, **61**, 1184 (1957).

Corrosion Mechanisms in the Reaction of Steel with Water and Oxygenated Solutions at Room Temperature and 316°C

Mary Boehm Strauss and M. C. Bloom

U. S. Naval Research Laboratory, Washington, D. C.

ABSTRACT

The corrosion products developed by steel when reacting with water of varying oxygen content at room temperature and at 316°C are described. The reaction was carried out in sealed steel capsules and followed by pH measurement of the solution and by microscopic, x-ray, and electron diffraction analysis of the corrosion product films. Data on the transformation behavior of the corrosion products involved and a summary of some of their physical properties are included.

Although the literature dealing with aqueous corrosion in ferrous systems is discouragingly voluminous, the amount of material dealing directly with the nature of the corrosion product films formed has, until recent years, been rather meager. A literature review (1) in 1955 indicated that the available information was far short of that needed for analysis of corrosion mechanisms of interest in connection with naval and nuclear steam generation problems, and a long-range program for obtaining some of the needed data was undertaken. This is a report of the preliminary explorations of that program. The conditions chosen for this preliminary exploration were room temperature (25°C) on the one hand and 316°C (600°F) on the other, a choice dictated by the practical considerations of naval and nuclear power steam generation applications.

Before discussing the experimental work, it may be useful to recall a few of the properties of the corrosion products with which we are concerned. These properties are listed in Table I. Neglecting FeO, with which we will not be concerned in this work, we see that color can sometimes be useful in distinguishing various forms. The structures are readily distinguishable by diffraction techniques with the exception of the two spinels Fe_3O_4 and γ-Fe_2O_3 which are built on the same framework. It may be noted that these two oxides are the only ferromagnetic species in this corrosion product system.

Experimental Techniques

The technique which was the major basis of the experiments was the use of mild steel specimens in the form of sealed capsules completely filled with the solution under test (17). The test specimens were prepared from mild steel tubing the composition of which appears in Table II. Attention is directed to the manganese content which will come into discussion later. Before fabrication into capsules, the steel tubing was hydrogen annealed 1 hr at 875°C, cooled

Table I. Corrosion products of iron

Composition (Mineral name)	Color	Structural type (3)	Magnetic character	Electrical resistivity	Density	Thermal behavior
$Fe_{0.950}O$ to $Fe_{0.888}O$ (Wustite) (2)	Black	NaCl	Paramagnetic (4)	Semiconductor (3)	5.4-5.73 (2, 11)	Melts at 1371°-1424°C. Below 570°C decomposes to Fe and Fe_3O_4 (2)
$Fe(OH)_2$	White	$Mg(OH)_2$ (Brucite)	Paramagnetic (5)	Insulator*	3.40 (12)	Decomposes at about 100°C to Fe_3O_4 and H_2† (14)
Fe_3O_4 (Magnetite)	Black	Spinel	Ferromagnetic (4)	Electronic conductor (8)	5.20 (4)	Melts at 1597°C (2)
γ-FeOOH (Lepidocrocite)	Orange	γ-FeOOH (Lepidocrocite)	Paramagnetic (6)	Insulator*	3.97 (13)	Dehydrates to‡ γ-Fe_2O_3 at about 200°C (16)
α-FeOOH (Goethite)	Yellow	α-FeOOH (Goethite)	Paramagnetic (6, 7)	Insulator (9)	4.20 (13)	Dehydrates to‡ α-Fe_2O_3 at about 200°C (16)
γ-Fe_2O_3 (Maghemite)	Brown	Spinel (with vacancies)	Ferromagnetic (4)	Semiconductor to insulator (10)	4.88 (4)	Transforms to‡ α-Fe_2O_3 above 250°C (16)
α-Fe_2O_3 (Hematite)	Brick red to black	Al_2O_3 (Corundum)	Paramagnetic (4)	Insulator (10)	5.25 (4)	Decomposes to magnetite at 1457°C and 1 atm (2)

* Color indicates that these are insulators.
† In contact with traces of oxygen $Fe(OH)_2$ is unstable at room temperature and transforms to γ-FeOOH, α-FeOOH, or Fe_3O_4 depending on the conditions of the system (15).
‡ Presence of water causes conversion to α-Fe_2O_3 at lower temperature.

Table II. Analysis of steel

Constituent	Weight %
C	0.09
P	0.017
S	0.032
N	0.007
Mn	0.57
Si	0.07
Cr	0.10
Ni	0.07
Fe (by difference)	99.05

in the hydrogen atmosphere to 60°C and then removed to the atmosphere of the room; subsequently, the tubing was annealed 1 hr at 875°C in a vacuum furnace maintained at a pressure of less than 10^{-5} mm Hg and cooled to room temperature in the furnace. The electron diffraction pattern obtained from the metal after this treatment was that of α-iron with occasional traces of the 311-line, the strongest line of the spinel pattern.

The prepared capsule specimens were exposed in sets of 6 to 12 each. The specimens were prepared, treated at room temperature for selected lengths of time, and then opened. Additional capsules were treated at room temperature for specific times, then placed in an oven at 316°C for one week, or twelve weeks, cooled to room temperature, and opened immediately thereafter. A typical capsule is shown in Fig. 1. The capsules were opened by carefully filing one corner until the metal was so thin that it could be puctured with a stainless steel syringe needle. The liquid was removed from each capsule into a glass syringe and the pH of the liquid measured promptly to avoid reaction with carbon dioxide from the atmosphere. The pH measurements were made using a Beckman "one drop" glass electrode and Model G pH meter. The individual measurements showed considerable scatter. The value reported is the average. In some cases samples of the liquid were dropped on copper electrodes coated with Apiezon wax, evaporated to dryness under an infrared lamp, and analyzed by emission spectroscopy. When liquid was withdrawn from a capsule, a magnet was used to test suspended solids for the presence of the spinel type oxides, Fe_3O_4 and γ-Fe_2O_3, which as previously indicated are the only ferromagnetic species in this corrosion product system. Solids suspended in the capsule liquids were collected on a Millipore filter and dried in a desiccator over Drierite (anhydrous calcium sulfate), x-ray diffraction patterns being obtained from the dry solids.

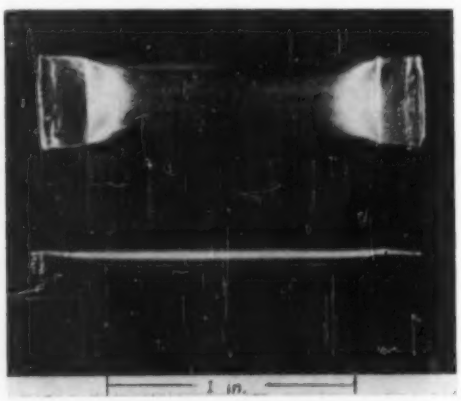

Fig. 1. Typical capsule

After removal of the liquid from the capsules, the walls were prepared for examination by filing away the lengthwise edges and shearing the transverse edges to yield two opposite wall surfaces. These were examined by use of a Geiger counter x-ray spectrometer using cobalt Kα radiation as well as by use of the diffraction attachment of an RCA (EMU-2) electron microscope. The x-ray patterns served to characterize the bulk of the corrosion product film when this film was thick enough. The electron diffraction patterns served for characterization of very thin films on the metal surfaces and of the exterior surface layers of thicker corrosion product films.

The corroded capsule walls also were examined microscopically to determine the character and extent of the corrosive attack as well as the appearance of the corrosion products.

In most cases, no attempt was made in this exploratory work to distinguish between Fe_3O_4 and γ-Fe_2O_3.

Corrosion Products Generated in Air-Saturated Distilled Water

The data obtained in the characterization of the corrosion products formed at room temperature in capsules initially filled with distilled water are shown in Table III. Each pH value reported in this and subsequent tables is the average of a number of measurements usually 6-12. An indication of the scatter can be seen from the following which show typical scatter for data in Table III:

Measured pH after 6 hr: 9.48, 9.72, 9.57, 9.40, 8.91, 9.30, average 9.4; after 1 week: 9.7, 9.4, 10.1, 10.0, 9.7, 9.6, average 9.8; after 52 weeks: 9.93, 9.96, 9.90, 9.71, 10.02, average 9.9.

The water was initially air-saturated and the small variation in pH at the outset is probably due to differences in the carbon dioxide content of the laboratory atmosphere. It may be noted that after 6 hr the pH has risen to 9.4. This is approximately the pH of a saturated solution of $Fe(OH)_2$. This rise in pH indicates that all the oxygen has been consumed (20). The pH thereafter steadily rises to 9.9 where it is found one year later. The rise to so high a pH puzzled us for some time, but seems explicable as due to the simultaneous presence of $Fe(OH)_2$ and $Mn(OH)_2$. Using the known solubility product data for these two hydroxides one may calculate the pH in the presence of both to be 9.92. A calculation of the amount of manganese required (5.5×10^{-7} g) to produce this amount of $Mn(OH)_2$ shows that 10^{-4} g of steel would be required to be dissolved to give this quantity of manganese. This seems a very reasonable quantity to expect to have been dissolved in the 12 week period where this pH is shown to be developed. An independent series of experiments confirmed the conclusion that the calculated equilibrium of 9.92 would be achieved by allowing mixtures of carbonyl

Table III. Corrosion products formed by the action of water* in mild steel capsules at 25°C

Solution pH before reaction†	Time metal was exposed to solution	Solution pH after reaction†	Appearance of solution	Appearance of metal	Corrosion products on metal
5.9	1 hr	8.5	Yellow tinge	Speckled with brownish yellow islands	γ-FeOOH
5.6	6 hr	9.4	Clear, colorless	Same as above	γ-FeOOH and possibly spinel
6.0	24 hr	9.5	Clear, colorless	Same as above	γ-FeOOH and spinel
6.0	1 wk	9.8	Clear, colorless	Same as above	γ-FeOOH and spinel
6.0	12 wk	9.9	Clear, colorless	Thin gray brown film	Spinel and some γ-FeOOH
6.0	52 wk	9.9	Few particles of spinel	Continuous black film	Spinel

* The water was initially air saturated.
† Each value represents the mean of 6 capsules.

Table IV. Corrosion products formed by the action of 0.2% H_2O_2 in mild steel capsules at 25°C

Solution pH before reaction	Time metal exposed to solution	Solution pH after reaction†	Solid corrosion products filtered from solution	Appearance of metal	Corrosion products on metal	Residual oxygen pressure
5.9	1 hr	7.1	*	Yellow islands on shiny metal	γ-FeOOH	Yes
5.9	24 hr	6.8	Spinel and some γ-FeOOH	Same as above	γ-FeOOH and spinel	No
5.8	1 wk	7.4	Spinel	Yellow islands on black film	Spinel and some γ-FeOOH	No
5.8	4 wk	8.6	Spinel	Few yellow islands on black film	Spinel and some γ-FeOOH	No
5.7	52 wk	10.0	Spinel	Nearly covered with brownish-black film	Spinel	No

* Insufficient material for analysis.
† Each value represents the mean of 8 to 12 capsules.

Table V. Corrosion products formed by the action of 1% H_2O_2 on mild steel capsules at 25°C

Solution pH before reaction	Time metal exposed to solution	Solution pH after reaction*	Solid corrosion products filtered from solution	Appearance of metal	Corrosion products on metal	Residual oxygen pressure
5.8	1 hr	6.9	None	Yellow islands on shiny metal	γ-FeOOH	Yes
5.9	24 hr	7.3	γ-FeOOH	Same as above	γ-FeOOH	Yes
5.7	1 wk	8.0	α-FeOOH	Yellow film covers metals	γ-FeOOH and α-FeOOH	Yes
5.9	4 wk	8.2	α-FeOOH	Same as above	γ-FeOOH and α-FeOOH	Yes

* Each value represents the mean of 8 to 12 capsules.

Table VI. Corrosion products formed by the action of 4% H_2O_2 in mild steel capsules at 25°C

Solution pH before reaction	Time metal exposed to solution	Solution pH after reaction*	Solid corrosion products filtered from solution	Appearance of metal	Corrosion products on metal	Residual oxygen pressure
5.8	1 hr	7.1	None	Shiny metal	γ-FeOOH	Yes
6.0	24 hr	7.3	γ-FeOOH	Nearly covered with yellow film	γ-FeOOH	Yes
5.9	1 wk	8.2	α-FeOOH	Same as above	γ-FeOOH and α-FeOOH	Yes
5.9	4 wk	8.6	α-FeOOH	Same as above	γ-FeOOH and α-FeOOH	Yes
Not measured	61 wk	8.5	α-FeOOH	Same as above	α-FeOOH and trace of γ-FeOOH	Yes(?)

* Each value represents the mean of 8 to 12 capsules.

iron and electrolytic manganese to corrode in water. These metals had a total metallic impurity content of the order of 100 ppm and a nitrogen content in the neighborhood of 20 ppm. In these experiments, metallic powders were allowed to remain in sealed platinum-lined capsules for 3 weeks at 25°C prior to sampling. The solutions then gave the following pH values

Powder	Observed pH	pH Calculated for saturation
Fe	9.37	9.32
Mn	9.95	9.92
Fe-Mn mixture	9.95	9.92

Next, attention is called to the fact that the initial product of reaction is γ-FeOOH. The approximately 8 ppm of oxygen introduced with the air-saturated water apparently has produced the ferric ions necessary for its formation. This phase shows up as islands on the otherwise unattacked metal.

Finally, it may be noted that within 24 hr, the spinel phase has made its appearance and eventually spreads over the entire surface of the specimen. The fact that the pH of the solution has reached 9.4 [approximately the equilibrium pH of $Fe(OH)_2$] at the time that the spinel phase appears suggests that $Fe(OH)_2$ is present also, and the rise to 9.9 is taken as an indication of the presence of solid $Mn(OH)_2$ along with the $Fe(OH)_2$. Linnenbom (18) has shown that under these pH conditions $Fe(OH)_2$ does not break down to form Fe_3O_4 in impurity-free solutions, but Evans and Wanklyn (19), as well as Shipko and Douglas (14), have shown that impurities may catalyze the reaction

$$3Fe(OH)_2 \rightarrow Fe_3O_4 + 2H_2O + H_2$$

and this would appear to be what is happening here unless nuclei of Fe_3O_4 formed by reduction of γ-FeOOH are serving a similar catalytic purpose.

Tables IV-VI show some data concerning the effect of the presence of more oxygen in these systems. The data were obtained by utilizing solutions of H_2O_2 in the capsules. These solutions decompose readily in the presence of ferrous or ferric ions to liberate oxygen and thus provide a simple means for introducing oxygen into the capsules. When the capsules were opened, fluid squirted out whenever the residual oxygen pressure was in excess of atmospheric and this phenomenon was used to give a qualitative indication of oxygen exhaustion inside the capsules. The column marked residual oxygen pressure is based on this criterion.

Table IV shows the data obtained using 0.2% H_2O_2 solutions at room temperature. The pH of 5.7 to 5.9 exhibited by the solution before reaction is undoubtedly due to absorption of carbon dioxide from the atmosphere. No explanation is offered for the apparent drop in pH during the first 24 hr. Perhaps this is experimental error. Attention is, however, called to the fact that no residual oxygen pressure was observed after 24 hr and that thereafter the solution pH began to rise as it did previously in the case where no peroxide was added. It may be noted that γ-FeOOH is the initial reaction product which gives way to spinel as the oxygen content decreases and the pH increases finally reaching the vicinity of the 9.9 associated with oxygen-free solutions.

Table V exhibits analogous data obtained with a 1% H_2O_2 solution. It may be observed that a residual oxygen pressure in excess of atmospheric was present in all cases. We note that the pH again rises with time of exposure but that now a new corrosion product, α-FeOOH, appears when the pH reaches 8. Data obtained using a 4% solution of H_2O_2 are shown in Table VI. Again we note the appearance of α-FeOOH when the pH gets above 8, and we may now note that the pH seems to reach a plateau in the neighborhood of 8.5-8.6 which it maintains even after a year of exposure.

The following explanation is suggested for the arrest of the pH in the 8.5 region when oxygen is present. In the presence of oxygen, saturation of the solution with $Fe(OH)_2$ is not attained due to oxidation of Fe^{++} (20) and the consequent generation of FeOOH instead of $Fe(OH)_2$. FeOOH is so insoluble (21) that a pH in excess of 7 would not be anticipated from this source.

In the manganese system we might expect that analogously $Mn(OH)_2$ would be oxidized by dissolved oxygen as this is the basis of the Winkler test (22) for dissolved oxygen in water. However, the nature of the corrosion product generated and the corresponding pH has apparently not been investigated. Therefore, a brief exploration was undertaken of the corrosion of manganese by dissolved oxygen at room temperature. For this purpose fragments of electrolytic manganese were immersed in water in a quartz-glass flask and exposed to an atmosphere of oxygen which had been purified by being passed through sulfuric acid, water, and basic barium chloride. At weekly intervals the pH of the water was measured. Starting at 6.4, the pH of the water rose to 8.8 in the first week and remained there for 2 additional weeks. The major corrosion product which accumulated out of contact with the metal was a brown powder with an x-ray diffraction pattern not included in the ASTM card index. It has similarities to the pattern of γ-FeOOH and is perhaps the manganese analogue of that structure.

It seems probable therefore that the pH arrest noted in the capsules in the region of pH 8.5-8.6 was due to the genesis of manganese oxidation products.

As an aid to interpretations of observations from the capsule corrosion studies, exploratory studies of the transformation behavior of the various oxides and hydroxides were conducted. Samples of the desired compounds, obtained from commercial sources, (see Table VII) were subjected to the following treatments: (*a*) treatment in mild steel capsules at 25°C in the presence of water, (*b*) treatment in platinum-lined capsules at 316°C in the presence and absence of water, (*c*) treatment in mild steel capsules at 316°C in the presence and absence of water. The nature of the transformation products was determined by x-ray diffraction, chemical analysis for Fe(II) and Fe(III) and observation of the presence or absence of ferromagnetism. The results of these experiments are shown in Tables VIII-X. The data indicated that when in contact with corrod-

Table VII. Chemical analyses of oxides and hydrated oxides

Material	Fe_2O_3	Fe_3O_4	Water	Al_2O_3	MnO	SiO_2	CaO	SnO_2	MgO	Total
γ-FeOOH	85.24	0.14	13.09	1.07	0.09	0.08	—	—	—	99.71
α-FeOOH	86.23	0.05	12.56	1.38	0.06	0.03	—	—	—	100.31
γ-Fe_2O_3	90.90	6.52	0.65	1.63	0.03	0.53	—	0.07	—	100.33
α-Fe_2O_3	97.51	0.20	0.50	1.86	0.05	0.06	—	—	—	100.18
Fe_3O_4	21.76	77.22	—	—	—	0.22	1.00	—	0.20	100.40

Table IX. Summary of observations on products formed when iron oxides and hydrated oxides are heated in sealed platinum-lined nickel capsules at 316°C

Substance	Treatment	Time at 316°C	Color of product	Ferromagnetic	Result of treatment
γ-FeOOH	Heated with H_2O	24 hr	Brick-red	No	Converted to α-Fe_2O_3
γ-FeOOH	Heated dry with air	24 hr	Brick-red	No	Converted to α-Fe_2O_3
α-FeOOH	Heated with H_2O	24 hr	Maroon	No	Converted to α-Fe_2O_3
α-FeOOH	Heated dry with air	24 hr	Brick-red	No	Converted to α-Fe_2O_3
γ-Fe_2O_3	Heated with H_2O	24 hr	Maroon	Partially	All but a slight amount converted to α-Fe_2O_3
γ-Fe_2O_3	Heated dry with air	24 hr	Brown	Yes	Unchanged
α-Fe_2O_3	Heated with H_2O	24 hr	Brick-red	No	Unchanged
α-Fe_2O_3	Heated with H_2O	2 wk	Brick-red	No	Unchanged
α-Fe_2O_3	Heated dry with air	24 hr	Brick-red	No	Unchanged
Fe_3O_4	Heated with H_2O	24 hr	Black	Yes	Unchanged
Fe_3O_4	Heated dry with air	24 hr	Black	Yes	Unchanged

Table X. Summary of observations on products formed when iron oxides and hydrated oxides are heated in sealed mild steel capsules at 316°C

Substance	Treatment	Time at 316°C	Color of product	Ferromagnetic	Result of treatment
γ-FeOOH	Heated with H_2O	Up to 4 hr (before cracking)	Red-brown	Partially	Converted to α-Fe_2O_3 and some Fe_3O_4
γ-FeOOH	Heated with H_2O	(All capsules tested cracked and leaked within 6 hr)			
γ-FeOOH	Heated dry with air	24 hr	Red	No	Converted to α-Fe_2O_3 and trace Fe_3O_4
α-FeOOH	Heated with H_2O	24 hr	Black-red	Yes	Reduced to Fe_3O_4 with trace α-Fe_2O_3
α-FeOOH	Heated dry with air	24 hr	Brick-red	No	Converted to α-Fe_2O_3 with trace Fe_3O_4
γ-Fe_2O_3	Heated with H_2O	24 hr	Black-brown	Yes	Converted to α-Fe_2O_3 and Fe_3O_4
γ-Fe_2O_3	Heated dry with air	24 hr	Brown (unchanged)	Yes	Slight reduction to Fe_3O_4 at Fe interface
α-Fe_2O_3	Heated with H_2O	24 hr	Brick-red (unchanged)	No	Slight reduction to Fe_3O_4
α-Fe_2O_3	Heated with H_2O	7 days	Very dark red	Partially	Considerable reduction to Fe_3O_4
α-Fe_2O_3	Heated dry with air	24 hr	Brick-red (unchanged)	No	Unchanged
Fe_3O_4	Heated with H_2O	24 hr	Black (unchanged)	Yes	Unchanged
Fe_3O_4	Heated dry with air	24 hr	Black (unchanged)	Yes	Unchanged

ing steel at room temperature, anhydrous oxides were more resistant to reduction to Fe_3O_4 than the hydrous ones and that the α-Fe_2O_3 was most resistant to this action. This reduction could be a reaction with corrosion-generated hydrogen or a precipitation reaction involving divalent iron from the corroding steel and dissolved species from the trivalent solids. A probable mechanism is the following: $Fe^{++} + 2FeO_2^- \rightarrow Fe_3O_4$. Evidence of rapid direct reaction of this kind is found in the experiments of Forrest, Roetheli, and Brown (23) in which "gelatinous precipitates of ferrous and ferric hydroxides" were mixed to produce Fe_3O_4.

It may be noted that at elevated temperatures in the absence of corroding steel the transformation of all trivalent species to α-Fe_2O_3 is markedly accelerated by the presence of water in accord with the observations of Gheith (16). The reduction of all trivalent oxides to Fe_3O_4 at the elevated temperature is most probably due to reduction by corrosion-generated hydrogen. The fact that γ-Fe_2O_3 did not transform to α-Fe_2O_3 when heated at 316° in the dry state is undoubtedly due to stabilization by the presence of the aluminum present as an impurity (24). The cracking of the capsules when heated with γ-FeOOH slurries was shown to be a stress corrosion phenome-

Table VIII. Behavior of iron oxide and hydrated oxide slurries in mild steel capsules at room temperature

Iron compound in prepared slurry	Solids present in slurry after 48 hr	Solids present in slurry after 4 wk
Fe_3O_4	Apparently unchanged	No change
γ-FeOOH	Apparently unchanged	γ-FeOOH and spinel*
γ-Fe_2O_3	Apparently unchanged	γ-Fe_2O_3 and traces of Fe_3O_4
α-FeOOH	Apparently unchanged	α-FeOOH and spinel*
α-Fe_2O_3	Apparently unchanged	Unchanged

* Chemical analysis was not used for these cases since Fe_3O_4 seems to be the only spinel species which could be developed. In both cases, prior experimentation (16) indicates complete stability to dehydration up to temperatures in the neighborhood of 100°C. Thus γ-Fe_2O_3 could not be developed by dehydration of γ-FeOOH. In the case of α-FeOOH, even dehydration would produce only the stable α-Fe_2O_3. Thus the only feasible way in which the spinel structure could be developed here is by reduction to Fe_3O_4.

non induced by the presence of a chloride impurity. This will be discussed in a subsequent publication.

All the data thus far discussed are summarized in Table XI, and the results of heating capsules to 316°C after 24 hr of room temperature exposure are shown in Tables XII and XIII.

The following conclusions may be drawn:

1. Steel in contact with air saturated water at 25°C in these capsules develops γ-FeOOH within an hour. This γ-FeOOH appears as islands on the metallic surface. The pH rises within 24 hr from an initial value of about 6.0 to 9.5, approximately the equilibrium value in contact with $Fe(OH)_2$, and continues to rise to 9.9 where it apparently remains indefinitely. This pH of 9.9 is the equilibrium pH of a solution in contact with both $Fe(OH)_2$ and $Mn(OH)_2$. This rise in pH is accompanied by the gradual elimination of γ-FeOOH and its replacement with a spinel which eventually covers the entire specimen as the oxygen is used up and the pH rises.

2. Steel in contact with H_2O_2 solutions under these conditions also develops γ-FeOOH which appears as islands on the metal within an hour. The rise in pH in this case, however, is much more gradual. With sufficient oxygen present ($\geqq 1\%$ H_2O_2) γ-FeOOH is at first produced, and then as the pH rises with time to a value of 8.0 or above, α-FeOOH appears. With sufficient oxygen present the pH reaches a plateau in the neighborhood of 8.5.

3. On long standing (1 year) with exhaustion of oxygen, the spinel phase appears and the pH rises to the vicinity of 9.9, the equilibrium value in contact with $Fe(OH)_2$ and $Mn(OH)_2$.

4. On heating at 316°C, any $Fe(OH)_2$ or γ-FeOOH generated by room temperature exposure of steel to water is converted to magnetite within 24 hr with a corresponding drop in pH to the neutral region.

5. On heating at 316°C, any γ- or α-FeOOH generated by room temperature exposure in H_2O_2 solutions is converted to α-Fe_2O_3 within 24 hr with a corre-

Table XI. Summary of corrosion products formed by the action of water and H_2O_2 solutions in mild steel capsules at 25°C

Time of exposure	H_2O		0.2% H_2O_2		1% H_2O_2		2% H_2O_2		4% H_2O_2	
	pH	Product	pH	Product	pH	Product	pH	Product	pH	Product
1 hr	8.5	γ-FeOOH	7.1	γ-FeOOH	6.9	γ-FeOOH	7.3	γ-FeOOH	7.1	γ-FeOOH
24 hr	9.5	γ-FeOOH and spinel	6.8	Spinel and some γ-FeOOH	7.3	γ-FeOOH	7.3	γ-FeOOH	7.3	γ-FeOOH
1 wk	9.8	γ-FeOOH and spinel	7.4	Spinel	8.0	α-FeOOH	8.3	α-FeOOH	8.2	α-FeOOH
4 wk	—	—	8.6	Spinel	8.2	α-FeOOH	8.1	α-FeOOH	8.6	α-FeOOH
1 yr	9.9	Spinel	10.0	Spinel	—	—	—	—	8.5	α-FeOOH

Table XII. Corrosion products formed by the action of water in mild steel capsules at 316°C

Solution pH before 316°C treatment	Time metal was treated at 316°C*	Solution pH after 316°C treatment†	Appearance of solution	Appearance of metal	Corrosion products on metal	Thickness of surface oxide
9.5	24 hr	6.9	Clear, colorless	Continuous gray black film	Spinel	Less than 1μ
9.5	1 wk	7.0	Clear, colorless	Same as above	Spinel	Less than 1μ
9.5	14 wk	7.0	Clear, colorless	Same as above	Spinel	1 to 3μ
9.5	52 wk	6.9	Clear, colorless	Same as above	Spinel	2 to 6μ

* The metal was exposed at room temperature for 24 hr before treatment at 316°C.
† Each value represents the mean of at least 5 capsules.

Table XIII. Summary of the corrosion products formed by the action of H_2O_2 solutions in mild steel capsules at 316°C

Solution and initial pH	Exposure at 25°C	Products on metals	Solution pH after 25°C treatment	Exposure at 316°C	Products on metal	Solution pH after 316°C treatment
0.2% H_2O_2	24 hr	γ-FeOOH and spinel	6.8	1 wk	Spinel and trace α-Fe_2O_3	6.8
5.8-5.9	1 wk	Spinel and some γ-FeOOH	7.4	1 wk	Spinel	7.2
				12 wk	Spinel	6.7
1.0% H_2O_2	24 hr	γ-FeOOH	7.3	1 wk	α-Fe_2O_3 and some spinel	6.4
5.7-5.9	1 wk	γ-FeOOH and α-FeOOH	8.0	1 wk	α-Fe_2O_3 and some spinel	6.4
				12 wk	Spinel and trace α-Fe_2O_3	6.9
2.0% H_2O_2	24 hr	γ-FeOOH	7.3	1 wk	α-Fe_2O_3 and some spinel	6.1
5.4-5.7	1 wk	γ-FeOOH and α-FeOOH	8.3	1 wk	α-Fe_2O_3 and some spinel	6.0
				12 wk	α-Fe_2O_3 and spinel	6.0
4.0% H_2O_2	24 hr	γ-FeOOH	7.3	1 wk	α-Fe_2O_3 and some spinel	6.1
5.9-6.0	1 wk	γ-FeOOH and α-FeOOH	8.2	1 wk	α-Fe_2O_3 and some spinel	5.9
				12 wk	α-Fe_2O_3 and spinel	5.8

sponding drop in pH to the neutral region. As the oxygen is consumed by the reaction, this α-Fe_2O_3 is slowly reduced to spinel (Fe_3O_4).

Acknowledgments

The authors are indebted to W. A. Fraser and G. N. Newport for assistance throughout the course of this work; to C. O. Timmons for the preparation and treatment of many of the specimens; to Evelyn Cisney and W. G. Sadler for x-ray diffraction patterns; to D. M. Price for metallography, to the Analytical Branch of this organization for chemical analyses, to A. J. Pollard for aid in the exploration of the oxidation of manganese, to Jeanne B. Burbank for assistance with the electron diffraction patterns, and to Dr. Morris Cohen of the Canadian Research Council for helpful discussion of the kinetics of $Fe(OH)_2$ oxidation.

Manuscript received July 16, 1959. This paper was prepared for delivery before the Ottawa Meeting, Sept. 28-Oct. 2, 1958.

Any discussion of this paper will appear in a Discussion Section to be published in the December 1960 JOURNAL.

REFERENCES

1. M. J. Boehm and M. C. Bloom, *Corrosion*, **13**, No. 2, 44 (1957).
2. L. S. Darken and R. W. Gurry, *Metals Handbook*, p. 1212, American Society for Metals (1948).
3. W. Huckel, "Structural Chemistry of Inorganic Compounds," Elsevier Publishing Co., New York (1951).
4. B. Mason, *Geol. Foren. i. Stockholm Forh.*, **65**, 97 (1943).
5. A. Quartaroli, *Gazz. chim. ital.*, **46 ii**, 224 (1916).
6. H. W. Albrecht, *Ber.*, **62**, 1475 (1929).
7. G. F. Huttig and H. Kittel, *Z. anorg. Chem.*, **199**, 129 (1931).
8. E. J. Verwey and J. H. deBoer, *Rec. trav. chim.*, **55**, 531 (1936).
9. T. W. Case, *Phys. Rev.*, **9**, (2), 305 (1917).
10. H. Sachse, *Z. Phys.*, **70**, 539 (1931).
11. E. R. Jette and F. Foote, *J. Chem. Phys.*, **1**, 29 (1933).
12. G. Natta and E. Casazza, *Atti accad. naz. Lincei*, **5**, (6), 803 (1927).
13. J. Bohm, *Z. Krist.*, **68**, 568 (1928).
14. F. J. Shipko and D. L. Douglas, *J. Phys. Chem.*, **60**, 1519 (1956).
15. J. E. O. Mayne, *J. Chem. Soc.*, 129 (1953).
16. a-M. A. Gheith, "Stability Relations of Ferric Oxides and Their Hydrates," Ph.D. Thesis, Univ. of Minn. (1951).
    b-L. A. Welo and O. Baudisch, *Chem. Rev.*, **15**, 45 (1934).
17. M. C. Bloom and M. Krulfeld, *This Journal*, **104**, No. 5, 265 (1957).
18. V. J. Linnenbom, *ibid.*, **105**, No. 6, 322 (1958).
19. U. R. Evans and J. N. Wanklyn, *Nature*, **162**, 27 (1948).
20. M. J. Pryor and M. Cohen, *This Journal*, **100**, No. 5, 208 (1953).
21. K. H. Gayer and L. Woontner, *J. Phys. Chem.*, **60**, 1569 (1956).
22. ASTM Standards, Part 10, p. 1004 (1958).
23. H. O. Forrest, B. E. Roetheli, and R. H. Brown, *Ind. and Eng. Chem.*, **23**, No. 6, 650 (1931).
24. F. E. DeBoer and P. W. Selwood, *J. Am. Chem. Soc.*, **76**, 3365 (1954).

Corrosion of Nickel Coated Mild Steel

B. C. Banerjee[1]

National Chemical Laboratory, Poona, India

ABSTRACT

A dissolution rate study of iron from mild steel disks coated with electrodeposited nickel having (100), (10$\bar{1}$0) + (211), (110), and (210) orientations has revealed that, in hydrochloric acid solution, coatings with (210) orientation gave the best protection to the iron. On the other hand, in neutral sodium chloride solution appreciable difference in the dissolution rate has not been observed. These results have been discussed with reference to the precipitation of basic iron salts, the electrochemical anisotropy of different faces of a single crystal, and also to the texture of the deposits.

The corrosion of a metal can be minimized by a coating of a nobler metal, for example, by electrodeposition of nickel on iron. Under the conditions of electroplating used in practice, the coating will be more or less porous and the protection efficiency is supposed to depend largely on the porosity of the coating (1, 2). It may be mentioned in this connection that the polycrystalline nickel coating is made up of a large number of single crystals. Such a coating may, however, develop different crystal orientations under varying conditions of deposition (3, 4) and thus affect the corrosion rate of the base metal due to electrochemical anisotropy of different faces of a single crystal (5-8). It was previously thought (3, 4) that the lateral growth of electrodeposited metals of the f.c.c. type, defined by the orientation of the more densely packed atomic planes such as (111), (100), or (10$\bar{1}$0) + (211) parallel to the substrate surface gives better protection than the outgrowth type of deposits defined by (110) or (210) orientations. For industrial electroplating, bath conditions corresponding to the former were therefore recommended (4). In what follows some preliminary results of dissolution of iron from a mild steel disk coated with electrodeposited nickel suggest a different type of behavior.

Experimental Results

Mild steel disks of 2 cm diameter were made out of a rod supplied by "TISCO" (India). They were carefully polished and the nonsignificant portions were thickly plated with nickel, and then covered with collodion. The significant surfaces (area 3.14 cm^2) of one set of such disks were hand polished with emery of different grades ranging from 1F down to 4/0 and the surfaces of another set were machine polished on a polishing cloth containing jeweller's rouge soaked with a continuous supply of xylene as lubricant. Machine polishing of different sets of disks also was carried out with jeweller's rouge soaked continuously with benzene, toluene, dioxane, decaline, etc., respectively. The machine polished disks contained no visible scratches, but a few scratches could be seen in hand polished disks. The surfaces thus obtained were cleaned thoroughly with acetone (A.R. grade) and distilled water to make them free from grease, etc., and then coated with nickel from a bath consisting of 280 g/l of nickel sulfate, 48 g/l of nickel chloride, and 31 g/l of boric acid. All chemicals were of C. P. grade. The bath was purified initially by electrolyzing the solution at a low current density, with a dummy brass cathode and a very pure nickel foil as anode. The pH of the bath was adjusted by adding an appropriate quantity of the acid or nickel carbonate. The solutions thus prepared were filtered to remove any suspended matter in them. In order to prevent possible leakage of iron through nonsignificant surfaces of a disk during experiments, thick coatings of beeswax also were applied on them. The deposit orientations, (210), (100), and (10$\bar{1}$0) + (211) were obtained at 25°C at pH of 2.1, 3.9, and 5.1, respectively, whereas the (110) orientation was developed at any one of the pH's at 60°C. The current density was 10 ma/cm^2 in all the above cases of deposition. The time of deposition which ensured an average thickness of 5.75 μ of nickel coating was noted from reference curves, previously determined for each one of the crystal orientations, by a method suggested by Blum and Hogaboom (1). The orientations were checked from electron diffraction patterns (reflection type, ~55 kv electrons, camera length ~50 cm).

The experiments on dissolutions of the plated disks were carried out in Pyrex beakers containing 40 cc of 0.5% HCl (pH ≈ 1) or 5% NaCl (pH ≈ 7) at 25°C with the disks immersed vertically for the specified time intervals in the stagnant solutions, kept open to air all the time. The disk was washed with distilled water, dried with filter paper, and dipped in a fresh solution every time. The solutions containing iron mostly in the form of Fe^{2+} ions were oxidized to the Fe^{3+} state by adding 3 cc of 4*N* nitric acid and boiling for 5 min. Then the concentration of iron was estimated spectrophotometrically after adding KCNS solution with a Unicam spectrophotometer using a light of $\lambda = 500$ mμ (10).

Figure 1 presents results for the dissolutions in 0.5% HCl solutions at 25°C when the initial surface was hand polished, Fig. 2 for machine polished surfaces (jeweller's rouge soaked with xylene as lubri-

[1] Present address: Department of Physics, Pennsylvania State University, University Park, Pa.

cant), and Fig. 3 for dissolution in 5% NaCl solution from the machine polished plated disks. However, results similar to Fig. 1 also were obtained with machine polished plated disks if benzene, toluene, dioxane, decaline, and many other similar hydrocarbons were used as soaking liquid for jeweller's rouge during machine polishing of initial surfaces of mild steel disks instead of xylene. In all the above cases averages from five different experiments are given. It may be seen that the rate of dissolution as given by the slope is higher initially and becomes steady after a few minutes. In the case of (210) orientation the initial rate of dissolution is higher compared with other orientations (Fig. 1 and 2), but later the rate becomes the lowest of all, irrespective of the method of polishing of the initial iron surfaces. This indicates that (210) orientation of nickel coating or the texture of the coating obtained under the stated bath conditions on mild steel ultimately gives the better protection from corrosion in the wet environments studied above.

In the salt solution (Fig. 3), however, no appreciable difference in the corrosion rates was observed

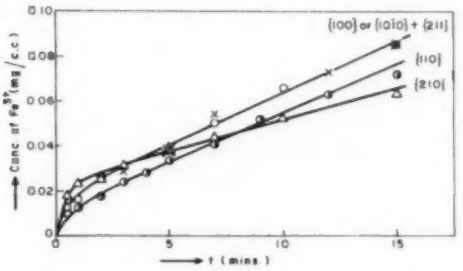

Fig. 1. Dissolution of Fe from hand-polished disk, coated with orientated nickel in 0.5% HCl solution.

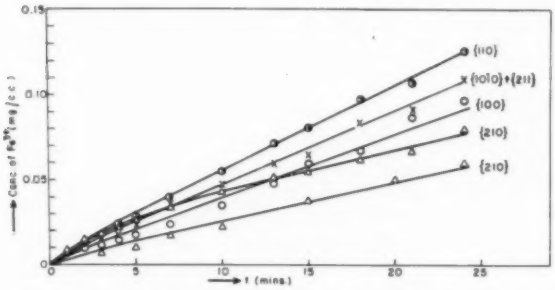

Fig. 2. Dissolution of Fe from machine-polished disk (xylene as soaking liquid) coated with orientated nickel in 0.5% HCl solution, (the lowest curve 0.25% HCl).

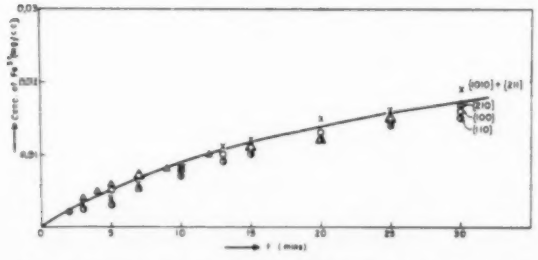

Fig. 3. Dissolution of Fe from machine-polished disk, coated with orientated nickel in 5.0% NaCl solution.

for the various crystal orientations. The higher dissolution observed in the case of hand-polished, compared to machine-polished, coated disks is obviously due to more irregularities on the surface leading to a less efficient protection by the coating.

Discussion

The corrosion of metals in acid solution involves essentially the transfer of one or more electrons by the metal atom to another species, followed by solvation in the aqueous solution. It could be assumed that the rate of dissolution will, *inter alia*, be dependent on the area of the exposed iron. The important question of the texture of the deposit involving such considerations as size, grain boundaries, orientations, and mutual arrangement of the discontinuities of the intercrystallites should be considered primarily (7-9).

It may be inferred that bath conditions depositing nickel with (210) plane parallel to the substrate surface might have produced the least porous surface. However, qualitative estimates of porosity by the usual hot water dip and ferrocyanide methods reveal that deposits with (210) and (10$\bar{1}$0) + (211) orientations are distinctly more porous and the results are in agreement with those of Rotinyan (13). This also can be appreciated in view of the fact that appreciable evolution of hydrogen occurs during the deposition of nickel with (210) crystal orientation and small gas bubbles would stick to cathode surface when the deposition is carried out (3-5). Although the above tests for porosity (1) do not give any quantitative estimate of the total area exposed as a result of discontinuities, etc., in the deposits, it is enough to suggest that the dissolution rate (vide Fig. 1 and 2) is not determined entirely by this exposed area, and the crystal orientation might have influenced the results (7-9).

It may be noted that the dissolution behavior as represented in Fig. 1 for (110) and (100) orientations of nickel coating is completely reversed in Fig. 2. This may be due to the adsorption of xylene (in some form or other) on the iron surface during machine polishing and the adsorbed matter could not possibly be removed by washing. Thus during electrodeposition of nickel on such surfaces, the adsorbed matter might have been trapped in the pores or other forms of discontinuities of nickel deposits and hence in the local corrosion cells during dissolution experiments. These trace quantities of trapped impurities (12) might have been responsible for influencing anodic and cathodic processes in each corrosion cell, ultimately giving the reversal effect.

It is well known that different single crystal faces have different electrochemical potentials (5, 6) and hence the oxidation and reduction rates differ considerably between them (7-9). We can visualize the existence of local cells at each pore consisting of large cathodes (oriented nickel) and small anodes (polycrystalline iron). The potentials of such cells are dependent on the orientations of nickel to such an extent as to affect the rate of dissolutions in the order suggested by our results. Further, the significant influence of other textural features as mentioned earlier cannot be ruled out.

Evans (2) pointed out that the combination of a large cathode and small anode gives rise to intense attack by corrosive agents. This will lead to a higher current density in the local corrosion cells favoring the dissolution of iron. In the prevailing stagnant condition of the acid solution in the pore, there will soon arise high anodic polarization due to the accumulation of Fe-ions which will oppose dissolution of iron progressively. Further, owing to the discharge of hydrogen at the cathode the liquid in the nickel/solution interfacial region will tend to be alkaline. Since the anode and the cathode are so near each other, iron/solution interface also will be at a pH much higher than that of the bulk solution. The precipitation of basic salts of iron in the pore thus are facilitated, and this decreases the dissolution rate with time. The absence of any appreciable difference in dissolution behavior of specimens having different crystal orientations in 5% sodium chloride solution in contrast with their behavior in dilute hydrochloric acid solutions may be attributed to the instantaneous formation of a protective oxide coating on the exposed areas in presence of neutral solution in the pores.

Acknowledgments

The author expresses his gratitude to Dr. A. B. Biswas for various suggestions and encouragements during the progress of the work and to Drs. A. P. B. Sinha, M. K. Gharpurey, and Hira Lal for stimulating discussions.

Manuscript received May 28, 1959.

Any discussion of this paper will appear in a Discussion Section to be published in the December 1960 JOURNAL.

REFERENCES

1. W. Blum and G. B. Hogaboom, "Principles of Electroplating and Electroforming," 3rd Ed., pp. 141 and 104, McGraw-Hill Book Co., New York (1949).
2. U. R. Evans, "An Introduction of Metallic Corrosion," Edward Arnold and Co., London (1950).
3. B. C. Banerjee and A. Goswami, *J. Sci. Ind. Res. (India)*, **14B**, 322 (1955).
4. B. C. Banerjee and A. Goswami, *This Journal*, **106**, 20 (1959).
5. H. Leidheiser, Jr., and A. T. Gwathmey, *Trans. Electrochem. Soc.*, **91**, 95 (1947).
6. W. E. Tragert and W. D. Robertson, *This Journal*, **102**, 86 (1955).
7. F. W. Young, Jr., J. V. Cathcart, and A. T. Gwathmey, *Acta Met.*, **4**, 145 (1956).
8. K. R. Lawless and A. T. Gwathmey, *ibid.*, **4**, 153 (1956).
9. "Semiconductor Surface Physics," R. H. Kingston Editor, p. 336, University of Pennsylvania Press (1956).
10. A. Vogel, "A Textbook of Quantitative Inorganic Analysis, Theory and Practice," p. 702, Longmans, Green and Co., London (1943).
11. A. L. Rotinyan, *et al*, *J. Appl. Chem. (U.S.S.R.)* (English edition), **30**, 756 (May 9, 1957).
12. B. C. Banerjee and A. Goswami, *J. Sci. Ind. Res. (India)*, **16B**, 144 (1957).

The Kinetics of the Corrosion of Low-Hafnium Zirconium in Aqueous Sulfuric Acid Solutions

Tennyson Smith

Atomics International, Canoga Park, California

ABSTRACT

The rates of corrosion of low-hafnium zirconium in aqueous sulfuric acid solutions, over the concentration range 9-97% by weight, have been studied. Corrosion was detected by measuring the concentration of zirconium in solution with a radioactive tracer, Zr^{95}. The samples first were etched in an aqueous hydrofluoric-nitric acid solution, then placed directly into the sulfuric acid solution. The initial corrosion followed a parabolic rate law which was followed by a constant rate. Corrosion during the constant reaction rate period was faster, by an order of magnitude or more, than rates reported in the literature (1-4) for unetched samples under similar conditions. This is thought to be due to the removal of the protective oxide film on etching and the subsequent growth of some less protective film in the sulfuric acid solution.

The corrosion rate was found to be first-order with respect to undissociated sulfuric acid over the concentration range 0.2-9M, "undissociated sulfuric acid," [31.4 to 81.1% H_2SO_4 by weight (5)]. An equation relating the corrosion rate and the concentration of undissociated sulfuric acid at 44°C and with pre-etching, is: $R = 4.0 \times 10^{-5} \times (H_2SO_4) + 1.0 \times 10^{-5}$, g cm^{-2} hr^{-1}. An approximate value for the activation energy determined over the temperature range 20°-72°C, is 7-8 kcal $mole^{-1}$. A discussion of possible mechanisms is given with suggestions for further research.

This paper reports the second part of a study to elucidate the kinetics of the corrosion of low-hafnium zirconium in aqueous acid solutions. Part one of this study has been reported previously (6) and concerned the dissolution of zirconium in aqueous hydrofluoric acid solutions.

Little has been reported in the literature about the kinetics of the corrosion of zirconium. Most of the work has been reported as engineering data, that is, spot checks at various temperatures and acid concentrations. The work reported here, although preliminary in nature, throws light on the mechanism of the corrosion of zirconium in sulfuric acid solutions and points the way to further experimentation.

To help understand the mechanism of the corrosion phenomenon, it is important to know the concentrations of the various species in solution. Much work has been done to identify the species present in aqueous sulfuric acid solutions. Most of the work has been done with the use of Raman spectra. It has been found that different species have characteristic lines, which are peculiar to them alone, the intensity of which is proportional to the concentration. Although most of the work has been concerned with identifying the Raman spectra with the individual species, two publications have been made which report the concentrations of the various species (H^+, $SO_4^=$, HSO_4^-, and undissociated H_2SO_4, hereafter represented as H_2SO_4) as a function of the stoichiometric sulfuric acid concentration. In 1949, Young and Blatz (5) reported calculations, based on the work of Rao (7), of the specific concentration of H^+, $SO_4^=$, HSO_4^-, and H_2SO_4 in aqueous sulfuric acid solutions. In 1951, Young (8) reported later work on the concentrations of these species.

The following reaction rate data are analyzed in terms of the specific concentrations of the various species in solution.

Experimental Procedure

Low-hafnium zirconium samples 5 x 5 x 0.32 cm had been irradiated with neutrons at the Oak Ridge National Laboratory. The isotope Zr^{95} (half life 65 days) was used as a tracer in these experiments. A detailed description of the zirconium history and the isotope detection apparatus is given in a previous paper (6). In brief, weighed samples were taken from the zirconium plates and were dissolved in hydrofluoric acid solutions. These solutions were used as standards for comparison with unknown concentrations of zirconium in solution. The apparatus, which continuously recorded the zirconium concentration in the hydrofluoric acid work (6), was not used because of the extremely slow corrosion rates in sulfuric acid below 80%.

The solutions were made with conductivity water and reagent grade sulfuric acid. All concentrations recorded in per cent refer to per cent by weight.

Four zirconium samples were suspended by polyethylene strings in four separate beakers which were in a constant temperature bath. Each beaker contained 750 ml of the appropriate sulfuric acid solution. Initial experiments showed that the corrosion of unetched zirconium samples in aqueous sulfuric acid solutions was too slow to be studied in the time available with the proposed experimental technique. Even samples that had been etched in aqueous hydrofluoric acid solutions, then rinsed in distilled water, corroded very slowly. Except for a few initial experiments, the zirconium samples were first etched for 1 min in a 4% hydrofluoric, 30% nitric acid, aqueous solution to remove any oxide film. The sample was then placed immediately into the sulfuric acid solution. Experiment showed that a sample etched then placed immediately into water put about 1 x 10^{-4} g of zirconium in solution as reaction products from the etchant. After placing samples in the sulfuric acid solution, samples of the solution were taken immediately and at regular time intervals and counted in the scintillometer. The amount of zirconium (1 x 10^{-4} to 2 x 10^{-4} g) in the first solution-sample then was subtracted from subsequent measurements, to determine the amount of corrosion.

In many of the initial experiments the solution was stirred at various rates (stirrer speed 0 to 1500 rpm), since no effect from stirring could be detected over the concentration and temperature range of the experiments stirring was discontinued.

Results

Figures 1, 2, and 3 show a few examples of 42 experiments that were made over a range of 9 to 97% sulfuric acid. Figure 1 shows the amount of zirconium that dissolved in a 16.9% solution of sulfuric acid as a function of time. Nine independent experiments were made at this concentration. Experiments 1, 2, 3, and 4 in Fig. 1 illustrate a phenomenon that occurred only a few times during the study, that of a sudden increase in the rate, or break away for a period of time, after which the corrosion rate returned to approximately the original value. These four experiments were started at the same time and were all in the same constant temperature bath. For simplicity, only curves showing trends are drawn through the points.

Figure 2 illustrates the shape of the curves that resulted when the weight of dissolved zirconium vs. time was plotted for 24.4% sulfuric acid solutions at 44°C. In most of the experiments, a constant rate was observed after the initiation period.

Figure 3 shows a plot of the corrosion of zirconium in 31.4% and 55% sulfuric acid over a period of 800 hr. The temperature was changed during some of the experiments to find the effect on the reaction rate. It is seen that the corrosion of zirconium in sulfuric acid, under the conditions of these experiments, is linear with respect to time over long periods.

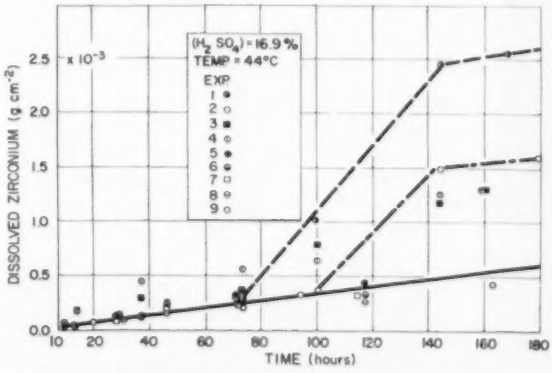

Fig. 1. Dissolved zirconium vs. time for a 16.9% sulfuric acid solution at 44°C. Shows break-away phenomenon.

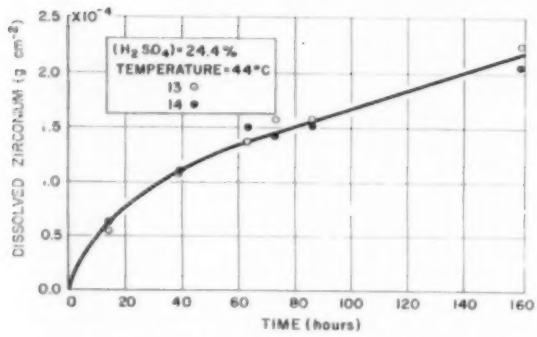

Fig. 2. Corrosion of zirconium in a 24.4% sulfuric acid solution at 44°C. Initial reaction follows the parabolic rate law.

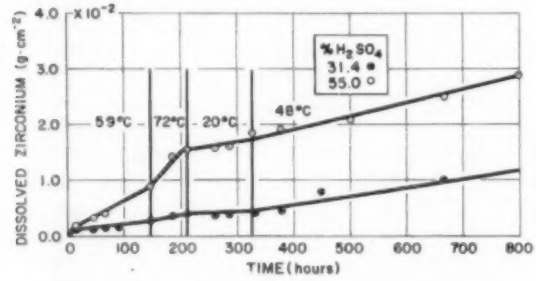

Fig. 3. Corrosion of zirconium in a 31.4 and 55% sulfuric acid solution, as a function of time and temperature.

Figure 4 is an Arrhenius plot for two experiments, one at 31.4% and the other at 55% sulfuric acid. An estimate of the activation energy from the experiment at 31.4% and 55% is about 7-8 kcal/mole.

Recorded in Table I is the rate of corrosion of zirconium at various concentrations of sulfuric acid, in weight per cent. The molarity of the sulfuric acid and the corresponding concentrations of the H^+, HSO_4^-, $SO_4^=$, and H_2SO_4 also have been recorded. These concentrations were estimated from the data given in the two reports by Young and Blatz (5) and Young (8) mentioned above.

Corrosion in solutions 9% or less was too slow to be detected in the time of the experiments. Between

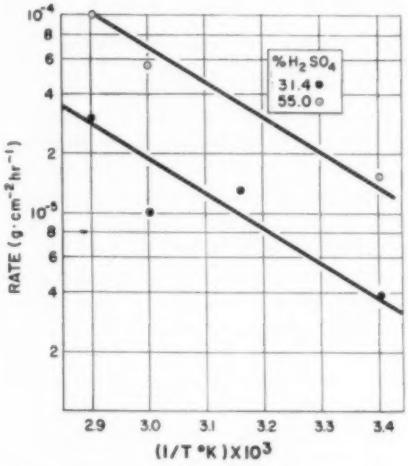

Fig. 4. An Arrhenius plot for zirconium corrosion in a 31.4 and 55% sulfuric acid solution.

9 and about 80% sulfuric acid the reaction rate was rapid at first then slowed down with time to a steady state. The samples had a clean metallic appearance while corrosion occurred, but were not bright. They appeared to have a very thin film that dulled their luster. At higher concentrations (around 80% or above) a white layer formed; some of this was scraped off and analyzed by x-ray diffraction. The x-ray diffraction pattern matched that of zirconium disulfate tetrahydrate as reported by Startzky and Singr (9) and also later by the National Bureau of Standards (10). At the highest concentrations (above 80%) the reaction rate was very fast and not reproducible. Black films formed that spalled and flaked off. The black material proved to be amorphous, giving broad peaks on x-ray analysis; many of the major peaks matched well in "d" value with those reported for ϵ zirconium hydride (ϵ-ZrH) by Hagg (11).

A weighed sample of zirconium turnings was reacted to completion in 96% sulfuric acid; the gas that evolved was collected and tested by infrared spectroscopy and by Orsat analysis. The gas proved to be

Table I. Corrosion rate of zirconium in sulfuric acid solutions as a function of concentration at 44°C

H_2SO_4, % by wt	Stoichiom conc. H_2SO_4, M	(H^+) M		$(SO_4^=)$ M		(HSO_4^-) M		(H_2SO_4) M		Rate‡ g cm⁻² hr⁻¹ x 10⁻⁴	Rate, mdd
		*	†	*	†	*	†	*	†		
16.9	1.87	2.6	1.9	0.6	0.1	1.4	1.7	—	0.08	0.033	7.9
24.4	2.80	3.8	2.7	0.9	0.1	2.0	2.5	—	0.18	0.086	20.6
31.4	3.74	5.0	3.6	1.2	0.2	2.6	3.2	—	0.29	0.230	55.2
37.9	4.67	6.2	4.4	1.5	0.2	3.2	4.0	—	0.47	0.230	55.2
44.0	5.61	7.2	5.3	1.6	0.3	4.0	4.7	—	0.67	0.380	91.2
55.0	7.48	9.1	6.5	1.7	0.3	5.7	5.9	—	1.22	0.670	160
64.7	9.35	10.6	7.3	1.4	0.3	7.8	6.7	—	2.35	1.04	250
69.1	10.28	11.2	7.3	1.2	0.3	8.8	6.7	—	3.30	1.46	350
73.3	11.22	12.2	6.8	1.0	0.2	10.2	6.4	—	4.71	2.30	552
77.3	12.15	13.0	5.9	0.8	0.1	11.4	5.7	—	6.53	2.60	624
81.1	13.09	13.6	4.0	0.5	0.0	12.6	4.0	—	8.85	3.60	876
88.0	14.96	12.6	2.6	0.0	0.0	12.6	2.6	2.0	12.50	—	—
94.0	16.83	8.0	1.3	0.0	0.0	8.01	1.3	8.1	15.60	—	—
100.0	18.70	0.0	0.0	0.0	0.0	0.0	0.0	15.0	18.70	—	—

* Concentrations estimated from Fig. 4, Ref. (8).
† Concentrations estimated from Table II, Ref. (5).
‡ Rates were determined over the period 20-100 hr, and are an average of a number of experiments at each concentration.

pure hydrogen; the amount was stoichiometrically correct for the oxidation of zirconium to the +4 state. The product of the reaction in solution would be zirconyl sulfate tetrahydrate according to Blumenthal (12).

To determine if the rate was affected by oxygen concentration, an experiment was conducted for which the solution had been boiled, cooled in an argon atmosphere, and saturated with argon. No change in the rate could be detected by thus changing the oxygen concentration.

Many of the experiments were made stirring the solutions at different rates, but no effect on the reaction rate could be noted.

One experiment was conducted with a solution approximately 1.5% sulfuric acid, for about 3 hr at varying temperature and pressure to see if corrosion would increase appreciably. The temperature ranged from 38° to 177°C and the pressure from 200 to 800 psig. No corrosion could be detected for zirconium in this short time experiment, although the titanium liner of the autoclave showed marked dissolution, forming a blue complex in solution.

Pitting corrosion was not observed during this study.

Discussion

Very low corrosion rates for unetched samples is in accord with rates reported in the literature (1-4), and this is usually ascribed to a protective layer of oxide on the zirconium surface.

To help understand the mechanism by which the reaction between zirconium and sulfuric acid is inhibited, samples were placed directly from the aqueous hydrofluoric acid solution into the sulfuric acid solution. It was felt that in this manner any oxide film adhering to the zirconium would be stripped off in the etchant, leaving a clean surface for the initial corrosion in sulfuric acid. In this way, the growth of any new film could be followed by the rate zirconium dissolved in solution.

Although the reaction during the initial period (20-60 hr) was not very reproducible, the curves generally had the shape as shown in Fig. 2.

A log log plot of the data in Fig. 2 is linear with a slope of 0.5. The initial corrosion follows a parabolic rate law which can be associated then with the growth of a corrosion product film (13).

The greatly increased corrosion rates that followed the initiation period, as compared to rates reported in the literature, indicate that this film is not an oxide film as found on unetched samples, but much more pervious. An attempt to discover the structure or composition of the film by x-ray analysis of the surface of a flat plate of zirconium proved unsuccessful. One can speculate that the composition is similar to that found at the higher acid concentrations, zirconium disulfate tetrahydrate, or zirconium hydride. Another possibility might be the formation of a film with small amounts of fluoride which acts as a catalyst to promote corrosion. The few instances where break-away took place (1, 2, 3, and 4, Fig. 1) may be attributed to the formation of an unstable film which occasionally breaks down, causing higher corrosion rates for a short interval until the film reforms.

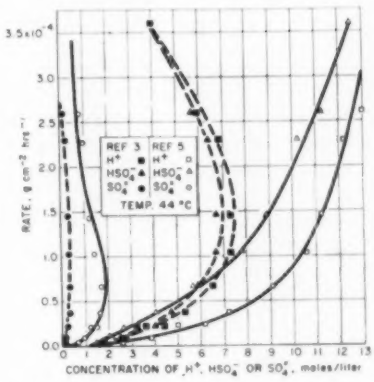

Fig. 5. Rate of corrosion of zirconium as a function of the concentration of H^+, HSO_4^-, and $SO_4^=$ ions.

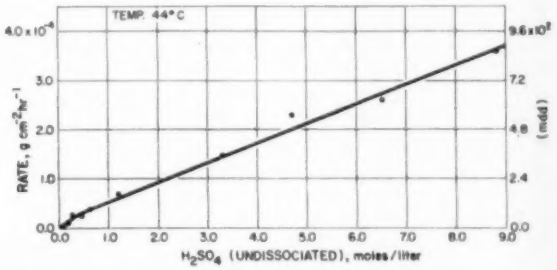

Fig. 6. Rate of corrosion of zirconium at various concentrations of undissociated H_2SO_4.

To find the effect of the individual ionic species on the rate of reaction, the steady-state corrosion rates were plotted as a function of the concentration of the ionic species separately in Fig. 5 and 6. The articles by Young and Blatz (5) and the later article by Young (8) report that, at low stoichiometric sulfuric acid concentrations, the major species are H^+ and HSO_4^-; at high acid concentrations H_2SO_4 increases rapidly. The article by Young and Blatz (5) reports that H^+, HSO_4^-, and $SO_4^=$ go through a maximum starting at a stoichiometric sulfuric acid concentration of about 6 to 7M. The later article by Young (8) gives the maximum for H^+ and HSO_4^- species at a much higher concentration, approximately 14M.

Figure 5 is a plot of the rate as a function of the concentrations of the H^+, $SO_4^=$, and HSO_4^- ions estimated from the two above mentioned articles. It is seen that, if the earlier report by Young and Blatz is correct, the rate is double valued for all of these species, and it can be concluded that the rate is independent of any of them. If the article by Young (8) is correct, the rate is still double valued for the sulfate ion and, although the curves for the H^+ and HSO_4^- ions are not double valued until much higher concentrations are reached, the shapes of the curves are such that it seems unlikely that the rate is a function of these ions in any case.

Figure 6 shows a plot of the rate as a function of the undissociated sulfuric acid concentration, based on the article by Young and Blatz (5). Within experimental error, the rate is directly proportional to the concentration of H_2SO_4. The points in Fig. 6 are

experimental, and the curve is a visual fit of these points.

Although the temperature at which Rao (7) did his work was not reported by him (he mentioned that he cooled his solutions by water), the temperature was probably close to room temperature or not far above this. Young (8) reported his later work was done at 25°C. The solutions used for the experiments reported in Table I were held at 44°C. In view of all the uncertainties involved, the values plotted in Fig. 5 and 6 probably have considerable error; however, the relative values and the shape of the curves should be reliable.

It seems reasonable to conclude that the species that controls the reaction rate is the undissociated sulfuric acid molecule, at least at the higher concentrations, and probably to as low as 0.5M. An equation for the linear portion of the curve in Fig. 6 is: $R = 4.0 \times 10^{-5} (H_2SO_4) + 1.0 \times 10^{-5}$ g cm^{-2} hr^{-1}, where R is the rate in grams of zirconium dissolving into solution per square centimeter of sample per hour.

By way of summary, the following observations have been made: under the conditions of these experiments the initiation reaction usually lasts from 20-40 hr and obeys a parabolic rate law. The initiation reaction is followed by a constant reaction rate which is somewhat higher than for unetched zirconium. The constant reaction rate appears to be a function of the undissociated H_2SO_4 concentration alone and is first order with respect to this species. At 44°C the specific reaction rate constant is 4.0×10^{-5} g cm^{-2} hr^{-1} moles^{-1} liter. The activation energy for the reaction slow step is 7-8 kcal mole^{-1}. No effect on the rate could be detected by stirring the solution or changing the oxygen concentration. No change in the appearance of the samples is detected until the solution becomes saturated with corrosion products, which crystallize as loose white crystals. The samples have a clean metallic appearance while corrosion occurs, but are not bright. They appear to have a very thin film that dulls their luster. Reaction of zirconium in solutions 80% sulfuric acid or higher gives rapidly increasing reaction rates, while loose films are formed that proved to be zirconium disulfate tetrahydrate. At the higher concentrations black films that flaked off are also formed; they are probably partly zirconium hydride. The gaseous reaction product is pure hydrogen; the amount evolved corresponds to that needed for zirconium to be oxidized to the +4 state.

Although these observations do not permit a very detailed account of the corrosion mechanism, they do allow the elimination of many of the possible mechanisms and point to further research which will narrow down the remaining possibilities.

The first order rate dependence on the undissociated sulfuric acid molecule and the low activation energy suggest the slow step to be some physical phenomenon involving this species, such as adsorption or diffusion. The initial reaction which follows a parabolic rate law indicates the growth of a reaction product barrier through which the reactants must diffuse. When the film reaches a limiting thickness, the reaction comes to a steady state as shown by the constant reaction rate which follows the initiation period. Another possibility could be that, as the reaction product film grows, it cracks, exposing only a small portion of the surface to reactants and that after the initiation period, exposure and closing off of reaction surface reaches a steady state.

Further experiments that would help elucidate the mechanism of corrosion of zirconium in sulfuric acid solution could be: electropolish the zirconium samples rather than etch them in hydrofluoric acid; weigh and measure the dimensions of both irradiated and unirradiated samples during corrosion, as a check on the tracer method, to see if irradiation affected the rate, and so that a material balance could be made accounting for the corrosion products that remained on the sample and that which dissolved in solution; investigate the reaction product film that adheres to the zirconium by electron diffraction and chemical analysis, if possible; and investigate the current potential relationships during the dissolution of zirconium in sulfuric acid solutions.

Acknowledgment

This research was supported by a grant from the Atomic Energy Commission. This paper was abstracted from a thesis submitted to the faculty of the University of Utah, Dept. of Fuel Technology, in partial fulfillment of the requirement for a Ph.D. degree, June 1956.

Manuscript received March 19, 1959.

Any discussion of this paper will appear in a Discussion Section to be published in the December 1960 JOURNAL.

REFERENCES

1. B. Lustman and F. Kerze, Jr., "The Metallurgy of Zirconium," McGraw-Hill Book Co., New York (1955).
2. L. B. Golden, "Zirconium and Zirconium Alloys," p. 305, American Society for Metals, Cleveland, Ohio, May (1953).
3. R. J. Gegner and W. L. Wilson, "The Corrosion Resistance of Titanium and Zirconium in Chemical Plant Exposures," Paper presented at the 15th annual conference, N.A.C.E., Chicago, Illinois, March 12-20, 1959.
4. W. E. Kuhn, "More Zr Facts", Col. 1, No. 2, p. 5, (1957), Publication of the Carborundum Metals Co., Akron, New York.
5. T. F. Young and L. A. Blatz, *Chem. Rev.*, **44**, 102 (1949).
6. T. Smith and G. R. Hill, *This Journal*, **105**, 117 (1958).
7. N. R. Rao, *Indian J. Phys.*, **14**, 143 (1940).
8. T. F. Young, *Record Chem. Prog.*, **12**, 81 (1951).
9. E. Startzky and J. Singr, *Anal. Chem.*, **28**, 553 (1956).
10. Nat. Bur. Standards *Circular* 539, **7**, p. 66 (1957).
11. G. Hagg, *Z. Phys. Chem.*, **11**, 433 (1930).
12. W. B. Blumenthal, *Ind. Eng. Chem.*, **46**, 528 (1954).
13. H. H. Uhlig, Editor, "The Corrosion Handbook," John Wiley & Sons, Inc., New York (1948).

The Relationship between Brightness and Structure in Electroplated Nickel

R. Weil and R. Paquin

Department of Metallurgy, Stevens Institute of Technology, Hoboken, New Jersey

ABSTRACT

Nickel deposits of various brightnesses were plated from Watts baths containing several different addition agents. The as-plated surfaces of the deposits were examined by electron microscopy. All bright deposits had a very fine-grained structure. However, some fine-grained deposits showed surface crevices and were therefore not bright. A linear relationship between the fraction of the surface area having a roughness less than 0.15 μ and the logarithm of light reflected as measured with a photocell was found. There is no direct relationship between the degree of preferred orientation and brightness, but the fiber axis is related to the type of structure observed, i.e., platelet, equiaxed crystallite, or spiral-type, and the addition agents in the plating bath.

The relationship between the light-reflecting property generally referred to as the brightness and the structure of electrodeposits has been the subject of many investigations. These studies have led to two theories. One theory advanced by Kohlschütter (1), Liebreich (2), and others states that electrodeposits are bright if their microstructure consists of crystallites smaller than the wave lengths of visible light, i.e., smaller than 0.4 μ. However, Read and Weil (3) and Denise and Leidheiser (4) have shown that not all very fine-grained deposits are bright.

The second theory which, among others, Hume-Rothery and Wyllie (5) and Blum, Beckman, and Meyer (6) have formulated, states that the more oriented the grain structure, the brighter the deposit. Smith, Keeler, and Read (7) and Denise and Leidheiser (4) found this relationship not to hold.

Therefore, the need for further study to determine what structural features determine brightness was indicated and this investigation was undertaken.

Experimental Procedure

Nickel electrodeposits having a range of brightnesses from dull gray to specular were plated from Watts baths containing the various addition agents listed in Table I. The baths were agitated by pumping solution from the region near the cathode into the anode bag, which also served as a filter. Three deposits were plated from each bath to a thickness of about 50 μ; for two deposits, the starting cathode was electropolished copper sheet and for the third, mechanically polished, mild steel.

The microstructures of the as-plated surfaces were examined by electron microscopy. Collodion replicas made in the manner described by Weil and Read (8) and carbon replicas prepared according to the method of Grube and Rouze (9) were used. In view of the claims found in the literature (10) that the microstructure of bright deposits cannot be resolved by electron microscopy, a thin surface layer of the deposit was examined directly in order to eliminate possible extraneous structural features resulting from shadowing or the replicating medium.

The thin surface layers were obtained by partially immersing one of the deposits plated on copper sheet in a copper-cyanide bath immediately after removal from the nickel-plating bath and rinsing in water. A copper layer approximately 1000Å thick was deposited. After rinsing again, part of the copper-plated nickel deposit was immersed again in the

Table I. Plating conditions and addition agents

Bath composition: 400 g/l $NiSO_4 \times 6H_2O$, 45 g/l $NiCl_2 \times 6H_2O$, 45 g/l H_3BO_3
Plating conditions: pH:4.0; temperature 60° ±2°C, current density 5 amp/dm²

Specimen No.	Addition agent
3000	None
3001	0.2 g/l 1-5 Naphthalene disulfonic acid
3002	0.4 g/l 1-5 Naphthalene disulfonic acid
3003	0.6 g/l 1-5 Naphthalene disulfonic acid
3004	0.6 g/l 1-5 Naphthalene disulfonic acid + 0.2 g/l chloral hydrate
3005	0.6 g/l 1-5 Naphthalene disulfonic acid + 0.6 g/l chloral hydrate
3006	1.0 g/l 1-5 Naphthalene disulfonic acid + 0.6 g/l chloral hydrate
3007	0.2 g/l p-Toluene sulfonamide
3008	0.6 g/l p-Toluene sulfonamide
3009	0.6 g/l p-Toluene sulfonamide + 0.2 g/l chloral hydrate
3010	0.6 g/l p-Toluene sulfonamide + 0.6 g/l chloral hydrate
3011	1.0 g/l Zinc + 0.6 g/l 1-5 naphthalene disulfonic acid
3012	1.0 g/l Zinc + 1.0 g/l 1-5 naphthalene disulfonic acid
3013	0.09 g/l Aniline
3014	0.18 g/l Aniline
3015	0.31 g/l Benzoic acid
3016	0.08 g/l Saccharin
3017	0.20 g/l Saccharin
3018	0.40 g/l Saccharin
3019	0.60 g/l Saccharin
3020	Harshaw Chemical Co. Nubrite addition agents

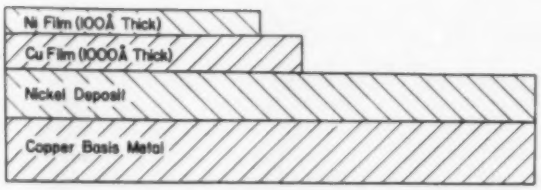

Fig. 1. Schematic representation of deposits for obtaining transparent nickel films.

original nickel bath and a thin nickel film, approximately 100Å thick, plated over the copper layer. Thus, the surface of this sample consisted partly of the original nickel plate, partly of the thin copper layer, and partly of the second nickel deposit as schematically represented in Fig. 1. Collodion replicas from the surfaces of the original nickel deposit, the copper film, and the nickel film were examined electron microscopically as were carbon replicas from the original nickel deposit and the nickel film. The purpose of these examinations was to determine if the nickel and copper films had copied the structure of the original nickel deposit. When this was found to be so, the nickel film was stripped by dissolving the copper layer in an aqueous solution of 50 g/l H_2SO_4 and 500 g/l CrO_3.

The light-reflecting properties of the deposits were determined by directing a beam from a zirconium arc through a slit onto the specimen and measuring the reflected light with a photocell. The incident beam made an angle of 10° with the normal to the sample and the photocell was placed along a line 10° to the normal on the other side. The brightnesses of the three areas of the sample represented in Fig. 1 as well as of the other two deposits were measured. In spite of the polishing there were some irregularities in the starting-cathode surface which resulted in lower brightness measurements. Therefore, the maximum reading is recorded in Table II. The various deposits also were arranged in five classifications of brightness as judged by eye. These data are also included in Table II. The order of brightness by eye evaluation, with one exception, was the same as that obtained with photocell measurements.

Table II. Experimental results

Specimen No.	Quantity of light reflected, ft. candles	Eye evaluation brightness group*	Percentage of area with roughness less than 0.15μ	Fiber axis‡
3000	4.5	I	7.4	(100)s
3001	47.5	IV	86.4	(311)+(111)w
3002	58.5	IV	93.4	(311)+(111)w
3003	58.5	IV	95.5	(311)+(111)w
3004	95.0	V	99.7	(100)s
3005	28.0	II	66.8	(100)s
3006a†	80.0	V	81.1	(100)s
3006b†	43.0	IV	100	(100)s
3007	53.5	IV	86.2	(100)s
3008	48.5	IV	84.5	(100)vs
3009	50.0	IV	84.9	(100)vs
3010	50.0	IV	84.0	(100)vs
3011	66.0	IV	93.4	(311)+(111)w
3012	>100	V	99.4	(311)+(111)w
3013	4.0	I	2.8	(110)m
3014	4.0	I	3.4	(110)m
3015	6.3	II	19.4	(110)m
3016	13.0	II	41.0	(100)m
3017	35.0	III	74.1	(100)s
3018	29.0	III	69.2	(100)s
3019	25.0	III	65.0	(100)s
3020	>100	V	100	(311)+(111)w

* Brightness increases with group number.
† Part of deposit was hazy (a), part bright (b).
‡ s = strong, vs = very strong, m = medium, w = weak.

The fiber axis of the deposits was determined by x-ray diffraction. The nickel deposit first was stripped off the copper basis-metal by dissolving the copper in the sulfuric acid-chromium oxide mixture mentioned previously. The nickel deposit was bent into a convex shape through an arc of a circle of 10 cm radius and an x-ray beam was directed along its surface. The results of these determinations are recorded also in Table II.

For reasons which will be explained later, measurements to determine the fraction of the surface area which had a roughness less than 0.15 μ were made on electron photomicrographs of collodion replicas. Polystyrene latex spheres which were 0.514 μ ±0.011 μ in diameter, obtained from the Dow Chemical Company, Midland, Michigan, were placed on the replicas and palladium evaporated on them subsequently. The heights of the various structural components were determined from the ratio of their shadows to those of the latex spheres. The area occupied by those components of the structure more than 0.15 μ above or below the surface then was measured with a planimeter and the value subtracted from the total area of the photograph in order to get that fraction of the whole surface which was reflecting light. The results of these measurements also are included in Table II.

Experimental Results

Three structural types corresponding to the three different fiber axes were observed in the deposits plated in the baths containing the various addition agents. The type of structure was affected by the addition agent, but the structures of all deposits plated from a given bath were the same regardless of the basis metal.

The deposits having a (100) fiber axis[1] were found to consist of platelets. A number of platelets were stacked parallel to each other and comprised a colony. In most of the deposits exhibiting this type of structure, a depression in the surface resembling a grain boundary existed between colonies of platelets. The thickness and the spacing of the platelets within a colony varied widely between deposits from different baths. Figure 2 shows coarsely spaced and relatively thick platelets and a large colony size. Figure 3 shows a finer spacing and a smaller colony size. A structure with still finer platelets, although possessing a larger colony size than shown in Fig. 3, can be seen in Fig. 4. The x-ray diffraction patterns of the structures with the (100) fiber axis showed the anomalous intensity maximum at the meridian which Clark and Simonsen (11) explained on the basis of a twinning relation between the platelets. Structures with platelets were found in deposits

[1] The term, fiber axis is used here in the same sense as in Ref. (7).

Fig. 2. Electron micrograph of nickel deposit showing coarse platelets and large colony size.

Fig. 3. Electron micrograph of nickel deposit showing medium-fine platelets and small colony size.

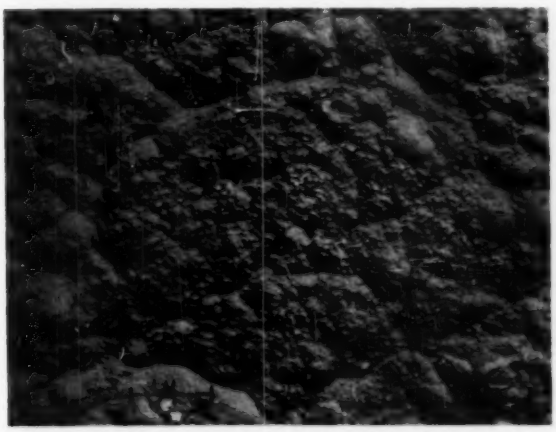

Fig. 4. Electron micrograph of nickel deposit showing fine platelets, but large colony size.

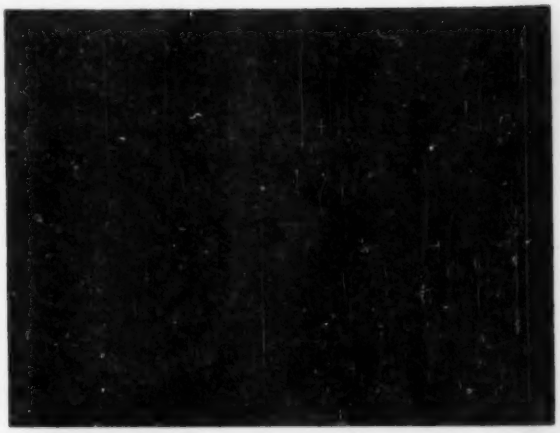

Fig. 5. Electron micrograph of specular nickel deposit

Fig. 6. Electron micrograph of hazy nickel deposit showing fine-grained structure with crevices.

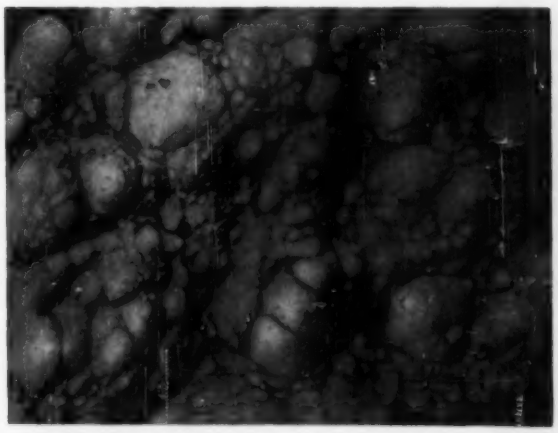

Fig. 7. Electron micrograph of dull nickel deposit showing spiral-type growth.

from plain Watts bath and from baths with chloral hydrate, p-toluene sulfonamide, and saccharin additions.

The second structural type, which was associated with a (311) + (111) fiber axis, consisted of fine crystallites which appeared equiaxed in the surface plane of the deposits. Most of the bright deposits exhibited this type of structure, but so did some hazy ones. Figure 5 shows the structure of a specular deposit as seen by transmission through the thin nickel surface film. In hazy deposits with this type of structure, depressions in the surface were observed. These depressions appear as dark areas in Fig. 6, which is an electron micrograph of a negative collodion replica, shadowed with palladium. The raised portions in

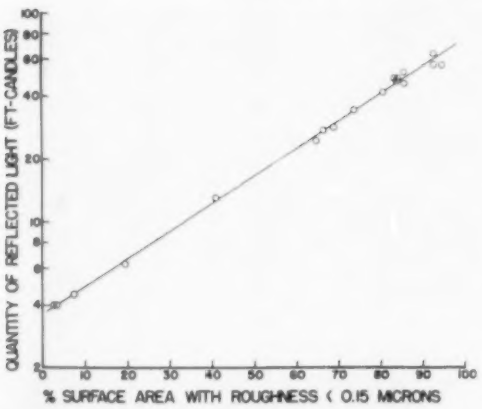

Fig. 8. Relationship between amount of light reflected and the fraction of the area with roughness less than 0.15 μ.

the replica result from depressions in the surfaces of the electrodeposit. Baths containing naphthalene disulfonic acid without chlorate hydrate and the bath containing the Harshaw Chemical Company proprietary brightener resulted in deposits of the second type.

Spiral growth was found in electrodeposits having a (110) fiber axis. This structure, represented by Fig. 7, was found in nickel plated from Watts baths containing aniline and benzoic acid. It is noteworthy that some deposits plated in an all-chloride bath without additives in connection with some other work performed by a graduate student at this institution also showed spiral-type growth. These deposits were found to have a (110) fiber axis. Banerjee and Goswami (12) reported the same preferred orientation under the same plating conditions. All deposits of this type were dull.

In attempting to relate microstructure and brightness, it was noted that all bright nickel samples in addition to having very small structural components also showed no crevices, deep grain boundaries, or protrusions which extended more than 0.15 μ from the surface plane. It therefore was assumed arbitrarily that only that fraction of the surface area with a roughness less than 0.15 μ specularly reflects light. This light-reflecting area was measured in the way previously described. A graph of brightness vs. fraction of surface area with a roughness less than 0.15 μ is shown in Fig. 8.

Discussion

It is apparent from Fig. 8 that the brightness depends on the degree to which the structural components of the surface of electrodeposits are in one plane. This, in turn, is determined by several factors such as grain size and orientation, the degree of preferred orientation, and codeposition of foreign substances. The grain size is important because the boundaries between large grains appear as deep crevices in the surface of electrodeposits. Structures composed of large platelets will show coarse steps between the plates. It is therefore necessary for bright deposits to be very fine-grained. However, it is also apparent from data in Table II that a small grain size is not a sufficient condition for brightness. The deposits showing spiral-type structures were dull even though some were fine grained because this type of growth results in crystals which have no light-reflecting plane parallel to the surface and consequently the tops of the grains protrude above the intergranular crevices. The orientation of the crystals which determines whether a light-reflecting plane is parallel to the surface therefore affects the brightness.

The size of the crevice between neighboring grains is certainly influenced by their relative orientations. It is expected that a group of crystallites with a common fiber axis would have very small crevices between them. As the degree of preferred orientation is only one of several factors which determines the surface roughness, it is not to be expected that there is a unique relationship between preferred orientation and brightness. Certainly, the findings previously cited (4, 7) that preferred orientation is not proportional to brightness have been substantiated. Even for a given fiber axis, no direct correlation has been found.

The smoothness of the surface has been shown by Beacon and Riley (13) to be dependent on the distribution of addition agents. By means of brighteners containing a radioactive atom, they showed that preferential codeposition takes place at protrusions, hindering crystal growth at these sites and thereby tending to eliminate the crevices. This could explain why there were no depressions in the surface with certain addition-agent concentrations.

The scatter of data for high light-reflecting values in Fig. 8 is probably due to the fact that, when most of the area has a roughness less than 0.15 μ, smaller changes in the morphology of the surface become significant. The photocell was also not as accurate at high light intensities as at lower ones. In the deposits with over 99% of their area having a roughness less than 0.15 μ, an increase in brightness and decreasing grain size was noted. The number of samples was not sufficient to definitely establish a relationship between brightness and grain size.

Conclusions

1. A direct relationship exists between the fraction of the surface roughness less than 0.15 μ and brightness in electroplated nickel.

2. The observations of others that fine-grained deposits need not be bright have been confirmed and explained.

3. A correlation between type of microstructure and fiber axis has been found.

4. There is no unique relationship between brightness and the degree to which the fiber axis is parallel to the corresponding crystallographic direction in each grain of the deposit.

Acknowledgments

Professor Harold J. Read of the Pennsylvania State University and Professors Alfred Bornemann and Theodore Gela of Stevens Institute of Technology read the manuscript and made valuable suggestions.

The work described in this paper was sponsored by the Office of Ordnance Research, U. S. Army.

Manuscript received Aug. 10, 1959. This paper was prepared for delivery before the Columbus Meeting, Oct. 18-22, 1959.

Any discussion of this paper will appear in a Discussion Section to be published in the December 1960 JOURNAL.

REFERENCES

1. V. Kohlschüter, *Trans. Electrochem. Soc.*, **45**, 229 (1924).
2. E. Liebreich, *Trans. Faraday Soc.*, **31**, 1188 (1935).
3. H. J. Read and R. Weil, *Plating*, **37**, 1239 (1950).
4. F. Denise and H. Leidheiser, Jr., *This Journal*, **100**, 490 (1953).
5. W. Hume-Rothery and H. R. Wyllie, *Proc. Royal Soc. (London)*, **181A**, 331 (1943).
6. W. Blum, A. O. Beckman, and W. R. Meyer, *Trans. Electrochem. Soc.*, **30**, 249 (1941).
7. W. Smith, J. H. Keeler, and H. J. Read, *Plating*, **36**, 355 (1949).
8. R. Weil and H. J. Read, *Metal Finishing*, **53**, [11], 60 (1955).
9. W. L. Grube and J. R. Rouze, *Proc. ASTM*, **52**, 573 (1952).
10. K. M. Gorbunova, J. Popova, A. A. Sutyagina, and V. M. Polukarvo, "Crystal Growth, Report of First Conference, 1956," p. 46, Consultants Bureau (English Transl.), New York (1958).
11. G. L. Clark and S. H. Simonsen, *This Journal*, **98**, 110 (1951).
12. B. C. Banerjee and A. Goswami, *ibid.*, **106**, 21 (1959).
13. S. E. Beacon and B. J. Riley, *General Motors Engrg. J.*, **6**, [2], 21 (1959).

The Adhesion of Electrodeposited Nickel to Chromium at Elevated Temperatures

Walter E. Reid, Jr. and Fielding Ogburn

Chemistry Division, National Bureau of Standards, Washington, D. C.

ABSTRACT

The use of a composite coating of electrodeposited nickel and chromium to protect molybdenum from oxidation at elevated temperatures has certain practical limitations. Examination of the composite coating showed that the problems of blister formation, weakening of the bond between nickel and chromium, and edge separation were interrelated. Blister formation was eliminated and edge separation reduced slightly by an improved treatment of the chromium surface prior to nickel plating. The weakening of the bond between nickel and chromium appears to be inherent in the coating system.

The application of a composite coating of electrodeposited nickel and chromium to protect molybdenum from oxidation at elevated temperatures has been described by Couch and co-workers (1). The use of this coating at elevated temperatures (800°-1200°C) has associated with it certain problems caused by the difference in the properties of the metals involved. Heating and thermocycling tests of the composite coating showed that (*a*) heating to 800° or 1000°C frequently, but not consistently, resulted in the formation of blisters between the chromium and nickel layers, (*b*) prolonged heating weakened the bond between the nickel and chromium layers, and (*c*) thermocycling between room temperature and 800° or 1000°C caused a separation of the nickel from the chromium, principally at sharp edges or corners.

An investigation of these three closely interrelated problems was necessary, since they represent practical limitations to the use of the coating system.

Blister Formation

Blister formation was observed on a number of specimens, electroplated with 0.007 in. of nickel over 0.001 in. of chromium, after they had been heated in a helium atmosphere to 850°C. These had been plated by the procedure described by Couch and co-workers. Examination of the blisters revealed that they always formed within the nickel-chromium diffusion alloy and not at the original nickel-chromium interface. Both nickel and chromium were detected chemically on the entire inner surface of the blister. Also the occurrence of blisters usually was accompanied by poor adhesion of the nickel to chromium on other parts of the specimen where blistering had not occurred.

Since blister formation is often caused by improper cleaning prior to plating, we examined a number of modifications in the plating cycle between the chromium and Watts nickel plating steps. Modifications included anodic and cathodic treatment of the chromium surface in different solutions, elimination of the water rinse, variation of current density for the nickel strike, and the immersion time in the nickel strike bath prior to electroplating.

The only change which eliminated blistering was the substitution of anodic etching in an acetic acid solution for the hydrochloric acid etch.

Acetic Acid Etch

Glacial acetic acid, to which had been added 10 to 15% H_2SO_4 by volume to increase the conductivity, constituted the etch solution. An inert cathode was used. Specimens were etched anodically in the solution at current densities of 3-7 amp/dm^2 until the surface of the chromium was covered uniformly with

a dark brown film. They were rinsed rapidly in water and placed in the Wood's nickel bath with electrical contact made beforehand so that plating began as the specimen was immersed. The specimens were plated at 25-30 amp/dm^2 for 2 to 4 min, then transferred directly to a Watts nickel bath.

A brief study of the etching process showed that an etching time of 5 min at 4 amp/dm^2 was usually sufficient. The time of exposure of the specimen to air after the water rinse and prior to insertion of the specimen into the Wood's nickel strike bath was not critical as long as it was brief and the specimen did not become dry. After adoption of this etch procedure in the plating cycle, blister formation was not encountered.

Adhesion

No difficulty was encountered with the adhesion of nickel to chromium in the "as plated" condition when either the plating procedure described by Couch and co-workers (1) or the acetic acid etch was used.

Heat treatment, however, caused a weakening of the bond between the chromium and nickel. This occurred when the nickel-chromium plated specimens were heated to 850°C in helium and held at this temperature for 1 hr. Very good adhesion was obtained with the acetic acid etch of chromium, even after extension of the heat treatment to 24 hr or with thermocycling (10 min in oven at 850°C, 10 min at room temperature) in air for 24 hr. Only a few such specimens were subjected to these more severe tests, but each one retained good bonding between the chromium and nickel.

A still more severe heat treatment of the same specimens, either at higher temperatures or for longer periods, resulted in a weakened bond. Thus, while it has been possible to improve the performance of the coating system with respect to bond failure, the problem still exists for prolonged heating at higher temperatures.

To gain additional insight into the weakening of the bond, a few experiments were conducted with short lengths of chromium plated nickel rods which were heat-treated to alloy the chromium and nickel. Additional nickel was plated over the chromium to serve as a grip for the measurement of the bond strength between the chromium and nickel rod by the Ollard method. Duplicate specimens were heated in helium at 850°C for 24 and 66 hr and compared with duplicate specimens in the as-plated condition. While the bond strength measurements were not highly reproducible, they showed a reduction in bond strength of 75 to 90%. This shows that bond strength is lost on heating when chromium is plated on nickel, just as when nickel was plated on chromium in the earlier experiments. Hence, it would appear that deterioration of the bond is an inherent property of the nickel-chromium system no matter how the nickel-chromium interface is prepared and is the result of the interdiffusion of nickel and chromium. The diffusion process leads to the formation of a weak layer which becomes the plane of separation. This weak layer could be simply an alloy of low tensile strength. It could also consist of a line of voids formed by the diffusion process (2) or a line of inclusions as observed by Couch and co-workers (1).

In summary, two factors can affect adversely the adhesion of the coating: (*a*) passivity of the chromium surface, and (*b*) alloying of the nickel and chromium. The first can be reduced by proper pretreatment of the chromium, but the second appears to be a property of the coating system.

Adhesion of Chromium to Molybdenum

As indicated above, the problem of blister formation was associated with the deposition of nickel on chromium. Usually, the adhesion of chromium to molybdenum was not a problem; however, an occasional lack of adhesion was encountered.

In the anodic etching of molybdenum in the sulfuric-phosphoric acid solution prior to plating, the metal becomes covered with a viscous film which is not entirely removed by simple rinsing in water. It was found that a subsequent short immersion in an acidified chromic acid solution (3) resulted in excellent adhesion. The composition of the immersion solution is given below. Other compositions were not considered, since no case of poor adhesion was encountered after adoption of this cleaning procedure.

Procedure.

1. Clean and anodically etch molybdenum in 1:1 H_2SO_4 (95%)-H_3PO_4 (85%) at 5-20 amp/dm^2 for 2 to 3 min.
2. Rinse thoroughly in water.
3. Immerse molybdenum for 3 min in an aqueous solution containing: 6% of CrO_3 by weight, 15% of H_2SO_4 by volume, and 15% of concentrated HCl by volume.
4. Rinse thoroughly in water.
5. Place in chromium bath about 30 sec before making electrical contact.
6. Plate in the chromium bath at 120 amp/dm^2 and 80° to 85°C.

"Edge Separation"

The resistance to thermal shock of a number of molybdenum specimens with a composite coating of chromium and nickel was evaluated by thermocycling them in air between room temperature and 800°-1100°C. The thermocycling was accomplished by lowering the specimens into a tube furnace at the desired temperature for 10 min and then withdrawing them to cool for 10 min. This cycle was repeated automatically for the duration of the test.

Microscopic examination of cross sections of specimens which had been cycled 6 times to 800°C revealed a slight parting within the coating in the immediate vicinity of a sharp corner or edge of a rectangular specimen. Specimens cycled for longer periods of time or at higher temperatures showed that the size of the void increased and also extended along the flat surfaces. In an extreme case, the separation of the coating extended over the entire circumference of a rod 0.25 in. in diameter after being cycled 16 times to 1100°C. The coating was intact, but was only very loosely held to the rod.

The "edge separation" always was observed as occurring within the nickel-chromium diffusion al-

loy. In view of this, the phenomenon of "edge separation" may be considered as another manifestation of the problem associated with the formation of a weak layer between the nickel and chromium.

Stresses due to Unequal Expansion of the Metals

A major factor contributing to the deterioration of the bond between the nickel and chromium when plated on molybdenum is the difference in the coefficients of expansion of the three metals. The expansion coefficient for nickel is about 2½ times that for molybdenum. Heating therefore would be expected to cause stresses which would tend to fracture the composite coating, especially where the radius of curvature is small. The equations used by Lander and Germer to explain spalling (4) also can be applied to this problem.

In these equations plastic flow is neglected and it is considered that a cylinder of metal A is plated with a metal B. They give for the normal pressure at the interface

$$P = \frac{2h}{d} (\alpha_B - \alpha_A) E_B t$$

and for the circumferential stress per unit area

$$S = (\alpha_B - \alpha_A) E_B t$$

where*: E is modulus of elasticity; α, coefficient of thermal expansion; d, diameter of cylinder; h, thickness of coating; and t, degrees Centigrade above room temperature. Though these equations do not include all the factors involved, they do help us to understand the stresses involved.

Since initial edge separation is governed by the stresses normal to the surface, the first equation is of primary interest. Consider a molybdenum surface with a radius of curvature of 0.3 in. plated with 0.008 in. of nickel over 0.001 in. of chromium. If this is heated to 800°C, the calculated normal stress is 5200 psi at the nickel-chromium interface and 1000 psi at the chromium-molybdenum interface. Thus the normal stress is greatest at the nickel-chromium interface and is of the order of the nickel-chromium (5) bond strength. The equation leads us to expect coating separation if the radius of curvature is small or the coating is thick.

These predictions are in qualitative agreement with the experimental evidence. Edge separation occurs initially at corners of rectangular specimens where the radius of curvature is small and at the chromium-nickel interface. If the corners are rounded off by increasing the thickness of chromium, edge separation is less likely. For example, two specimens were cycled 50 times to 980°C. One specimen had been plated with 0.004 in. of chromium and 0.006 in. of nickel, and the other with 0.001 in. of chromium and 0.006 in. of nickel. Edge separation occurred to a much greater extent on the specimen with the thinner layer of chromium.

The predicted low normal stress at the chromium-molybdenum interface is also verified by experiments for which rectangular molybdenum specimens were plated with 0.009 in. of chromium. After cycling 50 times to 980°C, no coating separation was observed.

Once the coating separation has been initiated, the analysis of the situation is different. Heating of the specimen causes the loose nickel layer to expand and the result is a high concentration of stress where the nickel joins the underlying metal. This stress concentration causes an extension of the void so that a peeling action of the coating occurs with continued thermocycling.

* The following quantities are used in the present discussion:

$\alpha_{Mo} = 5.5 \times 10^{-6}$/°C
$\alpha_{Cr} = 8.1 \times 10^{-6}$
$\alpha_{Ni} = 13.7 \times 10^{-6}$
$E_{Ni} = 30 \times 10^{6}$ psi
$E_{Cr} = 20 \times 10^{6}$ psi

Acknowledgment

The authors express appreciation to the Navy Department Bureau of Aeronautics, for financial support of the project and for permission to publish the results. Acknowledgment is also made to D. E. Couch and H. Shapiro, who did most of the experimental work on "edge separation."

Manuscript received July 30, 1959.

Any discussion of this paper will appear in a Discussion Section to be published in the December 1960 JOURNAL.

REFERENCES

1. D. E. Couch, H. Shapiro, J. K. Taylor, and A. Brenner, *This Journal*, **105**, 450 (1958).
2. R. S. Barnes and D. J. Mazey, *Acta Met.*, **6**, 1 (1958); R. S. Barnes, *Proc. Phys. Soc.*, **B65**, 512 (1952).
3. *Welding Engineer*, **44**, 41 (1959).
4. J. J. Lander and L. H. Germer, *Metals Tech.*, **14**, No. 2259 (1947).
5. A. Brenner, P. Burkhead, and C. W. Jennings, *Proc. Amer. Electroplaters' Soc.*, **34**, 32 (1947).

Temperature and Space-Charge Effects in Liquid Hydrocarbons

R. Coelho[1] and M. Bono[2]

Laboratory for Insulation Research, Massachusetts Institute of Technology, Cambridge, Massachusetts

ABSTRACT

Preliminary results on the residual d-c conduction and space-charge polarization in n-hexane and n-heptane under highly inhomogeneous field conditions (thin wire in coaxial cylinder) are presented. A residual current is observed under high applied voltage for either polarity of the test cell. At 20°C the current is one order of magnitude larger when the wire is the positive electrode. As temperature is increased, the residual current for the wire positive decreases and for the wire negative increases, until at 50°C it is about the same for both polarities. By heating only the wire, observations supporting and extending these findings were made. The gross features of the current-voltage characteristics can be explained by dissociation of polar impurities in the region of high field strength. The dependence on polarity can be explained by space-charge distortion of the field. For negative wire, field emission appears to occur from the wire, surrounding it with a current-limiting space charge.

For a number of years, work in this laboratory has emphasized the importance of field emission for certain types of electric breakdown in gases (1), liquids (2), and solids (3), and the role of space-charge buildup in front of the cathode as a means of providing the required gradient. Also, the charging-up of surface layers comes into play, as demonstrated impressively, for example, in the Malter effect (4) and in the work of Llewellyn Jones and co-workers (5).

The present investigation deals with space-charge phenomena in n-hexane and n-heptane, in continuation of the work by Green (2). His principal findings on d-c currents under nearly homogeneous field were that the current-voltage characteristics consist of a low-field region, dominated by the ions of the liquid, and of a high-field region in which the decisive role is played by the cathode as a source of field emission.

The main purpose of our measurements was to extend the study to a highly inhomogeneous electrode configuration (thin wire in large coaxial cylinder) that allows separation of anodic and cathodic effects.

Experimental

The test cell (Fig. 1) consisted of a platinum wire (1 mil diameter) stretched along the axis of a carefully polished platinum cylinder (about 10 mm diameter and 30 mm long) with ends rounded to avoid edge effects. The geometrical field strength on the wire is roughly 400 times greater than that on the cylinder surface. The cylinder was connected, through a 50-megohm resistor, to a reversible high-voltage 30-kv power supply (Beta Electric Co.) driven by a Sorensen a-c voltage regulator. The maximum ripple, observed with an oscilloscope, was less than 1.5 v peak to peak at 10 kv. The wire was connected to a vibrating-reed electrometer whose output was sent through a General Electric self-balancing potentiometer into an Esterline-Augus recorder (Fig. 2). The equipment in its shielded cage was tested up to 20 kv for the absence of corona.

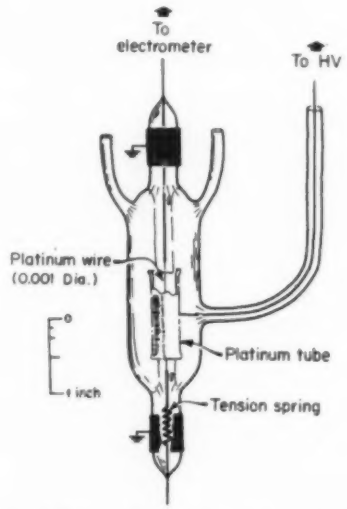

Fig. 1. Schematic drawing of the test cell

Test Samples and Procedures

"Pure grade" n-hexane and n-heptane (Philips Petroleum Co.) were repurified by passage through a 2-ft column of silica gel and an ultrafine fritted-glass filter; the initial fraction of the filtrate was discarded.

Ultraviolet absorption spectra, taken with a Cary spectrophotometer before and after treatment, show that bands initially observed around 2500Å are removed. This treatment seems to reduce the initial current slightly, but no significant change in residual current has been recorded.

Before final readings were taken, the cell was "conditioned" as follows.[3] After slowly raising the

[1] Present address: Laboratoire Central des Industries Electriques, Fontenay-aux-Roses, France.

[2] Present address: Torino, Italy.

[3] A similar technique has been used by House (6).

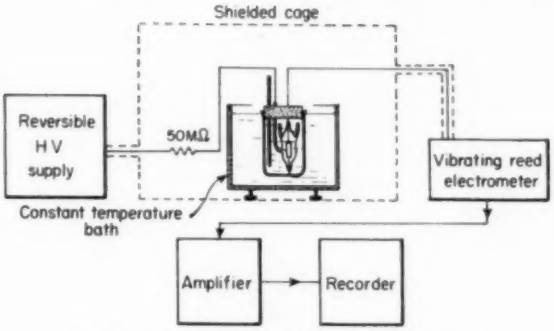

Fig. 2. Block diagram of the experimental setup

voltage to the onset of an erratic current, it was kept constant to permit the fluctuating current to decay gradually toward a steady state. Then the cycle was repeated three or four times until voltages of the order of 15 kv were reached. It is worth noting here that voltages up to 18 kv (which corresponds to 2.3 mv/cm at the wire for space-charge-free configuration) have been reached by this procedure. This treatment has a particularly strong effect in the negative-wire polarity (Fig. 3) supporting the belief that conditioning eliminates spots of high emissivity. The reproducibility of the final curves is shown by shaded areas which indicate the spread of the current values over a period of several weeks. The residual current is always noisy, especially when the wire is negative, and sudden fluctuations, superimposed on this noise, occasionally occur even after conditioning periods of 15 days. Hence, the current measured at intervals of several days was rarely reproducible within less than 40%.

In a second series of measurements, the test cell was thermostated to ±0.05°C and the steady current measured at constant voltage for various values of temperature as well as at constant temperature for different applied voltages.[4]

In a third series of experiments the wire alone was heated by a battery current and the average temperature of the wire estimated from its increment in resistance and the known temperature coefficient $d\rho/dt$ for platinum (4×10^{-3} ohm x cm x degree^{-1} between 0° and 100°C). In order to make sure that the leakage resistance to ground was not reduced when the heating current was turned on, the battery was connected permanently by one of its poles, and the whole circuit, including the switch, carefully insulated from ground. Potentials of 1.5, 3, 4.5, and 6 v were applied across the wire; at higher voltages the liquid at the wire surface started to boil. Since the volume of the wire is six orders of magnitude smaller than that of the liquid, only a very small fraction of the liquid near the wire surface is heated appreciably during the 1-min heating runs.

Time recordings of the charging and depolarization currents were also taken.

Behavior of the Residual Current

The residual current subsisting under both polarities after careful conditioning of the cell is shown in

[4] Since n-heptane is a liquid between −90.5° and +98.4°C, the data, thus far taken only over the range +13° to +50°C, should be extended. Some preliminary measurements in the wider range have been made but must be confirmed in detail before being reported.

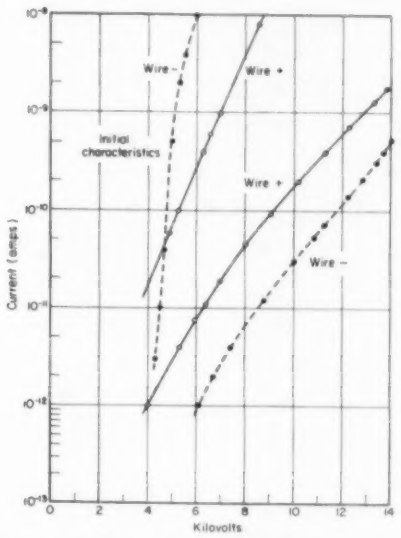

Fig. 3. Current-voltage characteristics in n-hexane showing the effect of conditioning. The shaded areas contain all the data taken over a period of several weeks, the points referring to the latest measurements.

Fig. 3 as a function of the applied voltage. The two curves, plotted on a log scale, are very similar in shape but the one corresponding to i_+ (positive wire configuration) lies above that corresponding to i_- (negative wire configuration).

Essentially the same results were obtained with a 1-mil diameter tungsten wire as the center electrode, although its surface roughness was much greater than that of the platinum wire. The residual current was larger under both polarities but the ratio i_+/i_- was nearly the same as for platinum (Fig. 4). Furthermore, fairly good agreement between the two sets of curves was obtained by scaling along the V axis. This seems to indicate that the highest field locally present in the cell, rather than the nature of the electrodes, is the significant factor.

The curves of Fig. 5, showing the temperature dependence of the current in n-heptane for various applied voltages, were obtained directly by varying the temperature under constant voltage. The same

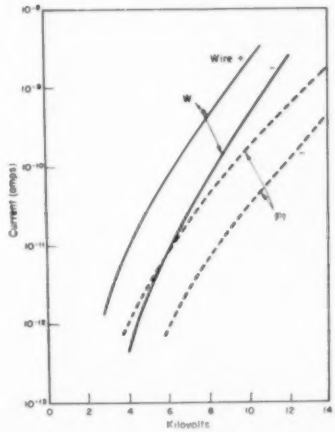

Fig. 4. Comparison of the current-voltage characteristics obtained with platinum and tungsten wire.

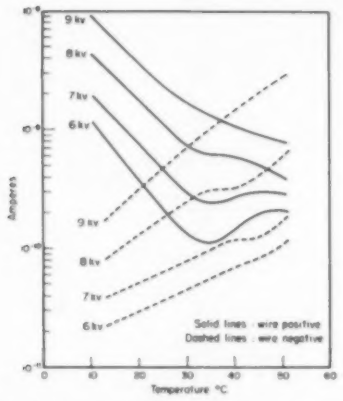

Fig. 5. Residual current vs. temperature in n-heptane for various applied voltages.

type of curves, constructed from a set of current-voltage characteristics at different temperatures, agree fairly well with those of Fig. 4. Although some details in the curves are not significant, the general trend shows that i_+ and i_- vary oppositely with temperature. While at room temperature i_+ is ten to twenty times larger than i_-, the two currents are of comparable magnitude at 50°C.

Current vs. Time (Wire Heated)

The results obtained when the wire was heated with 6 v applied are summarized in Fig. 6, which reproduces the essential trends of actual recordings. When the heating current is applied, the current drops suddenly regardless of polarity; then while i_+ keeps decreasing slowly, i_- tends to increase. When the wire current is switched off, the cell current rises sharply at first and then recovers its original value more slowly.

This effect is independent of the orientation (vertical or horizontal) of the test cell, the polarity of the battery, and the characteristics of the external circuit. Consequently, the sudden drop of the current must be caused by the heating of the wire and its immediate surroundings. However, transient phenomena related to the appearance of the thermal gradient are probably involved and complicate the interpretation. The slow variation, caused by the propagation of heat through the cell, is consistent

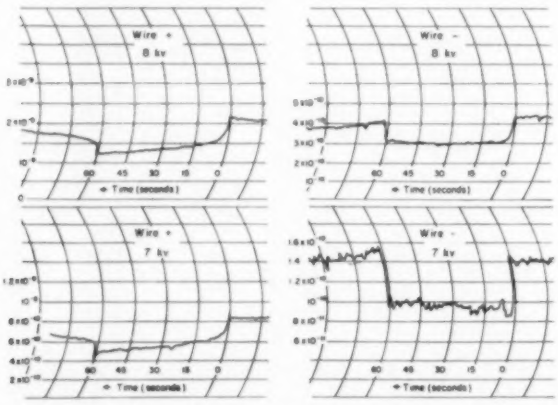

Fig. 6. Current recordings showing the effects of heating the wire alone.

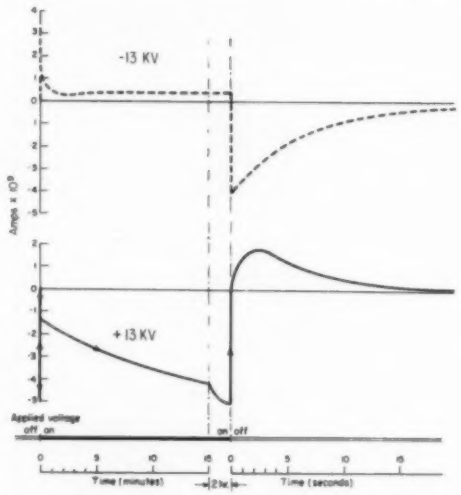

Fig. 7. Polarization and depolarization currents for both polarities.

with the results obtained by homogeneous heating of the whole cell. Table I shows the initial current drop in its relation to the wire temperature.

Polarization Currents

The cell generates a slowly decaying depolarization current when the applied voltage is removed after a steady state is reached. However, as Fig. 7 shows, the initial rise of this current is polarity dependent. When the applied voltage is restored, the current, after an initial jump, slowly recovers its initial value. It should be noted that i_+ increases significantly with time.

Discussion

The significant facts are: above a certain applied voltage, a residual current can be measured for both polarities. The current-voltage characteristics for i_+ and i_-, while of similar shape, vary oppositely when temperature is changed. The ratio i_+/i_- of the order of 10 at 20°C, approaches unity around 50°C.

A detailed analysis, due to Onsager (7), of the influence of an external field E on the dissociation constant K of a weak electrolyte shows that for the high-field limit,

$$K(E) = K(0)\ (2/\pi)^{1/2}\ (8b)^{-3/4} \exp \sqrt{8b} \qquad [1]$$

where $8b = 77.2\ E/\kappa T^2$.

Table I. Initial current drop through the cell upon heating of the wire

Voltage across the wire, v	Current in wire, ma	Resistance of wire, ohm	Temperature at wire surface, °C*	Initial current drop through cell, %
0	0	13.40†	20.5 (R.T.)	0
1.5	102.5	14.65	38.7	7
3.0	189	15.90	64.0	12-22
4.5	260	17.30	77.5	18-22
5.95	318	18.75	97	27-30

* Calculated from the formula $R_T = 0.725\ R_{20.5}\ (1 + \alpha T)/(1 + \alpha \times 20.5)$. The factor (.725 accounts for the difference between the temperature of the wire at its periphery and its average temperature. It was estimated from the fact that boiling started when the average temperature was about 135°C.
† Obtained by graphical extrapolation for zero current.

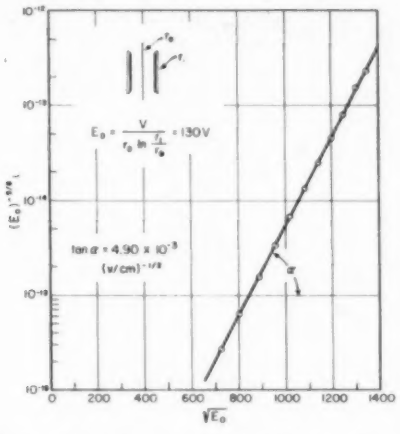

Fig. 8. Final characteristics of Fig. 3 (wire positive), plotted for a check of Onsager's theory.

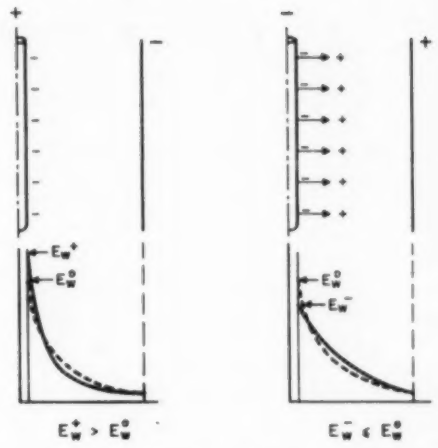

Fig. 9. Hypothetical model for the field distribution under both polarities (schematic).

Assuming that the dissociation products of both signs contribute equally to the current and that the mobility of the carriers does not vary in the field range of interest, the current is expected to vary with the field as $E\sqrt{K(E)}$, i.e. (in hexane at room temperature, $8b = 4.5 \times 10^{-4} E$), as

$$i \propto E^{9/8}\, 10^{4.6 \times 10^{-5} \sqrt{E}} \qquad [2]$$

In fact, if the residual characteristic for positive wire (cf. Fig. 3) is replotted on a log scale (Fig. 8) as $iE^{-5/8}$ vs. $\sqrt{E}$, the points fall on a straight line of angular coefficient 4.0×10^{-5}, as compared with the theoretical value of 4.6×10^{-5}.[5]

In view of the approximations involved in Eq. [1] and of the presence of the space charge which may distort the field at the wire, the agreement can be considered very good and strongly indicates that the carriers are created primarily by field ionization of impurities near the wire. Furthermore, the results obtained by other workers [in particular by House (6)] with more homogeneous field are consistent with this model. However, this mechanism fails to predict the temperature dependence of the residual current, in particular the effect of polarity (cf. Fig. 5). Since the polarization and depolarization currents (Fig. 7) suggest the presence of a different kind of space-charge for each polarity, it is logical to investigate whether the polarity effect can be ascribed to space-charge phenomena.

Let us call E_w^0 the field at the wire surface in the absence of space charge, and E_w^+ and E_w^- the actual field strengths at the wire positive and negative, respectively. If the wire is positive, a negative ionic space charge builds up at the wire surface, and $E_w^+ > E_w^0$ (Fig. 9). For increasing temperature the space charge expands by diffusion, hence E_w^+ decreases. For wire negative, field emission can occur.[6]

[5] The "effective radius" of the cell, defined as

$$\bar{r} = \int_{r_{in}}^{r_{out}} \left\{K[E(r)]\right\}^{1/2} r\,dr \Big/ \int_{r_{in}}^{r_{out}} \left\{K[E(r)]\right\}^{1/2} dr$$

with $E(r) = V/[r \ln(r_{out}/r_{in})]$ and $V = 9000$ v, has been calculated and found to be about twice the radius of the wire. Hence, no error in order of magnitude is made by using the geometric field $E(r_{in})$ in the plot of Fig. 7.

[6] E_w^0 is of the order of 10^6 v/cm for 8 to 10 kv applied. Surface irregularities make the field locally higher; furthermore, the potential barrier at the electrode is decreased by the dielectric.

The emitted electrons trapped by the liquid create a negative space charge, so that $E_w^- \leqq E_w^0$; as temperature increases, the space charge expands and E_w^- increases.

The inequality $E_w^- \leqq E_w^0 < E_w^+$ predicts the relative value of the current for both polarities, and the fact that E_w^- and E_w^+ become closer to E_w^0 as temperature increases is also in agreement with the observed temperature dependence.

To summarize, some evidence is given that the carriers are produced by field-induced dissociation and that the polarity dependence indirectly results from the fact that field emission is possible when the wire is negative. The species that dissociate under high field, the mobility of the charge carriers, and other problems of detail remain to be investigated. Experiments with other liquids and over a wider temperature range should help in clarifying the situation.

Acknowledgments

The authors are deeply grateful to Professor A. R. von Hippel for valuable discussions which contributed to the interpretation of the results, and to Mr. J. Kalnajs of this laboratory for his unfailing help in the realization of the experiment.

Manuscript received Sept. 16, 1959. This paper was prepared for delivery before the Philadelphia Meeting, May 3-7, 1959. Work on this paper was sponsored by the U.S. Office of Naval Research, Army Signal Corps, Air Force, and Atomic Energy Commission.

Any discussion of this paper will appear in a Discussion Section to be published in the December 1960 JOURNAL.

REFERENCES

1. A. von Hippel, *Z. Physik*, **80**, 19 (1933); D. R. Young, *J. Appl. Phys.*, **21**, 222 (1950).
2. W. B. Green, *J. Appl. Phys.*, **26**, 1257 (1955); **27**, 921 (1956).
3. A. von Hippel and R. S. Alger, *Phys. Rev.*, **76**, 127 (1949); A. von Hippel, E. P. Gross, J. G. Jelatis, and M. Geller, *ibid.*, **91**, 568 (1953); M. Geller, *ibid.*, **101**, 1685 (1956).
4. L. Malter, *ibid.*, **49**, 478 (1936).
5. F. Llewellyn Jones, *Repts. Prog. in Phys.*, **16**, 216 (1953).
6. H. House, *Proc. Phys. Soc. (London)*, **A170**, 913 (1957).
7. L. Onsager, *J. Chem. Phys.*, **2**, 599 (1934).

Silicon Nitride Thin Film Dielectric

Charles R. Barnes and Charles R. Geesner

Electronic Technology Laboratory, Wright Air Development Center, Wright-Patterson Air Force Base, Ohio

ABSTRACT

Thin adherent nonporous films of pure silicon nitride have been deposited from the vapor phase on hot molybdenum substrates by pyrolytic deposition. Such films, when incorporated between molybdenum plates to form capacitors, were found to maintain satisfactory dielectric properties up to and above 600°C. Silicon nitride coatings, deposited by the method herein described, also offer a convenient and effective method of encapsulation for protecting metal surfaces from atmospheric oxidation up to and above 1000°C.

As a result of the need for high temperature resistant electronic materials and miniaturized electronic equipment for use in space vehicles and satellites, thin films of silicon nitride were deposited pyrolytically and developed as a new dielectric material for capacitors capable of operating satisfactorily up to and above 600°C.

Pyrolytic deposition may be defined to include the following three chemical processes of deposition of materials on the surface of hot substrates: (*a*) the thermochemical decomposition of a properly selected chemical compound existing in the vapor state, (*b*) the reaction between two or more chemical vapors at the hot surface, and (*c*) the reaction of a vapor with the hot substrate itself. In the present case a process like (*b*) above was used.

The literature shows no record of the use of thin adherent nonporous films of pure silicon nitride as a dielectric for capacitors capable of satisfactory operation at 600°C. From the thermodynamic data of Kellogg (1), Brewer, Bromley, Gilles, and Lofgren (2), Powell (3) in a search for high-temperature protective coatings for metals predicted that silicon nitride might be vapor plated by means of the reaction of the combined vapors of silicon tetrachloride, hydrogen, and nitrogen at a substrate temperature of 1000°-1600°C. Powell further states that the probable deposit would be composed of a mixture of elemental silicon and silicon nitride.

In the present investigation it was imperative that a high temperature resistant dielectric material should not only be of high purity but should be pore-free in order to function properly in a thin film capacitor. To prevent the formation of pores in the deposit and to obtain a pure silicon nitride film the following precautions and requirements were adopted: (*a*) The metal substrate surface must be smooth and thoroughly cleansed. (*b*) Its temperature must be accurately controlled during the deposition. (*c*) A volatile silicon compound is required, such as silicon tetrabromide, capable of being relatively easily reduced to silicon which should react with nitrogen at temperatures below 1000°C to form pure Si_3N_4. (*d*) The reactant carrier gases, hydrogen and nitrogen, must be thoroughly purged of water vapor and oxygen.

Deposition of Silicon Nitride Dielectric

The silicon nitride dielectric films were deposited on smooth polished molybdenum disks 1 in. in diameter and 0.005 in. thick by means of the apparatus shown in Fig. 1. Before introducing the molybdenum disk into the plating apparatus, its surface is cleaned in succession with acetone, a hot water solution of sodium hydroxide, hot chromic acid, distilled water, and finally wiped dry with a fine clean grade of untreated tissue paper. The disk is then placed on the graphite core of the plating chamber (G), heated to the desired temperatures to be discussed later, deoxidized with hydrogen, and finally plated with silicon nitride dielectric.

In the actual plating process for silicon nitride dielectric illustrated in Fig. 1, commercial grades of hydrogen and nitrogen are allowed to flow through calibrated flowmeters (A) at the following flow rates expressed in milliliters per minute: 300 for hydrogen and 1100 for nitrogen. Both hydrogen and nitrogen gases then pass through deoxidizing units (B) and (C), respectively, for the purpose of removing con-

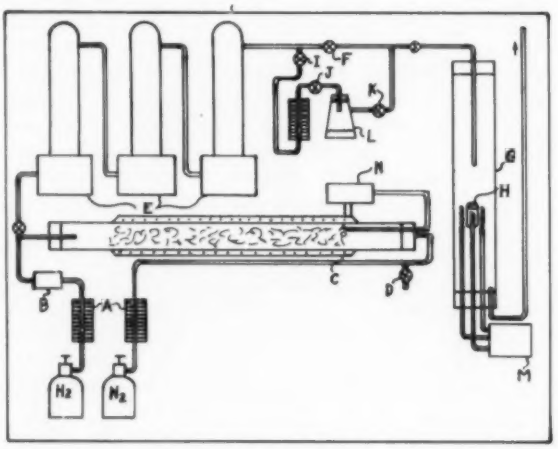

Fig. 1. Apparatus for depositing silicon nitride: (A) Flowmeters for hydrogen and nitrogen; (B) and (C) deoxidizers; (D) back-flush valve; (E) calcium hydride drying towers; (F), (I), (J), and (K) vapor control valves; (G) deposition chamber; (H) substrate; (L) silicon bromide evaporator; (M) induction heater with temperature controller; (N) deoxidizer temperature control.

taminating oxygen. For the hydrogen purification a Baker and Company Deoxo unit Model D is employed. The nitrogen gas is purified by passing over copper turnings maintained at a temperature of 750°C. The advantage of using a separate deoxidizing unit for the nitrogen is that the copper can be reactivated between runs by back flushing hydrogen through the hot oxidized copper turnings. As a result, a large quantity of water is removed from the system through outlet valve (D). This water would otherwise rapidly consume the drying agent in subsequent drying towers (E). The hydrogen and nitrogen both flow together through three drying towers each of which contains a bed of —4 to 40 mesh calcium hydride that is 7 in. in depth and 2 in. in diameter. The mixed purified carrier gases then flow through valve (F) and enter the plating chamber (G) through Vycor nozzle. Thus the carrier gases blow directly on the clean molybdenum disk substrate, the upper surface of which is maintained at a temperature of 960° ±2°C as measured by an optical pyrometer. The source of heat is a 7.5 kw induction heater whose water-cooled coils surround a cylindrical graphite core. By induction the graphite core is heated to approximately 1000°C which in turn heats the molybdenum disk substrate (H) resting on top. Finally the exhaust gases leave the heating chamber through the exhaust stack.

In starting the plating operation the carrier gases are allowed to flow until all air and moisture are flushed from the plating chamber. The induction heater is turned on and the temperature of the substrate raised to and maintained at 600°C for 10 min during which time the nitrogen flow is turned down to a trickle and hydrogen valve is opened to allow a flow of 1000 ml/min. The purpose of this short operation is to deoxidize and clean the substrate surface with hydrogen.

After the above purging operation the hydrogen and nitrogen flow rates are readjusted to 300 and 1100 ml/min, respectively, and the gas flow allowed to continue until equilibrium of the gas mixture is established in the Pyrex glass plating chamber. The temperatures of the graphite core and molybdenum disk are then increased until a substrate surface temperature of 960° ± 2°C is reached and maintained. To start the deposition of silicon nitride on the substrate, valves (I), (J), and (K) are opened and valve (F) is partially closed. By manipulation of valves (F) and (I) simultaneously the amount of carrier gas by-passed through the silicon bromide evaporator (L) is adjusted to 100 ml/min. As the gas mixture passes over the surface of the liquid, silicon bromide vapor is picked up and blown directly on the molybdenum disk substrate which is located 4¼ in. from the nozzle. Subsequently a deposit of silicon nitride (Si_3N_4) appears immediately on the molybdenum substrate discernible only by the moving rainbow formations which continue to grow as the deposition progresses. After continuing the deposition process for 1 hr, a silicon nitride dielectric film of 0.5 mil approximate thickness has grown on the molybdenum substrate. Finally, after turning off the silicon bromide vapor flow and in a few minutes shutting down the heater, the substrate with deposited film is allowed to cool and may be removed.

Although experiment showed that silicon nitride films can be deposited over a temperature span of 930°-1000°C, the best quality dielectric films were obtained at a substrate surface temperature of 960°C. These were smooth, clear, transparent, colorless, very adherent, free of pores, and suitable for capacitor construction. It was further determined that, by increasing the flow-rate of the carrier gases and silicon tetrabromide vapor, the deposition rate can also be increased. However, the best quality dielectric films were those which required at least 1 hr to obtain a thickness of 0.4-0.6 mil.

Construction of Silicon Nitride Capacitor

In order to measure the dielectric properties of silicon nitride a number of thin film capacitors were constructed and tested utilizing the dielectric films deposited on molybdenum disks as described above.

Before constructing the capacitor the molybdenum disk with a dielectric film of silicon nitride 0.5 mil thick on one side is turned over and plated on the opposite side with a coating of silicon nitride 0.3 mil thick which serves to encapsulate the molybdenum plate after it is incorporated in a capacitor.

Thickness of the films were measured by a metallurgical microscope with a mechanical stage graduated with one scale division equal to 1 μ of stage movement.

To construct the capacitor, a thin film of molybdenum of 0.5 mil thickness is plated on the silicon nitride dielectric which was previously deposited on the molybdenum substrate. As a source of molybdenum its pentachloride vapor carried by hydrogen gas to the substrate is employed, a procedure recommended by Powell (4). In the present case the apparatus of Fig. 1 is modified by removing the head assembly of the plating chamber and replacing with another (not shown) which contains an evaporator for furnishing molybdenum pentachloride vapor at a temperature of 195°C to the hydrogen carrier gas blowing at 1000 ml/min. The silicon nitride substrate surface temperature is 800°C. Five minutes are required to deposit a molybdenum film of 0.5 mil thickness. After cooling and removing the capacitor from the plating chamber the edge of the molybdenum film is etched back from the outer circumference for a distance of 1/32 in. Also a spot is etched away where it is desired to scratch through the silicon nitride dielectric in order to solder a lead to the base plate.

Platinum wire leads are then soldered with metallic gold, one to the molybdenum base plate and the other to the molybdenum film. To accomplish the gold soldering the capacitor is placed in the plating chamber and platinum wire leads are supported in such a manner that one tip of each rests against the bare molybdenum and adjacent to a tiny bead of gold placed at the attachment areas. Soldering is then accomplished in an atmosphere of hydrogen by heating the whole capacitor to the fluxing temperature of gold.

After the leads are attached the capacitor remains in the plating chamber and a final encapsulating film

Table I. Dielectric properties of silicon nitride

Temp, °C	Resistance in megohms at 100 V.D.C.	Volume resistivity, ohm-cm	Capacity at 1 kc	Dielectric constant at 1 kc	Dissipation factor at 1 kc	RC product, megohm-microfarads	Dielectric strength, v/mil
25	1.5×10^{8}	4.1×10^{16}	2714	12.7	<0.0001	407,000	1000
100	8.5×10^{7}		2719		<0.0001	231,000	
200	1.7×10^{7}		2725		<0.0001	46,300	
300	1.7×10^{6}		2737		<0.0001	4,600	
400	5.0×10^{5}		2747		0.0003	1,375	
500	3.2×10^{5}		2757		0.0006	881	
600	5.7×10^{4}	1.6×10^{15}	2763	13.5	0.0033	157	660

of silicon nitride 0.3 mil thick is plated over the molybdenum film and the attachment areas of the leads. The construction of an encapsulated high temperature thin film silicon nitride capacitor is now complete.

Summary of Dielectric Properties of Silicon Nitride

Several of the capacitors were recycled stepwise three times in a muffle furnace over a temperature range of 25°-600°C. Each capacitor was supported by two Vycor tubes through which the leads were passed. The tubes extended separately from the capacitor in the furnace through the port hole to the outside without touching each other or the walls of the furnace. Representative results of the temperature exposures up to 600°C are presented in Table I. Furthermore it is interesting to note that in one case a capacitor was heated to 1000°C in a flame without damage.

Manuscript received Sept. 18, 1959.

Any discussion of this paper will appear in a Discussion Section to be published in the December 1960 JOURNAL.

REFERENCES

1. H. H. Kellogg, *J. Metals*, **2**, 862 (1950).
2. L. Brewer, L. A. Bromley, P. W. Gilles, and N. L. Lofgren, "The Chemistry and Metallurgy of Miscellaneous Materials," L. L. Quill, Editor, pp. 40-75, McGraw-Hill Book Co., New York (1950).
3. C. F. Powell, I. E. Campbell, and B. W. Gonser, "Vapor Plating," p. 97, John Wiley & Sons, Inc., New York (1955).
4. C. F. Powell, I. E. Campbell, and B. W. Gonser, *J. (and Trans.) Electrochem. Soc.*, **93**, 258 (1948).

Tin-Activated Calcium Orthosilicate Phosphors

Richard W. Mooney

Chemical and Metallurgical Division, Sylvania Electric Products Inc., Towanda, Pennsylvania

ABSTRACT

A study of the tin-activated calcium orthosilicates disclosed two phosphors: a blue-emitting phosphor with a very broad excitation band having the β-Ca_2SiO_4 structure and a yellow-emitting phosphor with fair response to high-pressure mercury-vapor radiation having the α'-Ca_2SiO_4 structure. The β-Ca_2SiO_4:Sn phosphor is the more efficient of the two, comparing very favorably with other well-known blue phosphors. The efficiency of β-Ca_2SiO_4:Sn was studied as a function of activator concentration and compared with similar results for β-$CaSiO_3$:Sn. The difference in behavior between β-Ca_2SiO_4:Sn and β-$CaSiO_3$:Sn is attributed to differences in crystal structure.

The orthosilicates of calcium having the composition $2CaO \cdot SiO_2$ or Ca_2SiO_4 have been the subject of many investigations, since they are found commonly in blast furnace and open-hearth slags and used extensively in Portland cement and certain types of refractories. The present ideas on the chemistry and crystallography of dicalcium orthosilicate began in 1943 with the work of Bredig (1) whose ideas since have been confirmed and extended by many authors (2-6). It is now generally accepted that dicalcium orthosilicate occurs in four polymorphic modifications: namely, an alpha (α) or high-temperature modification stable above 1450°C; an alpha prime (α') modification occurring between 850° and 1450°C; a beta (β) modification, metastable at room temperature; and a gamma (γ) modification, which is stable at room temperature. The γ-, β-, and α'-modifications are found in nature and have the mineralogical names: calcio-olivine, larnite, and bredigite, respectively. It has been shown also that the additions of small amounts of many of the common oxides change the temperatures of both the α-β and the β-γ inversions, resulting in some cases in the stabilization of high-temperature forms (7, 8). For instance, less than 0.2 mole % of Na_2O will inhibit the β-γ transformation (9). Thus the specific crystallographic species formed by high-temperature solid-state reaction will be determined not only by the temperature of firing, but also by the particular modifying compounds present.

The only calcium orthosilicate phosphor previously reported was β-Ca_2SiO_4: Pb which, according to Studer and Fonda (10), emits at 334 mμ under 254 mμ excitation. The present investigation was undertaken as part of a general study of the tin-activated calcium silicates. The preparation and optical properties of the tin-activated calcium metasilicates were reported in a previous paper (11) while this paper gives corresponding data on the calcium orthosilicates activated by tin.

Experimental Procedure

Calcium carbonate and silicic acid were mixed in mole ratios which varied from 2CaO/0.95 SiO_2 to 2CaO/1.50 SiO_2 with 0.01-10.0 mole % of stannic or stannous oxide. The mixture was pebble-milled in a deionized water slurry, dried at 110°-120°C, and fired in silica trays at temperatures varying from 870°-1320°C. For maximum efficiency it was necessary to fire in a steam atmosphere, and since tin-activated phosphors luminesce only when the tin is in a lower valence state, a reducing atmosphere, usually a mixture of hydrogen, nitrogen, and steam, was maintained. All gas flows were controlled carefully in order to obtain reproducible results with optimum efficiencies being obtained at a nitrogen to hydrogen ratio of approximately unity.

The methods used for structure identification by x-ray diffraction, measurement of excitation and emission spectra, and determination of per cent tin by quantitative analyses were the same as those previously reported (11). In this paper the activator contents are expressed as gram-atom tin per gram-atom of calcium in the fired phosphor.

Relative efficiency measurments under 254 mμ excitation were made on a plaque tester of conventional design (12). Efficiency measurements under high-pressure mercury-vapor (HPMV) excitation were made on a similar instrument using as sources two General Electric C85H3 lamps with ultraviolet-transmitting envelopes. The predominant wave lengths present in the HPMV source were 313 and 365 mμ. The instrument was so constructed that efficiencies of various phosphors could be compared at room temperature, or the temperature dependence of fluorescence of a sample could be measured by raising the temperature of the sample at a constant heating rate of approximately 2°C/min. The output of a 1P21 photomultiplier detector was amplified by a Photovolt Model 520-M unit and fed into the Y-axis of a Mosely Autograf X-Y recorder. The signal from a chromel-alumel thermocouple imbedded in the phosphor sample was fed to the X-axis, thus giving a continuous plot of efficiency vs. temperature for a particular sample.

Results with β-Ca_2SiO_4:Sn

A deep blue-emitting phosphor having the β-Ca_2SiO_4 structure was formed over wide temperature and composition limits with temperatures between 1150° and 1230°C and compositions between 2.0 CaO/1.00 SiO_2 and 2.0 CaO/1.10 SiO_2 giving the best results. There was no evidence in any of the firings of the presence of γ-Ca_2SiO_4. The most efficient phosphors were produced at a SiO_2 content

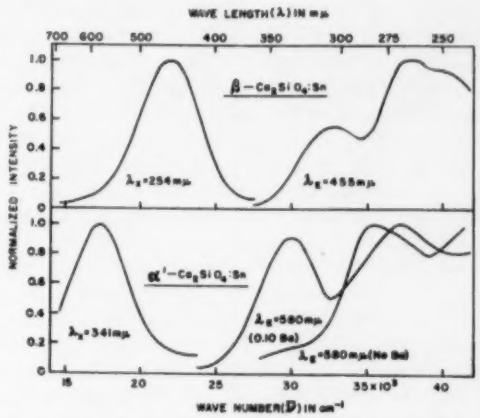

Fig. 1. Excitation and emission spectra of β-Ca_2SiO_4:0.003 Sn and α'-Ca_2SiO_4:0.003 Sn.

that gave a slight excess of SiO_2 over the theoretical Ca_2SiO_4 composition. The presence of a slight excess of CaO was extremely deleterious to phosphor brightness.

The excitation and emission spectra of β-Ca_2SiO_4:Sn are shown in the top half of Fig. 1. The emission spectrum consists of a single band peaking at 22,000 cm^{-1} or 455 mμ regardless of the energy of excitation. The excitation spectrum is broad, giving efficient excitation by both 254 mμ and HPMV radiation. The brightness of β-Ca_2SiO_4 compares very favorably with that of other blue-emitting phosphors. For instance, with 254 mμ excitation β-Ca_2SiO_4: 0.003 Sn is 25% brighter than $Sr_2P_2O_7$: Sn, which has its peak emission at 452 mμ, and under HPMV excitation it is 15% brighter than magnesium tungstate. Both comparisons were made at room temperature.

Results with α'-Ca_2SiO_4:Sn

As the firing temperature exceeded 1200°C for phosphors having a composition close to the theoretical Ca_2SiO_4 composition, there was a gradual decrease in blue emission and an equally gradual increase in yellow emission. This effect was most pronounced as the composition approached the Ca_2SiO_4 stoichiometric formulation and decreased as the excess SiO_2 increased. Concurrent with the shift in emission, there occurred a corresponding shift in the excitation spectrum with the yellow component being excited more easily by HPMV radiation than by 254 μ excitation. The yellow-emitting phosphor was identified by x-ray diffraction as α'-Ca_2SiO_4: Sn with emission and excitation spectra as given in the bottom half of Fig. 1.

The emission is dependent on the wave length of excitation, giving a single band at 17,300 cm^{-1} (578 mμ) when excited by 341 mμ. As the energy of the exciting wave length is increased, the position of the main emission band shifts from 578 mμ under 341 mμ excitation to 559 mμ under 268 mμ excitation, and in addition a very weak emission band develops at about 370 mμ. From the excitation data it is apparent that the intensity of the band in the neighborhood of 570 mμ is greatest at the peak in the excitation curve, i.e., under 285 mμ radiation.

It was also found that the substitution of small amounts of Mg, Zn, Sr, or Ba, in the range 0.10 gram-atom of modifying Group II metal, for an equivalent amount of Ca in the calcium orthosilicate formulation tended to promote the transition to the yellow-emitting α'-Ca_2SiO_4:Sn. A comparison of the results showed that the greater the difference in ionic size between calcium and the modifying cation, the greater the effect, i.e., barium and magnesium were more efficient in promoting the transition than zinc or strontium while cadmium had little, if any, effect. The most efficient yellow-emitting phosphor having the α'-Ca_2SiO_4 structure had the composition $Ca_{1.97}Ba_{0.03}SiO_4$:0.003 Sn. The excitation spectrum of the Ba-modified α'-Ca_2SiO_4:Sn phosphor as shown in the bottom half of Fig. 1 is very different from the unmodified sample as evidenced by the strong absorption of radiation at about 30,000 cm^{-1} (333 mμ) caused by the addition of barium. The addition of small amounts of alkali metals as, for example, 0.013 gram-mole of Li_2CO_3 to a Ba-modified Ca_2SiO_4:Sn phosphor was also effective in increasing the efficiency to HPMV radiation by increasing the absorption of 30,000 cm^{-1} radiation still further. Calcium orthosilicate phosphors fired at 1316°C displayed no evidence of fusion even in the presence of well-known fluxes such as Li_2CO_3 or $BaCO_3$.

Effect of Activator Concentration on β-Ca_2SiO_4:Sn

The effect of activator concentration, expressed as atom Sn found in the fired phosphor per atom Ca, on the relative efficiency of β-Ca_2SiO_4:Sn was studied and compared to similar results on the more efficient of the tin-activated calcium metasilicates, namely, β-$CaSiO_3$:Sn. The results for 254 mμ excitation for both β-Ca_2SiO_4:Sn and β-$CaSiO_3$:Sn are shown in the top half of Fig. 2. The normalized efficiency data were fitted to the equation

$$\eta = \frac{c(1-c)^Z}{c + (\sigma/\sigma')(1-c)}$$

where η is the relative efficiency, c is the activator concentration in atom Sn per atom Ca, and Z and σ/σ' are adjustable parameters (13). The parameter σ/σ' is the ratio of the capture cross sections of nonactivators to the capture cross sections of luminescent activators, while the parameter Z is defined as the number of lattice positions surrounding a given activator such that, if any one of these sites is occupied by another activator, luminescence is quenched. The efficiency of β-Ca_2SiO_4:Sn is relatively insensitive to activator concentration over the range 0.001-0.020 atom Sn/atom Ca for 254 mμ excitation, whereas the efficiency of β-$CaSiO_3$:Sn is sharply peaked at an activator concentration of about 0.001 atom Sn/atom Ca. The ratio of the capture cross section of nonactivators to activators is approximately constant for both phosphors, whereas Z increases by a factor of six in going from 10 for β-Ca_2SiO_4:Sn to 60 for β-$CaSiO_3$:Sn.

Since β-Ca_2SiO_4:Sn is also excited by HPMV radiation, the effect of activator concentration on the HPMV response was also studied, with results as given in the bottom half of Fig. 2. The efficiencies at elevated temperatures were calculated from the room-temperature efficiencies and measurements of the temperature dependence of fluorescence. The β-Ca_2SiO_4:Sn phosphors showed a gradual decrease in efficiency with temperature with the phosphor having the highest tin concentration giving the greatest drop in efficiency. Since the decrease in brightness is very gradual, the error due to nonequilibrium measurements should be negligible. As would be expected the maximum in the plot of efficiency vs. activator content shifts to lower activator concentrations with increasing temperature.

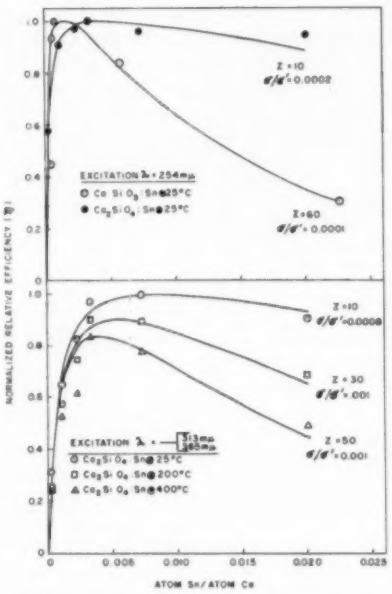

Fig. 2. Relative efficiency vs. activator concentration for β-Ca_2SiO_4:Sn with ultraviolet excitation.

Values of Z and σ/σ' for β-Ca_2SiO_4:Sn at 25°, 200°, and 400°C were calculated. The σ/σ' values for all three temperatures were approximately equal, i.e., about 0.001 or an order of magnitude greater than the σ/σ' values for 254 mμ excitation. The Z value found was the same at room temperature for low and HPMV excitation, but increased from 10 at room temperature to 50 at 400°C for HPMV excitation.

It is interesting that most of the tin added to the phosphor mix is lost during the firing process. Thus, for β-Ca_2SiO_4:Sn, 44% of the original tin present is retained at the lowest activator concentration. This amount decreases to a value of 13% in the neighborhood of the optimum activator concentration and then increases rapidly again to 40% for 0.10 gram-atom Sn added per gram-mole of Ca_2SiO_4. The per cent tin retained in β-$CaSiO_3$:Sn goes through a similar minimum starting at 45%, decreasing to a minimum of 2.5%, and increasing again to 42%.

Discussion

The predominance of the β-Ca_2SiO_4 structure and the complete lack of any evidence of the γ-Ca_2SiO_4 structure in the Ca_2SiO_4:Sn phosphors indicate that tin has a strong stabilizing effect on the metastable β-Ca_2SiO_4 crystal lattice. Another stabilizing influence on the β-Ca_2SiO_4 structure might be the small

particle size since Guinier and Yannaguis (5) found that, with crystals less than 10 μ in size, the β-phase only was stable. At very high temperature it is necessary to introduce a distorting cation whose radius is markedly different from that of calcium in order to promote the β-α' transition and stabilize the α'-structure at room temperature. The necessity of a slight excess of SiO_2 over the Ca_2SiO_4 composition for optimum efficiency is generally accepted in phosphor technology as is the use of reducing atmospheres for the firing of tin-activated phosphors.

It is interesting to compare the σ/σ' and Z values obtained on β-Ca_2SiO_4:Sn and β-$CaSiO_3$:Sn with those of another tin-activated phosphor, namely $Sr_{2.60}Zn_{0.20}(PO_4)_2$:Sn, recently studied (14). For 254 mμ excitation at room temperature, the σ/σ' values are all approximately constant, varying from 0.0001 and 0.0002 for the tin-activated silicates to 0.0005 for the tin-activated phosphate. The Z values of 10 and 60 for the silicates are higher than the previous $Z = 1$ value for the above phosphate, although a strict comparison of these figures is not entirely valid, since in the previous paper (14) the activator concentrations were expressed in terms of the unfired mix, whereas in the present paper they are given in terms of the tin actually present in the phosphor after firing. The latter method is much to be preferred due to the large and variable loss of tin during firing.

A comparison of the response of β-Ca_2SiO_4:Sn with $Sr_{2.60}Zn_{0.20}(PO_4)_2$: Sn under HPMV excitation gives similar results. Thus, σ/σ' is not changed very much, being in the neighborhood of 0.001 for the tin-activated silicates and varying with temperature from 0.003 to 0.005 for the tin-activated phosphate. The increase in Z with temperature is according to expectation, and at elevated temperatures there is good correlation between the Z value for $Sr_{2.60}Zn_{0.20}(PO_4)_2$:Sn of 36 at 377°C and the values of 30 and 50 for temperatures of 200° and 400°C, respectively, for β-Ca_2SiO_4:Sn.

Generalizing these results, it would appear that the ratio of the capture cross section of nonactivators to luminescent activators is relatively unaffected by environment, being a function largely of the activator itself and the energy of the exciting radiation. However, the parameter Z, which is related to the number of neighboring sites occupied sufficient to cause concentration quenching, is a function of the phosphor matrix.

More specifically, why is β-$CaSiO_3$:Sn with a Z value of 60 much more sensitive to activator concentration than is β-Ca_2SiO_4:Sn with a Z value of 10. One possible explanation for the difference lies in the fundamental difference in structure between wollastonite (β-$CaSiO_3$) and larnite (β-Ca_2SiO_4). Thus the structure of larnite has been shown by Midgley (15) to consist of isolated SiO_4 tetrahedra and Ca ions. On the other hand, the wollastonite structure has recently been reinvestigated (16, 17) and found to consist of infinite chains of Si_6O_{17} radicals arranged along endless columns of Ca-octahedra. Thus the activator sites in wollastonite, assuming isomorphous replacement of calcium by tin, are found in these Ca-octahedra columns, whereas the sites in β-Ca_2SiO_4:Sn are more or less randomly distributed among the isolated calcium sites in the crystal. It is proposed that the association of the activator sites by this column-type structure leads to a greater interaction between neighboring activators and therefore a greater sensitivity to concentration quenching as evidenced by a Z value of 60 for β-$CaSiO_3$:Sn vs. a Z value of 10 for β-Ca_2SiO_4:Sn.

The appreciable loss of tin during firing is undoubtedly explained by the work of Platteeuw and Meyer (18) who showed that at high temperatures SnO is a stable gas with an appreciable vapor pressure. The presence of H_2 in the gas mixture would undoubtedly favor the formation of SnO and thus lead to its subsequent dispersal through the system and partial loss to the surroundings. The presence of the activator in the vapor state might also explain the generally high efficiencies of tin-activated phosphors due to uniform incorporation in the lattice. The increase in the tin retained at the higher concentrations is evidently due to the inability of the phosphor to rid itself of excess tin during the period of firing used.

An analysis of the spectra of the Sn-activated calcium orthosilicates is considerably more difficult than that for the metasilicates. Studer and Fonda (10) found one emission band at 334 mμ for β-Ca_2SiO_4:Pb. However, recent measurements in this laboratory indicate that there are at least four emission bands with a corresponding number of excitation bands. As a consequence, it is completely impossible to relate the excitation or emission bands in β-Ca_2SiO_4:Sn to those in β-Ca_2SiO_4:Pb at this time.

Acknowledgment

The author is indebted to several of his colleagues for their help with the preparations and measurements. Specifically, he wishes to thank Dr. C. W. W. Hoffman for the x-ray identifications and Mr. G. J. Meisenhelter for the analytical determinations. The author also wishes to acknowledge the advice and encouragement of Dr. J. S. Smith during the progress of this work.

Manuscript received Aug. 26, 1959. This paper was prepared for delivery before the Philadelphia Meeting, May 3-7, 1959.

Any discussion of this paper will appear in a Discussion Section to be published in the December 1960 JOURNAL.

REFERENCES

1. M. A. Bredig, *Am. Mineral.*, **28**, 594 (1943); *J. Phys. Chem.*, **49**, 537 (1945); *J. Am. Ceram. Soc.*, **33**, 188 (1950).
2. G. Trömel, *Naturwissenschaften*, **36**, 88 (1949).
3. G. Yamaguchi, H. Miyabe, K. Amano, and S. Komatsu, *Yogyo Kyokai Shi*, **65**, 99 (1957).
4. N. A. Toropov, B. V. Volkonskii, and V. I. Sadkov, *Doklady Akad. Nauk S.S.S.R.*, **112**, 467 (1957).
5. A. Guinier and N. Yannaguis, *Compt. rend.*, **244**, 2613 (1957).
6. D. M. Roy, *J. Am. Ceram. Soc.*, **41**, 293 (1958).
7. E. S. Newman and L. S. Wells, *J. Research Nat. Bur. Standards*, **36**, 137 (1946).
8. G. V. Kukolev and M. T. Mel'nik, *Doklady Akad. Nauk S.S.S.R.*, **109**, 1012 (1956).
9. E. Thilo and H. Funk, *Z. anorg. u. allgem. Chem.*, **273**, 28 (1953).

10. F. J. Studer and G. R. Fonda, *J. Optical Soc. Am.*, **39**, 655 (1949).
11. R. W. Mooney, *This Journal*, **106**, 955 (1959).
12. K. H. Butler and R. W. Mooney, *Sylvania Technologist*, **9**, 121 (1956).
13. P. D. Johnson and F. E. Williams, *J. Chem. Phys.*, **18**, 1477 (1950).
14. R. W. Mooney, *This Journal*, **105**, 456 (1958).
15. C. M. Midgley, *Acta Cryst.*, **5**, 307 (1952).
16. K. Dornberger-Schiff, F. Liebau, and E. Thilo, *ibid.*, **8**, 752 (1955).
17. Kh. S. Mamedov and N. V. Belov, *Doklady Akad. Nauk. S.S.S.R.*, **107**, 463 (1956).
18. J. C. Platteeuw and G. Meyer, *Trans. Faraday Soc.*, **52**, 1066 (1956).

Luminescent Properties of Silver-Activated Magnesium Borate Phosphors

Yasuo Uehara, Yoshimasa Kobuke, and Isoo Masuda

Matsuda Research Laboratory, Tokyo Shibaura Electric Co., Ltd., Kawasaki, Japan

ABSTRACT

Silver-activated magnesium borate phosphors are extremely sensitive to reducing agents in the presence of water or moist air. With progressive reduction, the color of fluorescence turns from bluish white to green, yellow, orange, and red under excitation by 3650Å. At the same time the color of the phosphor powders changes from white to gray or black. Similar properties were found in some other crystals containing Ag. The characteristics of these phosphors show some similarities with photographic materials.

The fluorescence due to atomic silver in glasses and crystals containing silver has already been reported by Weyl and others (1). Reduction of the silver ions in these substances was effected by means of hydrogen, electron bombardment, and exposure to x- or γ-rays. It was found by the present authors that Ag-activated magnesium borate can be reduced by common reducing agents in the form of solutions and thus be made strongly fluorescent. These phosphors are extremely sensitive to reducing agents, and their fluorescence color under excitation by 3650Å radiation varies from an original whitish blue to orange or red with increasing degree of reduction; eventually they become nonfluorescent and dark gray. These phosphors are of interest in providing an analogy to photographic processes.

Preparation of Phosphor

Silver-activated magnesium borate phosphors of various compositions were prepared by firing mixtures of purified boric acid (H_3BO_3), basic magnesium carbonate ($3MgCO_3 \cdot MgO \cdot 4H_2O$), and silver nitrate with or without added aluminum hydroxide, for two 0.5 or 1 hr periods at 950°C. The initial firing was always made in air, and the second firing was carried out in various atmospheres, such as in air, oxygen, or nitrogen, after an intimate grinding between firings. Pure magnesium borates without added impurities were also prepared by the same method. The compositions studied were as follows: boric acid, 2 moles; basic magnesium carbonate, 0.5, 0.375, 0.25, and 0.125 moles; silver nitrate, $0\text{-}2\times10^{-2}$ moles; and aluminum hydroxide, $0\text{-}5\times10^{-3}$ moles. Furthermore, magnesium borates of composition $MgO \cdot B_2O_3$ containing 1 mole % Cu, Li, Be, Hg, Al, La, Tl, Ti, Ge, Zr, Sn, Pb, V, As, Sb, Bi, Se, Mn, Ce, Sm, U, and Th were prepared by the same method, except for phosphors with Ce and Sn which were fired in air or in a reducing atmosphere in the second heat treatment.

Reduction of phosphors.—A small amount of the phosphor is placed in a glass dish and wetted with an extremely dilute solution of a reducing agent. For most of the experiments, $10^{-5}N$ sodium sulfite ($Na_2SO_3 \cdot 7H_2O$) solution or the solution prepared by dissolving 1 cc Elon-Hydroquinon Borax (D-76) developer in 100 liters of water were used as reducing agents. With these dilute solutions of reducing agents, the fluorescence color of Ag-activated phosphors changes from an original whitish blue to green, yellow, orange, or red within a few minutes, while with concentrated solutions of reducing agents, such as D-76 developer itself, the phosphors turn into nonfluorescent black powders. On the other hand, pure magnesium borates of various compositions remained unchanged by the same reducing agents.

Filter paper or common white paper can also be used as convenient reducing agents. If a small amount of the dry phosphor powders is spread on a sheet of dry white paper in a layer of a few millimeter thickness, the reduction of the phosphor due to traces of reducing agents such as sulfite, which may be originally contained in the paper, occurs gradually and progresses from the interface between powder layer and paper to the upper layer of the powders. For example, the bluish white fluorescing phosphor spread on a sheet of paper turned completely into a green fluorescent phosphor during a few hours in air of about 70% relative humidity at room temperature, while the sample spread in a clean glass dish and wetted with distillated water showed no change of fluorescence color for a long time.

If the phosphor is first placed on a sheet of paper for several tens of minutes and then stored in a clean glass bottle, it turns into the reduced phosphor during a few months' time. Indeed, a phosphor spread on a sheet of paper for 30 min and then stored in a bottle in the dark for about five years turned into a dark gray powder producing only extremely weak red fluorescence under excitation by 3650Å, while the same phosphor stored from the beginning in a clean glass bottle turned into a strongly green fluorescent powder during the same length of time. The speed of reduction of the phosphor depends on temperature and moisture, as well as on the concentration of reducing agents. If the phosphor on a sheet of paper is moistened with hot steam, the color of fluorescence under excitation by 3650Å changes from whitish blue to green, yellow, orange or red, and finally to reddish dark gray within a few minutes. For the measurements of the optical properties of the reduced phosphor, the sample reduced on paper in air at room temperature was used since it was difficult to stop the reduction at the desired stage with reducing solutions.

Silver-activated phosphors reduced by electron bombardment or by means of hydrogen diluted with nitrogen in a third heat treatment at temperatures from 100° to 200°C showed weak fluorescence of various colors depending on the degree of reduction. When these phosphors were exposed to 2537 or 3650Å radiation and x- or γ-rays for 1 hr at room temperature they showed no changes of fluorescence color.

Emission and reflection spectra.—The spectral distribution of fluorescence under excitation by 3650Å and that of reflection were measured at room temperature by the same method as reported in a previous paper (2).

Experimental Results

Emission Characteristics

Silver-activated magnesium borate phosphors of approximate composition $MgO \cdot B_2O_3$: Ag (10^{-2} mole) and prepared by firing in air show a weak whitish blue fluorescence under excitation by 2537 or 3650Å, but not under excitation by cathode rays. The detailed hue of color and the intensity of fluorescence fluctuate from sample to sample, even when they are prepared under as nearly identical conditions as possible. This fluctuation of the luminescent properties may be due to slight differences of the atmosphere during preparation. The phosphors prepared by firing in oxygen or nitrogen in the second heat treatment are similar to those prepared by firing in air. At liquid air temperature, all of these phosphors produce strong bluish green or green fluorescence under excitation by 2537Å and 3650Å. The fluorescence of Ag-activated phosphors with different mole ratios of $MgO:B_2O_3$ was similar in color to that of the phosphor mentioned above, but weak in intensity. Pure magnesium borate showed no fluorescence under excitation by ultraviolet or cathode rays at room or liquid air temperature.

Silver-activated phosphors treated with reducing agents show a strong fluorescence whose color varies from bluish green to dark red depending on the degree of reduction of the phosphor, but only under excitation by 3650Å. The brightest fluorescence after reduction was obtained when the composition was $MgO \cdot B_2O_3$: Ag ($1\text{-}2\times10^{-2}$ moles). The fluorescent intensity of the phosphors emitting green, yellow or orange fluorescence is comparable to that of Cu-activated zinc or zinc·cadmium sulfide phosphors under excitation by 3650Å. Since the body color of the phosphor powder deepens from white to black with increasing degree of reduction, the intensity of the emerging red fluorescence of the gray colored powder is weak. The fluorescent intensity of Ag-activated phosphors of different mole ratios of $MgO:B_2O_3$ is weak after treatment with reducing agents as before. Pure magnesium borate without added impurities shows no fluorescence at all after reduction by the same reducing agents.

Among magnesium borates containing various elements other than Ag, several phosphors such as the ones containing Mn (red fluorescence under excitation by 3650Å or cathode rays), Tl (weak blue, 2537Å), Sm (orange, cathode rays), Ce(Ce^{3+}: strong violet, 2537Å) and Sn(Sn^{2+}: weak yellow white, 2537Å), produced fluorescence, but none of these phosphors showed a change of fluorescence color after treatment with the same reducing agents as before. Phosphors with 1 mole % Ag and increasing amounts of Al from 0.1 to 5 mole % showed a decreasing sensitivity to reducing agents as the Al concentration was increased. Thus a sample with 0.1 mole % Al was still strongly green fluorescent after the reduction, while one with 1% Al was already very weak.

The fluorescent spectrum of the bluish green phosphor obtainable by slight reduction on paper is shown by curve 1 in Fig. 1. After the phosphor was allowed to stand in air for 3 hr at room temperature, it gave the fluorescent spectrum shown by curve 2. As seen in this diagram, the normalized fluorescent spectra consist of at least two main bands peaking at about 4200 and 5300Å. With increasing degree of reduction, the intensity of the blue band decreases, while that of the green band increases.

The fluorescent spectrum of the green phosphor, which was reduced on paper in air, is shown by curve 1 in Fig. 2. The peak position is at about 5200Å in approximate agreement with that of the green band

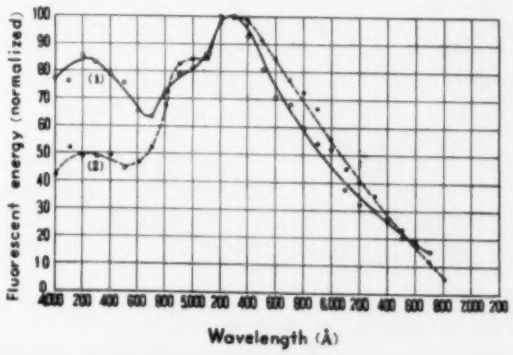

Fig. 1. Fluorescent spectrum of bluish white fluorescent magnesium borate phosphors with 1 mole % Ag, fired for two 0.5 hr periods at 950°C in air, under excitation by 3650Å at room temperature.

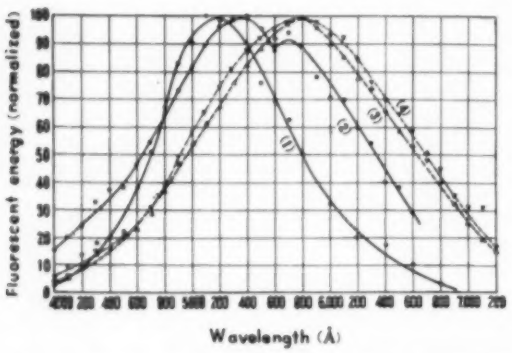

Fig. 2. Fluorescent spectrum of magnesium borate phosphors with 1 mole % Ag, fired for two 0.5 hr periods at 950°C in air, producing green (curve 1), yellow (curve 2) and orange (curves 3 and 4) fluorescence after reduction, under excitation by 3650Å at room temperature.

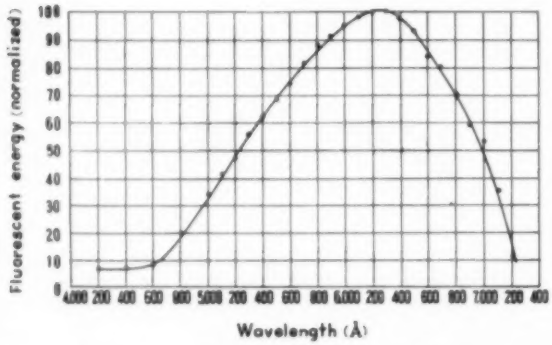

Fig. 3. Fluorescent spectrum of magnesium borate phosphor with 1 mole % Ag, fired for two 0.5 hr periods at 950°C in air, producing red fluorescence after reduction, under excitation by 3650Å at room temperature.

shown in Fig. 1. The fluorescent spectrum of the same phosphor exposed to 3650Å radiation for 6 hr in air at room temperature after the measurement of curve 1 in Fig. 1 is shown by curve 2 in Fig. 2. This spectrum shows two bands peaking at about 5400 and 5700Å which correspond to the bands peaking at about 5200 and 5800Å to be described below. The shift in peak position of the two bands may be due to the overlap of the two bands peaking at about 5200 and 5800Å.

The fluorescent spectra of samples which were allowed to stand in the dark in air for 24 hr, or for 18 hr followed by exposure to 3650Å for 12 hr, after the measurement of the spectrum shown by curve 2 in Fig. 2 was made, are shown by curves 3 and 4 in Fig. 2, respectively. The time required for the measurement of the respective fluorescent spectra mentioned above was about 30 min. The spectra shown by curves 3 and 4 in Fig. 2 are essentially identical and the peak wave length of the spectra is about 5800Å.

The fluorescent spectrum of a phosphor reduced on paper under irradiation by 2537Å for 30 hr at room temperature is shown in Fig. 3. The peak wave length of the spectrum is about 6300Å.

Reflection Spectra

The spectral reflection of pure magnesium borate of composition $MgO \cdot B_2O_3$ is shown by curve 1 in Fig. 4, relative to that of magnesium oxide. The reflection spectra of typical phosphors whose fluorescence spectra are illustrated by curve 1 in Fig. 1, by curves 1 and 2 in Fig. 2, and by Fig. 3 are shown by curves 2, 3, 4, and 5 in Fig. 4. All of these curves have a rather similar shape and show no narrow absorption bands over a wide range of the spectrum from about 2400 to 4800Å.

Discussion

Since the change of fluorescence color of phosphors treated with reducing agents was confined to the phosphors activated with Ag, the origin of this phenomenon must be ascribed to the presence of Ag. In Ag-activated magnesium borate phosphor prepared in oxidizing or neutral atmosphere, silver may be introduced into the matrix in the form of Ag^+ ions replacing Mg^{++} ions at the lattice sites. An O^{--} ion vacancy may be generated by the replacement of two Mg^{++} ions by two Ag^+ ions in order to satisfy the condition of charge neutrality in the phosphor, as has already been suggested for the Cu-activated calcium orthophosphate (2). The blue fluorescence band peaking at 4200Å may be ascribed to an Ag^+ activator center adjacent to an O^{--} ion vacancy.

Extending the assumption made above, the green, orange, and red bands in the reduced phosphor may be attributed to activator centers adjacent to O^{--} ion vacancies in which one, two, and three electrons are trapped, respectively. It is plausible to assume that one of the trapped electrons will combine with an Ag^+ ion and form an Ag-atom. If Ag-atoms aggregate into the colloidal form the phosphor powder will become gray or black colored.

It is further proposed that the surface O^{--} ions of the phosphor crystals react chemically with adsorbed reducing agents in the presence of water. For ex-

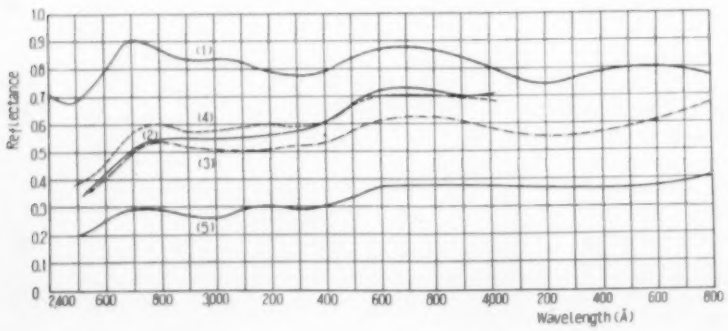

Fig. 4. Reflection spectrum of pure and Ag-activated magnesium borates: curve 1, pure magnesium borate; 2, bluish white fluorescent phosphor; 3, green fluorescent phosphor; 4, yellow fluorescent phosphor; and 5, red fluorescent phosphor.

ample, sulfite ions are thus oxidized to sulfate ions with the simultaneous release of free electrons. These free electrons then enter into the crystal via the conduction band and become trapped at O^- vacancies adjacent to Ag^+ ions. This may lead to a reduction of Ag^+ ions to Ag atoms. As a result, the concentration of surface O^- ions is greatly decreased. This establishes a steep gradient of O^- ion concentration in the region near the crystal surface, causing more O^- ions from the crystal interior to diffuse to to the surface. Repetition of these processes then leads to the progressive disintegration of the crystal until the last stage of reduction, namely the form of a black powder, is reached.

The strong interaction between activator center and lattice in the phosphor or the loose binding of trapped electrons with Ag^+ ions in the activator centers will be responsible for the rather flat reflection spectra shown in Fig. 4. Since the intensity of fluorescence of the phosphors producing green to orange fluorescence is comparable with that of Cu-activated zinc or zinc·cadmium sulfide whose quantum efficiencies have been reported to be about 0.5 at 3650Å, the quantum efficiency of these Ag-activated magnesium borate phosphors will be close to unity at 3650Å. This is estimated on the basis of their much lower absorption of 3650Å radiation compared with the sulfides.

With the incorporation of aluminum into Ag-activated magnesium borate, the number of O^- ion vacancies will decrease, since aluminum will be introduced into the matrix as Al^{+++} ions replacing Mg^{++} ions at the lattice sites. The effect of aluminum in lowering the intensity of fluorescence of the reduced phosphor is thus explained.

The properties of these phosphors resemble somewhat those of Ag-activated alkali halides or of pure silver halides as reported by Weyl and others (1, 3), but they are more complicated. In addition to the phosphors described, a number of other Ag-activated phosphors were prepared and reduced by the same method. Many phosphors, such as Ca or Sr silicate containing Ag, showed similar properties, but their intensity of fluorescence after reduction was lower than that of Ag-activated magnesium borate. Furthermore, it was found that silver nitrate crystals purified by repeated recrystallizations and stored in a clean glass bottle for about five years in the dark developed a number of bright specks under excitation by 3650Å, while nonpurified silver nitrate crystals turned into nonfluorescent gray crystals under the same conditions. The color and intensity of the fluorescent specks in the pure crystals were similar to those of magnesium borate phosphors shown by curves 3 or 4 in Fig. 2. These crystals containing orange fluorescent specks turned into nonfluorescent dark gray crystals after reduction by the same reducing agents as mentioned before. The luminescent centers of these crystals, therefore, seem to be identical with those of Ag-activated magnesium borates. We suggest that Ag^+ ions adjacent to negative ion vacancies in the phosphors correspond to the latent image in the photographic emulsion.

Acknowledgment

The authors wish to express their sincere thanks to Dr. Tsuneo Harada, the Director of Matsuda Research Laboratory, Tokyo Shibaura Electric Co., for his continuous support and encouragement. A major portion of this paper was presented at the Annual Symposium on Photochemistry, sponsored by The Chemical Society of Japan, The Photographic Society of Japan, and The Phosphor Circles of Japan, Tokyo, September 25, 1954.

Manuscript received April 22, 1959.

Any discussion of this paper will appear in a Discussion Section to be published in the December 1960 JOURNAL.

REFERENCES

1. W. A. Weyl, J. H. Schulman, R. J. Ginther, and L. W. Evans, *This Journal*, **95**, 70 (1949); J. H. Schulman, R. J. Ginther, C. C. Klick, R. S. Alger, and R. A. Levy, *J. Appl. Phys.*, **22**, 1479 (1951).
2. Y. Uehara, Y. Kobuke, and I. Masuda, *This Journal*, **106**, 200 (1959).
3. K. V. Shalimova and A. V. Belkina, *Zhur. Eksptl. Teoret. Fiz.*, **21**, 326 (1951); M. L. Kats, *Doklady Akad. Nauk S.S.S.R.*, **85**, 539 (1952); *Zhur, Eksptl. Teoret. Fiz.*, **23**, 720 (1952).

Chemical Etching of Silicon

II. The System HF, HNO_3, H_2O, and $HC_2H_3O_2$

H. Robbins and B. Schwartz

Hughes Semiconductors, Newport Beach, California

ABSTRACT

The kinetics of the reaction of silicon with solutions of hydrofluoric acid, nitric acid, and acetic acid are reported as a function of the composition of the etchant. The system qualitatively behaves in the same manner as the system hydrofluoric acid, nitric acid, and water, which has been reported previously. Quantitatively, the acetic acid diluted system shows a much higher tolerance for the diluent than does the water diluted system. The greater tolerance for acetic acid has been explained on the basis of the lesser ionization of nitric acid in acetic acid than in water. The reaction mechanisms postulated for the water diluted system have been found to apply equally well to the acetic acid diluted system.

Acetic acid is used widely as an additive to silicon etching solutions composed of hydrofluoric acid and nitric acid. This study was undertaken with the object of determining the role played by the acetic acid in the reaction, and also in the expectation that an understanding of the behavior of the acetic acid diluted system would lead to a better understanding of the water diluted system (1).

Experimental Procedure[1]

The kinetics of the system were determined by measuring the change in the dimensions of a silicon die, initially 0.125 x 0.125 in. in area and 0.025 in. thick, as a function of the composition of the etchant at constant initial temperature (25°C). The data were taken over the composition range where the decrement in die thickness exceeded 0.0001 in./min. The dice were n-type of approximately 3 ohm-centimeter resistivity; the two large surfaces were oriented along the (111) plane with an accuracy of approximately 90 min, whereas the remaining four surfaces were randomly oriented in the 111 zone. All surfaces were lapped with an abrasive grit; they were work damaged to an estimated depth of about ¼ mil.

The etching solutions consisted of mixtures, in various proportions, of nitric acid, hydrofluoric acid, and glacial acetic acid. No water was added to the solution. The only water in the solution was that contained in the concentrated hydrofluoric acid (51% H_2O) and nitric acid (30% H_2O). Before etching was begun, 20 ml of etching solution was placed in a small Teflon beaker and brought to 25°C in a constant temperature bath.

Two dice were placed in a small perforated polyethylene basket and etched simultaneously. Turbulent agitation was provided by rapidly swirling the basket through the solution, and quenching at the proper time was effected by rapidly transferring the basket to a large volume of water in a separate beaker. The decrement in die thickness was measured with a micrometer to ±0.0001 in.

The dice were etched three times, in separate portions of the same solution, and they were measured after each etch. The first etch was performed on an initially work damaged surface. The second etch was performed on a surface free from work damage, and the third etch was performed in the presence of a catalytic trace of sodium nitrite.[2]

Results and Discussion

Figure 1 depicts the etch rate corresponding to the catalyzed system as a function of the composition of the etchant. The solid curves correspond to the etching system in which acetic acid is the diluent, whereas the dashed curves correspond to the system in which water is the diluent. The curves are seen to converge on the zero diluent line, and to diverge as the amount of diluent is increased.

[1] Essentially the same experimental procedure was used here as was described in the first paper of this series.

[2] Small amounts of sodium nitrite have been found to enhance the rate of reaction in those instances where the supply of reagent by diffusion was not rate limiting (see below). Larger amounts of sodium nitrite caused inhibition of the reaction by formation of a protective film. This film is formed also in the presence of KNO_2 or NH_4NO_2, and on the basis of x-ray diffraction it has been identified as a fluosilicate.

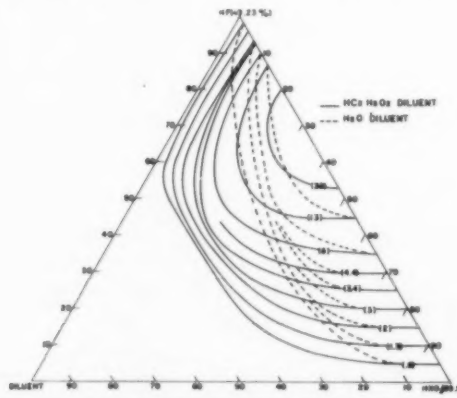

Fig. 1. Curves of constant rate of change of die thickness (mils/min) as a function of etchant composition in the system 49% HF, 70% HNO_3, and diluent.

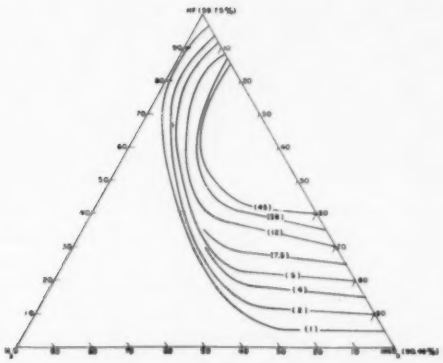

Fig. 2. Curves of constant rate of change of die thickness (mils/min) as a function of etchant composition in the system 60% HF, 90% HNO_3, and H_2O.

The etching behavior of the acetic acid diluted system is similar qualitatively to that of the water diluted system. The similarity is more striking when the acetic acid diluted system is compared with the more concentrated water diluted system shown in Fig. 2. There are three areas of general interest: the high nitric acid region, the high hydrofluoric acid region, and the region in the vicinity of the maximum etch rate. In the high nitric acid region the curves run parallel with lines of constant hydrofluoric acid, indicating that the hydrofluoric acid plays the kinetically important role here. In the high hydrofluoric acid region the course of the curves parallel with lines of constant nitric acid indicates that here the kinetically important reagent is nitric acid. In the region near the maximum etch rate both reagents play an important kinetic role.

The interpretation of the mechanism of the reaction in the water diluted system appears to be applicable also to the acetic acid diluted system. The mechanism involves a diffusion limited supply of reagents to the silicon surface, modified by autocatalytic factors as described earlier (1).

Effect of Diluent on the Reaction

The principal difference between the water diluted system and the acetic acid diluted system lies in the much greater tolerance of the latter for the diluent. Both systems initially show an indifference toward the addition of diluent in both the high hydrofluoric acid region and the high nitric acid region. When a critical amount of diluent has been added, however, the rates vanish rapidly upon the further addition of a small amount of diluent. In the high hydrofluoric acid region, the water diluted system of Fig. 1 already contains the critical amount of diluent so that no additional water can be tolerated if the etch rates are to retain their diffusion limited values.

Briner and co-workers (2, 3) have shown that the oxidizing power of nitric acid in concentrated solutions depends on the undissociated species, probably in the form of the pseudo acid $HONO_2$, which is involved directly in the oxidation. Cretella and Gatos (4) take a similar position with respect to the necessary role of undissociated nitric acid. They find that the rate of oxidation of germanium is proportional to the product of HNO_3 and undissociated HNO_2. They base their argument on the mechanism postulated by Vetter (5) as follows:

$$HNO_2 + HNO_3 \rightleftarrows N_2O_4 + H_2O$$

(slow and rate determining) [1]

$$N_2O_4 \rightleftarrows 2NO_2 \quad \text{(fast)} \quad [2]$$

$$NO_2 + e^- \rightleftarrows NO_2^- \quad \text{(fast)} \quad [3]$$

Here the active species is NO_2, which takes an electron from the germanium to form the nitrite ion. The nitrite ion then combines with a proton to regenerate the nitrous acid required for step [1]. This mechanism is in accord with the observed autocatalytic behavior of the reaction.

An additional possible interpretation of the mechanism is based on a paper by Schmid and Spahn (6) which considers the various equilibria involving nitrogen oxides and nitrous acid. The latter authors accept the basic ideas of Abel, *et al.* (7-9) that the active oxidizing agent is HNO_2 such that

$$2HNO_2 + R \rightarrow RO + 2NO + H_2O$$

(R = reducing agent) [4]

and that the formation of HNO_2 is rate determining.

$$HNO_2 + H^+ + NO_3^- \rightleftarrows N_2O_4 + H_2O$$

(slow, rate determining) [5]

$$N_2O_4 + 2NO + 2H_2O \rightleftarrows 4HNO_2 \quad \text{(fast)} \quad [6]$$

A portion of the HNO_2 is recycled through [5], and the remainder either reacts with the reducing agent to form more NO, which is again involved in the regeneration of HNO_2 as in [6], or diffuses away into the bulk of the solution. The net result is:

$$HNO_3 + R = RO + HNO_2 \quad [7]$$

On the basis of these equilibria which involve water, Schmid and Spahn come to the conclusion that there must be a maximum in the oxidizing ability of nitric acid at an optimum water content, since the removal of water past that point causes the reversal of Eq. [6] and thus a decrease in the concentration of the actual reactive species. As applied to the present research, this peak in the oxidizing ability of nitric acid would be leveled into a plateau by the diffusion mechanism, but would, in accord with our results to be discussed below, account for the ultimate falling off of the etch rates as the amount of water is decreased. We are not inclined to favor the point of view of Schmid and Spahn, since we have observed that in many instances the slowdown of the oxidation by nitric acid as the water content is decreased can be attributed to the formation of an insoluble film, and that in instances where the formation of the film does not take place, e.g., in the oxidation of substances such as sulfur, selenium, or phosphorus, the rates continue to increase monotonically as the amount of water is decreased. A further complication is the fact that the etching of silicon will take place in the presence of a slight excess of permanganate or cerate ions, which quantitatively remove all of the nitrogen existing in lower valence states, and which themselves attack silicon but slowly, if at

all. Under these conditions only the mechanism of Briner is possible. We are inclined to consider that it is this process that initiates the reaction, generating a surface concentration of catalyst that leads to the build-up of the etch rate to the steady-state value. In the steady state, the reaction probably takes a parallel path through the intermediate formation of HNO_2 within the boundary film in a mechanism similar to that postulated by Schmid and Spahn (6).

The difference between the two systems tolerance for diluent, shown in Fig. 1, reflects the difference in the basicity and dielectric constant of the diluents. Since the oxidizing power of nitric acid has been shown to depend on the undissociated HNO_3 molecule, the etch rates at constant nitric acid concentration should decrease as water is added to the system. However, as long as the reaction is diffusion governed, the reaction rates will remain constant in spite of the decreasing oxidizing power of the nitric acid as diluent is added. Upon the further addition of water, however, a point is reached ultimately where the oxidation potential has been reduced to the extent that the rate of oxidation of the suface during the induction period becomes slightly less than the possible rate of supply of reagents by diffusion. At this point, the reduction products of nitric acid begin to play a kinetically observable role, and, since the reaction is now sensitive to the catalyst concentration, there results a very rapid decrease in the rate of the initiation reaction on the further addition of only a small amount of diluent. Since a 49% HF solution already contains the critical amount of water, it is necessary to employ a 60% solution to observe this behavior.

When acetic acid is the diluent, it must be remembered that in the high HF region and at constant HNO_3 concentration, diluent is being substituted for an aqueous HF solution. Thus a very weak base of low dielectric constant is being substituted for a somewhat stronger base, water, and a substance having moderately acidic properties, HF. Initially this should result in a decrease in the dissociation of the nitric acid, since the solvent is initially more than 50% water. Because of the diffusion limitation, the etch rates do not respond to the increased free nitric acid concentration. On further dilution with acetic acid, the removal of HF, which is a stronger acid than acetic acid, probably counteracts the effect of the substitution of acetic acid for water, so that the concentration of undissociated HNO_3 probably goes through a maximum and then decreases. A critical composition with respect to diluent thus is reached ultimately, and the rates vanish on the slight further addition of acetic acid, for the same reason as in the water diluted system.

The same argument can be used to interpret the abrupt change of the curvature of the rate contours with increasing diluent in the high nitric acid region. The question may be raised that, if in the high HF region the reaction can be noncritical at 5% HNO_3, why does it become critical at 50% HNO_3 in the high nitric acid region of the acetic acid diluted system, and at a still higher value of HNO_3 in the water diluted system? We can only suggest that the difference lies in the nature of the silicon surface. In the high HF region the surface is essentially stripped of oxide, and the rapid decrease in the etch rate is the result of the slowdown of the oxidation reaction. In the high HNO_3 region the surface is essentially covered with an oxide mask. As the concentration of HNO_3 is decreased, this oxide becomes more tenuous, until a point is reached at which the HF reaction begins to slow down. The slowdown in the HF reaction causes a slowdown in the over-all reaction which then further affects the oxidation step through the mechanism of reduced catalyst production. This condition then requires an increased HF concentration to restore the etch rate to its previous value. It can be seen that in the critical region the rate contours run in the direction of constant acetic acid concentration, suggesting that the decrease in reactivity of the nitric acid as the latter is decreased in concentration may be compensated by the increase in the HF concentration. In this region the reaction is probably not strictly diffusion limited, since there is a finite surface concentration of both reagents. However, diffusion still plays a role in that the surface concentration does not equal the bulk concentration of reagents, and both the surface concentration of reagents and the nature of the surface itself affect the kinetics.

Chemical etching in solutions the compositions of which lie in the critical regions of Fig. 1 can be extremely frustrating. As an example, a mixture of 4.50 ml HF, 7.50 ml HNO_3, and 8.00 ml of $HC_2H_3O_2$ has always been found to etch a work damaged specimen, and etching always continued at the same rate even after all of the damage had been removed. A fresh solution did re-etch the specimen if the solution had been made up from 48.9% HF, but it did not re-etch the specimen if it had been made up from 48.5% HF. Furthermore, the addition of one drop of acetic acid to 20 ml of the solution that had been made up from 48.9% HF caused the solution to lose its ability to re-etch. The addition of a few milligrams of sodium nitrite then caused the solution to regain its etching ability. If an etching die were transferred to a fresh solution made up from 48.5% HF, it usually would continue to etch at the same rate, since a trace of catalyst reinitiates the reaction. If this die were transferred rapidly to a solution of the same composition, swirled to dissipate the catalyst, and then transferred to a third solution of the same composition, etching invariably would be quenched. In all cases, the etching rate was either in the vicinity of 1.8 mil/min or 0.

In view of this behavior, the reaction must proceed first through an induction period in which the autocatalytic factors cause a build-up of the etch rate to the steady-state value. The induction period depends greatly on the condition of the silicon surface. A work damaged surface has a short induction period, whereas an undamaged surface has a relatively long induction period, owing to the absence of catalyst initially. Whether or not the etch rate can build up to the steady-state value then depends on whether the catalyst can be conserved in the vicinity

of the surface in sufficient quantity to assure its involvement in the propagation of the reaction. The etch rates thus seem to be the result of a balance struck between the autocatalytic factors, which are explosive in nature, and some rate limiting mechanism. Since the rates are the result of the difference between these two large quantities, the system may be inherently unstable, and this may cause the measured etch rates to be nonreproducible.

Conclusions

The role of acetic acid in the etchant is primarily that of a diluent. As such it is able to provide control over the rate of the reaction by reducing the concentration of the kinetically important species. However, this function also can be performed with nitric acid as diluent in the compositions rich in nitric acid, or with hydrofluoric acid in the compositions rich in hydrofluoric acid. Excessive addition of acetic acid can cause the etch rates to become erratic and extremely critical with respect to small changes in composition. Water also can be used as a diluent, except that in the high hydrofluoric acid region the system is critical with respect to the addition of diluent.

The kinetics in the acetic acid diluted system are governed by the same factors that operate in the water diluted system. Thus the reaction rates are determined by the rate of diffusion of the kinetically important species to the surface of the specimen. The autocatalytic factors that operate in the water diluted system play the same role in the acetic acid diluted system. The quantitative differences between the two systems can be explained on the basis of the difference in the basicity and dielectric constant of the two diluents.

Manuscript received April 6, 1959. This paper was prepared for delivery before the Ottawa Meeting, Sept. 28-Oct. 2, 1958.

Any discussion of this paper will appear in a Discussion Section to be published in the December 1960 JOURNAL.

REFERENCES

1. H. Robbins and B. Schwartz, *This Journal*, **106**, 505 (1959).
2. E. Briner, *Helv. Chim. Acta*, **18**, 363 (1935).
3. E. Briner and P. Bolle, *ibid.*, **18**, 368 (1935).
4. M. Cretella and H. Gatos, *This Journal*, **105**, 487 (1958).
5. K. Vetter, *Z. physik. Chem.*, **194**, 199 (1950).
6. G. Schmid and H. Spahn, *Z. Metallkunde*, **45**, 128 (1955).
7. E. Abel and H. Schmid, *Z. physik. Chem.*, **132**, 55 (1928).
8. E. Abel and H. Schmid, *ibid.*, **134**, 279 (1928).
9. E. Abel, H. Schmid, and S. Babad, *ibid.*, **136**, 135 (1928).

High-Purity Silicon from an Iodide Process Pilot Plant

Carlyle S. Herrick and James G. Krieble[1]

Research Laboratory, General Electric Company, Schenectady, New York

ABSTRACT

Silicon tetraiodide is formed from commercial silicon and iodine in a fluid-bed reactor. Impurities are rejected by solvent recrystallization followed by fractional distillation. High-purity silicon is formed by thermal decomposition of the iodide on a silicon surface. Silicon made this way has a resistivity over a 1000 ohm-cm. Reproducible results are obtained which suggest the product quality is controlled by back-contamination from the decomposition and crystal growing steps. Data from the decomposition of silicon tetraiodide at 1000°C and low pressure are correlated by the relation:

$$\log p = 2.18 - \frac{m}{0.305}$$

where p = lb SiI_4 vapor feed/hr/ft^2 heated surface and m = fraction of $SiI_{4(g)}$ converted to $Si_{(s)}$. It is postulated that this reaction reaches equilibrium.

Iodide chemistry was developed by Van Arkel and de Boer (1) into a useful method for reducing the oxygen, nitrogen, or carbon content of such refractory materials as titanium, zirconium, hafnium, and silicon. Other impurities, aluminum, beryllium, boron, iron, and copper, are not rejected effectively by this simple iodide cycle and, as a result, further development of the iodide method has been necessary to produce the purity required in semiconductor silicon. The most fruitful approach has been to remove the iodide intermediate from the reaction system, subject it to additional purification, then decompose it to form a purer material.

Recrystallization (2), distillation (2-4), sublimation (5), and zone refining (5, 6) have been reported to be useful for the intermediate purification of sili-

[1] Present address: Lamp Metals & Components Department, General Electric Company, Cleveland, Ohio.

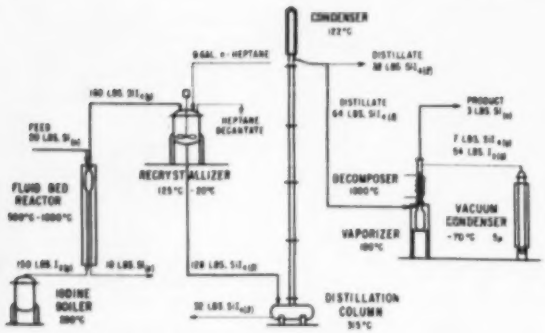

Fig. 1. Iodide process flowsheet

con tetraiodide. McCarty (2) in this laboratory has shown that silicon of 500 ohm-cm resistivity can be prepared by using a recrystallization step followed by a distillation step. The present work has been directed toward finding answers to the questions:

1. Can silicon of even higher purity be made by chemical means?
2. Can this silicon be made in large quantities?

Both questions can be answered in the affirmative when an iodide process is used.

Process Description

The flow sheet for this iodide process, Fig. 1, shows reaction of silicon and iodine to form silicon tetraiodide, purification of tetraiodide by recrystallization, then distillation, and decomposition to high-purity elemental silicon and iodine. This same sequence of events was used by McCarty (2); however the character of the reaction step, distillation and decomposition step used here have been modified substantially to improve their effectiveness.

Silicon tetraiodide is formed in a fluid bed reactor using commercial 99.9% silicon and research grade iodine at atmospheric pressure. The bed, charged with 44-100 μ diameter silicon powder is fluidized entirely by iodine vapor, although an inert gas diluent may be used if desired. Fluidization provides excellent heat transfer between particles and creates a uniform temperature throughout the bed. It has the advantage that an exothermic reaction involving a poor heat conducting solid can take place at constant temperature. Of course, constant reaction temperature means a constant reactivity for silicon and its impurities and a better separation between them based on reaction energies. Previously described small scale reactors have used the fixed bed principle and thus have not realized the full separating potential of the reaction step. Close observation of a fixed bed using iodine and silicon discloses that lack of temperature control causes a reaction zone to travel through the bed as a "hot spot," usually incandescent. Such lack of control is characteristic of fixed beds. Unreacted silicon enriched in impurities is discharged from the fluid bed at the end of an experiment.

Iodine residence time in the bed is short, 1-2 sec; however the reaction is rapid enough for the yield to be quantitative. As iodine is consumed from the vapor stream, the silicon tetraiodide product takes over the job of fluidizing the bed. Since the reaction appears to involve only iodine atoms and silicon, there is a 4 to 1 volume change during the reaction according to Eq. [1].

$$4\ I_{(g)} + Si_{(s)} \rightarrow SiI_{4(g)} \qquad [1]$$

This decrease in top-bed fluidizing velocity helps reduce powder entrainment.

Silicon tetraiodide leaving the reactor condenses in the recrystallizer where n-heptane is added in 1 to 1 mole ratio. The resultant slurry is warmed and then cooled to dissolve and recrystallize the tetraiodide. The n-heptane containing dissolved impurities is decanted, then the operation is repeated. The over-all yield for two recrystallizations is about 80%.

In the distillation column the tetraiodide is divided into a bottom fraction containing the less volatile impurities, a top fraction containing the more volatile impurities, and a second distillate of purified tetraiodide comprising 50% of the column charge.

This purified tetraiodide is fed to the vaporizer where evacuating and heating produce a low-pressure tetraiodide atmosphere around a heated silicon rod. Now the tetraiodide dissociates to the diiodide (7) and then to solid silicon according to reactions [2] and [3].

$$SiI_{4(g)} \rightarrow SiI_{2(g)} + 2\ I_{(g)} \qquad [2]$$

$$SiI_{2(g)} \rightarrow Si_{(s)} + 2\ I_{(g)} \qquad [3]$$

A deposit of high quality product silicon forms on the heated rod while the iodine atoms recombine after cooling and flow to the vacuum condenser along with unreacted tetraiodide. The diffusion rates of many impurities in silicon are comparable with the rate of product accumulation. Commercial semiconductor silicon was used for the heated decomposer surface to minimize diffusional contamination of the product silicon. The yield for this step was about 50%.

In the stoichiometry of Fig. 1, 20 lb of silicon and 150 lb of iodine are fed to the reactor for each 3 lb deposit of product silicon. It does not take account of the existing opportunities to reuse and recycle waste streams to bring consumption and production into better balance.

Except for impurities added during processing, it is assumed that impurities are present as iodides in silicon tetraiodide. Vapor pressure data from Brewer (8) and from Schäfer and Hönes (9) are shown in Fig. 2. Vapor pressures of Nb, Hg, Ga, Ge, Al, As, and Sb iodides fall in a band between those of tin and tantalum. Vapor pressures of most metal iodides are lower than for silicon tetraiodide so they will remain in the reboiler during distillation. Phosphorus and boron iodides are more volatile and must be removed at the top of the distillation column before purified silicon tetraiodide can be distilled overhead. At 1 atm CI_4 boils 19°C higher than SiI_4 and PI_3 63°C lower. The calculated relative volatilities are 3.4 for PI_3 with respect to SiI_4 and 1.4 for SiI_4 with respect to CI_4. Both volatilities are large enough to permit extensive separations with a moderate number of theoretical distillation plates.

This process scheme imposes stringent requirements on the materials of construction. Silicon tetra-

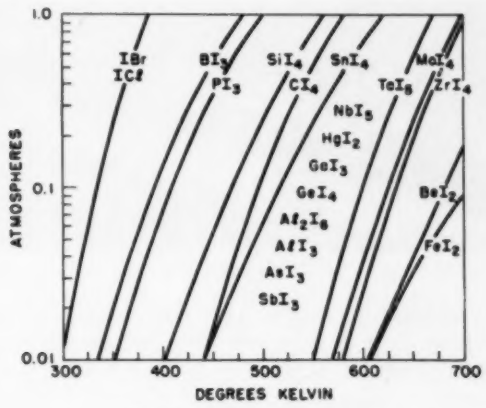

Fig. 2. Iodide vapor pressures

iodide in process is usually accompanied by some iodine and hydrogen iodide and this mixture is quite aggressive toward container materials at elevated temperatures. Quartz, due to its high chemical stability, was selected for the reactor, the distillation column, and the decomposer.

Process Equipment

The fluid bed reactor is a 4-in. diameter quartz tube 8 ft long mounted vertically in a furnace, Fig. 3. A porous-type gas distributor was used to eliminate stagnant zones and get uniform fluidization (10). Heat of reaction is removed from the bed by direct radiation to the furnace walls which are maintained about 50°C cooler than reaction temperature. The electric heating elements in the furnace are internally exposed to get maximum heat transfer and

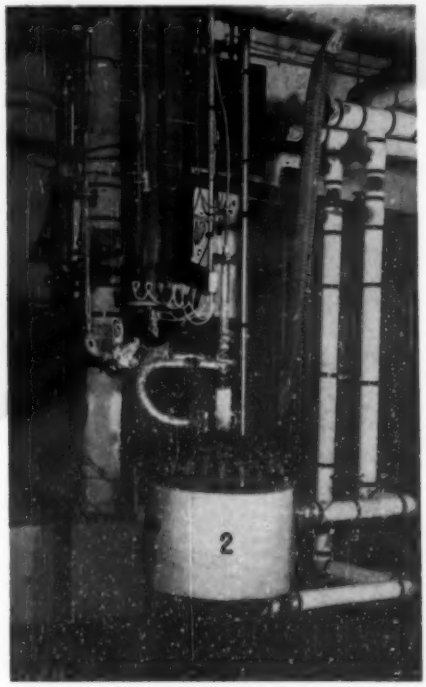

Fig. 3. Fluid bed reactor: 1, reactor furnace; 2. iodine boiler.

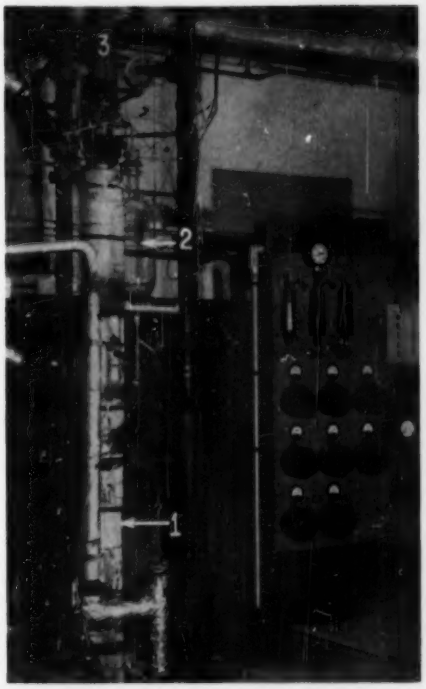

Fig. 4. Distillation column: 1, column upper sections; 2, product receiver; 3, condenser.

controllability. Iodine is vaporized in a 10-gal glass-lined steel iodine boiler jacketed with 230°C hot oil.

The recrystallizer is a 20-gal glass-lined steel agitated vessel jacketed for steam heating or water cooling. It is mounted on a base which permits weighing without disturbing the quartz piping connections.

The all-quartz distillation column consists of reboiler, four lengths of 3-in. diameter tubing, and a condenser, with an over-all height of 24 ft. At the bottom the 10-gal reboiler is heated by Calrod® units inserted in quartz tubes sealed lengthwise through the lower sector of the vessel. Direct radiant heat transfer from heater to boiling SiI, gives fast response and minimum superheating.

At the top of the distillation column, Fig. 4, a 3-ft length of 4-in. tubing serves as a condenser. It is provided with a 6-in. stainless steel jacket and a circulating hot oil coolant system. Each of the four column sections is packed with ⅜-in. quartz rashig rings with quartz packing supports and distributor plates. The entire asesmbly is supported by a system of weights and pulleys and is arranged for adiabatic operation. Thirty-two theoretical plates were measured at 1 atm using a n-heptane methylcyclohexane test mixture (11) and the Fenske equation (12).

Silicon tetraiodide is removed from the column in a 3-gal quartz receiver and placed in the vaporizer to become the bottom portion of the decomposer assembly. Figure 5 shows a Pyrex receiver of the same size holding 45 lb of tetraiodide. The discoloration is caused by iodine released by a photochemical oxidation which has not yet been identified. Heating silicon tetraiodide from room temperature to 100°C

® Registered Trademark.

Fig. 5. Product receiver

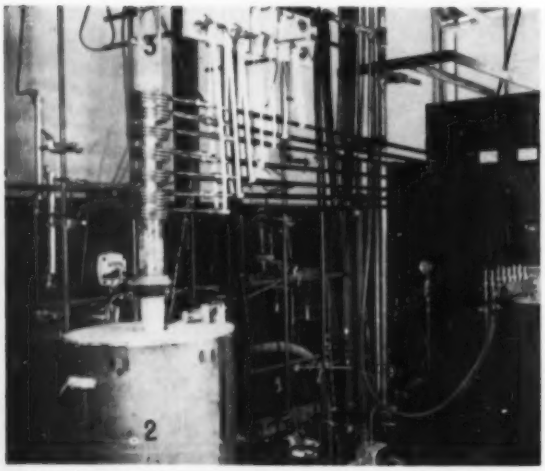

Fig. 6. Decomposer assembly: 1, induction heater; 2, vaporizer; 3, decomposer.

causes expansion forces strong enough to break glass or quartz containers. Melting the outer layer of the SiI_4 cake and reforming along one side of the vessel creates ample room for expansion without breakage.

The decomposer consists of a vertical 2-in. quartz tube mounted atop a 3 gal SiI_4 receiver just described. A silicon rod, ⅝ in. in diameter and 14 in. long, mounted inside the tube, is heated to 1000°C by external coils connected to an induction heater, Fig. 6. As SiI_4 decomposes in contact with the heated surface, silicon deposits on the rod which increases in diameter. Adjustment of the heating coils along the rod is necessary to obtain a uniform deposit.

Figure 7 shows a typical deposit obtained by heating a 10 in. length of rod. It is 1.25 in. in diameter

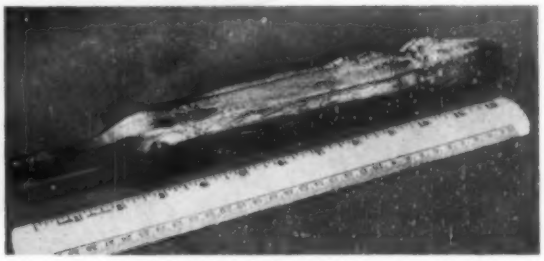

Fig. 7. Product silicon

and contains 1 lb of new silicon. Deposit and rod are separated by a sawing operation which produces sizes and shapes required for crystal growing.

Product Silicon Evaluation

Resistivity measurements were made on single crystals prepared by the Czochralski technique (13). The four point probe method (14) was used to measure resistivity profiles. Minority carrier lifetime was measured by the infrared photoconducting decay method (15).

Experimental results are listed in Table I. It should be recognized that the four point probe measurement is subject to large errors above 1000 ohm-cm. Furthermore, the crucible method of crystal growing contaminates the silicon, and at high resistivities this causes the seed end resistivity to change rapidly along the crystal so the region of maximum resistivity is difficult to locate. This effect is noticeable in Table I where resistivity values are reported at approximate 1-in. intervals along the crystals.

Resistivities as high as 3500 ohm-cm have not been reported previously for crucible grown silicon. Dissolution of quartz in molten silicon during crystal growth is known to occur (16, 17), and the accompanying impurities are expected to limit the maximum obtainable resistivity values. Practical values for such a limit have not yet been reported. Hannay (17) reports that the limit is higher than 300 ohm-cm p-type while Taft and Horn (16) report exceeding 300 ohm-cm in practice. The present work suggests that the practical limit is above 1000 ohm-cm p-type under the most favorable experimental conditions, i.e., minimum time elapses between the onset of melting and the cooling-off of the seed end of the pulled crystal.

Examinations in a cryostat for deep level compensation showed these effects to be absent. Each crystal did exhibit a photo-emf in ambient light; however, type reversals were not detectable by potentiomet-

Table I. Product silicon resistivity and lifetime

Lot No.	Decomposer Rod material	Rectification type	Speed end	Resistivity, ohm-cm		Sprout end	Lifetime, μsec
1	ZR	p	3400	1100	500	200	100
2	C	n	70	78	65	130	50
3	ZR	p	3500	700	400	130	100
4	ZR	p	3200	900	400	140	350

ZR—Zone refined silicon, 130 ohm-cm p-type.
C—Commercial grade silicon, 2 ohm-cm n-type.

ric probing or by applying an electric field to a barium titanate coated surface. The source of the photo-emf is not understood at present. While it did interfere somewhat with lifetime measurements, the values obtained are in a medium range for high-quality crucible grown silicon.

With all factors considered, it is concluded that the product silicon quality corresponds to a resistivity over 1000 ohm-cm. Measurements on crucible grown silicon in this resistivity range do not warrant a more quantitative statement at the present time.

The Table I data are a full sequence of lots without deletions or selections; thus the agreement between 3400, 3500, and 3200 ohm-cm resistivities is remarkable in view of the measurement uncertainties and may be fortuitous. The weight of evidence indicates to the authors, however, that this agreement is more real than circumstantial. It is believed to result from improved effectiveness and reproducibility in the processing steps and from skillful handling of the crystal growing problem.

Two different grades of silicon were used for the decomposer surface. One, the zone refined, had a resistivity of 130 ohm-cm; the other was a premelt rod of 2 ohm-cm commercial grade silicon. Both were prepared by the techniques of Taft and Horn (16). The low resistivity of product silicon in the second experiment correlates with the low resistivity of the silicon rod used in the decomposer. Since relative volumes of silicon and time of deposit were roughly equal in the four experiments, the data suggest that a proportional dilution effect controls product resistivity at about 27 times greater than the starting rod resistivity. It further suggests that the effect is roughly independent of resistivity over the range covered by the experiments.

Macroscopic examination of a transverse fraction in the product silicon gives the impresion of close-packed needlelike crystals with major axes radiating outward from the center of the rod. Hölbling (18) shows similarly oriented columnar crystals from the hydrogen reduction of SiI_4 on a carbon rod. Sangster, Maverick, and Croutch (19), on the other hand, show propagation of the original crystal structure when $SiBr_4$ is hydrogen reduced on a heated silicon filament.

The product silicon in this work was found to propagate the crystal structure of the original silicon rod. Figure 8 shows several crystal faces present after 2×10^5 atom layers of silicon have been deposited. The same crystal pattern was present in the rod before deposition. Microscopic examination of the product shows the individual crystals to have a large number of defects, presumably twins, Fig. 9. These twin lines are highly oriented in the growth direction. This degree of defect alignment would account for the observed fraction pattern as well as for the observation that the product material is much weaker when stressed in the transverse direction than is the original rod.

Fig. 8. Crystal faces preserved during deposition

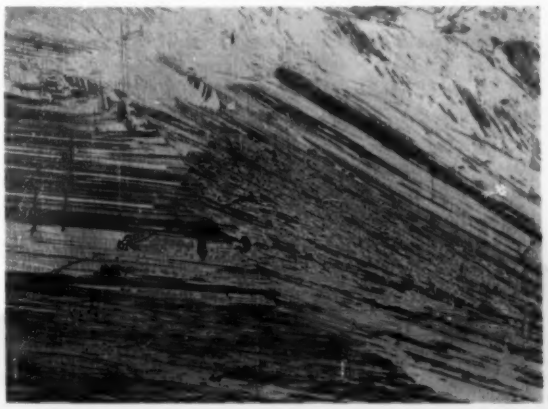

Fig. 9. Product silicon crystal structure. Magnification 200 X before reduction for publication.

Impurity Separations During Processing

A resistivity of 3500 ohm-cm requires the electrically active impurity content of the silicon to be about 8 atoms per hundred billion atoms. The contribution of each process step to the total separation has been estimated in Table II to indicate whether this purity level is a reasonable achievement for the process. Impurity concentrations are indicated only as to order of magnitude which is about the accuracy warranted by much of the supporting data. The starting silicon was commercial acid-leached 99.9% silicon. Spectrographic analyses of this material gave results in agreement with those reported by Szekely (4). The most concentrated impurity was present less than 1×10^{-4} atoms per atom Si. Analysis of the SiI_4 product from the fluid bed reactor by the same means shows the maximum impurity concentration to be a few parts per million. Similarly after the recrystallization step the impurity content is below the sensitivity of the analytical method. It is interesting to note that detectable amounts of boron are rejected in the solvent.

An indirect approach is necessary to estimate distillation column output purity. Calculations for the PI_3-SiI_4 system using the Fenske equation (12) and a relative volatility modified to dilute solution conditions according to the experience of Green and

Table II. Impurity separating ability of process steps

Process step	Atoms of most concentrated impurity per silicon atom		Separation factor
	Input	Output	
Fluid bed reactor	1×10^{-5}	10^{-6}	10^{1}
Recrystallizer	10^{-6}	10^{-8}	10^{2}
Distillation column	10^{-8}	10^{-10}	10^{2}
Silicon surface decomposer	10^{-10}	10^{-11}	10^{-1}

Kafalas (20) indicate a maximum separation factor of 5.5 x 10^{6} for this column and feed. It is probable, however, that column performance is limited to a factor of 10^{5} by an aerosol entrainment mechanism according to Manowitz, Bretton, and Horrigan (21). This factor applies to all iodide impurities except CI_4. Since carbon is one of the elements most effectively rejected by iodide chemistry the lower separation factor for this compound has not caused special problems.

The decomposer separation factor calculated as the difference between known input and output impurity levels gives 10^{-3} or a hundredfold contamination. This is consistent with the observed dependence of product purity on silicon rod purity. Moreover, the magnitude of the effect is reasonable for the impurity level of this step.

Two conclusions can be drawn from this analysis. First, product silicon in the 10^{-11} impurity range is within the capability of this process. Second, improvements in the decomposition step will probably yield product silicon of still higher purity.

SiI_4 Decomposition

The experimental observations on the decomposition step made at the General Electric Research Laboratory including this work and that of McCarty are correlated in Fig. 10. Equation [4] expresses the linear correlating function.

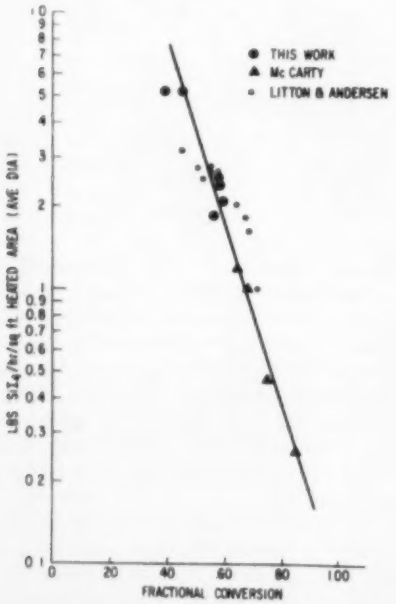

Fig. 10. Correlation of decomposition reaction data

$$\log p = 2.18 - \frac{m}{0.305} \qquad [4]$$

when p = pounds of SiI_4 vapor feed to the decomposer per hour per square foot of heated surface (arithmetic average) and m = fractional conversion of SiI_4 to Si.

The correlation holds for the over-all reaction of Eq. [5] at 1000°C and a condenser pressure of 1 to 10 μ.

$$SiI_{4(g)} \rightleftharpoons Si_{(s)} + 2\,I_{2(g)} \qquad [5]$$

The basic significance of this correlation is not understood at present, and no theoretical treatment exists to support it. Undeniably it correlates the data well. The results of Litton and Andersen (3), who have published the only data on thermal decomposition of SiI_4, have been recalculated and are compared with Eq. [4] in Fig. 10. Although the Litton and Andersen data show some scatter, the quantitative agreement is good. The decomposer vessels used in these three investigations differ widely in geometry. In this work decomposition occurred on a 5/8-in. diameter rod in a 2-in. diameter vessel. McCarty decomposed inside a 1.25-in. diameter cylinder while Litton and Andersen decomposed on a 0.1-in. diameter wire formed into an open helix inside a 2.75-in. diameter vessel. The fact that data taken under such widely different circumstances fit the same correlation suggests that chemical equilibrium exists in each type of equipment over the experimental range covered.

It is interesting to note that in all three studies each datum is really the average result of an entire experiment conducted at a continuously changing iodide vaporization rate, hence the instantaneous conditions corresponded with the average for a short time only. The form of the correlating equation $p = e^{m}$ is such that the derivative dp/dm is also equal to e^{m}. In this case, if the average diameter is replaced by the instantaneous diameter, the correlation will apply to the variables on an instantaneous basis. This condition is a prerequisite to having Eq. [4] represent an equilibrium relation.

One should note that the units, pounds per hour per square foot heated area, are actually unconventional units of pressure. Although no investigator has yet reported decomposer pressure measurements for reasons of contamination and corrosion, in principle sufficient data are now available to calculate an experimental equilibrium constant. The constant for equilibrium Eq. [5] is given by [6].

$$K_p = \frac{[I_2]^2}{[SiI_4]} \qquad [6]$$

In Table III experimental pressure values taken from the correlation have been recalculated to the more familiar units microns Hg. K_p has been calculated on the hypothesis that the experimental pressure is the total pressure in the system, i.e., the plug flow case or flow with no back-mixing. The variation between values of K_p is less than a factor

Table III. Experimental equilibrium constant

Lb SiI_4/hr/ft²	Pressure, μHg	K_p, mm
0.20	0.94	1.3×10^{-4}
0.30	1.4	1.2
1.0	4.4	1.4
3.0	13	1.9
6.0	25	2.2

of 2 which is firm evidence for equilibrium conditions during the decomposition reaction.

Acknowledgments

The authors appreciate the guidance and assistance of L. V. McCarty throughout the work, also C. B. Collins, F. H. Horn, and R. O. Carlson who took part in many helpful discussions. R. O. Carlson and G. W. Ludwig evaluated the product silicon, and W. C. Dash supplied silicon rods for the decomposer. R. J. Sullivan, R. L. Richard, and D. A. Reed assisted in carrying out the experimental work.

Manuscript received Jan. 22, 1959. This paper was prepared for delivery before the Buffalo Meeting, Oct. 6-10, 1957.

Any discussion of this paper will appear in a Discussion Section to be published in the December 1960 JOURNAL.

REFERENCES

1. A. E. Van Arkel and J. H. deBoer, *Z. anorg. u. allgem. Chem.*, **148**, 345 (1925).
2. L. V. McCarty, *This Journal*, **106**, 1036 (1958).
3. F. B. Litton and H. C. Andersen, *ibid.*, **101** 287 (1954).
4. G. Szekely, *ibid.*, **104**, 663 (1957).
5. B. Rubin, G. H. Moates, and J. R. Weiner, *ibid.*, **104**, 656 (1957).
6. G. H. Moates and B. Rubin, Paper presented before Electronics Division 113th meeting, Electrochem. Soc., New York, April 1953.
7. H. Schäfer and B. Morcher, *Z. anorg. u. allgem. Chem.*, **290**, 279 (1957).
8. Brewer, *et. al.*, "The Chemistry and Metallurgy of Miscellaneous Materials, Thermodynamics," L. L. Quill, Editor, McGraw-Hill Book Co., New York (1950).
9. H. Schäfer and W. J. Hönes, *Z. anorg. u. allgem. Chem.*, **238**, 68 (1956).
10. E. W. Grohse, *AIChE Journal*, **1**, 358 (1955).
11. E. C. Bromily and D. Quiggle, *Ind. Eng. Chem.*, **25**, 1136 (1933).
12. M. R. Fenske, *ibid.*, **24**, 482 (1932).
13. J. Czochralski, *Z. Physik Chem.*, **92**, 219 (1918).
14. A. Coblenz and H. L. Owens, "Transistors: Theory and Measurement," p. 208, McGraw-Hill Book Co., New York (1955).
15. R. L. Watters and G. W. Ludwig, *J.Appl. Phys.*, **27**, 489 (1956).
16. E. A. Taft and F. H. Horn, *This Journal*, **105**, 81 (1958).
17. N. B. Hannay, "Recent Advances in Silicon," Progress in Semiconductors, Vol. 1, p. 7, Heywood, London (1956).
18. R. Hölbling, *Z. Angew. Chem.*, **40**, 655 (1927).
19. R. C. Sangster, E. F. Maverick, and M. L. Croutch, *This Journal*, **104**, 317 (1957).
20. M. Green and J. A. Kafalas, *J. Chem. Soc.*, **5943**, 1604 (1955).
21. B. Manowitz, R. H. Bretton, and R. V. Horrigan, *Chem. Eng. Prog.*, **51**, 313 (1955).

The Preparation and Properties of Aluminum Antimonide

W. P. Allred, W. L. Mefferd, and R. K. Willardson

Battelle Memorial Institute, Columbus, Ohio

ABSTRACT

An improved method of growing single crystals of aluminum antimonide is described. Oxide from the aluminum has been eliminated by a vacuum heat-treating technique which also removes volatile impurities. The mobility of the positive carriers in AlSb at 300°K is found to be greater than 400 cm^2/v-sec. Values as high as 5000 cm^2/v-sec have been measured at 50°K. The p-type impurities have an activation energy of about 0.02 ev in AlSb. A maximum is observed at 4000 gauss in the magnetic-field dependence of the Hall coefficient at 77°K.

Considerable interest has been shown over the past few years in the development of semiconductors which are capable of operating at high ambient temperatures. The electrical properties of some of the Group III-V compounds are especially interesting for this application. Among these compounds, aluminum antimonide, with an energy gap of 1.6 electron volts (ev) shows particular promise. The major problem in producing device-quality aluminum antimonide is concerned with the removal of impurities from the compound or its constituents (1). Schell (2) reports that zone refining AlSb has produced p-type material with resistivities as high as 14 ohm-cm and carrier concentrations of 3×10^{18}/cm^3. However, these samples have low carrier mobilities, 150 cm^2/v-sec. Aluminum antimonide crystals with resistivities as high as 30 ohm-cm have been obtained by doping p-type AlSb with selenium (3). Again, the mobility of the positive carriers in the base p-type AlSb was low, about 100 cm^2/v-sec. Resistivities as high as 200 ohm-cm have been obtained by adding lithium to aluminum antimonide (4). In this case, the mobility was extremely low, about 0.02 cm^2/v-sec. While doping can produce interesting samples for optical studies, it drastically decreases the carrier mobilities and the purity of the

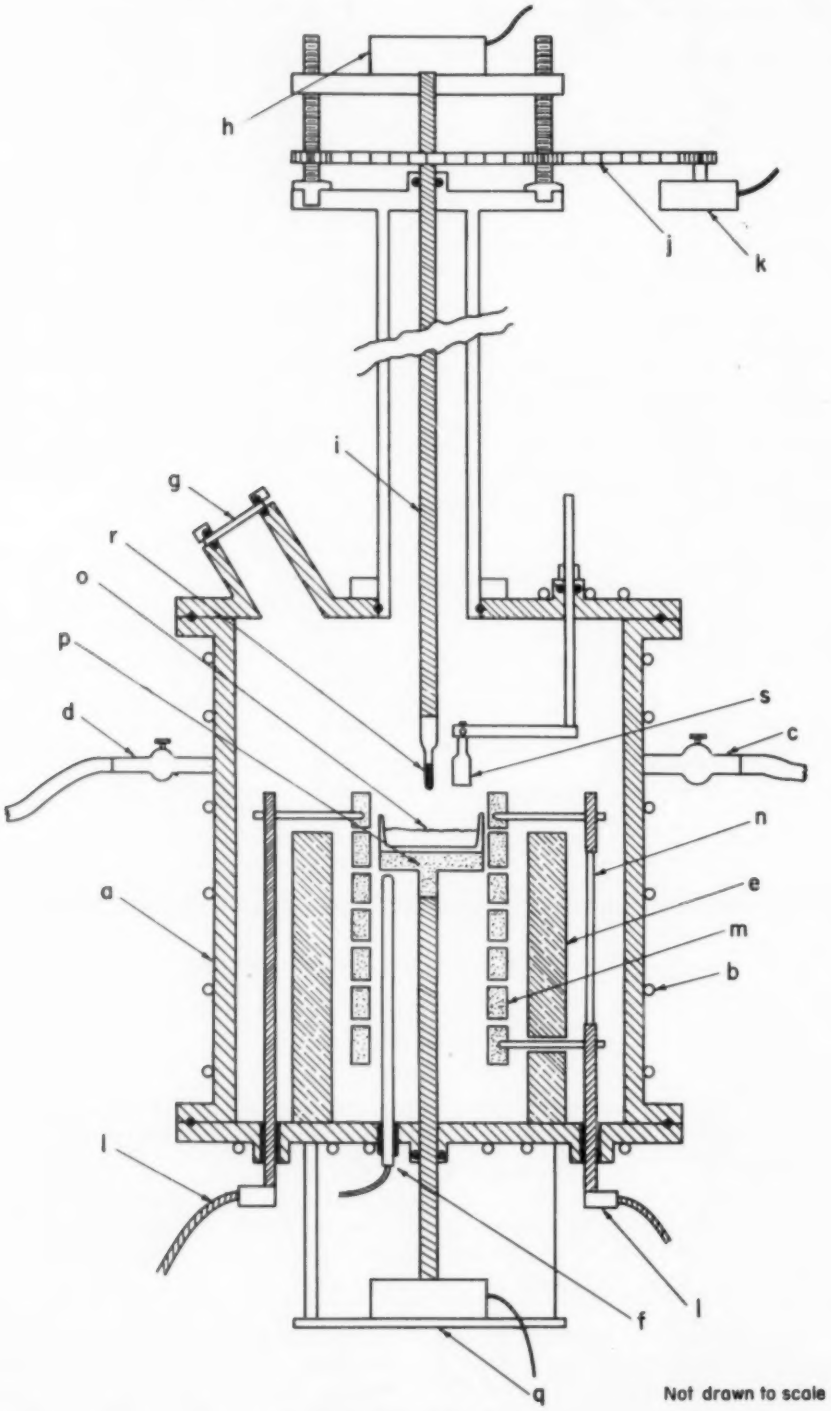

Fig. 1. Crystal growing furnace

aluminum antimonide. Nasledov and Slobodchikov (5) have prepared p-type aluminum antimonide with hole mobilities as high as 240 cm²/v-sec and carrier concentrations of nearly 10^{18}/cm³.

Results of this investigation show that the majority of the p-type impurities found in aluminum antimonide come from the aluminum. It also shows that the concentration of the major p-type impurity in aluminum antimonide can be reduced by heat treating the aluminum at 1000°C in a vacuum. A relatively easy method for heat treating the aluminum and producing p-type aluminum antimonide single cystals with mobilities as high as 400 cm²/v-sec and carrier concentrations in the 10^{16}/cm³

range is described. The purity of the aluminum antimonide is indicated by the temperature dependence of the Hall coefficient and the mobility data.

Growing of Single Crystals

The crystal-growing furnace shown in Fig. 1 is a steel vacuum tank (a) surrounded by cooling coils (b). Helium gas used for atmosphere while growing crystals enters the furnace through valve (c). A vacuum pump is connected to valve (d). Fused quartz is used for shielding (e) in this system, and the thermocouple well (f) is porcelain.

The viewing port (g) at the top is so located as to reduce condensation of volatile materials on the viewing glass. An electric motor (h) rotates the stainless steel seed holder (i). This motor is attached to a platform that is raised or lowered by the rotation of two long screws which are turned by a chain (j) driven by a variable-speed motor (k). The electrical feed-throughs (l) are stainless steel which contact the graphite heating element (m) through molybdenum rods. One side of the heating element is mechanically supported by a porcelain rod (n). The Morganite Al_2O_3 crucible (o) is mounted on an AUC graphite pedestal (p) and rotated counterclockwise by motor (q), while the seed (r) rotates clockwise. Both the seed and the crucible are normally rotated at 6 rpm, giving a net rotational rate of the seed with respect to the melt of 12 rpm.

Although aluminum is etched prior to its reaction with antimony, it still retains an oxide surface that floats on the aluminum antimonide melt and provides nucleation centers which produce additional crystals when the oxide particles come in contact with the seed or the crystal being pulled.

Originally this oxide was removed by lowering the aluminum oxide paddle (s) into the melt. The entire surface of aluminum antimonide was allowed to freeze to the paddle. Then this surface plus the oxide could be lifted out of the crucible, leaving a melt clear of oxide.

The oxide coating on the seed is a second source of nucleation. In order to minimize this nucleation, the crystal being grown is necked down to approximately ⅛ in. before it is allowed to grow out to the desired diameter. This necking down forces out crystals nucleated by the oxide on the surface of the seed.

During the pulling of aluminum antimonide crystals, it was observed that single crystals could not be grown when pulling at speeds above 3 in./hr. Pulling rates exceeding this value caused the ingot to grow as if pulled from a nonstoichiometric melt. This and other experiments indicate that the maximum pulling rate for single crystal growth depends on the magnitude of the deviation of the melt from the stoichiometric ratio. The greater the deviation from stoichiometry the more slowly the crystal must be pulled.

At pulling speeds less than ½ in./hr it was observed frequently that the ingot was covered with a yellow-white glasslike substance. This coating was identified as vitreous antimony trioxide by index-of-refraction measurements. The vitreous coating of Sb_2O_3 varied from 8 to 26 μ in thickness. It is expected therefore that all of the aluminum antimonide crystals pulled from the melt have a thin coating of antimony trioxide glass. Based on oxide coating thickness found at different pulling rates, ingots pulled at 2 in./hr would have a coating of Sb_2O_3 about 4 μ thick. This thickness would of course vary with the pressure of the inert gas and the amount of oxygen present.

Starting Materials

Since neither the antimony nor the aluminum was of sufficient purity as a starting material, purification by zone refining was attempted. The aluminum was given 20 zone-melting passes at 2 in./hr, while the antimony was given 20 passes at 1 in./hr. Both the aluminum and the antimony were zone refined in AUC graphite boats. Following the zone refining, both elements were etched to remove oxides from their surfaces. The aluminum was etched in a solution composed of 95% phosphoric acid and 5% nitric acid, and the antimony was etched in CP-4. Deionized water was used for washing the materials after etching.

In general, pulled aluminum antimonide crystals produced from zone-refined aluminum and antimony reacted in an aluminum oxide crucible contain p-type impurities on the order of $6 \times 10^{17}/cm^3$. Since high-purity indium antimonide can be made with antimony of the same quality as that used in the preparation of aluminum antimonide, the impurity content of the antimony is at least two orders of magnitude below this $6 \times 10^{17}/cm^3$ level.

To investigate the possibility of the melt being doped with contaminants in the aluminum oxide crucibles, two aluminum antimonide crystals were pulled from a high-purity, single-crystal sapphire crucible. These crystals showed no significant differences in electrical properties from the previously obtained material. It was concluded that this level of p-type impurities, i.e., $6 \times 10^{17}/cm^3$, does not come from the crucible.

Therefore, it is probable that the source of the observed impurities in aluminum antimonide is the aluminum. Various impurities which should act as acceptors in aluminum antimonide are found (spectrographically) in the aluminum. Significant quantities of magnesium and copper are among these impurities. An ingot of aluminum antimonide was pulled from a melt doped with 1 part magnesium to 10^4 parts aluminum. As would be expected, the acceptor concentration increased from 6×10^{17} to $2.5 \times 10^{18}/cm^3$. More significantly, little change in carrier concentration along the crystal was observed, indicating that magnesium segregates slowly in aluminum antimonide.

Heat Treatment of the Aluminum

The aluminum was heat treated in vacuum at 1000°C for several hours in an attempt to reduce the concentration of volatile impurities. Magnesium should be one of these impurities removed, since the vapor pressure of magnesium is quite high with respect to that of aluminum. After evacuating and flushing the system with dry helium several times, the system was maintained at 1×10^{-5} mm Hg. Then

Table I. Electrical properties of crystals pulled from AlSb Melts (300°K)

Crystal	Hall coefficient, cm³/coulomb	Mobility, cm²/v-sec	Number of carriers, n/cm³	Preparation of aluminum
1	10.3	230	6.0×10^{17}	As received
4	11.0	230	5.6×10^{17}	Zone refined
8	14.6	250	4.5×10^{17}	Heat treat 1000°C for 7 hr
10	41.0	300	1.5×10^{17}	Heat treat 1000°C for 16 hr
16	53.3	340	1.2×10^{17}	Heat treat 1000°C for 40 hr
15	66.2	330	9.4×10^{16}	Heat treat 1000°C for 54 hr

the aluminum, in an aluminum oxide crucible, was heated to 1000°C for several hours. After heating the aluminum about 3 or 4 hr, the oxide skin which always appears on the aluminum began to disappear. The mechanism involved is probably the Al_2O_3 reduction by aluminum to Al_2O, which subsequently evaporates (6).

After the heat treatment of the aluminum, the system was filled with dry helium and a positive pressure of 10 psi maintained. The antimony which had been fastened to the aluminum oxide probe during the heat-treatment of the aluminum was lowered into the hot zone and allowed to melt into the crucible. This method allowed the aluminum and the antimony to react without the necessity of opening the system; a surface completely clear of oxide particles was produced.

Table I shows the electrical properties of crystals pulled from aluminum antimonide melts when using as-received, zone refined, and heat-treated aluminum. It is apparent from these properties that zone refining the aluminum does very little to reduce the p-type impurities in aluminum antimonide crystals. However, the crystals pulled from melts containing aluminum that had been heat treated had p-type impurity concentrations almost an order of magnitude lower than those observed for crystals made from as-received aluminum.

Figure 2 is a graphical presentation of a portion of the data in Table I. The concentration of p-type impurities in pulled aluminum antimonide crystals is plotted as a function of heat-treatment time of the aluminum. As has been noted, initially the surfaces of the aluminum melts are covered with oxide, which gradually disappears as the aluminum is retained in the molten state. The vaporization of magnesium and other volatile impurities from the melt is inhibited undoubtedly by the oxide coating, which may be a cause of the scatter of points observed in the initial part of the curve in Fig. 2. Since the rate of the removal of p-type impurities seems to decrease rapidly at heat-treatment times above 16 hr, it is probable that most of the volatile impurities have been removed by this time and that the remaining impurities are not highly volatile and therefore are difficult to remove by this method. Such an impurity could be copper, which is known to be present in the aluminum also.

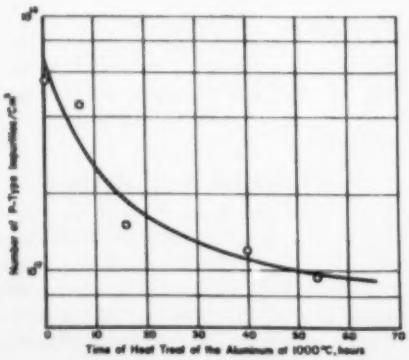

Fig. 2. Concentration of p-type impurities in pulled crystals of AlSb as a function of heat-treating time.

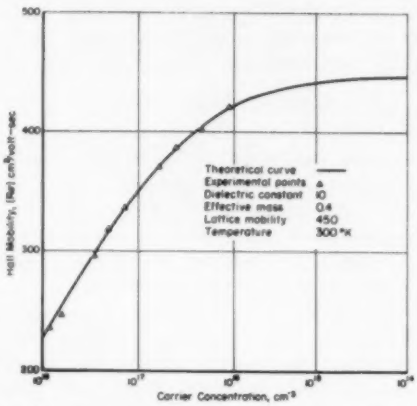

Fig. 3. Hole mobility at 300°K vs. carrier concentration of AlSb.

In Fig. 3 the mobility of the positive carriers in aluminum antimonide is shown as a function of carrier concentration. The theoretical curve was calculated on the basis of a dielectric constant of 10 for aluminum antimonide, an effective mass of 0.4 m_o, and a lattice mobility of 450 cm²/v-sec at 300°K. The close agreement of the experimental points to the theoretical curve indicates that vacuum heat treatment of the aluminum significantly reduces the impurities in aluminum antimonide. The observed re-

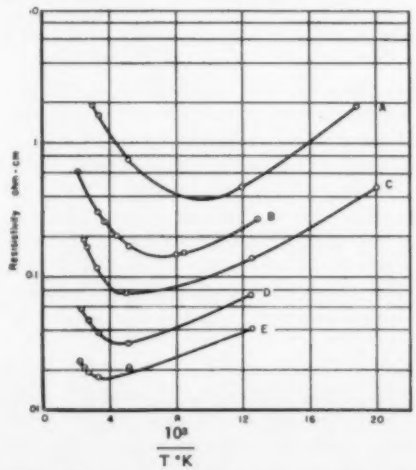

Fig. 4. Resistivity as a function of temperature for single crystals of AlSb.

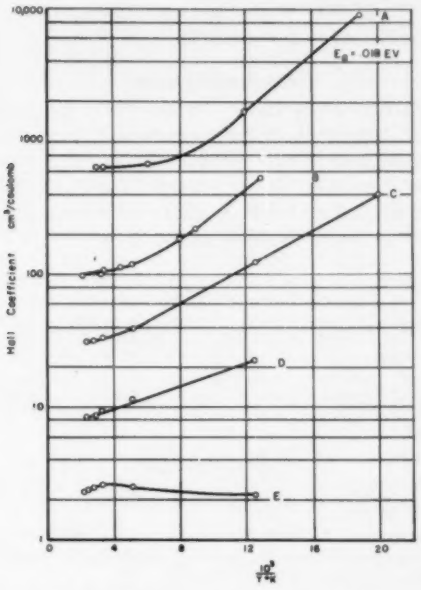

Fig. 5. Hall coefficient as a function of temperature for single crystals of AlSb.

duction in carrier concentrations therefore is not due to compensation.

Figure 4 shows the resistivity as a function of temperature of Hall samples cut from pulled aluminum antimonide crystals. Samples A, B, and C were taken from crystals pulled from melts containing aluminum that had been vacuum heat treated at 1000°C for 16 hr. Sample D is from an aluminum antimonide crystal made from aluminum that had been zone refined but not heat treated. Crystals grown from melts containing zone-refined aluminum show little, if any, improvement over crystals grown from melts containing aluminum in as-received condition. Sample E was cut from the aluminum antimonide crystal that had been doped with 1 part magnesium to 1 x 10^4 parts of aluminum.

Figure 5 shows the Hall coefficient as a function of temperature for the five crystals in Fig. 4. The slope of curve A was used to compute the energy level of the acceptor impurity. The energy level calculated from this slope is 0.018 ev. The minority impurity concentration calculated is consistent with the amount of compensation predicted by a comparison of the mobility data with the theoretical curve in Fig. 3.

The Hall sample cut from the magnesium-doped crystal giving curve E is degenerate throughout the entire temperature range of measurement. The critical concentration of p-type impurities in AlSb for which the ionization energy disappears is about 2 x 10^{18}/cm³, compared with 6.5 x 10^{18}/cm³ for silicon (7). It is expected that the effective activation energy will increase somewhat from 0.018 ev as the acceptor concentration is decreased and that it will be different for the various p-type impurities. However, it appears likely that the acceptor levels in AlSb are, in general, nearer to the valence band than those in silicon; probably the activation energies in AlSb are about a factor of two less than those in silicon.

Figure 6 is a plot of mobility as a function of temperature, as computed from the resistivity and Hall coefficient curves in Fig. 4 and 5. The mobility of the positive carriers decreases more steeply than $T^{-3/2}$ in the lattice-scattering range. In fact, the slope of the lattice mobility vs. temperature appears to be greater than T^{-2}. Magnetoresistance data suggest the presence of both light and heavy mass valence bands in AlSb. Thus, with the relatively impure samples presently available and the uncertainty in the values of r relating the Hall coefficient at a given magnetic field to the carrier concentration, the only conclusion possible is that the temperature dependence of the mobility in p-type AlSb is similar to that of p-type germanium and silicon.

Measurements of the Hall coefficient as a function of magnetic field between 600 and 20,000 gauss have

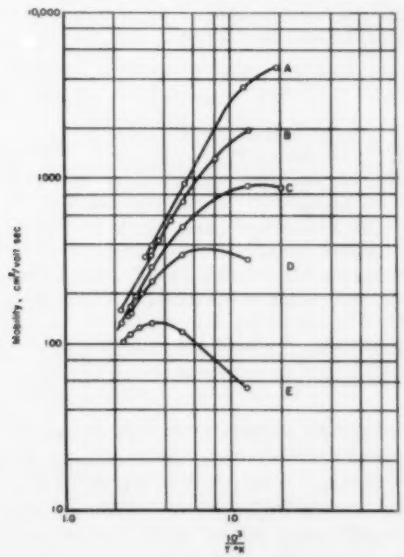

Fig. 6. Mobility as a function of temperature for single crystals of AlSb.

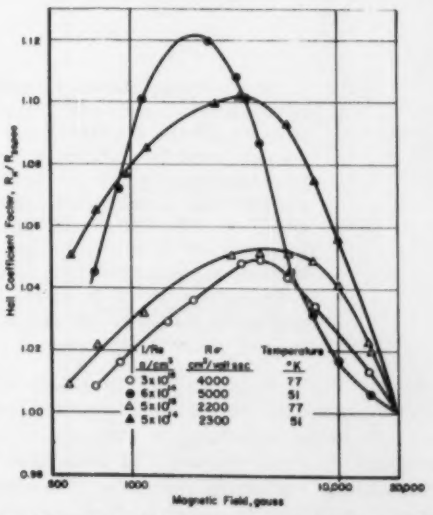

Fig. 7. Magnetic field dependence of the Hall coefficient in p-type AlSb.

been made at 77° and 51°K on a 1.6 ohm-cm sample of p-type aluminum antimonide with an $R\sigma$-value of 400 cm²/v-sec at room temperature. These measurements (shown in Fig. 7) indicate a maximum in the Hall coefficient at about 4000 gauss at 77°K and 2000 gauss at 51°K. A maximum also has been reported in the Hall coefficient of silicon at 77°K and a magnetic field of 20,000 gauss (8). In the case of silicon this maximum appears to be caused by a warping of the heavy mass band. One might expect a similar situation in p-type AlSb. It should be pointed out however that the maximum in the Hall coefficient occurs at a much lower magnetic field in AlSb. This could imply that the maximum in the Hall coefficient in p-type AlSb is related to the structure of the light mass band (9). Other factors, such as the polar character of the zinc blende structure, might affect the magnetic-field dependence of the Hall coefficient.

Summary

The p-type impurities in AlSb have been reduced by an order of magnitude by heat treating the aluminum. The major impurity remaining is probably copper; therefore, methods for removing minute amounts of copper and other nonvolatile impurities from the aluminum need to be developed. The oxide that hinders the growth of single crystals of aluminum antimonide can be eliminated completely by vacuum heat treatment of the aluminum. The activation energies of p-type impurities in AlSb are about one-half those for silicon. The mobility and the temperature dependence of the mobility of the majority carrier in p-type AlSb are almost identical with those in silicon. Finally, as in silicon, a maximum is observed in the magnetic-field dependence of the Hall coefficient in p-type AlSb.

Acknowledgments

The authors wish to thank Dr. H. L. Goering and Dr. A. C. Beer for helpful suggestions. They are especially indebted to F. J. Reid and J. J. Duga for making the electrical measurements. They also wish to acknowledge helpful conversations with R. L. Batdorf of the Bell Telephone Laboratories.

Manuscript received July 21, 1959. This research was supported by the Aeronautical Research Laboratory, Wright Air Development Center. This paper was prepared for presentation at the Philadelphia Meeting, May 5, 1959.

Any discussion of this paper will appear in a Discussion Section to be published in the December 1960 JOURNAL.

REFERENCES

1. W. P. Allred, B. Paris, and M. Genser, *This Journal*, **105**, 93 (1958).
2. H. A. Schell, *Z. Metallkunde*, **49**, 140 (1958).
3. A. Herczog, R. R. Haberecht, and A. E. Middleton, *This Journal*, **105**, 533 (1958).
4. F. Kover, "On the Electrical and Optical Properties of Aluminum Antimonide," International Conference on Solid State Physics in Electronics and Telecommunications, Brussels, June 2-7, 1958.
5. D. N. Nasledov and Slobodchikov, *J. Tech. Phys. (U.S.S.R.)*, **28**, 715 (1958).
6. R. F. Porter, P. Schissel, and M. G. Inghram, *J. Chem. Phys.*, **23**, 339 (1955).
7. G. L. Pearson and J. Bardeen, *Phys. Rev.*, **75**, 865 (1949).
8. A. C. Beer and R. K. Willardson, *ibid.*, **110**, 1286 (1958).
9. A. C. Beer, *J. Phys. Chem. Solids*, **8**, 507 (1959).

A Phase Equilibrium Study of the System Na_2WO_4-Na_2CO_3-H_2O

R. L. Pilloton and G. E. Crawley, Jr.

Metals Research Laboratories, Union Carbide Metals Company, Division of Union Carbide Corporation, Niagara Falls, New York

ABSTRACT

A phase equilibrium diagram representing the binary system Na_2WO_4-H_2O between −7.5° and +35°C was constructed. This curve shows the regions of stability of the dihydrate and decahydrate of sodium tungstate. There is a eutectic point for the system ice-$Na_2WO_4 \cdot 10H_2O$ at −7.5°C and 30.1% Na_2WO_4, a transformation point for $Na_2WO_4 \cdot 10H_2O$-$Na_2WO_4 \cdot 2H_2O$ at 6.2°C, and 42.5% Na_2WO_4 and a metastable eutectic point for ice-$Na_2WO_4 \cdot 2H_2O$ at −13°C and 42.5% Na_2WO_4. Phase equilibria for the ternary system Na_2CO_3-Na_2WO_4-H_2O between −8° and +35°C are represented by a ternary diagram. Projections showing temperature contours and crystallization paths are given. The regions of initial crystallization of the various salts are presented. Applications of the diagram to fractional crystallizations are discussed.

Although solutions of sodium tungstate and of sodium tungstate plus sodium carbonate play an important part in the metallurgy of tungsten, information concerning phase equilibria of these systems is still incomplete. Published values for the solubility of sodium tungstate in water at low temperature (1, 2) are based on work done by Funk in 1900 (3). He indicated the existence of sodium tungstate decahydrate but did not study the exact range of stability of this salt. Furthermore, his solubility measurements are not sufficient to construct phase diagrams representing phase equilibria of the system Na_2WO_4-H_2O at low temperatures.

The only recent investigation of the ternary sys-

tem Na_2CO_3-Na_2WO_4-H_2O was reported by Sei and co-workers (4) in 1954 and concerns solubilities only at 19° and 29°C.

The first objective of the present work was to study the phase equilibria of the systems Na_2WO_4-H_2O and Na_2WO_4-Na_2CO_3-H_2O in the temperature and concentration regions close to those found in industrial applications. A second objective was to use the data for investigating the fractional crystallization of sodium carbonate from aqueous solutions containing both sodium carbonate and sodium tungstate.

General Procedures

To determine the solubilities, solutions of reagent-grade sodium carbonate and sodium tungstate containing an excess of one salt were agitated for several hours at constant temperature and the resulting solutions analyzed.

For experiments at or above 0°C, the samples were equilibrated in a water bath, the temperature of which was kept constant within 0.1°C. For experiments below 0°C, a glycol bath in a low-temperature chamber was used. After attainment of equilibrium, samples of the solution were withdrawn and filtered in the chamber at constant temperature. The length of time necessary to attain equilibrium was determined by analyzing aliquots from a number of solutions at regular intervals.

The densities of the solution samples were measured with a Westphal balance at room temperature. The dissolved sodium tungstate was determined by precipitating the tungsten as WO_3 in an acidified solution in the presence of cinchonine, igniting and weighing the oxide. Sodium carbonate was determined by weighing the $BaCO_3$ formed by absorption of the acid-displaced CO_2 in $Ba(OH)_2$ solution. Water was determined by difference. All analytical results were converted to weight percentages for the graphical representation. These results were found to be reproducible within a precision of 0.5%. The hydrate formulas were calculated from chemical analyses of the crystals which separated on cooling the solutions. Any solution attached to these crystals was carefully separated by absorption with filter paper. Crystals of ice were also analyzed to verify that they did not contain any Na_2WO_4 or Na_2CO_3.

In order to verify the course of crystallization, particularly in the "ice" region of the tungstate-carbonate diagram, a number of thermal analyses were made. In these experiments, solutions containing known quantities of Na_2CO_3 and Na_2WO_4 were cooled and time-temperature curves drawn. In most cases, a 4°C supercooling was observed. The temperatures of initial crystallization were determined from the curves.

Experimental results of the solubility measurements are given in Table I and represented by the phase diagram of Fig. 1.

The experiments showed that in most cases only crystals of $Na_2WO_4 \cdot 2H_2O$ were obtained even when saturated solutions of sodium tungstate were cooled to −5°C. The points representing the composition of the solution were then on branch FG of the curve in Fig. 1. However, by completely freezing a sodium tungstate solution at −15°C and then slowly raising the temperature to 0°C, long needles of a new hydrate were obtained. This compound was identified as $Na_2WO_4 \cdot 10\,H_2O$ by chemical analysis. The colorless crystals of this hydrate turned white and converted to $Na_2WO_4 \cdot 2H_2O$ and water at +6.2°C. By keeping the decahydrate at a low temperature, it was possible to prevent its decomposition and to

Table I. Solubility of Na_2WO_4 in water

Temp, °C	Density d^{25}_{25}	Weight % Na_2WO_4	Weight % Water	Solid phase
−1.7	—	9.6	90.4	Ice
−3.5	—	17.2	82.8	Ice
−4.7	1.27	23.6	76.4	Ice
−4.8	—	24.3	75.7	Ice
−5.6	—	25.7	74.3	Ice
−6.1	—	27.2	72.8	Ice
−6.8	—	28.2	71.8	Ice
−6.7	—	28.4	71.6	Ice
−7.2	—	29.4	70.6	Ice
−7.6	—	30.4	69.6	Ice
−8.0	—	32.2	67.8	Ice
−8.6	1.41	33.2	66.8	Ice
−9.8	—	35.5	64.5	Ice
−6.7	1.35	31.1	68.9	$Na_2WO_4 \cdot 10H_2O$
−6.0	1.37	31.4	68.6	$Na_2WO_4 \cdot 10H_2O$
−4.7	1.39	32.5	67.5	$Na_2WO_4 \cdot 10H_2O$
0.5	—	37.5	62.5	$Na_2WO_4 \cdot 10H_2O$
5.0	—	41.5	58.5	$Na_2WO_4 \cdot 10H_2O$
29.9	—	42.2	57.8	$Na_2WO_4 \cdot 2H_2O$
15.0	—	42.5	57.5	$Na_2WO_4 \cdot 2H_2O$
20.0	—	42.9	57.1	$Na_2WO_4 \cdot 2H_2O$
5.0	1.56	42.7	57.3	$Na_2WO_4 \cdot 2H_2O$ metastable
5.0	1.57	42.5	57.5	$Na_2WO_4 \cdot 2H_2O$ metastable
0.0	1.56	43.0	57.0	$Na_2WO_4 \cdot 2H_2O$ metastable
0.0	1.56	42.5	57.5	$Na_2WO_4 \cdot 2H_2O$ metastable
−2.5	1.56	42.5	57.5	$Na_2WO_4 \cdot 2H_2O$ metastable
−4.5	1.56	42.4	57.6	$Na_2WO_4 \cdot 2H_2O$ metastable

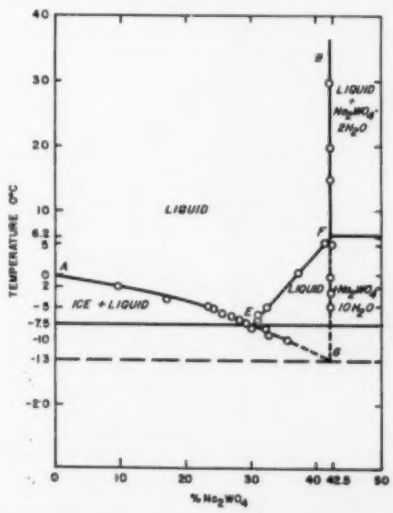

Fig. 1. Phase diagram for the system sodium tungstate-water.

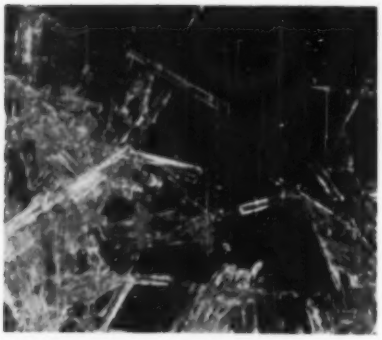

Fig. 2. Crystals of $Na_2WO_4 \cdot 10H_2O$. Magnification ~10X

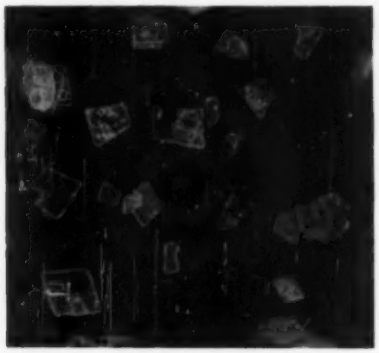

Fig. 3. Crystals of $Na_2WO_4 \cdot 2H_2O$. Magnification ~10X

use the crystals to seed other solutions. Branch EF of the curve was obtained by the procedure of seeding the solution after cooling below 6°C. Crystals of $Na_2WO_4 \cdot 10\ H_2O$ and $Na_2WO_4 \cdot 2H_2O$ are shown in Fig. 2 and 3.

The diagram shows that the freezing points of the solutions vary from 0 to −7.5°C along branch AE of the curve when the sodium tungstate concentration is lower than 30.1%. An aqueous solution containing 30.1% Na_2WO_4 by weight freezes invariantly at −7.5°C to give a binary eutectic E consisting of crystals of ice and of $Na_2WO_4 \cdot 10\ H_2O$. When the composition is lower than 42.5% and higher than 30.1% Na_2WO_4, crystals of $Na_2WO_4 \cdot 10\ H_2O$ may form between −7.5° and +6.2°C along branch EF of the diagram. However, in many cases, because of a "metastable supercooling" phenomenon, crystals of ice are formed along EG or crystals of $Na_2WO_4 \cdot 2H_2O$ along branch FG. Point F gives the temperature and

Table II. Solubility of Na_2CO_3-Na_2WO_4 in water

Temp, °C	Density d^{20}_{20}	Solubility-weight %			Solid phase
		Na_2CO_3	Na_2WO_4	Water	
−2.5	—	1.7	9.1	89.2	Ice
−3.0	—	3.5	9.2	87.3	Ice
−3.8	1.12	5.0	9.1	85.9	Ice
−4.1	—	1.7	17.0	81.3	Ice
−4.6	—	3.1	16.7	80.2	Ice
−5.9	—	1.5	24.7	73.8	Ice
−6.0	1.53	1.8	24.7	73.5	Ice
+20	1.40	11.7	20.9	67.4	$Na_2CO_3 \cdot 10H_2O$
+20	1.33	13.6	15.3	71.1	$Na_2CO_3 \cdot 10H_2O$
+20	—	15.8	8.1	76.1	$Na_2CO_3 \cdot 10H_2O$
+15	1.40	8.7	24.6	66.7	$Na_2CO_3 \cdot 10H_2O$
+15	1.31	10.0	17.5	72.5	$Na_2CO_3 \cdot 10H_2O$
+15	1.22	11.9	9.2	78.9	$Na_2CO_3 \cdot 10H_2O$
+15	1.52	5.3	33.2	61.5	$Na_2CO_3 \cdot 10H_2O$
+10	1.40	5.6	26.7	67.7	$Na_2CO_3 \cdot 10H_2O$
+10	1.30	7.3	20.2	72.5	$Na_2CO_3 \cdot 10H_2O$
+10	1.20	8.6	9.6	81.8	$Na_2CO_3 \cdot 10H_2O$
+10	1.25	9.1	9.8	81.1	$Na_2CO_3 \cdot 10H_2O$
+10	1.52	3.9	36.2	59.9	$Na_2CO_3 \cdot 10H_2O$
+10	1.52	5.4	29.8	64.8	$Na_2CO_3 \cdot 10H_2O$
+5	1.39	4.1	27.8	68.1	$Na_2CO_3 \cdot 10H_2O$
+5	1.29	4.8	19.7	75.5	$Na_2CO_3 \cdot 10H_2O$
+5	1.18	6.8	11.3	81.9	$Na_2CO_3 \cdot 10H_2O$
+5	1.25	9.3	6.6	84.1	$Na_2CO_3 \cdot 10H_2O$
+5	1.56	4.0	35.6	60.4	$Na_2CO_3 \cdot 10H_2O$
+5	1.54	3.9	34.2	61.9	$Na_2CO_3 \cdot 10H_2O$
0	1.38	3.7	29.2	67.1	$Na_2CO_3 \cdot 10H_2O$
0	1.29	4.2	22.0	73.8	$Na_2CO_3 \cdot 10H_2O$
0	1.17	5.9	11.8	82.3	$Na_2CO_3 \cdot 10H_2O$
0	1.25	7.7	9.4	82.9	$Na_2CO_3 \cdot 10H_2O$
−3.8	—	5.0	9.1	85.9	$Na_2CO_3 \cdot 10H_2O + H_2O$
−4.6	—	3.1	16.7	80.2	$Na_2CO_3 \cdot 10H_2O + H_2O$
−6.7	—	3.0	22.0	75.0	$Na_2CO_3 \cdot 10H_2O + H_2O$
+15	1.51	2.6	38.8	58.6	$Na_2WO_4 \cdot 2H_2O$
+10	1.51	2.4	37.3	60.3	$Na_2WO_4 \cdot 2H_2O$
0	1.54	1.4	34.9	63.7	$Na_2WO_4 \cdot 10H_2O$
−2	1.54	1.5	33.2	65.3	$Na_2WO_4 \cdot 10H_2O$
−4	1.54	1.2	31.8	67.0	$Na_2WO_4 \cdot 10H_2O$

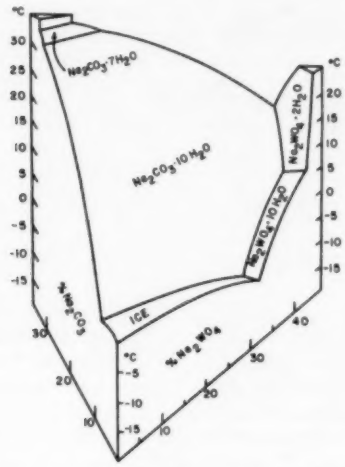

Fig. 4. Surface of initial crystallization for the system Na_2CO_3-Na_2WO_4-H_2O.

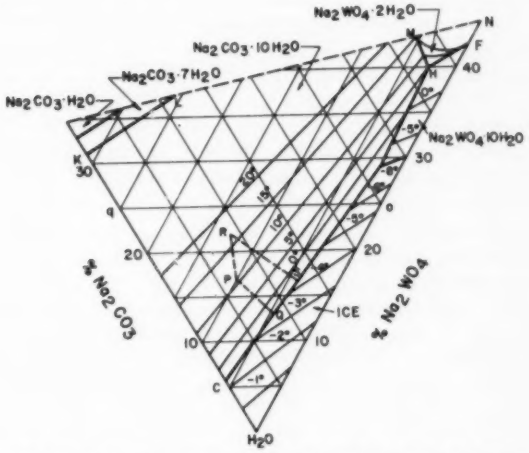

Fig. 5. Projection of the system Na_2CO_3-Na_2WO_4-H_2O showing temperature contours.

composition of the liquid in equilibrium with both di- and decahydrate. Point G, at −13°C, is the metastable binary eutectic point of the dihydrate and ice. Branch FB of the curve corresponding to saturation of the dihydrate is nearly vertical, indicating that there is little solubility change above +6.2°C.

The System Na_2CO_3-Na_2WO_4-H_2O

Graphical representation.—The three dimensional representation derived from the solubility measure-

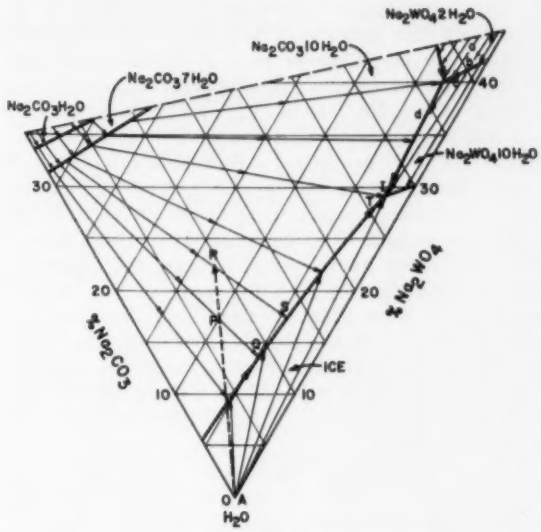

Fig. 6. Projection for the system Na_2CO_3-Na_2WO_4-H_2O showing crystallization paths.

ments given in Table II is shown in Fig. 4. This diagram covers concentrations up to 35% Na_2CO_3 and 45% Na_2WO_4. Figures 5 and 6 are projections showing temperature contours and crystallization paths, respectively.

The different regions and the most important points and lines are lettered. Table III summarizes the state of the phases for various compositions with corresponding letters.

Peritectic reactions.—The "ice" region is a region of congruent crystallization; in other words, the composition of the solid phase being formed lies within the boundaries of its field of primary crystallization. On the other hand, solutions in the region corresponding to crystallizations of $Na_2CO_3 \cdot 10\,H_2O$ and of $Na_2WO_4 \cdot 10\,H_2O$ undergo incongruent crystallizations. Because of these phenomena, conversions of one crystal species into another are observed at the upper borders of these regions. For example, on cooling solution a in Fig. 6, crystals of $Na_2WO_4 \cdot 2H_2O$ are obtained first while the composition of the solution moves from a to b. From b to c, the crystals of $Na_2WO_4 \cdot 2H_2O$ are converted into $Na_2WO_4 \cdot 10\,H_2O$. At c, when all the dihydrate has been converted to decahydrate, the point representing the composition of the solution leaves the binary eutectic line and moves across the field $Na_2WO_4 \cdot 10\,H_2O$ to reach the binary eutectic

Table III. Salient features in the system Na_2WO_4-Na_2CO_3-H_2O

System composition	State of phases	Solid phases	Temp, °C
C	Binary eutectic	H_2O-$Na_2CO_3 \cdot 10H_2O$	−2.1
K	Binary peritectic	H_2O-$Na_2CO_3 \cdot 10H_2O$-$Na_2CO_3 \cdot 7H_2O$	31.2
E	Binary eutectic	H_2O-$Na_2WO_4 \cdot 2H_2O$	−7.5
F	Binary peritectic	H_2O-$Na_2WO_4 \cdot 2H_2O$-$Na_2WO_4 \cdot 10H_2O$	+6.2
H	Ternary peritectic	$Na_2WO_4 \cdot 2H_2O$-$Na_2WO_4 \cdot 10H_2O$-$Na_2CO_3 \cdot 10H_2O$	+5
I	Ternary eutectic	H_2O-$Na_2WO_4 \cdot 10H_2O$-$Na_2CO_3 \cdot 10H_2O$	−8
KLMHIC	One component saturation	$Na_2CO_3 \cdot 10H_2O$	−8 to 32
CIEA	One component saturation	H_2O	0 to −8
EIHF	One component saturation	$Na_2WO_4 \cdot 10H_2O$	−8 to 6.2
FHM	One component saturation	$Na_2WO_4 \cdot 2H_2O$	Above +5

line corresponding to crystallization of a mixture of $Na_2CO_3 \cdot 10\,H_2O$ and $Na_2WO_4 \cdot 10\,H_2O$. Upon further cooling, the invariant point I is reached, and the whole solution freezes solid to give a mixture of crystals of ice, $Na_2CO_3 \cdot 10\,H_2O$, and $Na_2WO_4 \cdot 10\,H_2O$.

Application to the crystallization of sodium carbonate.—The diagrams show that large quantities of sodium carbonate can be crystallized by cooling solutions containing both sodium tungstate and sodium carbonate in quantities comparable to those found in industrial sodium tungstate liquors. The course of the crystallization can be followed on Fig. 6. An example of a possible solution is represented by point P, which is in the Na_2CO_3-$10\,H_2O$ region. Upon cooling, the composition of the solution varies first from P to Q, while crystals of $Na_2CO_3 \cdot 10\,H_2O$ are formed. At Q, around −3°C, the binary eutectic line is reached, and a mixture of crystals of ice and of $Na_2CO_3 \cdot 10\,H_2O$ appears. More of these crystals form when the temperature is lowered further and the composition of the solution moves toward I along line QI. The temperature to each composition is found in Fig. 5. If cooling is stopped before a temperature of −8°C is reached at point I of the diagram, only crystals of ice and of sodium carbonate are formed, and there is no precipitation of sodium tungstate. Since sodium tungstate stays in solution, the amount of sodium carbonate and of water per gram of Na_2WO_4 before and after cooling indicates the yield of the crystallization. For example, point P of the diagram corresponds to the composition (by weight) $Na_2CO_3 = 10.2\%$, $Na_2WO_4 = 7.2\%$, water = 82.6%; consequently, there are 1.42 g of Na_2CO_3 and 11.5 g of water per gram of Na_2WO_4. At the end of the crystallization at, say, −7°C, the composition T is $Na_2CO_3 = 2.0\%$, $Na_2WO_4 = 28\%$, water = 70% which corresponds to 0.071 g of Na_2CO_3 and 2.5 g of water per gram of Na_2WO_4. The percentages of sodium carbonate and of water separated by crystallization are, respectively:

$$Na_2CO_3 \quad \frac{1.42 - 0.07}{1.42} \times 100 = 95.0\%$$

$$H_2O \quad \frac{11.5 - 2.5}{11.5} \times 100 = 78.3\%$$

The compositions of the final solutions and the percentages of water and of sodium carbonate removed by crystallization when solution P is cooled down to −4°, −5°, −6°, and −7°C are given in Table IV.

Table IV. Water and sodium carbonate crystallization from solution P (Fig. 6) at various temperatures

Final Temp, °C	Final composition, %			Removed percentage	
	Na_2WO_4	Na_2CO_3	Water	Na_2CO_3	Water
−3	8.5	5.0	86.5	56.5	11.3
−4	10.0	5.0	85.0	64.8	26.1
−5	16.0	4.4	79.6	80.6	56.7
−6	22.0	3.0	75.0	90.4	70.4
−7	28.0	2.0	70.0	95.0	78.3

If water is evaporated from the solution prior to cooling, the point representing the solution moves from P to R on line APR. The temperature at which crystallization of R starts is given by the temperature contour passing through R in Fig. 5. Upon cooling the solution, the composition follows paths RS and SI (Fig. 6).

Conclusions

This study of the solubility of sodium tungstate in water indicates that solid phases existing at temperatures between −7.5° and +35°C are ice, $Na_2WO_4 \cdot 10\,H_2O$, and $Na_2WO_4 \cdot 2H_2O$. The eutectic point for ice-$Na_2WO_4 \cdot 10\,H_2O$ is at −7.5°C and 30.1% Na_2WO_4, the peritectic point for $Na_2WO_4 \cdot 2H_2O$-$Na_2WO_4 \cdot 10\,H_2O$ at +6.2% and 42.5% Na_2WO_4, and the metastable eutectic point for ice-$Na_2WO_4 \cdot 2H_2O$ at −13°C and 42.5% Na_2WO_4.

The ternary diagram representing the system Na_2CO_3-Na_2WO_4-H_2O shows a ternary eutectic containing 2% Na_2CO_3, 27% Na_2WO_4, and 71% H_2O at −8°C. This diagram indicates that large quantities of sodium carbonate can be crystallized fractionally from solutions containing quantities of Na_2WO_4 and Na_2CO_3 comparable to those present in industrial liquors.

Manuscript received May 18, 1959. This paper was prepared for delivery before the New York Meeting, April 27-May 1, 1958.

Any discussion of this paper will appear in a Discussion Section to be published in the December 1960 JOURNAL.

REFERENCES

1. K. C. Li and Chung Yu Wang, "Tungsten," p. 284, Reinhold Publishing Co., New York (1956).
2. Gmelin's Hanbuch der anorganischen Chemie, 8 Auflage, System Number 54, Wolfram, 215 (1933).
3. R. Funk, *Ber.*, **33**, 3696 (1900).
4. Rempei Sei, Genichi Nakazawa, and Koichi Ito, *J. Mining Inst. Japan*, **70**, 513 (1954).

Production of Thorium Powder by Calcium Reduction of Thorium Oxide

N. Fuhrman,[1] R. B. Holden,[1] and C. I. Whitman

Sylvania-Corning Nuclear Corporation, Bayside, New York

ABSTRACT

A process for the preparation of high-purity thorium powder by calcium reduction of thorium oxide has been developed, Calcined thorium oxide is reduced in an inert atmosphere at 950°C with high-purity calcium metal in the presence of calcium chloride. The reduction vessel is fabricated of type 446 stainless steel to avoid pick up of iron and nickel impurities and permit break out of the reduction cake. The thorium powder so produced has essentially the same purity as the thorium oxide starting material. Important factors controlling yield and quality of the thorium powder are discussed.

The purpose of this investigation was to examine the direct reduction of thorium oxide with calcium as a potential production process, to determine the yields and the quality of the metal so obtained, and to develop a standard procedure for preparing small batches of metal by this process.

Investigations of the calcium reduction of thorium oxide date back to the beginning of this century. Huppertz (1) suggested the use of calcium vapor, and Burger (2) employed this method with some success. Kuzel and Wedekind (3) subsequently patented a process using calcium vapor, and Wedekind (4) carried out further studies.

Results of the first critical study of thorium metal preparation were presented by Marden and Rentschler (5, 6) who, with the aim of producing a metal powder capable of being consolidated into homogeneous metallic bodies, conducted an investigation of calcium reduction of the oxide. Their method involved the reduction of thoria with a three-mole excess of calcium and one part of calcium chloride to one part of the oxide. The authors claim that after compacting and sintering, the solid metal assayed was 99.7 to 99.8% thorium.

Kroll (7) also investigated this process, essentially following the procedure of Marden and Rentschler. This method was also used on a large scale with some modifications in Germany during World War II, as reported by Espe (8, 9).

Rentschler, *et al.* (10) eliminated the calcium chloride in the charge and used a thin-walled molybdenum cup instead of the steel bomb. The reduction took place in a Vycor bell jar under argon at a maximum temperature of 1400°C, the heat being supplied by high-frequency induction. The thorium powder was recovered by leaching the charge directly out of the cup.

A variation of the above procedure was used by Marden (11) in the experimental preparation of several 12-lb batches of powder.

[1] Present address: Metallurgical Laboratories, Olin Mathieson Chemical Corporation, New Haven, Connecticut.

Meyerson (12) has described the development of the calcium reduction process in the U.S.S.R. Except for the production of thorium powder of much lower purity, his results are in agreement with those of the present work. Although the efforts were entirely independent, some of his reported procedures are similar to those developed here.

Process Description

The raw materials in the charge for reduction are: (*a*) thorium oxide, (*b*) redistilled calcium metal, and (*c*) anhydrous calcium chloride. Thorium fines may be added as a means of recycling the relatively impure metal powder which is not recovered as primary material in the leaching step.

The thorium oxide employed in the charge was supplied by the U.S. Atomic Energy Commission. A typical analysis of AEC thorium oxide is presented in Table I. It is apparent that special attention has been given to the removal of impurities of high thermal neutron absorption cross section. The overall quality of the material was fairly consistent from lot to lot. Raw thoria is fired for removal of absorbed carbon dioxide prior to preparation of the charge. Two methods have been used to accomplish this (*a*) continuous calcining at about 880°C in an experimental rotary unit, and (*b*) batch calcining in stainless steel boats for 40 hr or more at 800°C. The fired oxide is then handled in a CO_2-free atmosphere during the charge preparation and reduction. This procedure substantially reduces the carbon content of the metal product.

Redistilled calcium metal[2] was utilized as-received in the form of 6-mesh nodules. Typical analyses of the Domal and Nelco redistilled calcium indicate that they are of similar quality. Anhydrous calcium chloride, meeting the American Chemical Society specifications, is obtained in the form of 20-mesh granules and is used in the charge as-received.

[2] Obtainable from either Dominion Magnesium, Ltd. or Nelco Metals, Inc.

Table I. Comparison of impurity levels of thorium metal powder and thorium oxide feed material

Impurity spectrochemical	ThO_2— Lot FP-125* (oxide basis)	Thorium powder run 84† (metal basis)
Ag		a 0.5
Al	<10	<10
As		<5
B	0.2	<0.2
Be	<1	—
Bi	<2	<1
Ca	200	a 200
Cd	<0.2	<0.1
Co	1	—
Cu	35	a 30
Fe	35	55
Mg	15	120
Mn	2	a 6
Mo	2	—
Ni	20	7
P	<40	—
Pb	25	2
Sb		—
Si	<10	a 25
Sn	2	<2
V	<10	—
Zr	<10	—

Notes: All values are ppm. a = approximate; — = not detected; < = less than.
* Analysis supplied by National Lead of Ohio.
† Analysis performed by New Brunswick Laboratory of AEC.

The following charge composition is typical for the runs involving thorium fines recycle: 7000 g prefired ThO_2; 925 g thorium fines; 2800 g anhydrous $CaCl_2$; 2760 g redistilled calcium. The amount of $CaCl_2$ is 40% of the weight of ThO_2. The amount of calcium is 30% more than that required to react with the ThO_2. Whether or not thorium fines are recycled in this manner depends on the quality of thorium powder desired as a product.

The charge ingredients are weighed in an argon dry box into a 5-gal can which is then sealed and tumbled on a drum roller. Because of occasional poor yields of metal resulting from incomplete reduction, it is believed that blending may not be thorough enough with this equipment. An alternate blending method utilizes a 0.33 ft^3 double cone blender in which about half the charge is tumbled at one time. The latter procedure, on the basis of a limited number of experiments, appears to produce higher yields.

Fig. 1. Calcium reduced thorium oxide reduction cake. Type 446 stainless steel reduction vessel.

The blended charge is transferred to a tapered reactor fabricated of type 446 stainless steel. A flat reactor cover is secured to the reduction vessel, shown in Fig. 1, by means of a clamping ring. A pipe welded to the reactor cover admits argon into the reactor during the fastening operation as well as during the subsequent heating period, so that the reduction may take place in an inert atmosphere. An argon head of 5 in. of Hg is usually employed.

The loaded reactor is heated to 950°C by high-frequency induction heating and held there while the charge is soaked for about 5 hr. After reduction, the reactor generally is quenched in water to hasten the cooling process. The reduction product remains under argon until it is cold.

After cooling, the head is removed from the reactor and the reduction product or "cake" broken out by jolting the inverted reactor once or twice. A typical reduction cake is shown in Fig. 1.

Primary size reduction of the reduction cake is performed by crushing the cake between flat plates with a hydraulic press. Normally, about a 20- to 30-ton load is required to crack the cake. The large chunks are further reduced in size with a jaw crusher. A uniform crushed cake of about ¼ in. particle size is thus obtained.

A leaching apparatus consisting of a 55-gal stainless steel drum and a ½ hp "Lightnin" mixer, is used to disintegrate the crushed cake. First, the crushed reduction product is introduced into 35 gal of agitated tap water. After 15 to 30 min hydrogen evolution has almost ceased and agitation may be stopped. Any remaining unleached cake is allowed to disintegrate statically. After 2 hr the reduction cake is almost completely leached; however, in current practice, it is allowed to stand overnight. The supernatant liquor, containing suspended thorium fines, as well as $Ca(OH)_2$, is pumped to a settling tank for later recovery of the fines. The resulting thorium powder is then subjected to from three to five successive tap water washes to remove more of the $Ca(OH)_2$ leach product. These washes are carried out in a 20-gal stainless steel pot with agitation provided by a ¼ hp "Lightnin" mixer. After a settling interval of about 5 min, the supernatant liquor is pumped to the settling tanks. When practically all of the $Ca(OH)_2$ has been removed by this method, the thorium powder is ready for acid washing.

The powder is subjected to two successive washes of 1:8 nitric acid and then successive washes with demineralized water until the supernatant liquor is neutral. This treatment removes residual calcium and $Ca(OH)_2$ from the powder.

The wet powder is filtered and washed on a 9 in. diameter stainless steel Buchner funnel with three rinses of acetone followed by three rinses with petroleum ether (boiling range, 30° to 60°C) and then vacuum dried overnight at a pressure of <1 mm of Hg.

The wet powder can also be dried in a vacuum shelf dryer. The thorium powder is sufficiently dry when a vacuum of 35 μ of Hg is attained. It should be noted that in this drying method there is a possibility of obtaining an incompletely dried product which, because of its possible sensitiveness to ignition, is a safety hazard.

Thirty-seven reductions were carried out on an 11-lb. scale (the largest nominal batch size produced during the development program) with yields running as high as 91% of theoretical. The term "yield" refers to the coarse thorium powder obtained after the drying process. Early in this work it was shown that the yield of metal averaged over 99% when the metal fines were included and hence the conversion of oxide to metal is essentially complete.

The usual procedure for determining the quality of the thorium powder is chemical analysis. The following impurities are determined in each run: (*a*) carbon, (*b*) nitrogen, (*c*) hydrochloric acid insolubles (ThO_2), (*d*) iron, and (*e*) chromium. Occasionally, spectrochemical analyses are obtained, especially for elements with a high thermal neutron absorption cross section.

A typical spectrochemical analysis of the thorium powder produced is presented in Table I along with that of the ThO_2 starting material. A comparison of the two indicates that there is no substantial pickup of impurities in the process. In this case, an exception is magnesium which is readily removed, however, during consolidation by arc melting. Table II shows the chemical analyses of thorium powder produced during a series of ten consecutive runs on the 11-lb scale when the process was under control and before significant changes were made in the operating conditions. It is seen that the calcium reduction process is capable of consistently producing a high-purity thorium in good yield.

As a supplement to chemical analysis, another approach to quality measurement has been found useful, namely, the evaluation of the hardness and the surface appearance of arc melted buttons. For this evaluation, a 30-g sample of thorium powder is melted in an argon atmosphere of 7 in. of Hg absolute pressure in an arc furnace (button type). The Rockwell F hardness and button density are then determined. Since the button hardness is very sensitive to a small quantity of carbon and larger amounts of metallic impurities such as nickel, this method serves as a rapid means of determining relative quality. The presence of an unusually high oxide content is easily ascertained from the appearance of an oxide film on the button surface. Powder with a low oxide content (less than 0.3% HCl insolubles) normally results in a bright metallic surface. Button hardnesses of the material produced in the ten runs cited above are also shown in Table II.

Table II. Thorium powder chemical analyses, button hardness and yield data for a series of 11-lb scale production runs

Run No.	Chemical analysis					Button hardness, R_F	Yield % of theoretical
	Nitrogen, ppm	Carbon, ppm	ThO_2, %	Iron, ppm	Chromium, ppm		
60	40	160	0.16	11	11	40	83
61	50	140	0.19	35	13	35	78
62	40	210	0.15	46	9	41	80
63	40	200	0.14	44	10	36	91
64	30	150	0.24	41	17	31	85
65	30	200	0.17	46	22	34	88
66	40	120	0.57	43	20	40	80
67	40	190	0.12	42	17	38	86
68	40	200	0.17	39	28	36	85
69	50	140	0.04	48	26	36	78

Fig. 2. Arc melted thorium button, run No. 58, bright field, 200X, 0.37% ThO_2.

A typical photomicrograph of an arc melted button is presented in Fig. 2. The main inclusion constituent is probably ThO_2, since chemical analysis indicates the presence of 0.37% HCl insolubles in the button.

To recover the very fine thorium powder which has been pumped to settling tanks during the leaching and acid washing steps for recycle through the reduction step, the settled thorium sludge is washed with 1:8 HNO_3. Enough nitric acid is added to insure the complete dissolution of $Ca(OH)_2$. After a 1-hr settling period, the supernatant liquor is pumped to the settling tanks. The supernatant liquor contains a small amount of dissolved thorium which may be periodically recovered as the hydroxide by precipitation with NH_4OH. The thorium fines are then washed with demineralized water at least three times to remove the acid. The fines are collected and dried by either of the two drying methods described previously.

Coarse thorium powder has been stored for periods as long as 4 months in air without any detectable deterioration. The usual practice is to store the powder from each run in a separate metal container. During the course of the development program described in this report, no case of spontaneous ignition of the powder was ever observed. However, at the termination of the project, a serious explosion did occur when some scrap fines were being burned in a disposal operation. It is suggested, therefore, that thorium powder be handled by procedures recommended for the handling of zirconium metal powders.

Various methods of consolidating thorium metal powder have been investigated extensively at this laboratory. These methods are: (*a*) consumable electrode arc melting (14), (*b*) hot compaction (15-17), and (*c*) cold compaction and sintering (17). By far, the most advantageous of these is the

first, since such impurities as calcium, magnesium, and hydrogen are reduced by a factor of about 10 during the arc melting. In addition, ingot densities as high as 11.69 g/cc [theoretical is 11.71 g/cc (18)] are obtained in a single melting operation.

Process Development

The standard operating procedure described in the previous section evolved from fifty-seven experiments made on a smaller scale. In these experiments the important factors controlling the yield and quality of thorium metal powder produced were ascertained. The most important results of these experiments are summarized below.

According to the thermodynamic data compiled by Coughlin (13), the equilibrium for the reduction of thorium oxide with calcium is favorable below the boiling point of calcium. It appears from our work that the reduction is not highly exothermic, i.e., there is no sudden increase in the temperature of the reactor as it is heated slowly to the reduction temperature. A calculation of the heat of reaction at 950°C predicts a value of −12.4 kcal for the reduction of a gram mole of thorium oxide with liquid calcium as follows:

$$ThO_2 + 2Ca \rightarrow 2CaO + Th$$

This small quantity of heat evolved is apparently easily dissipated.

In practice, a calcium metal excess of 25% or more is usually added to effect complete reduction. In addition calcium chloride is required to provide a fluid medium for contact between the reactants. It has been suggested by Marden and Rentschler (5) that the compound $CaO \cdot CaCl_2$ is formed (between the flux and the reaction product CaO), which removes the CaO as it is formed, driving the reaction to completion. This assumption cannot be entirely correct since it was found in the present work that complete reduction is attained with a relatively small amount of $CaCl_2$, much less than that contained in the compound $CaO \cdot CaCl_2$.

The subsequent leaching of the thorium metal from the reduction product releases heat through reaction of CaO and excess Ca metal with water and acid. For removal of this heat, some cooling mechanism must be provided; otherwise, local overheating may cause excessive oxidation of the thorium metal. The leaching and acid washing may be carried out with a large volume of water to dissipate the heat, or a cooling coil may be introduced into the leaching tank.

It was found that impurities in the calcium and calcium chloride such as nitrogen and aluminum would appear in the thorium metal product. The use of redistilled calcium and calcium chloride granules which conformed to American Chemical Society specifications reduced the nitrogen content from greater than 100 to less than 60 ppm and aluminum from greater than 2000 ppm to less than 10 ppm. Carbon in the thorium metal product was traced to the absorption of CO_2 from the atmosphere by thorium oxide raw material. For example, small samples of thoria were found to contain 80 ppm carbon immediately after calcining. This same material, after exposure to an air stream for 30 min was found to have increased in carbon content to 400 ppm. Either batch or continuous calcining of the thoria was found to be a suitable technique for reducing the carbon content in the thorium metal product to levels rarely exceeding 200 ppm.

The development of a suitable container for carrying out the reduction proved to be a major problem in this program. Ordinary steel is unsuitable because of its lack of oxidation resistance. When a nickel stainless steel or Inconel container was used, the reduction cake adhered so firmly to the container wall that it was necessary to leach the charge in place in the container. Also, the thorium metal produced generally contained several hundred ppm of nickel impurity. Lining of the reactor with overlapped sheets of molybdenum was not satisfactory in preventing nickel pickup. A calcium oxide liner was dissolved in the reduction melt. A graphite liner eliminated the breakout problem but resulted in carbon contents of about 500 ppm.

It was found eventually that the use of a tapered reactor of type 446 stainless steel (which contains no nickel) reduced the nickel content in the product to as low as 7 ppm and also permitted removal of the reduction cake by the simple process of inverting the container and jolting it on a hard surface. In addition, to minimize atmospheric contamination, it was found necessary to admit argon throughout the reduction process through a tube leading into the cover of the reactor.

Experiments were made with varying proportions of calcium and calcium chloride, reduction times, and reduction temperatures. In general, a longer reduction time resulted in an increased yield of thorium powder, probably through agglomeration of fine thorium particles into larger ones. This was counter-balanced by a slightly increased pickup of such impurities as iron and chromium from the reactor. When the excess of calcium was decreased from 50% down to 25%, it became necessary to increase the soaking time from 2½ hr to 5 hr to insure complete reduction of thorium oxide. An optimum temperature for reduction is 950°C because at higher temperatures breakout difficulty can be encountered and, in addition, impurities in the thorium powder increase.

It was noted that increased periods of agitation during the leaching of the reduction cake had an adverse effect on thorium yield because larger particles are comminuted to fines. Both impeller agitation and tumbling barrel techniques were satisfactory for leaching thorium powder.

A typical analysis of fines is illustrated in Table III. It should be noted that the impurity level is somewhat higher than in primary yield thorium powder. These fines can be recycled into the process in several ways. If necessary, fines can be dissolved, reprecipitated as thorium oxalate, and calcined to form thorium dioxide, although economically this is least attractive. As noted earlier, fines can also be introduced directly into the metal reduction charge and with good results. Finally, the fines can be consolidated directly with the primary yield coarse thorium

Table III. Chemical analysis of thorium fines

	%
Nitrogen	0.010
Carbon	0.036
HCl insol.	0.83
Iron	0.012
Chromium	0.0058

powder at an apparent sacrifice in the quality of the metal produced. This was demonstrated in an experiment by comparing the button hardness of the product resulting from the two latter methods of recycle using the same lot of fines and a 15% recycle basis. The hardness of the metal produced by direct consolidation was R_r 58 and that prepared by recycle to the reduction step was R_r 47.

Conclusions

It has been shown that the calcium reduction of thorium oxide is capable of producing a high-purity thorium metal. This can be accomplished only through use of high-purity starting materials and by careful attention to charge preparation, reduction conditions, containers, materials, and powder leaching procedure. Extension of the process to manufacture of larger quantities should be straightforward.

Manuscript received Nov. 17, 1958. This paper was prepared for delivery before the Philadelphia Meeting, May 3-7, 1959. The work was sponsored by the U. S. Atomic Energy Commission at the Atomic Energy Division of Sylvania Electric Products, Inc., now Sylvania-Corning Nuclear Corporation.

Any discussion of this paper will appear in a Discussion Section to be published in the December 1960 JOURNAL.

REFERENCES

1. H. Huppertz, *Chem. Zentr.*, **1**, 1383 (1904).
2. K. Burger, Dissertation, Basel (1907); Gmelin Kraut, "Handbuch der Anorganische Chemie," III, Part 1, 1207.
3. H. Kuzel and E. Wedekind, U. S. Pat. 1,088,909 (1914).
4. E. Wedekind, *Edel-Erden und-Erze*, (3) Nos. 19-20, 109 (1922).
5. J. W. Marden and H. C. Rentschler, *Ind. Eng. Chem.*, **19**, 97 (1927).
6. J. W. Marden and H. C. Rentschler, U. S. Pat. 1,814,-719 (1931).
7. W. Kroll, *Z. Metallkunde*, **26**, 30 (1936).
8. W. Espe, *Powder Met. Bull.*, **3**, 100 (1948).
9. W. Espe, *ibid.*, **4**, 257 (1949).
10. H. C. Rentschler, W. C. Lilliendahl, and J. Gray, U. S. Pat. 2,446,062 (1948).
11. J. W. Marden, AEC Research and Development Report No. N-2139.
12. G. A. Meyerson, "Powder Metallurgy of Thorium," 1955 Geneva Conference A/Conf. 8/P/635.
13. J. P. Coughlin, Bulletin 542, Bureau of Mines (1954).
14. R. Witt, AEC Report, SEP-209, "Consumable Electrode Arc-Melting of Cold Compacted Thorium Powder," April 19, 1956.
15. R. H. Witt, J. Nylin, and H. M. McCullough, AEC Report, SEP-221, "A Study of the Hydride Process for Producing Thorium Powder," June 10, 1956.
16. R. H. Witt and H. M. McCullough, AEC Report, SEP-224, "Hot Pressing of Electrolytic Dehydrided and Calcium-Reduced Thorium Powders," Oct. 9, 1956.
17. R. B. Wagner and S. Storchheim, AEC Report, SEP-168, "Preparation and Consolidation of Thorium and Thorium Hydride Powders," August 9, 1954.
18. H. A. Saller and J. R. Keeler, "The Fabrication and Properties of Thorium," presented at the Nuclear Engineering and Science Congress, Dec. 12-16, 1955, Cleveland, Ohio.

Batteries with Solid Ion-Exchange Membrane Electrolytes

II. Low-Temperature Hydrogen-Oxygen Fuel Cells

W. T. Grubb and L. W. Niedrach

Research Laboratory, General Electric Company, Schenectady, New York

ABSTRACT

Hydrogen-oxygen fuel cells employing a commercial ion-exchange membrane as the electrolyte are described. Some performance data on this type of cell operating at room temperature with a cation membrane in the hydrogen form and with hydrogen and oxygen at 1 atm are presented. The open circuit EMF is about 0.3 v below the value of 1.23 expected for a reversible cell. This deficiency is found to be caused by the oxygen electrode which does not achieve the reversible half-cell potential. Equilibration of the membrane electrolyte with sulfuric acid prior to cell assembly results in improved polarization characteristics. Favorable features of these cells include their simple construction and their small unit thickness. In addition, the presence of as much as 67% CO_2 in the hydrogen feed gas is found to have little effect upon performance. Since the electrolyte is a cross-linked, water-saturated polymer, the electrolyte is locked into the structure and cannot be leached from the cell when it is operated within the stability limits of the polymer. No dilution occurs from the water formed at the oxygen electrode during cell operation because it is rejected from the saturated electrolyte.

In previous work (1), the behavior of ion-exchange membranes as electrolytes in cells employing metal electrodes was described. Their behavior suggests a strong analogy with aqueous solution elec-

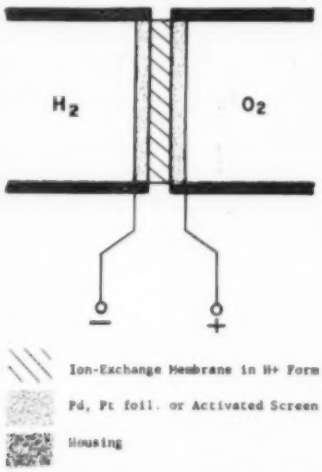

Fig. 1. Schematic diagram of ion-exchange membrane fuel cell.

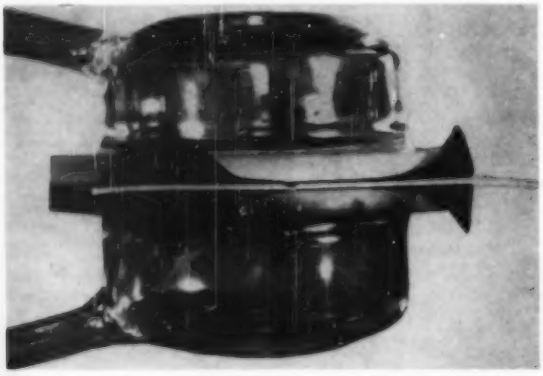

Fig. 2. Type 1 ion-exchange membrane fuel cell, active area, 25 cm².

trolytes. Since the permeability of gases through ion-exchange membranes is low, they appeared to be ideally suited to serve as both the gas separator and the electrolyte in fuel cells (2, 3). The present work was undertaken therefore to study the properties of some simple systems of this type. This has resulted in a new type of low-temperature, hydrogen-oxygen fuel cell.

Experimental

Two types of cells were used in the experimental work. In both cases construction was such that the electrodes were in intimate contact with the electrolyte material as shown schematically by the diagram in Fig. 1. Immediately adjacent to the electrodes, gas chambers for the hydrogen and oxygen were formed by the cell housings.

A commercially available ion-exchange membrane was used in all of this work. For this purpose Amberplex C-1[1] was selected. This is a heterogeneous membrane consisting of particles of sulfonated, cross-linked polystyrene bonded into sheet form with an inert binder. These membranes, which were employed in the hydrogen form, have a conductivity that approximates that of a 0.1*N* H_2SO_4 solution (4). They are also stable chemically and have high flexibility and mechanical strength. Some electrochemical properties of Amberplex C-1 have been reported by Winger, *et al* (5).

Nickel screens activated by platinum black were used as the electrodes in most cases although a few experiments were performed with platinized platinum and palladium foil electrodes. Platinizing of the nickel screens was accomplished by simply immersing the screen into an acidified platinum chloride solution containing a trace of lead acetate (6). When palladium or platinum was employed, electrodeposition of the black was necessary, and the method of Reilly and Rae (6) was used.

A photograph of the simple cell (type 1) employed for the first experiments is shown in Fig. 2. The effective cell area was 25 cm² and the thickness of the electrolyte layer 0.06 cm to provide a cell constant of about 420. This type of cell was used with both screen and foil electrodes. Because of the relatively small area and the use of flat electrodes, good contact was obtained between the electrolyte and the electrodes with only the pressure of the flanges on the periphery of the housing.

In later work a larger version of the cell was designed. Two views of this cell (type 2) are shown in Fig. 3 and 4. In this model the electrodes were held in place against the membrane by backing plates with suitable baffles arranged to promote gas distribution. A uniform pressure was applied to the electrodes by placing rubber spacers between the backing plates and the face plates of the cell. These

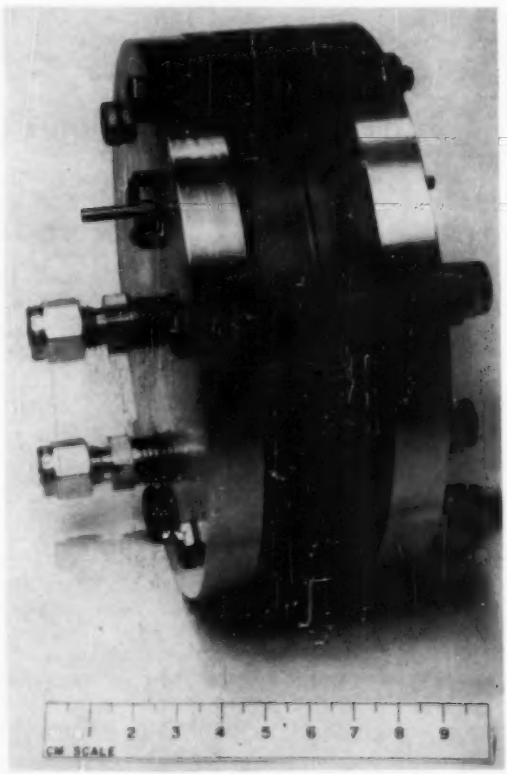

Fig. 3. Type 2 ion-exchange membrane fuel cell, assembled, active area, 50 cm².

[1] Rohm and Haas Co., Philadelphia, Pa. A similar product is available as Permaplex C-10 from Permutit Corp. Ltd., London, England.

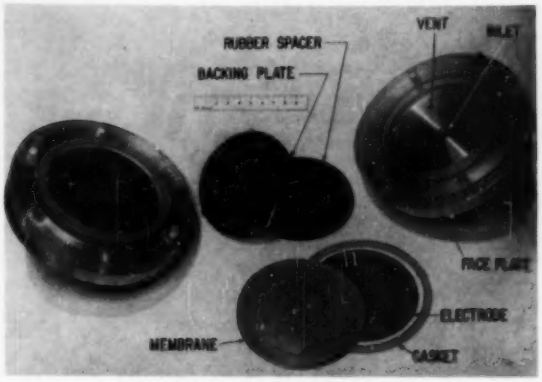

Fig. 4. Type 2 cell, not assembled

parts are shown in Fig. 4. In operation the feed gases were admitted through inlets on the axis of the cell. After radial distribution over the electrodes, the waste gases were then vented through the exit ports. Silicone rubber gaskets were employed as seals. Over-all diameter of the cell was 12.7 cm (5 in.) and the diameter of the electrodes was 8.3 cm (3¼ in.). Total active area was approximately 50 cm².

The cells were operated by admitting hydrogen and oxygen, respectively, to the two gas chambers and measuring the electrical output. In order to maintain ion exchange membranes in highly conducting form, they must be kept at 100% humidity, and this was accomplished by bubbling the input gases through water. Water formed by the cell in operation can help to maintain the hydration of the membranes. Actual dilution of the electrolyte cannot occur since the membranes reject water when they are saturated.

Polarization curves were obtained under various conditions by measuring currents with a sensitive galvanometer and cell potentials with a Rubicon potentiometer. In the initial work with the type 1 cells (Fig. 2), measurements were taken 10 sec after applying the load. This procedure has been recommended by Davtyan (7) and proved adequate for the purpose of comparing various modifications. In the work with type 2 cells, steady-state data were obtained. Establishment of equilibrium generally required several minutes after a change in load was made. All of the data were obtained at room temperature (25° ± 3°C).

In order to permit comparison of data obtained with the two types of cells, all current measurements were converted to current densities. This was done by dividing the measured current by the geometrical area covered by the circular electrodes.

Results and Discussion

The initial polarization curves, shown in Fig. 5, were obtained on type 1 cells with platinum foil electrodes. Platinized platinum foils as thin as 0.0002 cm (0.08 mil) were used in order to minimize diffusion effects through the metal. Only fairly low currents could be obtained from these cells. For this reason, attention was quickly directed toward cells with metal screen electrodes.

Polarization curves obtained with the type 1 cell using platinized screen electrodes are depicted in Fig. 6. All screen cells were found to afford higher currents than the foil types. The screen electrodes were made from nickel screen 150 x 150 (per inch) mesh. This mesh is woven from 0.0076 cm (0.003 in.) diameter nickel wire. The original screen thickness is 0.015 cm (0.006 in.) at the points where the wires of the mesh cross. The three curves were obtained with screens that had been rolled to different thicknesses before being platinized. It was observed that, as a result of the successive rolling, the surface of the screen became flatter and facilitated a larger area of contact between the electrode and electrolyte. This correlates with the fact that less polarization occurs with the more extensively rolled samples since lower effective current densities at the electrode surface would result from the better contact. The best type 1 cell achieved 60 ma at 0.75 v after 10 sec under load and a steady-state current of about 40 ma on the same load resistance.

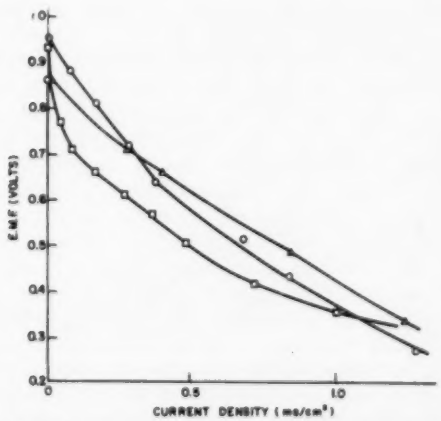

Fig. 5. EMF vs. current density for hydrogen-oxygen type 1 cells with platinum foil electrodes; cell area, 25 cm². ○, 0.5 mil foil platinized; △, 0.08 mil foil platinized; □, 0.05 mil lightly platinized.

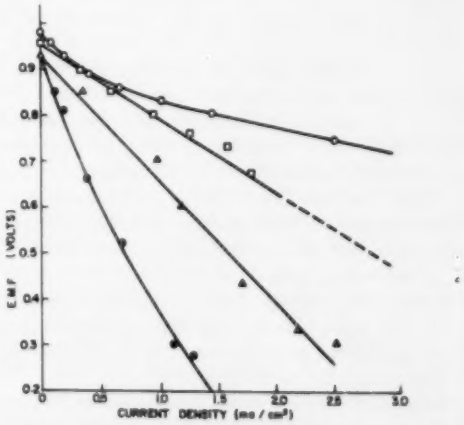

Fig. 6. EMF vs. current density for hydrogen-oxygen type 1 cells with various electrodes; cell area, 25 cm². ○, rolled screen* 2 mil thickness; □, rolled screen* 4 mil thickness; △, unrolled screen* 6 mil thickness; •, 0.08 mil foil cell (cf. Fig. 5).

* Platinized nickel screen.

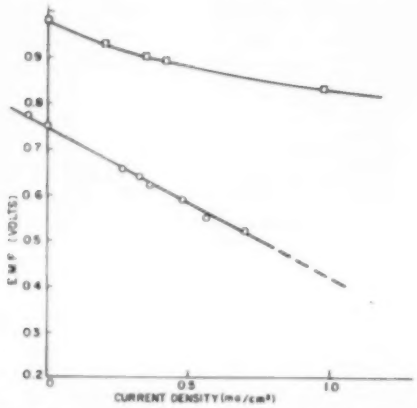

Fig. 7. EMF vs. current density for zinc-hydrogen and oxygen-hydrogen cells with platinized nickel screen electrodes. Cell, type 1; area, 25 cm². □, H_2-O_2 cell; ○, H_2-Zn cell.

The form of the polarization curves and the value of the open-circuit voltage both suggest irreversibility at one or both electrodes in this cell. In order to separate the effects of the anode and cathode, the hydrogen electrode was placed in a separate cell against a zinc electrode which is already known to behave reversibly (1). The following cell was used: zinc metal/zinc ion membrane/hydrogen ion membrane/platinized screen/hydrogen gas at 1 atm. The polarization curve of this cell is plotted in Fig. 7 along with that of the best cell of Fig. 6 for comparison. The emf of the H_2-Zn cell at zero current is observed to be 0.75 v, whereas in the analogous cell in which aqueous solutions at 25°C are employed with unit ionic activities the emf is 0.763 v (8). It is concluded that the H_2/platinized screen/H^+ membrane half-cell must be operating approximately at the reversible emf. The open-circuit emf of the H_2-O_2 cell is 0.90-0.96 v as compared with 1.23 v to be expected from the value of free energy of formation of water at 25°C. A deficiency of about 0.25-0.30 v at the O_2 electrode must therefore be present. This result is not surprising in view of published work on the behavior of platinum electrodes with oxygen at room temperature in sulfuric acid solutions (9).

The data presented above were obtained during short periods of operation using the type 1 cell of Fig. 2. It was of interest to consider performance under continuous operation. For this purpose a test run of approximately 15-hr duration was made on the type 2 cell of Fig. 3 and 4. In this run platinized nickel electrodes were used. In addition, the fuel gas was a mixture of 2 moles CO_2 to 1 mole of H_2. Flowing gases were used. At the start of the run the current was 45 ma at 0.69 v. After approximately 15-hr operation the cell current was 47 ma at 0.73 v. Initial and final polarization curves for this run are shown in Fig. 8.

Since it is known that ion-exchange membranes have a capacity for free acid, it was of interest to determine the effect of such acid on cell performance. For this purpose a membrane was equilibrated with 6M H_2SO_4 and after being blotted dry was assembled into a cell. The pronounced effect of the free acid on cell performance is shown by a comparison of the

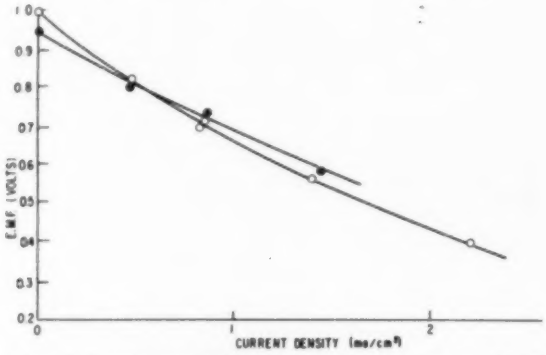

Fig. 8. Steady-state EMF vs. current density for type 2 cell operating on dry O_2 (flow rate 7 cc/min) and a 1:2M mixture of H_2 and CO_2 saturated with water (flow rate 10 cc/min). ○, Initial operation; •, after 15 hr of operation at 1 ma/cm². Electrodes 500X 500 mesh nickel screen activated with platinum black.

two curves in Fig. 9. The lower curve in the figure is representative of steady-state performance of cells operating with untreated membranes on pure hydrogen and oxygen.

While addition of free acid to the membrane does improve the cell performance, this does not appear to be a satisfactory, long range approach because of the corrosion problems that are thereby introduced. In addition, this acid can be leached from the membrane by the water produced in the cell reaction unless proper conditions are maintained to remove water by evaporation.

Summary and Conclusions

The use of ion-exchange membranes as the electrolyte in hydrogen-oxygen fuel cells is attractive. As solid, nonleachable electrolytes, these membranes permit the construction of cells that require a minimum of external components and controls, e.g., pumps, etc. Another important advantage of the ion-exchange membrane electrolyte is its very favorable geometry. The cells described here have a total active thickness of less than 1 mm. Such a favorable space factor helps to compensate for the lower current density of this cell relative, for example, to that of Bacon (3). In addition, because such membranes are used in their acid form, operation on gases containing large amounts of CO_2 is possible and has been demonstrated.

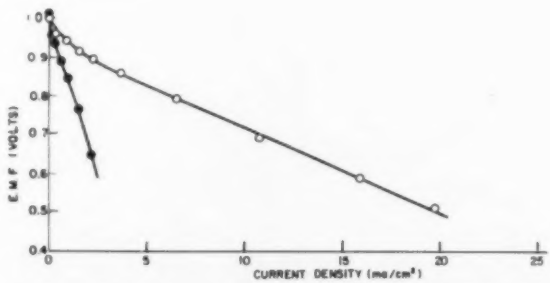

Fig. 9. Effect of free acid on cell operation. EMF vs. current density for type 2 cell with 200 x 200 mesh nickel screen electrodes (rolled to 0.002 in. thickness) platinum activated. •, Leached membrane H^+ form; ○, membrane H^+ form in equilibrium with 6M H_2SO_4 and wiped dry superficially.

Saturation of the membrane-electrolyte with sulfuric acid improves the performance of the cell. The treatment has some disadvantage in that it causes corrosion problems and other complications related to the dilution and leaching out of the free acid.

The indicated directions of improvement for cells of this kind are in mechanical construction to improve the electrical contact between the electrodes and the membrane and in the oxygen electrode surface to provide a more nearly reversible O_2 half-cell.

Acknowledgment

The authors are indebted to Drs. H. A. Liebhafsky, J. L. Weininger, and D. L. Douglas for a number of helpful discussions during the course of this investigation.

Manuscript received Oct. 2, 1959.

Any discussion of this paper will appear in a Discussion Section to be published in the December 1960 JOURNAL.

REFERENCES

1. W. T. Grubb, *This Journal*, **106**, 275 (1959) (Part I of this series).
2. R. G. H. Watson, *Research*, **7**, 34 (1954).
3. F. T. Bacon, *Beama Journal*, January (1954).
4. W. T. Grubb, *J. Phys. Chem.*, **63**, 55 (1959).
5. A. G. Winger, G. W. Bodamer, and R. Kunin, *This Journal*, **100**, 179 (1953).
6. J. Reilly and W. R. Rae, "Physico-Chemical Methods," Vol. 2, p. 608, D. Van Nostrand Co. Inc., New York (1953).
7. O. K. Davtyan, "Direct Conversion of Energy of Fuels to Electrical Energy," pp. 1-48, Academy of Science of the USSR, Moscow (1947).
8. W. M. Latimer, "Oxidation Potentials," 2nd ed., Prentice-Hall, Inc., New York (1952).
9. J. O'M. Bockris and A. K. M. S. Huq, *Proc. Royal Soc. (London)*, **237A**, 277 (1956).

The Influence of Cations on the Differential Capacity of the Dropping Mercury Electrode in Solutions of Electrolytes in Methanol and Ethanol

S. Minc and J. Jastrzebska

Department of Electrochemistry, University of Warsaw, Warsaw, Poland, and Department of Electrochemistry, Polish Academy of Sciences, Warsaw, Poland

ABSTRACT

Differential capacities of the electrical double layer of LiCl, NaCl, $MgCl_2$, and $SrCl_2$ in methanol have been measured. The capacities have been found to be higher in the presence of large cations (of low polarizability), which undergo chemisorption according to Frumkin's theory, by comparison with values observed in the presence of cations of high polarizability. In addition, the effect of concentration of the electrolyte on the differential capacity increases with decreasing polarizability of the cation. The solvent effect on the differential capacity has been found to be greatest near the zero charge potential, the decrease of the differential capacity relative to its value in water solutions being proportional to the decrease in dielectric constant.

In recent papers on electrocapillary phenomena, two different points of view have been advanced regarding the effect of cations on the structure of the electrical double layer. According to Grahame (1-3) the differential capacity of the inner part of the double layer is independent of the kind of cation if it is monatomic. Small differences of capacity observed for aqueous solutions in the region of strong cathodic polarization in the presence of different cations are due, according to Grahame's theory (4), to incomplete dielectric saturation of the solvent by some cations. There are more facts which could hardly be explained by Grahame's theory. For instance, it is known that the presence of large cations in the solutions increases the rate of electroreduction of some anions, e.g., $S_2O_8^{2-}$, and/or shifts the potential of desorption of anions toward more negative values (5-7).

Frumkin has concluded (6, 8) that some large cations, e.g., Rb^+, Cs^+, are chemisorbed at the surface of mercury. The aim of our work has been to contribute further experimental data to the solution of this problem (9). It was expected that the effects of chemisorption of cations ought to be more pronounced in some organic solvents. Methyl and ethyl alcohols have been chosen as solvents because of their high compressibility, high electrostriction in electrical fields, and their ease of dielectric saturation (10, 11). In consequence, the influence of cations on the structure of the double layer should be determined more precisely.

Experimental

An a-c symmetrical bridge was used in measurements of the differential capacity of the dropping mercury electrode. Our circuit differed from that of Grahame (12, 13) in that the stray capacitances of the bridge ratio resistors were balanced. A ferrite core choke or large inductance was introduced into the circuit (14). The application of balanced ratio

resistors and a large inductance in measurements with organic solvent solutions of low conductivity resulted in greater accuracy. The polarization of the dropping mercury electrode was achieved by a conventional polarographic technique.

Differential capacities were measured for potentials between −0.1 v and −1.8 v, with the aqueous saturated calomel electrode (S.C.E.) as reference. The surface area was evaluated by Grahame's method. The calculated differential capacity per unit area has been plotted against the potentials in Fig. 1-10.

Methyl and ethyl alcohols were distilled on a 30-plate column and the appropriate fractions collected. Water was distilled three times through a quartz condenser. Its specific conductivity was 4×10^{-6} ohm^{-1} cm^{-1}. Magnesium chloride, after being recrystallized from water, was heated in mixture with ammonium chloride at 360°C in platinum. Sodium chloride was brought down from a saturated solution by means of gaseous hydrogen chloride. Other salts were recrystallized from methyl alcohol and dried at 180°C to constant weight. Mercury was washed with dilute nitric acid, then with water, and finally distilled in vacuum. Nitrogen used for removing oxygen from the solutions was purified by means of activated carbon, potassium hydroxide solution, and silica gel impregnated with Cu_2O (15). The purity of solutions was checked polarographically.

Results and Discussion

Figure 1 shows differential capacity curves for 0.1M LiCl, 0.1M NaCl, and saturated KCl (about 0.05M) in methyl alcohol. In the region of high cathodic polarization the differential capacities differ in the presence of different cations and increase from Li^+ to K^+ in a manner similar to that observed for water solutions, except that the effect is more pronounced in alcohol. Similar curves determined for 0.1M methanol solutions of $MgCl_2$, $CaCl_2$, and $SrCl_2$ are shown in Fig. 2. The divalent cations affect the differential capacity only slightly and then only in the region of high cathodic polarization. In summary, it may be said that the differential capacity of the electrical double layer on mercury in the cathodic region is higher in the presence of cations of low polarizability (large radii). These ions, according to Frumkin's theory, undergo specific adsorption (chemisorption). There is no doubt that the high compressibility and electrorestriction of methyl alcohol molecules cause a more pronounced interaction of cations with the metal surface.

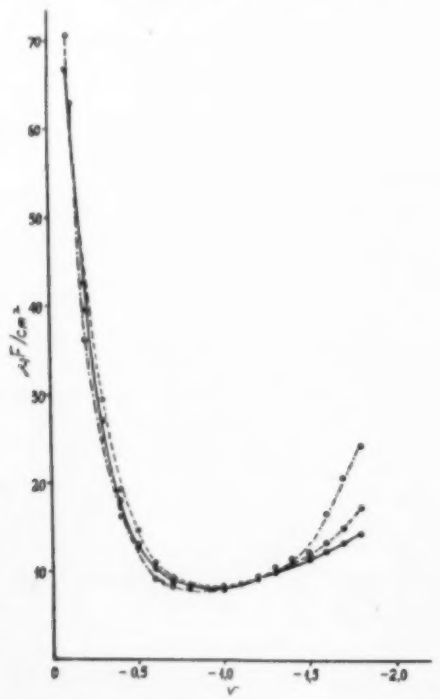

Fig. 1. •— 0.1M LiCl in methanol; o— — 0.1M NaCl in methanol; o- — satd. KCl in methanol.

Figs. 1-10. In the ordinate is the differential capacity of the mercury-solution interface in microfarads per square centimeter, the abcissa is the potential relative to the aqueous S.C.E., in volts.

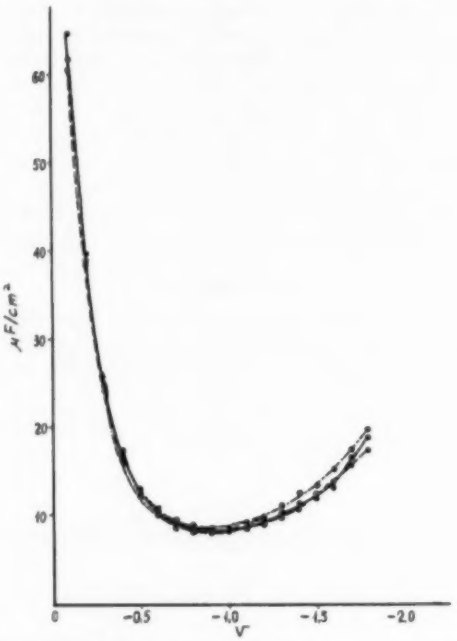

Fig. 2. •— 0.1M $MgCl_2$ in methanol; o— — 0.1M $CaCl_2$ in methanol; o- — 0.1M $SrCl_2$ in methanol.

Results shown in Fig. 1 and 2 make it clear, however, that the differential capacity is affected not only by the nature of the solvent, as postulated by Grahame (11, 16), but also by the nature of cations, especially those of low polarizability. If Frumkin's hypothesis of specific adsorption of some cations is true, an unusually strong effect of concentration of the electrolyte on the differential capacity is to be expected when these cations are present in solution. The measurements performed to test this expectation are presented in Fig. 3-8. The differential capacities have been measured for aqueous, methanol, and ethanol solutions of LiCl and KF in the concentration range from 0.05 to 0.5M.

For aqueous solutions of LiCl and KF the effect of concentration on the differential capacity is small and nearly the same for both cations in the cathodic region (Fig. 3 and 4). This is in accordance with the

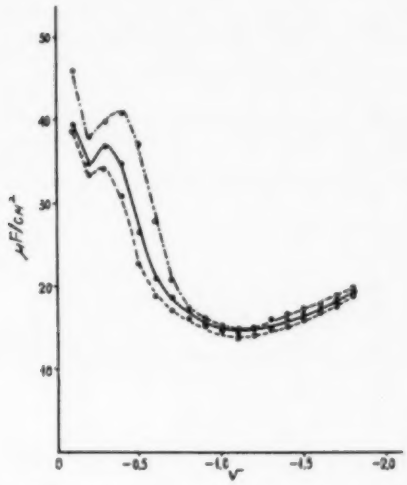

Fig. 3. Effect of concentration o— — 0.05 M LiCl in water; •— 0.1 M LiCl in water; o- — 0.5 M LiCl in water.

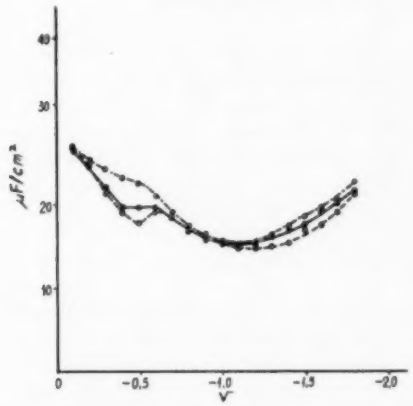

Fig. 4. Effect of concentration. o— — 0.05M KF in water; •— 0.1M KF in water; o- — 0.5M KF in water.

conclusion that neither Li^+ nor K^+ are chemisorbed on mercury from water. The small effect of concentration on the differential capacity of LiCl solutions in all three solvents (Fig. 3, 5, and 6) may be accourted for on the basis of the theory of electrostatic interaction of ions with metal surface developed by Grahame (1, 2, 11).

The marked concentration dependence found for high cathodic polarizations in alcoholic KF solutions (Fig. 7 and 8) cannot be due to the effect of concentration on the capacity of the diffuse part of the double layer as this effect could not be so different for the two cations investigated. It may be considered as evidence in support of the hypothesis of chemisorption of K^+ ion from methanol and ethanol.

Further measurements were undertaken to determine the desorption potentials of halide ions in methanol (Fig. 9 and 10). The only reason for the lower differential capacities in the cathodic region for saturated (about 0.05M) KCl in methanol as compared with 0.1M solutions of the potassium halides (Fig. 10) is evidently the difference in concentration. The differential capacities of saturated KCl (Fig. 1) and of 0.05M KF (Fig. 7) are practically the same. It is worth stressing that the desorption potentials found in this work for F^- and Cl^- ions in the presence of K^+ ion in methyl alcohol are nearly the same as those given by Grahame (11) for the same anions and solvent in the presence of NH_4^+.

In order to characterize the solvent effect, the curves for 0.1M LiCl in water (Fig. 3), methanol

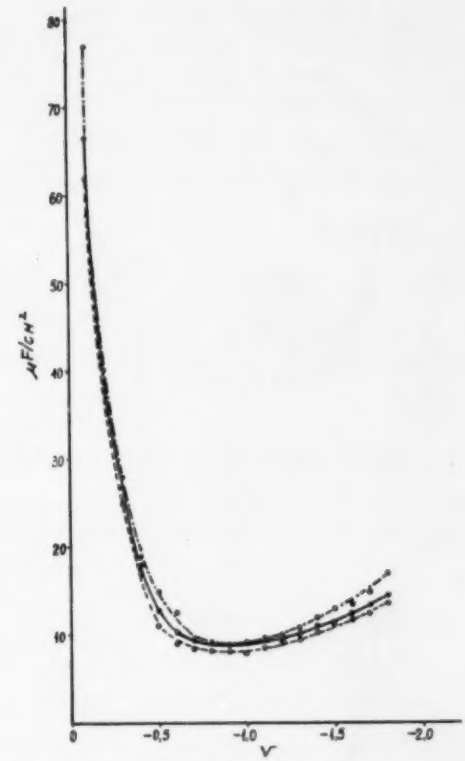

Fig. 5. Effect of concentration. o— — 0.05M LiCl in methanol; •— 0.1M LiCl in methanol; o- — 0.5M LiCl in methanol.

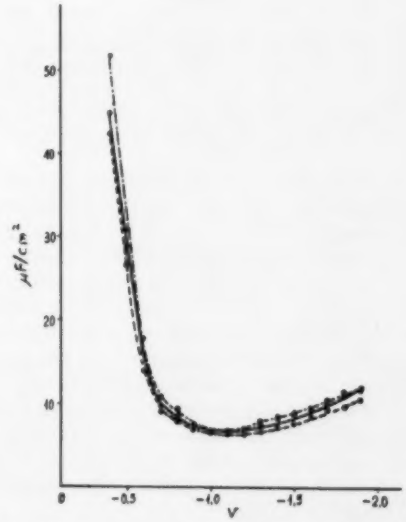

Fig. 6. Effect of concentration. o— — 0.05M LiCl in ethanol; •— 0.1M LiCl in ethanol; o- — 0.5M LiCl (satd.) in ethanol.

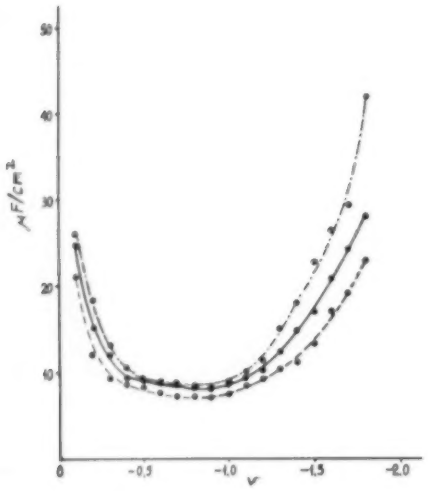

Fig. 7. Effect of concentration. o— — 0.05M KF in methanol; •— 0.1M KF in methanol; o- — 0.5M KF in methanol.

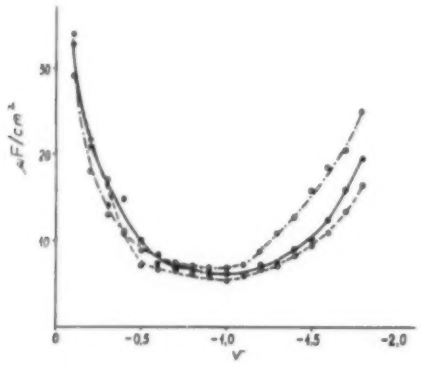

Fig. 8. Effect of concentration. o— — 0.05M KF in ethanol; •— 0.1M KF in ethanol; o- — satd. KF in ethanol.

(Fig. 1 and 5), and ethanol (Fig. 6) can be compared. The strongest effect of the solvent occurs near the zero charge potential (about −0.6 v). In this region, the decrease of the differential capacity when water is replaced by alcohol is nearly proportional to the decrease of the dielectric constant of the solvent. Also worth noting is the fact that the differential capacities of alcohol solutions show no peaks in the region of low anodic polarizations (about −0.3 to −0.4 v to S.C.E.); such peaks are observed in aqueous solutions (Fig. 3). This observation seems to favor the explanation given by Grahame (16) according to which this effect is due to the pseudocrystallic structure of water.

Manuscript received June 11, 1959.

Any discussion of this paper will appear in a Discussion Section to be published in the December 1960 JOURNAL.

REFERENCES

1. D. C. Grahame, *Chem. Rev.*, **41**, 441 (1947).
2. D. C. Grahame and B. A. Soderberg, *J. Chem. Phys.*, **22**, 449 (1954).
3. D. C. Grahame, *Z. Elektrochem.*, **59**, 773 (1955).
4. D. C. Grahame, *This Journal*, **98**, 343 (1951).
5. A. N. Frumkin, *Izvesti Akad. Nauk S.S.S.R.*, **12**, 1421 (1957).

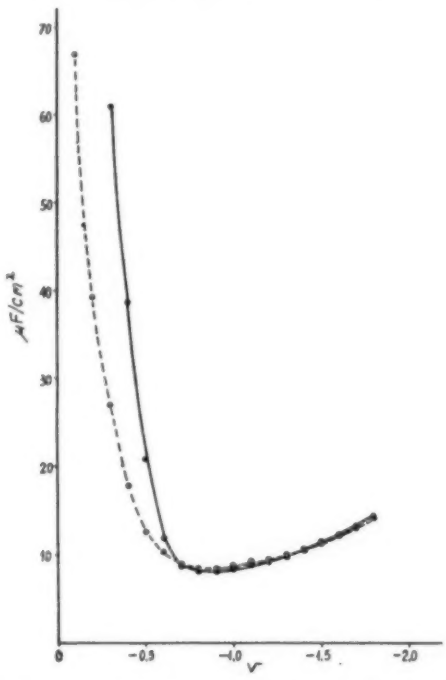

Fig. 9. Differential capacity in presence of specific adsorption of some anions. o— — 0.1M LiCl in methanol; •— 0.1M LiBr in methanol.

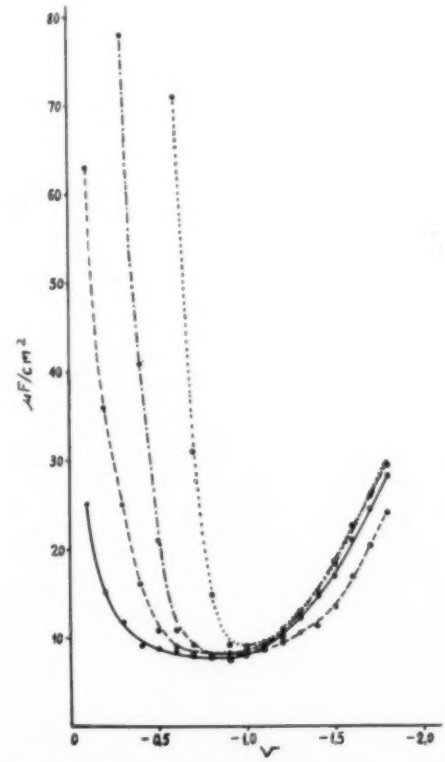

Fig. 10. Differential capacity in presence of specific adsorption of some anions. •— 0.1M KF in methanol; o— — satd. KCl in methanol; o- — 0.1M KBr in methanol; o- - - - 0.1M KI in methanol.

6. A. N. Frumkin, B. Damackin, and N. Nikolajeva-Fiedorovic, *Doklady Akad. Nauk S.S.S.R.*, **115**, 751 (1957).
7. J. J. Lothe and L. B. Rogers, *This Journal*, **101**, 258 (1954).
8. B. Damackin, N. Nikolajeva-Fedorovic, and A. N. Frumkin, *Doklady Akad. Nauk S.S.S.R.*, **121**, 129 (1958).
9. S. Minc and J. Jastrzebska, *ibid.*, **120**, 114 (1958).
10. R. J. Macdonald, *J. Chem. Phys.*, **25**, 364 (1956).
11. D. C. Grahame, *Z. Elektrochem.*, **59**, 740 (1955).
12. D. C. Grahame, *J. Am. Chem. Soc.*, **63**, 1207 (1941).
13. D. C. Grahame, *ibid.*, **71**, 2975 (1949).
14. S. Minc and J. Jastrzebska, *Rocz. Chem.*, **31**, 1339 (1957).
15. F. Meyer and G. Konge, *Angew. Chem.*, **52**, 637 (1939).
16. D. C. Grahame, *J. Am. Chem. Soc.*, **79**, 2093 (1957).

Technical Notes

Chloride Content of the Diffusion Layer at a Silver Anode

Paul A. Krasley[1]

Chemistry Division, National Bureau of Standards, Washington, D. C.

A technique for isolating the diffusion layer at an electrode was developed by Yannakopoulos and Brenner (1). It involves the drawing off of the diffusion layer through a microporous electrode. These authors applied the method only to the study of the decrease of metal concentration that occurred at a cathode during metal deposition. The study reported here is an extension of the method and deals with the depletion of chloride ion that occurs at an attackable anode of silver.

The diffusion layer that forms at a silver anode during electrolysis of a sodium chloride solution contains a lower concentration of salt than the body of the solution, and the lowest concentration exists at the interface of the solution and the anode. The reduction in concentration results from the precipitation of chloride ions as silver chloride and the migration of sodium ions toward the cathode.

Experimental

Preparation of a microporous silver electrode.—Yannakopoulos and Brenner used a microporous, cylindrical, stainless steel electrode in their experiments. This shape has the advantage of providing a large electrode surface and a small volume. Efforts to prepare a microporous cylinder from porous silver sheet were unsuccessful for several reasons. The pores in the silver sheet were closed through cold-welding during the fabrication of the cylinder, and the sheet was so brittle that it cracked in shaping. A silver plated stainless steel cylinder was unsatisfactory because the stainless steel was attacked anodically through the pores in the silver coating.

Plane microporous silver anodes 2 in. in diameter were made by placing "spherical silver powder" in a soapstone form, covering with a disk of soapstone, and sintering in a preheated furnace at 900°C for 0.5 hr. This procedure yielded disks having a ratio of voids to volume of 30-50%. Both acicular and electrolytic silver powder were also tried in the fabrication, but the spherical silver powder was most satisfactory.

Attempts to form the silver disks by the application of pressure alone, up to 2000 lb/in.^{2}, were not successful, because the silver did not cold-weld sufficiently to form a mechanically strong disk. The combination of compacting by pressure followed by sintering at 900°C had no advantage over heating alone.

The porous silver disks were made as thin as possible in order to reduce the amount of solution required to rinse the porous disks before collecting a sample of the interface of the bath. Disks having a thickness of about 0.09 in. were the thinnest able to withstand the handling in the cleaning procedure and the slight vacuum applied during sampling.

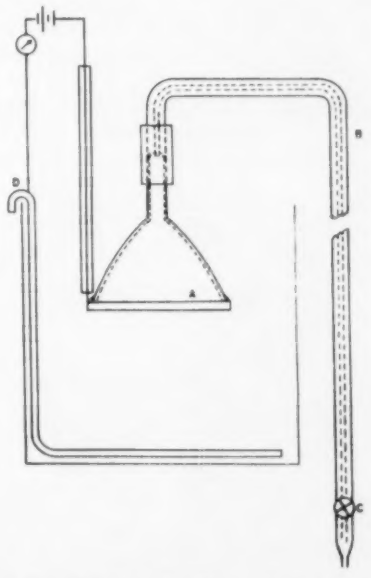

Fig. 1. Apparatus for desalting water: A, microporous silver anode; B, siphon; C, pinchcock; D, nickel anode.

[1] Present address: Bureau of Engraving and Printing, Washington, D. C.

Apparatus and Procedure

The apparatus shown in Fig. 1 consisted of a microporous silver anode, A, attached to an inverted funnel with Apiezon wax. The funnel was provided with a long capillary syphon, B. A pinchcock, C, regulated the rate of sampling of the interface. The nickel cathode, D, was bagged to minimize turbulence due to hydrogen evolution.

The apparatus was made ready for an experiment in the following way. The inverted funnel attached to the silver anode was filled with an organic liquid immiscible with water. To do this the anode assembly was partially immersed in water while the organic liquid was poured in from the top. An organic liquid more dense than water was chosen so that the aqueous solution subsequently collected would rise to the top. The following liquids were tried: a toluene-chloroform mixture (density 1.07^{20}), perfluorotriethylamine (density 2.7^{20}), and tetrabromoethane (density 2.95^{20}). Tetrabromoethane was used in most of the experiments.

The filled anode assembly was attached to the capillary syphon and was suspended in the bath. Electrolyses at various anodic current densities and rates of sampling were performed. Since the pores of the silver anode were filled with the water, the first several milliliters of liquid collected in an experiment were discarded before a sample representative of the electrode-solution interface was collected.

Results

The data in Table I represent typical results for the electrolysis of sodium chloride solutions. One disk was used for the 3% electrolysis and another disk was used for the 1% electrolysis. Because the formation of silver chloride plugged the interstices of the disk and caused a considerable increase in resistance both to current flow and to the flow of liquid, a single disk could not be used to make many successive experiments for determining effects of current density and of the rate of collection of the sample. For this reason the concentration of sodium chloride was reduced to 1%. The order of collection of data was the same as appears in Table I. Run No. 9 and definitely Run No. 10 can be attributed to the plugging of the disk. The plugging is accompanied by the evolution of gas which doubtless disturbs the diffusion layer.

Table I. Results of the electrolysis of NaCl solutions using porous silver anodes

Run No.	Conc. of electrolyte, %	Current density, amp/dm²	Rate of sampling of diffusion layer, min/ml	Reduction in chloride, %
1	3	2	3.3	17.8
2	3	3	3.3	24.5
3	3	1	7	39.4
4	3	2	7	45.6
5	1	0.25	7	18.5
6	1	0.50	7	34.3
7	1	0.25	14	32.2
8	1	0.5	14	73.0
9	1	0.75	14	80.9
10	1	0.75	17.5	27.0

Discussion

The investigation of the removal of chloride ion in the diffusion layer of a silver anode was carried only far enough to indicate that the process was theoretically feasible. The plugging of the silver disks showed that the use of this particular electrode was impracticable as a means of desalting water. However, it is possible that a more satisfactory electrode system can be developed.

Theoretically, a continuous desalting process could be devised which would utilize two porous silver-silver chloride electrodes. They would be placed close together, and initially the desalted water would be collected from one electrode. At intervals the direction of the current would be changed to regenerate the electrode and at the same time the collection of the desalted water from the other electrode would be started. If the two electrodes were placed close together to lessen resistance, the consumption of electrical energy would be small.

The desalting of water by the continuous collection of solution at the anode-solution interface differs in principle from the removal of chloride ion by use of a silver anode and cathode in a confined volume of solution. In the latter process, even though all the chloride ion were eventually removed by the silver anode, an equivalent content of sodium hydroxide would replace it, so that the solution would not be demineralized. The microporous electrode method, on the other hand, is envisaged to operate in a large volume of flowing solution, such as an ocean, so that the anode is always immersed in a solution of constant composition and the products formed at the cathode are swept away.

Murphy (2) has utilized silver-silver chloride electrodes to separate dissolved chlorides by an electro-gravitational method. His method is not directly comparable with the microporous electrode method, since its operation depends on the continued treatment of a solution for several hours either in a fixed volume or as it flows along the electrodes.

Manuscript received Aug. 19, 1959.

Any discussion of this paper will appear in a Discussion Section to be published in the December 1960 JOURNAL.

REFERENCES

1. Theodore Yannakopoulos and Abner Brenner, *This Journal*, **105**, 521 (1958).
2. G. W. Murphy, *ibid.*, **97**, 405 (1950); G. W. Murphy and D. Batzer, *ibid.*, **99**, 520 (1952).

Oxidation Rates of K and Rb between −79°C and −20°C

J. V. Cathcart and G. P. Smith

Metallurgy Division, Oak Ridge National Laboratory, Union Carbide Corporation, Oak Ridge, Tennessee

A study of the oxidation characteristics of the alkali metals was undertaken as a part of an investigation of the factors which determine the degree of protectiveness of thin oxide films formed on metals. Previously published data (1) relative to the oxidation kinetics of Na indicated that in purified oxygen Na formed a highly protective oxide film at room temperature or below but that the film became nonprotective after long periods of oxidation in the vicinity of 50°C. A similar study of the oxidation rates of K and Rb between −79° and −20°C showed that these metals likewise formed protective films at low temperatures but that the transition from protective to nonprotective oxidation occurred at a lower temperature than for the case of Na.

Experimental Procedure

Oxidation rates of K and Rb were determined by measuring the changes in pressure in a closed reaction chamber as oxidation proceeded. A sensitive differential manometer served as the pressure sensing device. Samples of K and Rb were purified by careful vacuum distillation (2), and the oxidation specimens were prepared by depositing relatively thick films of K or Rb on the walls of the oxidation chamber at a pressure of approximately 10^{-7} mm Hg. Details of the apparatus and the experimental procedure have been described elsewhere (1).

Results and Discussion

Rate measurements were made for K at −79°, −50°, −20°C and for Rb at −79° and −50°C. Results of typical experiments are shown in Fig. 1 and 2. In each figure the number of moles of oxygen consumed per square centimeter of apparent surface area is plotted against the time of oxidation measured in minutes.

Both K and Rb exhibited a marked lack of reactivity in pure oxygen in the temperature range cited. If it is assumed that the oxide formed as a uniform surface layer on the specimens, the films produced on K at −50° and −79°C were not more than 100Å thick after 100,000 min (about 70 days) of oxidation. At higher temperatures, −20°C for K and −50°C for Rb, the maximum film thicknesses attained were probably between 2000 and 3000Å. More precise figures are not given for the film thicknesses because of the uncertainty as to the exact oxide compositions and because of the likelihood that thickness inhomogeneities existed in the films (3).

It will be noted that the oxide films formed on K at −50° and −79°C were almost completely protective, but at −20°C a transition from protective to nonprotective oxidation was observed. A similar transition occurred in oxide films formed on Rb at −50° and −79°C. These results are also consistent with the oxidation characteristics of Na for which a comparable behavior was observed at 48°C. Thus a transformation from protective to nonprotective oxidation occurred for all three of the alkali metals investigated, and the temperature at which this transformation was observed varied inversely with the electropositive character of the metals.

Because of the extreme thinness of the oxide films and their sensitivity to moist air, no satisfactory method has as yet been devised for determining their compositions. The super oxides, KO_2 and RbO_2, have been reported as the major products formed during the burning of K and Rb in oxygen (4). However, several other oxides have been reported in the literature for both K and Rb (5), although complete metal-oxygen phase diagrams are available

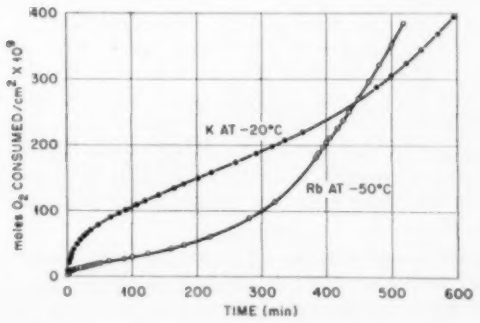

Fig. 1. Oxidation of K at −20°C and Rb at −50°C

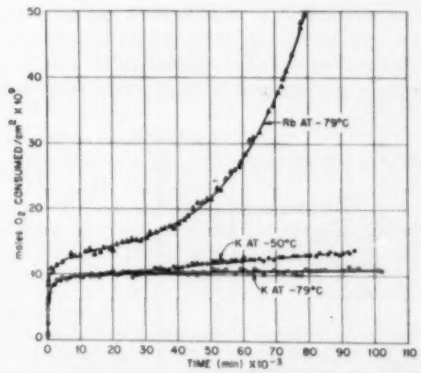

Fig. 2. Oxidation of K at −50° and −79°C and Rb at −79°C.

for neither. Since the metal was by no means completely consumed in the experiments reported here, it is probable that the oxide films consisted of several oxide phases in addition to the super oxides.

Efforts to determine rate curves at temperatures higher than −50°C for Rb and −20°C for K were unsuccessful because the rates of oxidation were too rapid to be measured with the manometric technique utilized in this research. At room temperature, actual burning of the metal occurred. It was noted, however, that, if the specimens were first exposed to oxygen at a lower temperature, e.g., −79°C, and then the system brought to room temperature, a drastic reduction in the oxidation rate occurred. Instead of the burning such as occurred when the clean metal was exposed to oxygen at room temperature, a slow uptake of gas was found to take place over a period of several days. Thus the oxidation rates of K and Rb, as is the case for many other metals, proved to be markedly dependent on the prior history, especially the surface condition, of the metal specimens.

Manuscript received March 23, 1959.

Any discussion of this paper will appear in a Discussion Section to be published in the December 1960 JOURNAL.

REFERENCES

1. J. V. Cathcart, L. L. Hall, and G. P. Smith, *Acta Met.*, 5, 245 (1957).
2. G. W. Horsley, "The Purification of Commercial Potassium," Atomic Energy Research Establishment No. M/R 1371.
3. W. W. Harris, F. Ball, and A. T. Gwathmey, *Acta Met.*, 5, 574 (1957).
4. H. Remy, "Lehrbuch der Anorganischen Chemie," Vol. 1, p. 165, Akademische Verlasgesellschaft, Leipzig (1953).
5. L. Brewer, *Chem. Rev.*, 52, 1 (1953).

The A-C Resistance of a Polarized Stainless Steel Wire Cathode

G. M. Schmid and Norman Hackerman

Department of Chemistry, University of Texas, Austin, Texas

Resistance measurements are used currently to determine the amounts of adsorbed gas on thin metal films (1). It also should be possible, in principle, to determine the growth of an oxide layer on a thin metal film in solution by this method. However, it is uncertain how the resistance of an electrode is affected by the solution and by a polarizing current.

The a-c resistance of palladium wires increases when the metal is in certain electrolyte solutions while being cathodically charged (2-4). Prolonged charging at higher current densities results in a resistance decrease. The increase is due to H_2 absorption and it has been suggested by Knorr and coworkers (5, 6) that the decrease is due to leakage through the surrounding electrolyte. Conductivity by way of the electrolyte must occur via a coupling which is provided by disturbing of the electrical double layer (edl). In order to eliminate the effect of H_2 absorption the a-c resistance of stainless steel electrodes was followed in this study. The structure of the edl was altered by passing a d-c polarizing current of 1-40 ma/cm².

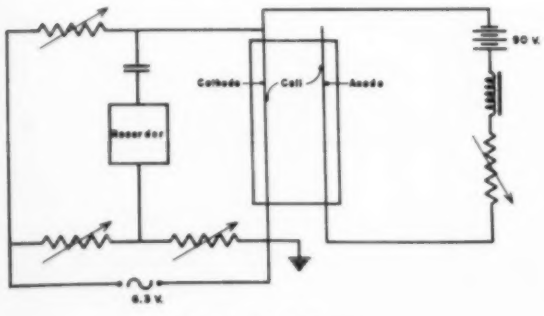

Fig. 1. Circuit diagram

Experimental and Results

The cell consisted of a glass tube and two straight type 302 stainless steel wires, 0.038 cm in diameter and 30-100 cm long (Fig. 1). The a-c resistance of the wire serving as the cathode was measured. The second wire was the anode and was held parallel to the first, generally more than 0.1 cm away. The electrolyte was 0.01-1.0M Na_2SO_4.

The resistance measurements, with or without d-c polarization, were obtained with a standard Wheatstone-Bridge, using 60 cps a-c. A Brown-Honeywell recorder with its converter stage by-passed was used as an automatic balancing instrument. Any d-c pickup was eliminated by the transformer in the automatic balancing unit of the recorder and by using a 100 μf capacitor in the circuit. The voltage drop along the grounded cathode was about 0.1 v. Resistance changes of 0.005 ohm could be measured easily. The polarizing current was furnished by a 90 v battery using a set of resistors to control the current and a 10 henry choke to minimize a-c pickup from the bridge circuit. In order to get significant resistance changes the cathode had to be polarized to the hydrogen evolution potential (at least to −1.1 v vs. SCE).

Addition of solution alone has no influence on the resistance of the cathode, causing changes of no more than 0.01 ohm, provided the anode was more than 1 mm away. On the other hand, Fig. 2 shows that the resistance of the cathode drops when polarized at current densities greater than 0.5 ma/cm², thus indi-

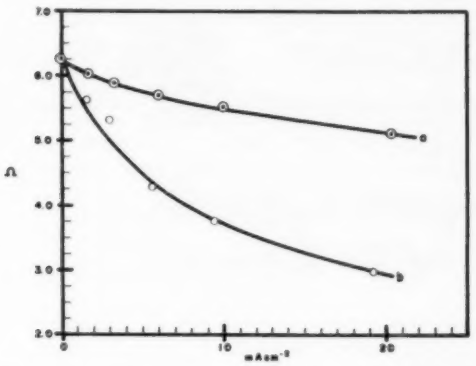

Fig. 2. Dependence of resistance on electrode-distance, cathode surface area 11.1 cm^2, 18-8 stainless steel, 1.0M Na_2SO_4. Curve a, electrode-distance 2.1 cm; curve b, electrode-distance 0.1 cm.

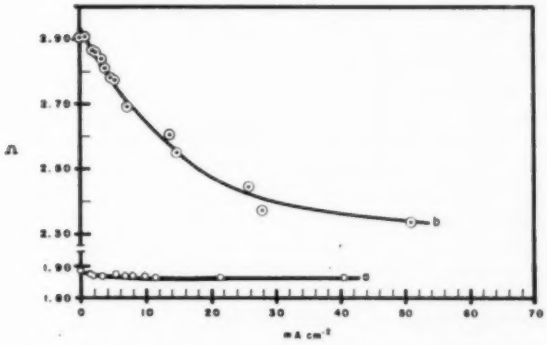

Fig. 3. Dependence of resistance on electrolyte concentration, electrode-distance 1.0 cm. Curve a, 0.01M Na_2SO_4, length of wire 29 cm, surface area 3.5 cm^2; curve b, 1.0M Na_2SO_4, length of wire 44 cm, surface area 5.2 cm^2.

cating additional conduction by the surroundings. The resistance changes are related nonlinearly to the length of the wire in solution.

Aside from immersed wire length, the resistance decrease at constant polarizing current density was influenced by the distance between anode and cathode. This indicates that the anode as well as the electrolyte is part of the a-c conducting system at small separations (Fig. 2). The influence of solution concentration is shown in Fig. 3. Under the same conditions except with 0.001M Na_2SO_4 there was no resistance change.

In all cases the resistance changes occurred in less than 2 sec, indicating the absence of hydrogen diffusion effects. The i^2R-effect was negligibly small, values obtained being steady over a 5-min period. The changes were reversible and, for a given electrolyte, a given distance between anode and cathode, and a given "air" resistance of anode and cathode, entirely reproducible.

Discussion

Coehn and Specht (7) carried out similar experiments on palladium and also observed drops in resistance proportional to the polarizing current. They explained their effects by the additional conductivity by hydrogen in the metal in excess of saturation concentration. This explanation is not suitable for stainless steel because of the rapid resistance changes and the rapid recovery of original resistance after switching off the d-c polarizing current. This makes diffusion effects highly improbable.

The transition resistance between cathode and surroundings seems to be very high as long as the cathode is not polarized. After the polarizing current has shifted the potential of the electrode to a high enough negative value, the a.c. is able to oxidize and reduce some species according to its own frequency, thus passing into solution. Moreover, with increasing current density, i.e., increasing negative potential, the cathode metal is sufficiently displaced from its zero point of charge so that there should be an adsorbed layer of cations and oriented water dipoles in close contact. This may cause a further drop in resistance.

The same effect, with reverse sign, should be expected at the anode, and this was verified experimentally. The resistance changes are in the same order of magnitude.

It seems therefore that the resistance of the system in a polarized state consists of the resistance of the cathode and the anode plus a transition resistance or coupling capacitance on either side plus the resistance contributed by the electrolyte. All these additional resistivities cannot be considered as parallel to the cathode but rather as diffuse and effective over the whole cathode surface. Thus a linear relationship between resistance change and length of the cathode should not be expected.

In order to get conclusive data concerning oxide films on thin working electrodes by observing its resistance change, one has to work in electrolytes of very low conductivity, otherwise the data taken during the flow of a d-c polarizing current are meaningless.

Further studies in this field should include the frequency dependence of the transition resistance and the effects of specifically adsorbed ions and surface active substances.

Acknowledgment

This work was carried out as part of Contract Nonr 375(02) with the Office of Naval Research. The authors take this opportunity to express their appreciation for this aid. Financial assistance by the Robert A. Welch Foundation is also appreciated.

Manuscript received June 5, 1959.

Any discussion of this paper will appear in a Discussion Section to be published in the December 1960 JOURNAL.

REFERENCES

1. Especially Suhrmann and co-workers, e.g., *Z. Elektrochem.*, **63**, 155 (1959).
2. F. Fischer, *Ann. phys.*, **20**, 503 (1906).
3. A. Coehn and H. Juergens, *Z. Phys.*, **71**, 179 (1931).
4. D. P. Smith, "Hydrogen in Metals," University of Chicago Press, Chicago (1948).
5. C. A. Knorr and E. Schwartz, *Z. Elektrochem.*, **39**, 281 (1933).
6. Just as this paper was being submitted an abstract of a paper given by Knorr and Roemer at the Bunsen-Meeting 1959 in Darmstadt/Germany on "Dependence between Polarization Resistance and Resistance of Hydrogen-Containing Palladium Wires" was received.
7. A. Coehn and W. Specht, *Z. Phys.*, **62**, 1 (1930).

Brief Communication

Measurement of the Segregation Coefficients of Impurity Elements in Aluminum Antimonide

D. Hazelby and J. L. Parmee

B.T.H. Group Research Laboratory, Rugby, England

Some approximate figures have already been quoted (1) for segregation coefficients in aluminum antimonide, but it was considered necessary to obtain accurate values for those elements which influence the electrical properties of the compound, and also those which are common impurities.

The technique adopted was to use radioactive tracers, prepared by irradiating each impurity in the B.E.P.O. pile at Harwell. Since no suitable isotope of carbon could be made by this method, carbon-14 was obtained from the radiochemical center at Amersham. It was found convenient to measure activities with a liquid counter. As the energy of the beta radiation from carbon-14 and from sulfur-35 was too weak to be detected with this counter, they were precipitated with carriers as barium sulfate and carbonate, respectively, and measured with an end window Geiger counter. Magnesium was used in the inactive form and estimated with a mass spectrograph, although the accuracy of this method was somewhat less than would be obtained by the radiochemical method.

The impurity concentration at any point along an ingot produced by normal freezing is

$$C = kC_o (1 - g)^{k-1} \qquad [1]$$

where C is the concentration at the point where a fraction g of the ingot has solidified, C_o is the original concentration in the melt, and k is the segregation coefficient.

At the front of the ingot, where g is almost equal to zero, the equation becomes

$$C = kC_o \qquad [2]$$

Thus, by measuring the concentration at the front of the ingot and the average concentration, k can be determined.

The conditions of our experiment did not conform strictly to those required for equilibrium segregation and so the measured values of k can be regarded only as observed values, i.e., as would be encountered in practice.

Milligram quantities of each impurity element were melted by high-frequency induction heating with 35 g of aluminum antimonide in a "Purox" alumina boat in an atmosphere of pure, dry argon. The melt was held at 1200°C for 5 min, during which time the stirring induced by the high-frequency field produced thorough mixing. The boat then was drawn out of the furnace at a rate of 5 in. hr^{-1}, causing normal freezing along the whole length of the charge.

The front 5% of the ingot was cut off, and this and the remaining piece weighed and dissolved in a mixture of hydrochloric and nitric acids. A suitable aliquot was taken from each solution and the activity was measured. The activity of the smaller piece gave the concentration of the front of the ingot C, and that of the larger piece was taken to be the average concentration C_o. The slope of the normal freezing curve at the front of the ingot is small for all values of k; there is thus no significant loss of accuracy in taking C to be the average concentration of the front 5%. The segregation coefficients of several elements are quoted in Table I.

It was noticed in some cases that an appreciable amount of activity was being lost by volatilization. Consideration of vapor pressures indicated that this was likely with zinc, cadmium, sulfur, selenium, and tellurium. This loss increased along the length of the ingot, being greatest at the end which was last to freeze, and so lowered the impurity concentration and hence the measured value of C_o. This gave a very high apparent value for the segregation coefficient, using Eq. [2].

In the practical use we are interested in the overall purification by both evaporation and segregation.

Table I.

Impurity element	Segregation coefficient	Purification factor
Magnesium	0.1	
Carbon	0.6	
Silicon	0.1	
Germanium	1.2	
Tin	1.0	
Iron	0.02	
Copper	0.01	
Manganese	0.01	
Cobalt	0.002	
Zinc		0.02
Cadmium		0.002
Sulfur		0.003
Selenium		0.003
Tellurium		0.01

This can be obtained by taking the ratio of the concentration of the activity in the front 5% of the ingot, to that of the impurity originally added, and gives an indication of the purification obtained under conditions in which volatilization is occurring. These ratios, which we have described as purification factors, are also given in Table I. Although they are clearly dependent on the conditions of the experiment, they do give an indication of the behavior of these impurities that could be expected on zone refining aluminum antimonide.

Acknowledgments

The authors express indebtedness for encouragement and assistance in this work to colleagues in the B.T.H. Group Research Laboratory.

Manuscript received Oct. 12, 1959.

Any discussion of this paper will appear in a Discussion Section to be published in the December 1960 JOURNAL.

REFERENCE

1. W. P. Allred, B. Paris, and M. Genser, *This Journal*, **105**, 93 (1958).

Corrections

In the discussion of the paper by P. E. Lake and E. J. Casey, "The Anodic Oxidation of Cadmium, I. Mechanism of Film Formation," which appeared in the June 1959 JOURNAL, in column 1 on page 533 it should read $R_z = \frac{I\,t'_p}{t_c + t'_p}$ rather than $R_z = \frac{I\,t'_p}{t_c\,t'_p}$.

* * *

In the paper by B. Schwartz, "The Use of Organo-Substituted Hydrolyzable Silanes on Silicon Devices," which appeared in the October 1959 JOURNAL, the following corrections should be made:

Page 871, column 1, paragraph 2, line 4—". . . while R is an organic . . ." should read ". . . where R is an organic . . ."

Page 871, column 2, paragraph 1, line 5—". . . this technique is the one preferred to . . ." should read ". . . this technique is the one referred to . . ."

Page 872, Table I, column 6, and Table III, column 1—"I_b, μa" should read "I_b, $m\mu a$"

Page 873, column 2, paragraph 3, line 3—". . . creating a silicon coating on the surface . . ." should read ". . . creating a silicone coating on the surface . . ."

Page 873, Reference 3—"*General Electric Rec.*" should read "*General Electric Rev.*"

Monographs of The Electrochemical Society

ECS Series

The following are books developed and sponsored by The Electrochemical Society and published by John Wiley & Sons, Inc., 440 Fourth Ave. New York 16, N. Y. Members of The Electrochemical Society can receive a 33 1/3% discount by ordering volumes from Society Headquarters, 1860 Broadway, New York 23, N. Y. Book and invoice will be mailed by John Wiley & Sons. Nonmembers (including subscribers) should order direct from Wiley.

Corrosion Handbook. Edited by Herbert H. Uhlig. Published 1948, 1188 pages, **$16.00**

Modern Electroplating. Edited by Allen G. Gray. Published 1953, 563 pages, **$8.50**

Abstracts of the Literature on Semiconducting and Luminescent Materials and Their Applications. Compiled by Battelle Memorial Institute.

Vol. I, 1953 Issue—published 1955, 169 pages, **$5.00** (soft cover)

Vol. II, 1954 Issue—published 1955, 200 pages, **$5.00** (soft cover)

Vol. III, 1955 Issue—Edited by E. Paskell; published 1957, 322 pages, **$10.00** (hard cover)

Vol. IV, 1956 Issue—Edited by E. Paskell; published 1959, 456 pages, **$12.00** (hard cover)

Electrochemistry in Biology and Medicine. Edited by Theodore Shedlovsky. Published 1955, 369 pages, **$11.50**

Vapor Plating (The Formation of Metallic and Refractory Coatings by Vapor Deposition), by C. F. Powell, I. E. Campbell, and B. W. Gonser. Published 1955, 158 pages, **$5.50**

High-Temperature Technology (Materials, Methods, and Measurements). Edited by I. E. Campbell. Published 1956, 526 pages, **$15.00**

Stress Corrosion Cracking and Embrittlement. Edited by W. D. Robertson. Published 1956, 202 pages, **$7.50**

Arcs in Inert Atmospheres and Vacuum. Edited by W. E. Kuhn. Published 1956, 188 pages, **$7.50**
(Papers Presented at the Symposium on Arcs in Inert Atmospheres and Vacuum of the Electrothermics and Metallurgy Division of The Electrochemical Society, April 30 and May 1, 1956, San Francisco, Calif.)

Technology of Columbium (Niobium). Edited by B. W. Gonser and E. M. Sherwood. Published 1958, 120 pages, **$7.00**
(Papers Presented at the Symposium on Columbium—Niobium of the Electrothermics and Metallurgy Division of The Electrochemical Society, May 15 and 16, 1958, Washington, D. C.)

The Structure of Electrolytic Solutions. Edited by Walter J. Hamer. Published 1959, 441 pages, **$18.50**
(Based on a Symposium held in Washington, D. C., in May 1957, sponsored by The Electrochemical Society, New York, and The National Science Foundation, Washington, D. C.)

Vacuum Metallurgy

Vacuum Metallurgy, third printing, 1958. Edited by J. M. Blocher, Jr.; 216 pages; **$5.00,** less a 20% discount to ECS members only. Available from Electrochemical Society Headquarters, 1860 Broadway, New York 23, N. Y.

(Papers Presented at the Vacuum Metallurgy Symposium of the Electrothermics and Metallurgy Division of The Electrochemical Society held in Boston, Mass., October 6 and 7, 1954)

Current Affairs

An Electrochemist Awarded the Nobel Prize in Chemistry for 1959

Professor J. Heyrovsky at an apparatus for oscillographic polarography

Professor Jaroslav Heyrovsky was awarded the Nobel Prize in Chemistry for 1959 by the Royal Swedish Academy of Science, for his discovery of polarography and for his development of polarographic analysis. The formal presentation took place on December 10, 1959, in Stockholm.

Professor Heyrovsky was born in 1890 in Prague as the fifth child of Leopold Heyrovsky, Professor of Roman Law at the Czech University, Prague. He started his studies in this university in 1909, taking courses in chemistry, physics, and mathematics. Later on, he continued his studies at University College, London, under Professor Sir W. Ramsay and G. F. Donnan. The latter suggested to him, as the subject of his Thesis, the determination of the electrode potential of aluminum. During the study of this problem, Heyrovsky first used the dropping amalgam electrode, a type of electrode to which he later devoted practically his whole scientific career. His interest in this type of electrode was aroused mainly during his Ph.D. examination at the Charles University of Prague, shortly after the end of World War I. His examiner, Professor Kucera, during the examination turned Heyrovsky's attention to the anomalies of the electrocapillary curves obtained in the presence of oxygen when using a dropping mercury electrode. After years of tireless experiments, Heyrovsky once tried to follow the current flowing during the electrolysis and register its dependence on potential. In these experiments, polarography was born. The first papers concerning electrolysis with a dropping mercury electrode appeared in Czech in 1922 (*Chemické listy*) and in English in 1923 (*Philosophical Magazine*), and the results were presented at a General Discussion of the Faraday Society in London, 1923.

Later on, Heyrovsky spent all his time, effort, and interest in the explanation of transport and electrolytic phenomena occurring at the dropping mercury electrode. In 1925, he invented, together with his Japanese collaborator M. Shikata, an apparatus, called a polarograph, enabling automatic registration of the current-voltage curves. Professor Heyrovsky attracted devoted collaborators and students by his enthusiasm as well as by his charming and inspiring personality. In his laboratories originated the concepts of migration, diffusion (Ilkovic), kinetic (Wiesner, Brdicka), catalytic (Brdicka), and adsorption (Brdicka) currents, of half-wave potentials, the equations for polarographic waves, as well as many other important contributions to polarographic theory and practice.

His efforts, results, and successes were reflected in a rapidly rising academic career. In 1922, he was appointed assistant professor and in 1926 full (*Ordinarius*) professor of physical chemistry at the Charles University. In 1950, he became head (as its first director) of the Polarographic Institute at Prague, which became, in 1952, a part of the Czechoslovak Academy of Science. Here he works in a quiet laboratory in an old mansion in an ancient quarter of Prague. During the last decade, he has been interested mainly in oscillographic polarography, a method he invented in 1942. The dV/dt-V curves obtained by this method allow him to draw further conclusions concerning the electrolytic and adsorption processes occurring on a single mercury drop.

In addition to being a member of many other scientific societies and academies, Professor Heyrovsky has been an Active Member of The Electrochemical Society since about 1927 (with an interruption due to World War II). He has received a number of honorary degrees and awards, including the Medal of the Polarographic Society (London) awarded last August on the occasion of the

Second International Congress on Polarography at Cambridge. He was the first recipient of this Medal.

Professor Heyrovsky has very intimate, friendly relations with electrochemists all over the world. His relations with chemists in the U.S.A. started early in 1933, when he spent a half year as the Carnegie Visiting Professor, lecturing on polarography at the University of California at Berkeley and at the California Institute of Technology, besides visiting a number of universities in the middle and eastern States. The relations were renewed and strengthened by the visits of American chemists to Prague, where visitors from overseas rarely omit coming to see Professor Heyrovsky's laboratory (this year e.g., Professors P. J. Elving and O. H. Müller). It is a pity that due to ill health Professor Heyrovsky was unable to take part in the Symposium on Electrode Processes, held last May in Philadelphia at The Electrochemical Society meeting.

Polarography has grown up from an analytical method to an important tool in electrochemistry, enabling us to study electrode processes, the rate and adsorption phenomena accompanying them, to determine reaction rates and equilibria in solutions, and to follow the effects of structure on reactivity of several types of compounds. The knowledge gained by use of the dropping mercury electrode has enabled the electrochemist also to understand processes on some other types of electrodes. It was thus not an overstatement when it was said that the invention of polarography opened a "renaissance of electrochemistry."

As Professor Heyrovsky is not only the originator of an important method to which at present more than 10,000 scientific papers have been devoted, but as he also recognized many of the advantages and possibilities of this method and nurtured its development, the Nobel Prize in Chemistry, 1959, is well deserved.

P. Zuman

Section News

Indianapolis Section

The Indianapolis Local Section of the Society held its first technical meeting of the current season on Tuesday, November 24, 1959, at the Student Union Bldg. of Butler University in Indianapolis. Dr. Earl A. Gulbransen, of the Westinghouse Electric Corp., spoke on "Effect of Substructure, Defects, Stress, and Environment on the Chemical Reactivity of Metals."

After a review of chemical and electrochemical concepts of corrosion and some of the inadequacies of each, Dr. Gulbransen presented the results of his experiments involving the use of electron optical procedures to examine the oxidation of certain metals and alloys under widely varied gaseous environments. Results clearly demonstrated that reactions were initiated at isolated sites involving only a small fraction of the total surface, even on the purest available forms of the metal. Variations in both the nature and distribution of the reaction products with different gaseous environments were illustrated, along with acceleration of effects under stress. Reaction products were identified and a model was presented to explain these phenomena in terms of either the chemical or electrochemical concepts of corrosion. A discussion period concluded the evening's activities.

T.C. O'Nan, *Secretary-Treasurer*

Pittsburgh Section

The Pittsburgh Local Section held its fall symposium on "Electrothermics and Metallurgy" at the Alcoa Research Labs. in New Kensington.

Dr. L. M. Foster described the "Characterization of Molten Salts," concluding that many of the apparent anomalies in the molten salts can be explained by assuming partial dimerization of alkali halides and appreciable holes or vacancies in the structure.

Dr. Everett Gorin reviewed the state of the art of "Fuel Cells," pointing out that hydrogen-burning cells are in a high state of development but offer limited commercial application. High-temperature cells suitable for burning fuel gases are potentially of much greater interest but more work is required before they can achieve commercial stature.

Dr. Neill Weber described an "Electrochemical Method of Tempering Glass" operating through the replacement of surface sodium ions with potassium ions by the application of an electric current in a fused salt.

Mr. M. A. Orehoski described the metal handling and vacuum equipment being used for vacuum casting of large steel ingots in a chamber 16 ft in diameter x 28 ft high, evacuated to 0.5 mm Hg at rates up to 100,000 cfm.

Mr. H. C. Ludwig described an optical method developed for measuring temperatures in electric welding arcs by measuring the intensity of specific spectral lines.

Dinner and a trip to the Alcoa Research Labs. followed the presentation of the papers.

W. E. Haupin, *Secretary*

San Francisco Section

The first meeting of the 1959-1960 season was held on September 23, 1959, at the University of California Men's Faculty Club. The speaker was Mr. H. F. Bauman, senior scientist at the Missile and Space Division of Lockheed Aircraft Corp. His subject was "Survey of Primary Cells as Power Sources."

Mr. Bauman described the various types of primary cells commercially used and their chemical and physical characteristics. Special cells also were mentioned, such as cells using organic materials as cathodes, cells containing liquid ammonia, and remotely activated cells. The speaker then described some of the special design features and operating characteristics of the batteries used in military applications.

The second meeting of the season was held at the International House in Berkeley on November 18, 1959. Dr. William Shockley, president of Shockley Transistor Corp., spoke on "Introduction to Semiconductor Physics."

Dr. Shockley first described the five essential imperfections in semi-

Notice to Members

According to the Constitution of the Society, Article III, Section 9, "Any member delinquent in dues after April 1 of each year shall no longer receive the Society's publications. . . ." Such delinquents will not receive the May issue of the JOURNAL. A reminder notice will be mailed to delinquents about the middle of February and a final notice about the middle of March.

conductor physics and their functions in transistor electronics. The theory and characteristics of junction transistors were discussed. Methods of transistor production were described briefly.

An interesting question and discussion period followed the formal part of the talk.

R. E. De La Rue, *Vice-Chairman*

Division News

"Symposium on Electrochemical Engineering," Spring 1960

A "Symposium on Electrochemical Engineering," sponsored jointly by the Theoretical Electrochemistry and Industrial Electrolytic Divisions, is being planned for the Chicago Meeting of the Society to be held May 1-5, 1960.

The purpose of this symposium is to present selected topics in fundamental and applied electrochemistry, particularly in areas which pertain to the design and operation of full-scale electrochemical reactors. The program will include ten invited papers in the areas: thermodynamics, applied electrode kinetics, mass transport and hydrodynamics factors, heat transfer, potential distribution, electrode materials and materials of construction, scale-up, and measurements on the plant scale. In addition, panel discussions will follow the first and second halves of the program.

Chairman of the symposium is Charles W. Tobias, University of California, Berkeley. Richard Bechtold of the Dow Chemical Co. in Pittsburg, Calif., is in charge on the panel discussions. Plans are being formed to publish the papers and the tape-recorded material of the panel discussions in a "Symposium" volume.

Charles W. Tobias, *Chairman*
Theoretical Division

New Members

In November 1959, the following were elected to membership in The Electrochemical Society by the Admissions Committee:

Active Sustaining Member

W. E. Hanley, Peerless Roll Leaf Co., Inc., 4511 New York Ave., Union City, N. J. (Battery)

Active Members

Robert Agenet, International Metalloids, Inc.; Mail add: 516 Cesar Gonzales St., Hato Rey, Puerto Rico (Electronics)

T. A. Alessi, Detroit Edison Co.; Mail add: 5711 Somerset Rd., Detroit 24, Mich. (Battery, Corrosion, Theoretical Electrochemistry)

L. W. Austin, National Steel Corp.; Mail add: 3821 Marland Hts. Rd., Weirton, W. Va. (Electrodeposition)

G. L. J. Bailey, The Mond Nickel Co., Ltd., Wiggin St., Birmingham 16, England (Battery, Corrosion, Electrodeposition, Electrothermics & Metallurgy, Theoretical Electrochemistry)

A. J. Borofsky, Sylvania Electric Products Inc.; Mail add: 59 Hazelhurst Ave., West Newton 65, Mass. (Electronics)

P. F. Bruins, Polytechnic Institute of Brooklyn, 333 Jay St., Brooklyn 1, N. Y. (Battery)

D. D. Bump, Chrysler Corp.; Mail add: 29105 Lorraine, Warren, Mich. (Theoretical Electrochemistry)

R. E. Carr, Bradley Semiconductor Corp., 275 Welton St., New Haven, Conn. (Electronics)

G. R. Clark, Catalyst Reasearch Corp.; Mail add: 912 Starbit Rd., Towson 4, Md. (Battery)

G. W. Cullen, RCA Laboratory, Princeton, N. J. (Electronics)

Thomas De Vries, Dept. of Chemistry, Purdue University, Lafayette, Ind. (Electro-Organic)

R. R. Dion, Products Development Lab., International Business Machines Corp., Poughkeepsie, N. Y. (Electronics)

C. E. Earhart, Texas Instruments, Inc.; Mail add: 4306 Southcrest Rd., Dallas 29, Texas (Electronics)

Pierre Egre, Centre d' Information du Nickel, 47 bis Ave. Hoche, Paris (8e), France

M. B. Epstein, Colgate Palmolive Co.; Mail add: 2700 De Witt Terrace, Linden, N. J. (Theoretical Electrochemistry)

Adolph Fischbach, U. S. Army Signal Research and Development Lab.; Mail add: 12 Cypress Ave., Elberon Park, N. J. (Battery)

D. J. Fischer, Dow Corning Corp.; Mail add: 4508 Huron Dr., Midland, Mich. (Electrodeposition, Electronics, Electrothermics & Metallurgy)

C. A. Forbes, Westinghouse Electric Corp.; Mail add: 1416 Ridge Ave., Coraopolis, Pa. (Electrodeposition)

R. M. Frey, Kyle Products Plant, Line Material Industries; Mail add: 9311 W. Forest Park Dr., Hales Corners, Wis. (Corrosion, Electric Insulation, Electronics)

C. A. Graf, Merck & Co., Inc., Electronic Chemical Div.; Mail add: 38 Devonshire Place, Glen Rock, N. J. (Electronics)

Herman Graff, Librascope, Inc., 808 Western Ave., Glendale 1, Calif. (Electronics)

W. W. Haase, P. R. Mallory & Co., Elkon Div.; Mail add: 944 South Lake Dr., DuQuoin, Ill. (Electronics)

P. J. Hagon, Lansdale Tube Co.; Mail add: 338 Butler Ave., Ambler, Pa. (Electronics)

D. J. Heiser, Air Reduction Co.; Mail add: 12 Neiers Lane, Watchung, N. J. (Theoretical Electrochemistry)

Franz Huber, Philco Corp.; Mail add: 225 E. Penn St., Philadelphia 44, Pa. (Electric Insulation, Electronics)

Melvin Kowal, Radio Corp. of America; Mail add: 188 Phillips Rd., New Brunswick, N. J. (Electronics)

J. F. Llopis, Instituto "Rocasolano" de Quimica Fisica; Mail add: Ardemans-83-C 2, Madrid, Spain (Corrosion, Theoretical Electrochemistry)

W. M. McNevin, Dept. of Chemistry, Ohio State University, Columbus 10, Ohio (Theoretical Electrochemistry)

L. V. McCarty, Lamp Development Dept., General Electric Co., Nela Park, Cleveland 12, Ohio (Electronics)

B. G. Nanney, Champion Paper & Fibre Co., Carolina Div., Canton, N. C. (Corrosion, Industrial Electrolytic)

W. A. Pliskin, International Business Machines Corp.; Mail add: 31 Greenvale Farms Rd., Poughkeepsie, N. Y. (Electronics)

Reinhardt Schuhmann, Jr., Purdue University; Mail add: 1206 Hayes St., West Lafayette, Ind. (Electrothermics & Metallurgy, Theoretical Electrochemistry)

R. N. Rhoda, International Nickel Co., Inc.; Mail add: 1020 Boulevard, Westfield, N. J. (Electrodeposition)

(Continued on page 36C)

By action of the Board of Directors of the Society, all prospective members must include first year's dues with their applications for membership.

Also, please note that, if sponsors sign the application form itself, processing can be expedited considerably.

Pictorial High Lights of the Columbus Meeting

Photographs by R. P. Jones, W. G. Jurevic, and R. E. Durtschi

Row 1—President W. C. Gardiner presenting Certificate of Appreciation to Past President R. M. Hunter; R. K. Shannon, Mrs. H. B. Linford, and Dr. and Mrs. L. I. Gilbertson; Dr. and Mrs. I. E. Campbell. **Row 2**—Dr. and Mrs. Clyde Williams (Dr. Williams was the 1000th registrant—he holds his ticket); E. M. Sherwood (Columbus Committee—Transportation) and Mrs. Sherwood; C. A. Snavely (Vice-Chairman, and in charge of Hotel Arrangements, Columbus Meeting) and Mrs. Snavely (Ladies' Committee). **Row 3**—P. S. Brooks, Dr. and Mrs. G. W. Heise, and Mrs. Brooks; L. D. McGraw, (Columbus Committee—Registration) and Mrs. McGraw (Ladies' Committee); H. H. Uhlig, Mrs. F. W. Fink (Chairman Columbus Ladies' Committee), and F. W. Fink. **Row 4**—R. M. Burns; R. N. Rhoda and C. V. King; A. C. Loonam, Lottie Fink, and Mrs. Loonam; R. J. McKay, R. M. Hunter, and Mrs. McKay. **Row 5**—Dr. and Mrs. C. L. Faust (General Chairman Columbus Meeting, and member Ladies' Committee, respectively), Dr. and Mrs. G. B. Carson, and Dr. and Mrs. W. C. Gardiner; J. H. Bartlett, H. B. Linford, Sherlock Swann, Jr., and H. A. Laitinen; Henri Andre. **Row 6**—Pei Wang, J. L. Porter, George Wallis and R. B. Soper; H. Wissenberg, John Griffin, and A. H. Beebe; Arnold Borofsky; F. W. Koerker.

Row 1—Mrs. N. M. Winslow, R. M. Hunter, Dr. and Mrs. C. A. Hampel, and N. J. Johnson; Mrs. M. G. Fontana, Mrs. R. B. Mears, and M. G. Fontana; Jan Meyering. **Row 2**—Mrs. J. H. Winkler, H. H. Uhlig, Dr. and Mrs. H. H. Pray, and C. L. Faust; Leo Esaki, Toshio Misawa, and Arthur Tang; J. F. Schaefer and O. H. Bauer. **Row 3**—S. A. Corren, T. A. Alessi, R. C. Smith, and F. W. Martin; Dr. and Mrs. M. W. Mallett; C. Thompson and W. H. Brattain; Serving line at Wednesday evening Buffet Supper. **Row 4**—R. G. Olsson, Monroe Goldberg, R. E. Coffman, Leonard Stein, Victor Sils, Kenneth Rankin, and Donald Lyon; Miriam Minamoto, Kurt Lehovec, John Madigan, Mr. and Mrs. Bernd Ross; K. Hauffe.

Brattain Among Noted Speakers at ECS Columbus Meeting

Dr. Walter Houser Brattain, research physicist and Nobel Prize winner, was among the distinguished scientists who presented papers at the Columbus Meeting of the Society held October 18-22, 1959.

Dr. Brattain presented the Keynote speech, "Introduction to the Physics and Chemistry of Surfaces," at the Corrosion—Electronics Joint Symposium on "The Surface Chemistry of Metals and Semiconductors," sponsored by the Office of Naval Research and The Electrochemical Society.

He was awarded the Nobel Peace Prize in Physics in 1956, jointly with Dr. John Bardeen and Dr. William Shockley, for his contribution to developing the transistor. Other contributions to the world of science in general, and electronics in particular, have been the discovery of the photo effect at the free surface of a semiconductor, and work leading to a better understanding of the surface properties of germanium.

Dr. Brattain, who has been with Bell Telephone Laboratories since 1929, lists as his chief field of research the surface properties of solids. His early work was concerned with thermionic emission and adsorbed layers on tungsten. He then continued into the field of rectification and photo effects at semiconductor surfaces, beginning with a study of rectification at the surface of cuprous oxide. This work was followed by similar studies of silicon. He also has carried on research on electron collisions in mercury vapor, piezoelectric frequency standards, magnetometers, and infrared detectors.

Among the honors bestowed on Dr. Brattain are the Stuart Ballantine Medal of the Franklin Institute (jointly with Dr. Bardeen), and the John Scott Medal (jointly with Dr. Bardeen). He also is the holder of four honorary Doctor of Science degrees, and is a Fellow of the American Association for the Advancement of Science, the American Physical Society, and the American Academy of Arts and Sciences.

New Members

(Continued from page 33C)

La Vern Rice, Union Carbide Nuclear Co.; Mail add: 132 E. Arrowwood Rd., Oak Ridge, Tenn. (Corrosion)

M. J. Rice, Jr., C. B. S.-Electronics; Mail add: 42 Dakin Rd., Sudbury, Mass. (Electronics)

D. E. Semones, Battelle Memorial Institute, 505 King Ave.,Columbus 1, Ohio (Battery, Corrosion, Electrodeposition)

J. W. Shackelford, Arkansas Louisiana Chemical Corp., P. O. Box 95, Pine Bluff, Ark. (Industrial Electrolytic)

A. H. Sharbaugh, General Electric Research Lab.; Mail add: 39 Pine St., Scotia 2, N. Y. (Electric Insulation)

J. S. Shaw, General Transistor Corp., Research and Development Div., 87-11 130th St., Richmond Hill 18, N. Y. (Electrodeposition)

Paul Smisko, Stackpole Carbon Co.; Mail add: 152 Center St., St. Marys, Pa. (Industrial Electrolytic)

R. C. Smith, Westinghouse Research Labs., Beulah Rd., Churchill Boro., Pittsburgh 35, Pa. (Electrodeposition, Electronics, Electrothermics & Metallurgy, Industrial Electrolytic, Theoretical Electrochemistry)

T. H. Smith, P. R. Mallory & Co.; Mail add: 408 E. North St., DuQuoin, Ill. (Electronics)

H. M. Stahr, General Electric Co.; Mail add: 33 Wilson Ave., South Glens Falls, N. Y. (Electric Insulation, Electro-Organic)

R. A. Staniforth, Monsanto Chemical Co., 800 N. Lindbergh Blvd., St. Louis 66, Mo. (Electronics)

G. W. Trytten, University of Michigan Research Institute; Mail add: 1635 S. Harris Rd., Ypsilanti, Mich. (Electronics)

C. F. Viglotti, Dept. of the Navy, Bureau of Ships; Mail add: 4000 Massachusetts Ave., N. W., Washington 16, D. C. (Battery)

B. B. Winter, Handy & Harman, 82 Fulton St., New York 38, N. Y. (Battery)

T. K. Worthington, International Business Machines Corp.; Mail add: Losee Rd., Wappingers Falls, N. Y. (Electronics)

R. S. Yatsko, U. S. Army Research and Development Labs.; Mail add: 646 Old Corlies Ave., Neptune, N. J. (Electronics)

Associate Members

D. A. Allen, Electro-Optical Systems; Mail add: 983 Del Rey, Pasadena, Calif. (Electronics)

ECS Membership Statistics

The following three tables give breakdown of membership as of Jan. 1, 1960. The Secretary's Office feels that a regular accounting of membership will be very stimulating to membership committee activities. In Table I it should be noted that the totals appearing in the right-hand column are *not* the sums of the figures in that line since members belong to more than one Division and, also, because Sustaining Members are not assigned to Divisions. But the totals listed are the total membership in each Section. In Table I, Sustaining Members have been credited to the various Sections.

Table I. *ECS Membership by Sections and Divisions*

Section	Division: Battery	Corrosion	Electric Insulation	Electrodeposition	Electronics	Electro-Organic	Electrothermics & Met.	Industrial Electrolytic	Theoretical Electrochem.	No Division	Total as of 1/1/59	Total as of 1/1/60	Net Change
Boston	18	30	6	37	75	8	26	14	30	6	151	168	+17
Chicago	15	32	5	41	29	9	14	10	26	15	132	134	+ 2
Cleveland	52	29	2	53	41	8	30	33	36	13	198	198	0
Columbus, Ohio	3	17	0	15	10	2	26	2	11	4	49	62	+13
Detroit	13	20	4	52	11	6	8	6	24	18	91	97	+ 6
India	8	7	2	19	8	6	8	10	15	3	35	35	0
Indianapolis	14	9	6	12	15	6	10	3	10	2	39	53	+14
Midland	9	15	0	6	3	3	8	14	11	1	43	43	0
Mohawk-Hudson	4	17	16	7	17	2	9	1	19	5	54	70	+16
New York	96	111	31	148	170	35	74	70	108	40	517	575	+58
Niagara Falls	13	25	1	25	13	6	78	68	29	18	183	180	− 3
Ontario-Quebec	9	24	1	15	8	3	39	30	12	14	82	93	+11
Pacific Northwest	6	9	0	9	3	1	10	11	10	10	44	43	− 1
Philadelphia	32	28	4	36	78	9	26	20	47	30	185	205	+20
Pittsburgh	2	47	4	30	30	7	43	18	36	10	133	136	+ 3
San Francisco	9	13	1	20	24	4	16	20	20	4	71	78	+ 7
S. Calif.-Nevada	19	26	3	33	49	5	25	18	34	10	105	135	+30
Washington-Baltimore	39	40	7	37	25	3	11	10	34	6	129	140	+11
U. S. Non-Section	71	92	14	92	100	42	65	83	125	30	408	452	+44
Foreign Non-Section	47	67	10	68	39	33	43	61	81	92	262	285	+23
Total as of Jan. 1, 1960	479	658	117	755	748	198	569	502	718	331		3182	
												+271	
Total as of Jan. 1, 1959	441	638	103	723	621	190	549	486	656	329	2911		
Net Change	+38	+20	+14	+32	+127	+8	+20	+16	+62	+2			

Table II. *ECS Membership by Grade*

	Total as of 1/1/59	Total as of 1/1/60	Net Change
Active	2538	2761	+223
Faraday (Active)	30	32	+ 2
Deutsche Bunsen Gesellschaft (Active)	15	18	+ 3
Delinquent	70	88	+ 18
Active Representative Patron Members	10	10	0
Active Representative Sustaining Members	99	111	+ 12
Total Active Members	2762	3020	+258
Life	17	17	0
Emeritus	49	48	− 1
Associate	31	33	+ 2
Student	46	57	+ 11
Honorary	6	7	+ 1
Total	2911	3182	+271

The figures pertaining to Patron and Sustaining Member Representatives, and Faraday and Deutsche Bunsen Gesellschaft members subscribing to the JOURNAL, have been added to reflect reclassifications and changes in membership status.

Table III. *ECS Patron and Sustaining Membership*

	Total as of 1/1/59	Total as of 1/1/60	Net Change
Patron Member Companies	5	5	0
Sustaining Member Companies	148	160	+ 12

S. P. Carbone, Sprague Electric Co., 11 Doncaster Rd., Lynnfield, Mass. (Theoretical Electrochemistry)

Gurion Meltzer, R.C.A. Semiconductor Div.; Mail add: 40 Brookside Ave., Somerville, N. J. (Electronics)

J. R. Norman, Texas Instruments, Inc.; Mail add: 125 West Ave. "E," Garland, Texas (Electronics)

D. L. Patorius, Varian Associates; Mail add: 770 Coleman Ave., Apt. F, Menlo Park, Calif. (Electrodeposition)

Student Associate Members

M. C. Banta, Dept. of Chemistry, University of Texas, Rm. 123, Austin 12, Texas (Theoretical Electrochemistry)

H. D. Cole, Dept. of Chemistry, University of Texas, P. O. Box 7737, Austin 12, Texas (Theoretical Electrochemistry)

W. F. Drinkard, Jr., North Carolina State College; Mail add: 1039 Nichols Dr., Raleigh, N. C. (Theoretical Electrochemistry)

T. F. Kassner, Purdue University; Mail add: 118-13 Marshall Dr., West Lafayette, Ind. (Electrothermics & Metallurgy)

George Schick, Corrosion Lab., Massachusetts Institute of Technology, 8-206, Cambridge 39, Mass. (Corrosion)

C. C. Seastrom, Ohio State University; Mail add: 69 E. 18 Ave., Columbus 1, Ohio (Corrosion)

Transfers from Associate to Active Membership

A. J. Carlan, Mellon Institute, 4400 Fifth Ave., Pittsburgh, Pa. (Electronics)

H. I. Moss, R.C.A. Laboratories; Mail add: 73 Myrtle Ave., North Plainfield, N. J. (Electronics)

Transfer from Student to Associate Membership

B. J. Kim, J. F. D. Manufacturing Co.; Mail add: 118 Park Place, Brooklyn 17, N. Y. (Electrodeposition, Electronics)

Reinstatements to Active Membership

H. D. Stanley, Price Battery Corp., Grant St., Hamburg, Pa. (Battery)

M. G. Vucich, Research and Development Dept., National Steel Corp., Weirton, W. Va. (Corrosion, Electrodeposition)

News Items

1959 Annual Index

The Annual Index for Vol. 106 (1959) of the JOURNAL appears on pp. i-xi of this issue. Reprints of the Index can be obtained about the middle of March by writing to The Electrochemical Society, 1860 Broadway, New York 23, N. Y.

ECS Chicago Meeting, May 1-5, 1960

The Spring Meeting of The Electrochemical Society will be held in Chicago, Ill., from May 1 through 5, 1960. Headquarters will be at the Lasalle Hotel.

Sessions will be scheduled on Electric Insulation (including a symposium on "Electrolytic Capacitors"), Electronics (including Luminescence, Semiconductors, and Thermionics), Electrothermics and Metallurgy (including symposia on Refractory Metals, "High-Purity Vanadium—Its Preparation, Properties, and Alloys" and on Rhenium, and a round table on "Methods of Reducing Iron Ores"), Industrial Electrolytics, and Theoretical Electrochemistry (general sessions, and a symposium on "Electrochemical Engineering" co-sponsored by the Theoretical and Industrial Electrolytic Divisions).

The complete program, including general information and 75-word abstracts of papers to be presented, will appear in the March JOURNAL.

W. A. Hamor Retires as Senior Director of Research, Mellon Institute

Dr. William Allen Hamor, senior director of research, Mellon Institute, Pittsburgh, retired on December 31, 1959 after 45 years at the Institute and more than a half-century of distinguished service to science.

Since joining the Institute in 1914, Dr. Hamor has continued in the supervision of public relations and in research management. He has served as adviser to several hundred different Fellowships, most recently as adviser to the Fellowships in Air Purification, Food Varieties, Industrial Hygiene, Paper, and Petroleum, as well as to three research programs in industrial pathology.

Long acknowledged to be one of the nation's leading research authors and editors, Dr. Hamor has been called "the greatest living American authority on the literature of chemistry." He is the author or co-author of nearly 200 articles and publications, including five books. He also has edited, during his years as a key figure in Mellon Institute's progress, some 3000 articles, books, and other publications. Since 1947, he has been editor of the American Chemical Society's Chemical Monograph series.

He was born in Du Bois, Pa., on March 27, 1887, and spent his boyhood in New Kensington, graduating from New Kensington High School in 1904. He studied at the University of Pittsburgh (at that time the Western University of Pennsylvania) as a special student in chemistry, receiving his M.A. degree in 1913.

For his contributions to research management and the application of human relations to research, Dr. Hamor has received many honorary degrees. Also, in 1950, he received the Pittsburgh Award of the American Chemical Society for "outstanding service to chemistry" for his achievements in research management, and was the recipient of the Science Award of the Pittsburgh Junior Chamber of Commerce in 1951.

In addition to The Electrochemical Society, Dr. Hamor is associated with many professional organizations in this country and abroad.

National Science Foundation Announces Academic Year Institute Program

The National Science Foundation, Washington, D. C., recently announced the award of grants totaling about $9,200,000 to 33 colleges and universities to support Academic Year Institutes for science and mathematics teachers. This will be the fifth year of this program, whose purpose is to help teachers improve their subject matter knowledge through a year's advanced study on a full-time basis.

Approximately 1600 experienced teachers will be enrolled in the Institutes in the 1960-1961 academic year, of whom the great majority will be secondary school teachers. A limited number of openings for college teachers also will be available in some of the Institutes. Each teacher will pursue a program of study in science or mathematics planned especially for him and conducted by scientists noted both for competence in their fields and for skill in presentation.

The Academic Year Institutes program has, in its four preceding years, helped about 3400 science and mathematics teachers improve the quality of their teaching by enabling them to keep abreast of the latest scientific developments. Reports from participants in the program, from their supervisors, and from observers strongly indicate that the influence of these trained teachers on others raises the general level of science in-

struction in secondary schools and tends to motivate students to undertake science careers.

The Foundation grants will provide stipends of $3000 for each participant, with additional allowances for dependents, books, and travel. Some Institutes will provide an additional summer training program to enable teachers more easily to fulfill graduate degree requirements. Supplementary allowances will be provided for teachers participating in this extended program.

Support of these Institutes by the National Science Foundation encourages colleges and universities to offer special programs in subject-matter instruction for teachers already in service, as well as providing financial support for teachers so that they can undertake advanced studies.

Scientific Information Projects in Chemistry and Metallurgy to be Supported by National Science Foundation

The National Science Foundation has announced support totaling $286,900 for three projects to develop mechanized systems and other advanced methods for improving the availablity of scientific information in the fields of chemistry and metallurgy.

Chemical Abstracts Service of the American Chemical Society, at Columbus, Ohio, received grants totaling $127,700 for two projects. A third grant for $159,200 will support a test program at the Center for Documentation and Communication Research, School of Library Science, Western Reserve University, Cleveland, Ohio, according to Dr. Alan T. Waterman, Foundation director.

"Scientific progress increasingly depends upon solution of the scientific information problem—how best to provide the scientist with the information he needs to do his work," Dr. Waterman said. "These grants represent fundamental attempts to provide long-range solutions as part of a Foundation effort to further the development of more comprehensive and versatile information tools for scientists."

Investigation of mechanical aids to chemical documentation will be performed by Chemical Abstracts Service with a $69,800 grant for a period of one year. The project will seek ways to exploit more fully the chemical information which the Service collects and organizes in carrying on its primary function of indexing and abstracting chemical literature. Processing techniques and equipment will be reviewed, preparatory to the development and experimental testing of applicable systems and methods.

One aspect of the project will involve ways to mechanize chemical data in order to correlate structures of chemical compounds with their properties and uses. The development of a system for correlating these data would permit the Service to answer, for example, a question regarding the number of chemical compounds containing a particular element that also have boiling points within specific ranges. This type of information search, which cannot now be done readily with *Chemical Abstracts*, would be of great use to industrial, governmental, and institutional research laboratories.

A second grant to Chemical Abstracts Service, $57,900 for one year, involves research into the semantic content of chemical literature. Part of a Chemical Abstracts program to mechanize wherever possible the processing and searching of information in chemistry, the study will attempt to determine methods for reducing the variety of word forms needed to express concepts in a subdiscipline such as biochemistry. Concept dictionaries will be prepared and applied experimentally to the processing of abstracts. Experimental searches will be conducted, using machine techniques. Machine programming needed to convert stored information automatically back to an intelligible form will be investigated.

The Western Reserve University grant will help support a large-scale test program to evaluate procedures developed for the automatic processing and searching of literature of interest to metallurgists. The funds will be used by the Center in working with not only the metallurgical literature proper, but also material of interest to metallurgists in such fields as physics, chemistry, and engineering. The program ultimately will include test searches and related studies designed to evaluate the results achieved with the mechanized procedures. In addition, the use made of the mechanized searching service by metallurgists will be analyzed.

This project also has the support of the American Society for Metals, and a committee of the society will lend active and continuing assistance to the project staff members at Western Reserve in developing details of the test program. In addition, the National Academy of Sciences—National Research Council has agreed to appoint an ad hoc commit-

Manuscripts and Abstracts for Fall 1960 Meeting

Papers are now being solicited for the Fall Meeting of the Society, to be held at the Shamrock Hotel in Houston, Texas, October 9, 10, 11, 12, and 13, 1960. Technical sessions probably will be scheduled on Batteries, Corrosion, Electrodeposition, Electronics (Semiconductors), and Electrothermics and Metallurgy.

To be considered for this meeting, triplicate copies of abstracts (*not exceeding 75 words in length*) must be received at Society Headquarters, 1860 Broadway, New York 23, N. Y., *not later than June 1, 1960. Please indicate on abstract for which Division's symposium the paper is to be scheduled, and underline the name of the author who will present the paper.* Complete manuscripts should be sent in triplicate to the Managing Editor of the JOURNAL at the same address.

Papers submitted for presentation at the meeting become the property of The Electrochemical Society and may not be published elsewhere, in whole or in part, unless permission is requested and granted by the Society. Papers already published elsewhere, or submitted for publication elsewhere, are not acceptable for oral presentation except on invitation by a Divisional program Chairman.

* * *

The Spring 1961 Meeting will be held in Indianapolis, Ind., April 30, May 1, 2, 3, and 4, 1961, at the Claypool Hotel. Sessions will be announced in a later issue.

tee of information specialists and metallurgists to participate actively in the further planning of the test program, to advise on questions that may arise throughout the program, and to assume responsibility for evaluating the results, including the planning of studies needed for their proper evaluation.

G. E. Reveals Details of Process for Making Diamonds

The General Electric Research Laboratory, Schenectady, N. Y., recently revealed the details of one of its major scientific and engineering achievements, the process for making diamonds. Man-made diamonds were first announced by the Laboratory in 1955; less than a tenth of a carat in size, they have been manufactured at G.E.'s Metallurgical Products Dept. in Detroit and have been sold in commercial quantities since October 1957. Until recently, the process was covered by U. S. Government secrecy restrictions, which have been removed with G.E.'s achievement of a large-scale production of man-made diamonds.

The essential breakthrough that enabled carbon to be transformed into diamonds was the use of a molten metal catalyst which acted as a thin film between the carbon and the growing diamond crystal. According to Dr. Guy Suits, G.E. vice-president and director of research, the molten catalytic film and the development of new superpressure and high-temperature apparatus made possible the long-sought transformation. Without the catalytic action, it is estimated that pressures of 3,000,000 psi and temperatures of over 7000°F would be required to transform carbon into diamond. There is no equipment in existence that could produce such a combination of sustained pressure and temperature.

Geological evidence has long suggested that natural diamonds were formed when carbon underwent extremely high temperatures and pressure deep within the earth, but the details of the rare process were unknown. For four years, a group of scientists in the Chemistry Research Dept. of the G.E. Research Laboratory investigated many combinations of materials, pressure, temperatures, process times, and catalysts, and constructed various pressure chambers that extended the capacity of high-pressure and high-temperature apparatus. Finally, a system for making diamonds was evolved.

In this system, carbon and a catalyst metal are placed in a pressure cell and subjected simultaneously to pressures from 800,000 to 1,800,000 psi and temperatures from 2200° to 4400°F.

The nature of the starting material used to supply the carbon has some effect on the kind and number of diamonds formed. Best results are obtained with substantially pure graphite, but other carbonaceous material, such as carbon black, sugar charcoal, or carburizing compound, may be used.

The catalyst metal can be chromium, manganese, iron, cobalt, nickel, ruthenium, rhodium, palladium, osmium, iridium, or platinum. Tantalum is particularly effective for inducing the growth of small diamond crystals, although under some circumstances it may not be as active as the other catalysts.

It also was discovered that new diamond can form whether or not diamond seed crystals are present, and that the diamond can grow at very high rates. The formation of man-made industrial diamonds (80 mesh and finer) is completed within a few minutes.

Of particular significance was the discovery that the shape of the diamond crystal varies according to the temperature of formation. Cubes predominate at the low end of the critical temperature range; mixed cubes, cubo-octahedra, and dodecahedra at the intermediate point; and octahedra at the upper limits of the range.

Color also was found to be governed by the temperature of formation, varying from black at low temperatures through dark green, light green, and yellow to white at the highest temperatures.

In tests and actual use in production, man-made diamonds have surpassed natural diamonds for various uses, although their small size keeps them within the range of industrial rather than gem stones.

By controlling shape and other characteristics, it will be possible to tailor diamonds more nearly to the requirements of industry for special cutting, grinding, and polishing applications.

Notice to Members and Subscribers
(Re Changes of Address)

To insure receipt of each issue of the JOURNAL, please be sure to give us your old address, as well as your new one, when you move. Our records are filed by states and cities, not by individual names. The Post Office does not forward magazines.

One of several devices invented by G. E. scientists for sustaining the ultrahigh pressures and temperatures required to change carbon into diamond, called the "belt," makes use of conical, Carboloy cemented-carbide pistons that push into each end of a specially doughnut- or "belt"-shaped Carboloy cemented-carbide chamber. An important feature of the "belt" is its pressure sealing technique in which conical gaskets of pyrophyllite are used for the dual purpose of holding pressure and yet allowing motion through compression and flow. A unique characteristic of pyrophyllite is that its melting point is raised from 2400° to 4800°F by pressure. Pyrophyllite is also used to hold the sample, which consists of the graphite and the metal catalyst. The high temperature is obtained by the passage of electrical current through the sample. The pyrophyllite, in addition to transmitting the pressure of the converging pistons, serves as a thermal and electrical insulation, enabling the pistons to remain comparatively cool, thus increasing their effective strength and extending their useful life.

Asia Foundation Books for Asian Students Program

The Asia Foundation, San Francisco, Calif., is a nonprofit, nonpolitical organization founded by private American citizens and incorporated in the State of California. Its purpose is to strengthen Asian educational, cultural, and civic activities with private American assistance.

One of the Foundation's projects is the Books for Asian Students Program, begun about four years ago. By April 1959, over one million books and a quarter of a million journals had been sent to thousands of recipients in Asia. Program materials are of a selective nature meeting rigid criteria and are sent to recipients with known, definite needs.

A recently proposed book project concerns the Federation of Malaya, which is served by 15 teacher-training institutions. These schools train almost all the teachers who, in the future, will serve the primary and secondary schools of Malaya. Mr. J. E. Tod, Director of Teacher-Training in the Ministry of Education, has discussed the book and journal needs of these schools with the Asia Foundation personnel in Kuala Lumpur. Titles in education, geography, history, arts and crafts, reference books —titles in all categories useful to educators—are needed because these schools have very few books. The Foundation's book program has been asked to furnish each of these

schools, over a period of time, with a basic library of 2500 volumes.

This project and other new ones such as those to assist education in North Borneo and Sarawak, together with growing commitments for books in other Asian countries made in the past five years, require the program to seek the cooperation of individuals or organizations who are in touch with sources of books.

The Asia Foundation will pay transportation costs from the donor to San Francisco and thence to Asia.

For further information on the program, please contact: Books for Asian Students, 21 Drumm St., San Francisco 11, Calif.

Chemstrand Assigns Representative to Mellon Research Program

Chemstrand Corp., Dacatur, Ala., is the first company to assign a representative to Mellon Institute as a visiting scientist under the Institute's new program for industrial affiliation with fundamental research. Chemstrand, which supports part of the Institute's basic research in polymers, was one of the first companies to become an affiliate.

The company's research appointee, who will have the rank of Fellow, is Dr. Robert Chiang, a Chinese-born scientist. He will spend approximately one year working under the guidance of the Institute's Research Directorate on the effect of crystallinity on high-polymer properties. The arrangement is one of the privileges available to companies supporting fundamental research through the Institute's affiliation program.

Dr. Chiang received his B.S. degree from National Central University, Nanking, China, and his Ph.D. from the University of Wisconsin.

Union Carbide to Convert Power Distribution System at Niagara Falls

Plans for conversion of the electrical distribution system from 25 to 60 cycles at plants of two divisions of Union Carbide Corp. in Niagara Falls, N.Y., have been announced by the corporation. Plants of National Carbon Co. and Union Carbide Metals Co., both divisions of the corporation, will be involved in the several-million-dollar project.

The new facilities will accept and distribute 145,000 kw of 60-cycle power from the Niagara Mohawk Power Corp., which power will be obtained from the new Niagara Generating Plant of the New York State Power Authority. The power will be used exclusively for the operation of plant facilities. The conversion project became necessary as a result of a rock slide about three year ago which almost destroyed the Schoellkopf power station, the major producing unit for 25-cycle power at Niagara Falls, N.Y.

New Linde Liquid Hydrogen Plant in Operation

A new liquid hydrogen facility is now in operation at the Tonawanda, N.Y., laboratories of Linde Co., Division of Union Carbide Corp. Hailed as a major advance in industrial cryogenics, this facility will make substantial quantities of liquid hydrogen available for the first time in the northeastern United States. Deliveries initially will be made in Linde's new highly efficient low-loss liquid hydrogen containers, in quantities ranging up to thousands of liters per truck load.

The unit can produce more than 25,000 l per month of liquid hydrogen with less than 2 ppm impurities. In addition to high purity, liquid hydrogen produced by this unit has high parahydrogen content. Parahydrogen, the stable form of liquid hydrogen, usually may be present in only ¼ of all hydrogen which is liquefied, but this unit makes a product with a minimum of 95% parahydrogen and 5% orthohydrogen.

Since electrical conductors show a great increase in conductivity when subjected to extremely low temperatures, liquid hydrogen is becoming increasingly important in electrical and electronic research. In addition, the ultracold fluid is widely used in liquid hydrogen bubble chambers for nuclear research and for hydrogen-oxygen fuel cell experimentation. Its prime use in large volumes, is as a missile fuel.

Termed "the ultimate chemical fuel" by Air Force missile experts, liquid hydrogen delivers about 40% more "specific thrust" than any other rocket fuel known today.

This facility is the product of an extensive pilot plant operation conducted for several years at Tonawanda. It is also the precursor of a large-scale liquid hydrogen plant being built by Linde at Torrance, Calif., to provide the National Aeronautical and Space Administration and other users with tonnage quantities of liquid hydrogen for missile activities.

Book Reviews

"Repartition du Potentiel et du Courant dans les Electrolytes," by Robert H. Rousselot. Published by Dunod, Paris, 1959. 85 pages; price 980 francs.

The subject of current distribution in electrolytic cells is the "missing chapter" of electrochemistry textbooks. The author's version of this chapter is directed toward a textbook of electrodeposition, however, rather than one on general electrochemistry. By careful selection of a few, perhaps too few, potential distribution maps, he has achieved an introductory treatment that is both concise and easily readable. The fundamental concepts, and the experimental determination of potential and current distribution, are emphasized.

As expected in so short a book, theoretical calculations of potential distributions are largely omitted. Other omissions, however, are less logical. The important case of concentric spheres is specifically excluded. The discussion of experimental potential mapping includes only those geometries which may be represented by a planar model. The usefulness of wedge-shaped tanks and the circuitry involved are not even mentioned.

While this book should prove useful, primarily to the electroplater, it does not obviate the need for a more comprehensive chapter on current distribution in electrochemistry. The latter must include current distribution on the surface of a corroding metal and around capillary tips used in electrode polarization measurements. Perhaps the author will consider expanding his treatment along these lines in a second edition.

S. Barnartt

Gmelins Handbuch der Anorganischen Chemie. Magnetic Materials. Magnetic and Electrical Properties. Supplement 2 to System No. 59, Iron, Part D. Published by Verlag Chemie, Weinheim, Germany, 1959 (order through any American book importer). XXXVIII + 580 pages; $78.24.

This supplements the volume on iron (System No. 59) and the volumes on cobalt, nickel, manganese, and chromium (No. 58, 57, 56, and 52, respectively). It does not include data which have been presented in some of the earlier volumes in the series, but reference to these earlier volumes is made at appropriate places. The data section of the book is preceded by a 24-page chapter which summarizes the present conception of the behavior of ferromagnetic materials and the pertinent

theories, outlines galvanomagnetic and thermomagnetic effects, and devotes some paragraphs specifically to magnetoresistance and Hall effect. The data are classified by material rather than by magnetic properties (e.g., under iron, or cobalt, or cobalt alloys, rather than under such headings as thermoelectric power, or gyromagnetic effects). Thus, all the data on cobalt, for example, are contained in pages 185-195, whereas data on magnetoelastic effects, for example, are found distributed throughout the volume.

Location of data is facilitated by the thoroughness of the table of contents which occupies 38 pages, and is presented in both German and English. Each page of the table of contents is divided into two columns so that the German and English versions may be presented side by side. Another feature is a set of marginal notations, in English, which appear throughout the volume, and indicate the subject matter of each paragraph. The allocation of space within the volume is as follows: iron, 26 pages; alloys of iron, 121; cobalt, 11; alloys of cobalt, 13; nickel, 63; alloys of nickel, 42; alloys of manganese, 22; alloys of chromium, 2; ferromagnetic semiconductors, 121. Also included is a listing of approximately 800 patents which deal with preparation and heat treatment of magnetic materials, and with magnetic materials with unusually high or low resistivity. This patent listing is followed by an alphabetical listing of the materials named in the patents, with references to the patents in which they were named.

William Miller

High Altitude and Satellite Rockets, A Symposium Sponsored by the Royal Aeronautical Society, the British Interplanetary Society, and The College of Aeronautics, held at Cranfield, England, July 18-20, 1957. Published by Philosophical Library, New York, 1959. 136 pages; $15.00.

The 1959 world of Sputniks, Explorers, and Luniks, and of accomplished "far side" lunar surveys is not likely to receive with much excitement the publication of the proceedings of a symposium on high altitude rocketry held in England two and a half years ago, less than three months before Sputnik I was placed in orbit.

The reason for this is not that the papers presented at the symposium lacked quality or technical interest. It is merely that, since its rude awakening on October 4, 1957, the West has made such advances in the art of rocketry that specialists in this field will find in these papers little that is not already part and parcel of their working theoretical and methodological equipment.

As a historical document, however, these proceedings should be of considerable interest to the general reader as well as to technicians in rocketry.

Rèné Bussiere

Molecular Science and Molecular Engineering. Edited by Arthur R. von Hippel. Published jointly by the Technology Press of Massachusetts Institute of Technology and by John Wiley & Sons, Inc., New York, 1959. 446 pages; $18.50.

This is the third and final volume in a series on modern materials research. Previous volumes were called "Dielectrics and Waves" (Wiley, 1954) and "Dielectric Materials and Applications" (Wiley, 1954). The present volume is the outcome of a Summer Session at M.I.T. in 1956 in which Professor von Hippel and 22 colleagues attempted to cover the fields of molecular theory and practice. To quote from the inside of the dust jacket: "Proceeding from classical to molecular science, the chapters advance in unifying vision from the structure of atoms and molecules and the behavior of charge carriers in gases to the formation and structure of condensed systems, to dipoles and their spontaneous alignment in ferroelectrics and ferromagnetics, and finally to ions and electrons in liquids and solids. Thunderstorms and explosions, gas-discharge and solid-state devices, the molecular concepts producing masers and memory systems, transducers, transistors, parametric amplifiers, ion-exchange resins, etc., appear in an exciting sequence of contributions."

This is one of the most attractive books that this reviewer has ever seen. The line drawings are large, clear, and well executed, and the pictures are stunning, particularly those of Lichtenberg figures. The table of contents is detailed and the index is unusually complete. A table of symbols is given at the end of the book.

The first seven chapters are concerned with the theoretical background, description, and applications of the conduction of electricity through gases. At first, steady direct currents are taken up, then alternating current conduction in gases, with a splendid chapter on microwave breakdown by S. C. Brown. This group of chapters ends with clear and comprehensive descriptions of technical gas discharge devices, and a fine chapter by B. Lewis on explosions.

Chapter 8 is an abridged textbook of thermodynamics, kinetic theory, and statistical mechanics, all in 30 pages. An amazing amount of material is covered succinctly and understandably. O. K. Mawardi and A. von Hippel are to be congratulated for their pedagogic skill in assembling so much material in so few pages.

Chapters 9-14 are concerned mainly with details of crystal structure and growth. There are many well-drawn diagrams and a large table listing the seven crystal systems with their Bravais lattices, crystal classes, and space groups. The crystal structures of the elements are displayed on a large periodic table. The structure of polymers and reaction mechanisms in liquid systems are given careful treatment.

Chapters 15-20 contain a tremendous amount of information about ferroelectric and antiferroelectric substances, ferromagnetic and antiferromagnetic systems, and piezoelectric crystals. The use of such materials in various kinds of amplifiers and masers is also included.

June 1960 Discussion Section

A Discussion Section, covering papers published in the July—December 1959 JOURNALS, is scheduled for publication in the June 1960 issue. Any discussion which did not reach the Editor in time for inclusion in the December 1959 Discussion Section will be included in the June 1960 issue.

Those who plan to contribute remarks for this Discussion Section should submit their comments or questions in triplicate to the Managing Editor of the JOURNAL, 1860 Broadway, New York 23, N. Y., *not later than March 1, 1960.* All discussion will be forwarded to the author(s) for reply before being printed in the JOURNAL.

The book ends with electrolytic conduction in various electrolytes, with ion-exchange resins, and with rectifiers and transistors. In 430 large pages (two columns per page), there is contained a whole world of physics, expertly and at times brilliantly unfolded to the reader.

This book has something in it for practically every kind of physicist and physics student, as well as for many chemists and engineers.

Mark W. Zemansky

New Products

Bright Nickel Process. Hanson-Van Winkle-Munning Co. has announced the availability of a new bright nickel process, Superlume. Superlume, according to the manufacturer, gives the brightest, smoothest nickel deposit obtainable today. The process yields deposits which are exceptionally bright at high and low current density areas and has the ability to level-out scratches to an extraordinary degree.

For complete information, write to Hanson-Van Winkle-Munning Co., Church St., Matawan, N. J., for the Superlume Instruction Manual describing its preparation, operation, maintenance, and equipment requirements.

Aluminum Tinning Process. Allied Research Products, Inc., supplier of metal finishing chemicals, equipment, and engineering services, has announced the availability of a new process for the immersion tinning of aluminum parts. Called ARP #200 Stannate "M," this new product is a special compound for make-up and maintenance of Stannate-type tin baths. It produces a smooth, adherent tin coating on the work from only a 4-min immersion in the bath at 165°-175°F.

Further information and samples can be obtained from Allied Research Products, Inc., 4004 E. Monument St., Baltimore 5, Md.

Aluminum Etchant in Solid Form. After nearly a year of field testing in the plants of a number of major aluminum fabricators, Pennsalt Chemicals Corp. has introduced a new aluminum etchant in solid form, which is dustless, nonscaling, and has no heat of solution. Called AE-16S, the new compound is an improvement over Pennsalt's widely-used aluminum etchant AE-16 in flake form.

Data sheets and other additional information on AE-16S are available from Pennsalt Metal Processing representatives or by writing to Metal Processing Dept., Pennsalt Chemicals Corp., 3 Penn Center, Philadelphia 2, Pa.

Two New Zinc Plating Brighteners. Two new brightening agents for zinc plating have been developed by Allied Research Products, Inc. Named Isobrite #354 and Isobrite #355, both are supplied in liquid form in either 5-gal lined pails or Allied's Auto-Flo-Pak container. They are extremely stable, providing effective brightening even after weekend shutdowns. Liquid form eliminates mixing, and simplifies control. They will tolerate wide variations in zinc bath formula. Both have been extensively tested in actual field use with satisfactory results.

Isobrite #354 produces a white, bright plate directly from the barrel even without bright dipping. This liquid brightener is the first to match the powder compounds in efficiency and economy.

Isobrite #355 produces a bright zinc deposit with a slight yellow cast from barrels, or rack plating tanks. However, its fine grain, uniform deposit produces a plate with clarity and sparkle after bright dipping. Isobrite #355 provides true economy of operation, with long life and performance over a wide range of conditions.

Further information can be obtained from Allied Research Products, Inc., 4004 E. Monument St., Baltimore 5, Md.

Employment Situations

Positions Available

Metallurgist, Chemist, Chemical Engineer — Ferrous metallurgical background for research and development on high and low temperature corrosion problems of fuel burning equipment. Chattanooga, Tennessee, location. Salary commensurate with experience. *Reply to Box A-281, c/o The Electrochemical Society, 1860 Broadway, New York 23, N. Y.*

Research Chemists, Mathematicians, Metallurgists, and Physicists —The Civil Service Commission is searching for qualified scientists in the fields of chemistry, mathematics, metallurgy, and physics for research work in various Federal establishments in the Washington, D. C., area. Persons appointed will work with some of the nation's foremost scientists in attractive and promising assignments and will have outstanding opportunities for advancement. The entrance salaries range from $4490 to $12,770 a year.

Most appointments are made to the following agencies: National Bureau of Standards, Dept. of the Air Force, Agricultural Research Service, Walter Reed Army Medical Center, Diamond Ordnance Fuze Labs., Geological Survey, Bureau of Mines, Food and Drug Administration, and the National Institutes of Health. The research laboratories in these agencies are among the finest equipped in the world. The basic and applied research being done is highly diversified and affords many challenges in the field of physical science.

Candidates must have completed appropriate college study leading to a bachelor's degree. In addition, for positions paying $5430 and above, graduate study or professional experience is required. College graduates may also qualify for positions paying a beginning salary of $5430 a year if they have a superior scholastic record, or through passing an appropriate written test.

Further information regarding these positions is contained in Civil Service Announcements 209B and 210B. The announcements and application forms can be obtained at many post offices throughout the country, or from the U.S. Civil Service Commission, Washington 25, D.C. Applications will be accepted by the Board of U.S. Civil Service Examiners, National Bureau of Standards, Washington 25, D.C., until further notice.

Chemists and Chemical Engineers —We need physical, organic and inorganic chemists, and chemical engineers to carry out engineering and development work in the rapidly growing power sources field. Research & Development center located in Minneapolis near University of Minnesota. Battery experience preferred but not required. Send résumés to: J. W. Baxter, Employee & Labor Relations, Gould-National Batteries, Inc., E. 1326 First National Bank Bldg., St. Paul 1, Minnesota.

Advertiser's Index

General Motors Research Laboratories 27C
Great Lakes Carbon Corp., Electrode Division ..... Cover 2
E. H. Sargent & Company 23C
Stackpole Carbon Company 29C

The Electrochemical Society

Patron Members

Aluminum Co. of Canada, Ltd.,
Montreal, Que., Canada
International Nickel Co., Inc.,
New York, N. Y.
Olin Mathieson Chemical Corp.,
Niagara Falls, N. Y.
Industrial Chemicals Div., Research
and Development Dept.
Union Carbide Corp.
Divisions:
Union Carbide Metals Co.,
New York, N. Y.
National Carbon Co., New York, N. Y.
Westinghouse Electric Corp., Pittsburgh, Pa.

Sustaining Members

Air Reduction Co., Inc.,
New York, N. Y.
Ajax Electro Metallurgical Corp.,
Philadelphia, Pa.
Allen-Bradley Co., Milwaukee, Wis.
Allied Chemical & Dye Corp.
General Chemical Div., Morristown, N. J.
Solvay Process Div., Syracuse, N. Y.
(3 memberships)
Allied Research Products, Inc.,
Detroit, Mich.
Alloy Steel Products Co., Inc., Linden, N. J.
Aluminum Co. of America,
New Kensington, Pa.
American Machine & Foundry Co.,
Raleigh, N. C.
American Metal Climax, Inc.,
New York, N. Y.
American Potash & Chemical Corp.,
Los Angeles, Calif. (2 memberships)
American Zinc Co. of Illinois,
East St. Louis, Ill.
American Zinc, Lead & Smelting Co.,
St. Louis, Mo.
American Zinc Oxide Co., Columbus, Ohio
M. Ames Chemical Works, Inc.,
Glens Falls, N. Y.
Auto City Plating Company Foundation,
Detroit, Mich.
Basic Inc., Maple Grove, Ohio
Bell Telephone Laboratories, Inc.,
New York, N. Y. (2 memberships)
Bethlehem Steel Co., Bethlehem, Pa.
(2 memberships)
Boeing Airplane Co., Seattle, Wash.
Burgess Battery Co., Freeport, Ill.
(4 memberships)
C & D Batteries, Inc., Conshohocken, Pa.
Canadian Industries Ltd., Montreal, Que.,
Canada
Carborundum Co., Niagara Falls, N. Y.
Catalyst Research Corp., Baltimore, Md.
Chrysler Corp., Detroit, Mich.
Ciba Pharmaceutical Products, Inc., Summit,
N. J.
Columbian Carbon Co., New York, N. Y.
Columbia-Southern Chemical Corp.,
Pittsburgh, Pa.
Consolidated Mining & Smelting Co. of
Canada, Ltd., Trail, B. C., Canada
(2 memberships)
Continental Can Co., Inc., Chicago, Ill.
Cooper Metallurgical Associates, Cleveland,
Ohio
Corning Glass Works, Corning, N. Y.
Crane Co., Chicago, Ill.
Diamond Alkali Co., Painesville, Ohio
(2 memberships)
Dow Chemical Co., Midland, Mich.
Wilbur B. Driver Co., Newark, N. J.
(2 memberships)
E. I. du Pont de Nemours & Co., Inc.,
Wilmington, Del.
Eagle-Picher Co., Chemical Div., Joplin, Mo.
Eastman Kodak Co., Rochester, N. Y.
Thomas A. Edison Research Laboratory, Div.
of McGraw-Edison Co., West Orange, N. J.
Electric Auto-Lite Co., Toledo, Ohio
Electric Storage Battery Co.,
Philadelphia, Pa.
Englehard Industries, Inc., Newark, N. J.
(2 memberships)
The Eppley Laboratory, Inc., Newport, R. I.
(2 memberships)
Erie Resistor Corp., Erie, Pa.
Exmet Corp., Tuckahoe, N.Y.
Fairchild Semiconductor Corp., Palo Alto,
Calif.
Federal Telecommunication Laboratories,
Nutley, N. J.
Food Machinery & Chemical Corp.
Becco Chemical Div., Buffalo, N. Y.
Westvaco Chlor-Alkali Div., South
Charleston, W. Va.
Foote Mineral Co., Paoli, Pa.
Ford Motor Co., Dearborn, Mich.
General Electric Co., Schenectady, N. Y.
Chemistry & Chemical Engineering
Component, General Engineering
Laboratory
Chemistry Research Dept.
General Physics Research Dept.
Metallurgy & Ceramics Research Dept.
General Instrument Corp., Newark, N. J.

(Sustaining Members cont'd)

General Motors Corp.
Brown-Lipe-Chapin Div., Syracuse, N. Y. (2 memberships)
Guide Lamp Div., Anderson, Ind.
Research Laboratories Div., Detroit, Mich.
General Transistor Corp., Jamaica, N. Y.
Gillette Safety Razor Co., Boston, Mass.
Globe-Union, Inc., Milwaukee, Wis.
Gould-National Batteries, Inc., Depew, N. Y.
Grace Electronic Chemicals, Inc., Baltimore, Md.
Great Lakes Carbon Corp., New York, N. Y.
Hanson-Van Winkle-Munning Co., Matawan, N. J. (3 memberships)
Harshaw Chemical Co., Cleveland, Ohio (2 memberships)
Hercules Powder Co., Wilmington, Del.
Hill Cross Co., Inc., New York, N. Y.
Hoffman Electronics Corp., Evanston, Ill.
Hooker Chemical Corp., Niagara Falls, N. Y. (3 memberships)
Houdaille Industries, Inc., Detroit, Mich.
Hughes Aircraft Co., Culver City, Calif.
International Business Machines Corp., Poughkeepsie, N. Y.
International Minerals & Chemical Corp., Chicago, Ill.
Jones & Laughlin Steel Corp., Pittsburgh, Pa.
K. W. Battery Co., Skokie, Ill.
Kaiser Aluminum & Chemical Corp.
Chemical Research Dept., Permanente, Calif.
Div. of Metallurgical Research, Spokane, Wash.
Kennecott Copper Corp., New York, N. Y.
Keokuk Electro-Metals Co., Keokuk, Iowa
Libbey-Owens-Ford Glass Co., Toledo, Ohio
M. & C. Nuclear, Inc., Attleboro, Mass.
Mallinckrodt Chemical Works, St. Louis, Mo.
P. R. Mallory & Co., Indianapolis, Ind.
McGean Chemical Co., Cleveland, Ohio
Merck & Co., Inc., Rahway, N. J.
Metal & Thermit Corp., Detroit, Mich.
Minnesota Mining & Manufacturing Co., St. Paul, Minn.
Monsanto Chemical Co., St. Louis, Mo.
Motorola, Inc., Chicago, Ill.
National Cash Register Co., Dayton, Ohio
National Lead Co., New York, N. Y.
National Research Corp., Cambridge, Mass.
National Steel Corp., Weirton, W. Va.
New York Air Brake Co., Vacuum Equipment Div., Camden, N. J.
Northern Electric Co., Montreal, Que., Canada
Norton Co., Worcester, Mass.
Olin Mathieson Chemical Corp., Niagara Falls, N. Y.
High Energy Fuels Organization (2 memberships)
Peerless Roll Leaf Co., Inc., Union City, N. J.
Pennsalt Chemicals Corp., Philadelphia, Pa.
Phelps Dodge Refining Corp., Maspeth, N. Y.
Philco Corp., Philadelphia, Pa.
Philips Laboratories, Inc., Irvington-on-Hudson, N. Y.
Pittsburgh Metallurgical Co., Inc., Niagara Falls, N. Y.
Poor & Co., Promat Div., Waukegan, Ill.
Potash Co. of America, Carlsbad, N. Mex.
Radio Corp. of America, Harrison, N. J.
Ray-O-Vac Co., Madison, Wis.
Raytheon Manufacturing Co., Waltham, Mass.
Reynolds Metals Co., Richmond, Va. (2 memberships)
Rheem Semiconductor Corp., Mountain View, Calif.
Schering Corporation, Bloomfield, N. J.
Shawinigan Chemicals Ltd., Montreal, Que., Canada
Speer Carbon Co.
International Graphite & Electrode Div., St. Marys, Pa. (2 memberships)
Sprague Electric Co., North Adams, Mass.
Stackpole Carbon Co., St. Marys, Pa.
Stauffer Chemical Co., New York, N. Y.
Sumner Chemical Co., Div. of Miles Laboratories, Inc., Elkhart, Ind.
Sylvania Electric Products Inc., Bayside, N. Y. (2 memberships)
Tennessee Products & Chemical Corp., Nashville, Tenn.
Three Point Four Corp., Yonkers, N. Y.
Titanium Metals Corp. of America, Henderson, Nev.
Tung-Sol Electric Inc., Newark, N. J.
Udylite Corp., Detroit, Mich. (4 memberships)
Universal-Cyclops Steel Corp., Bridgeville, Pa.
Upjohn Co., Kalamazoo, Mich.
Victor Chemical Works, Chicago, Ill.
Western Electric Co., Inc., Chicago, Ill.
Wyandotte Chemicals Corp., Wyandotte, Mich.
Yardney Electric Corp., New York, N. Y.